

---

Master's Thesis

To acquire the academic degree  
Master of Science (MSc)

**Characterisation and affinity maturation of DARPins binding  
human ROR1**



Author  
Wolfgang Koch

Supervisor  
Dr. Birgit Dreier  
Prof. Dr. Andreas Plückthun  
Prof. Dr. Florian Rümer

2016

Performed at  
Laboratory of Prof. Andreas Plückthun  
Department of Biochemistry  
University of Zurich  
Switzerland

Submitted at  
Department of Biotechnology  
University of Natural Resources and Life Sciences, Vienna

---

---

Master's Thesis

To acquire the academic degree  
Master of Science (MSc)

**Characterisation and affinity maturation of DARPins binding  
human ROR1**



Author  
Wolfgang Koch

Supervisor  
Dr. Birgit Dreier  
Prof. Dr. Andreas Plückthun  
Prof. Dr. Florian Rümer

2016

Performed at  
Laboratory of Prof. Andreas Plückthun  
Department of Biochemistry  
University of Zurich  
Switzerland

Submitted at  
Department of Biotechnology  
University of Natural Resources and Life Sciences, Vienna

---

*Dedicated to  
my parents Elisabeth and Ferdinand Koch  
for their unconditional support throughout my whole life*

## Abstract

The human receptor tyrosine kinase-like orphan receptor 1 (ROR1) represents a crucial factor for tumour progression and metastasis in a great variety of blood and solid malignancies. Its selective cell surface expression and essential role in cancer progression has further made this receptor a novel and promising target for tumour therapy. Yet, only very few molecules and derivatives able to bind tightly to the target exist in research, limiting therefore its potential for further investigation of receptor biology in basic research and approaches towards therapies of aggressive malignancies related to human ROR1.

In course of this thesis the selection and characterisation of Designed Ankyrin Repeat Proteins (DARPin), a novel class of binding molecules with favourable biophysical properties, specific for human ROR1 is described. Previously selected DARPins from combinatorial libraries were initially screened by ELISA and characterised. To expand the panel of binders a new screening of single clones after 3 + 4 selection rounds was performed in this work using HTRF. Binders with picomolar affinities were obtained that were entirely monomeric and could be expressed in high yields using *Escherichia coli*. Several clones specifically bound human ROR1 with affinities of up to  $K_D = 39$  pM and revealed 3 epitope regions being targeted. Epitope region 1 appeared to be the most dominant, with binders exhibiting the highest affinities. By using an additional stringent off-rate selection to improve the affinities of Epitope 2 + 3 binders, DARPins that showed improved binding to cells expressing human ROR1 could be generated, resulting in binders with up to 2.5-fold stronger cell binding than conventional antibodies. DARPins generated and characterised in this study therefore represent novel tools for basic research and therapeutic strategies for malignancies in which human ROR1 is involved.

# Contents

<b>1</b>	<b>Introduction</b>	<b>1</b>
1.1	Human ROR1 . . . . .	2
1.2	Alternative Protein Scaffolds . . . . .	5
1.2.1	Designed Ankyrin Repeat Proteins . . . . .	8
1.3	Ribosome Display . . . . .	12
1.4	Current state of research . . . . .	16
1.5	Aim of the thesis . . . . .	18
<b>2</b>	<b>Material and Methods</b>	<b>19</b>
2.1	Material . . . . .	19
2.1.1	Buffer . . . . .	19
2.1.2	Reagents for Ribosome Display selection . . . . .	26
2.1.3	Plasmid Vectors . . . . .	28
2.1.4	Strains . . . . .	29
2.1.5	Media . . . . .	29
2.1.6	DNA and Protein Standards . . . . .	30
2.1.7	Antibodies . . . . .	31
2.1.8	Cell lines . . . . .	31
2.1.9	Chemicals . . . . .	32
2.1.10	Instruments . . . . .	33
2.1.11	Devices . . . . .	34
2.2	Methods . . . . .	35
2.2.1	Methods in Molecular Biology . . . . .	35
2.2.2	Ribosome Display selection . . . . .	37
2.2.3	Microbiology . . . . .	42
2.2.4	Methods in Biochemistry . . . . .	42
<b>3</b>	<b>Results</b>	<b>51</b>
3.1	Characterisation of DARPins evolved from previous selections . . . . .	51
3.1.1	Homogenous Time Resolved Fluorescence (HTRF) . . . . .	51
3.1.2	Sequence Analysis . . . . .	58
3.1.3	Expression and Purification of DARPins . . . . .	60
3.1.4	Analytical Size Exclusion Chromatography (SEC) . . . . .	61
3.1.5	Multi Angle Light Scattering (MALS) . . . . .	64
3.1.6	Qualitative ELISA . . . . .	66
3.1.7	Cell Binding . . . . .	67
3.1.8	Affinity Determination . . . . .	71
3.1.9	Epitope Binning . . . . .	74
3.2	Affinity maturation of DARPins binding to the human ROR1 ECD . . . . .	77
3.2.1	Introduction of Additional Diversity . . . . .	77
3.2.2	Ribosome Display selection - Round 5 . . . . .	79

3.2.3	Ribosome Display selection - Round 6 . . . . .	80
3.3	Characterisation of DARPins evolved from affinity maturation . . . . .	83
3.3.1	Crude extract ELISA . . . . .	83
3.3.2	Sequence Analysis . . . . .	87
3.3.3	Expression and Purification of DARPins . . . . .	94
3.3.4	Analytical Size Exclusion Chromatography (SEC) . . . . .	95
3.3.5	Multi Angle Light Scattering (MALS) . . . . .	97
3.3.6	Cell Binding . . . . .	99
3.3.7	Affinity Determination . . . . .	102
3.4	Summary of evolved DARPins . . . . .	104
<b>4</b>	<b>Discussion</b>	<b>107</b>
4.1	Characterisation of DARPins evolved from previous selections . . . . .	107
4.1.1	Screening of selected clones . . . . .	107
4.1.2	Sequence Analysis . . . . .	107
4.1.3	Monomeric Behaviour . . . . .	108
4.1.4	Cell Binding . . . . .	108
4.1.5	Binding Kinetics . . . . .	108
4.1.6	Epitope Regions . . . . .	109
4.2	Ribosome Display selection . . . . .	109
4.3	Characterisation of DARPins evolved from off-rate selection . . . . .	110
4.3.1	Screening of selected clones . . . . .	110
4.3.2	Sequence Analysis . . . . .	111
4.3.3	Monomeric Behaviour . . . . .	111
4.3.4	Cell Binding . . . . .	112
4.3.5	Binding Kinetics . . . . .	112
<b>5</b>	<b>Conclusion</b>	<b>114</b>
	<b>References</b>	<b>116</b>
	<b>Appendices</b>	<b>133</b>

# Abbreviations

<b>aa</b> .....	amino acid
<b>Ab</b> .....	Antibody
<b>Ad</b> .....	Adenovirus
<b>Amp</b> .....	Ampicillin
<b>AP</b> .....	Alkaline Phosphatase
<b>BSA</b> .....	Bovine Serum Albumin
<b>bp</b> .....	base pair
<b>CV</b> .....	Column Volumes
<b>C-terminal</b> .....	Carboxyterminal
<b>DARPin</b> .....	Designed Ankyrin Repeat Protein
<b>dNTP</b> .....	Deoxynucleotide triphosphate
<b>DMSO</b> .....	Dimethyl sulfoxide
<b><i>E. coli</i></b> .....	<i>Escherichia coli</i>
<b>EDTA</b> .....	Ethylenediaminetetraacetic acid
<b>ELISA</b> .....	Enzyme-linked immunosorbent assay
<b>ECD</b> .....	Extracellular Domains
<b>FRET</b> .....	Fluorescent Resonance Energy Transfer
<b>FZD</b> .....	Frizzled Domain
<b>HTRF</b> .....	Homogeneous Time Resolved Fluorescence
<b>Ig</b> .....	Immunoglobulin
<b>IMAC</b> .....	Immobilized metal ion affinity chromatography
<b>IPTG</b> .....	Isopropyl- $\beta$ -D-thiogalactoside
<b>KRD</b> .....	Kringle Domain
<b>MALS</b> .....	Multi-Angle Light Scattering
<b>MBP</b> .....	Maltose binding protein
<b>MW</b> .....	Molecular Weight

**N-terminal** ..... Aminoterminal

**NTA** ..... Nitrilotriacetic acid

**OD** ..... Optical Density

**O/N** ..... Overnight

**PBS** ..... Phosphate buffered saline

**PCR** ..... Polymerase chain reaction

**pNPP** ..... Para-nitrophenylphosphate

**TBS** ..... Tris(hydroxymethyl)aminomethane buffered saline

**RD** ..... Ribosome Display

**ROR1** ..... Receptor tyrosine kinase-like orphan receptor 1

**RU** ..... Response Unit

**SDS-PAGE** ..... Sodium Dodecyl Sulfate Polyacrylamide gel electrophoresis

**SEC** ..... Size Exclusion Chromatography

**SPR** ..... Surface Plasmon Resonance

# Chapter 1

## Introduction

Cancer is a global burden that affects all of humankind. As of today cancer represents a major cause of morbidity and mortality worldwide, with an estimated 14 million new cases and 8 million cancer-related deaths every year, underpinning its role as one of the major global burden in human health. [1] It is genetic disease that involves dynamic changes in genes related to crucial cell functions and control mechanisms that leads to abnormal cell growth and potential spreading to other organs.[2, 3] Among all cancers, lung cancer remains the most common and prevalent in terms of both new cases and deaths, followed by breast, prostate and colorectal cancer.[4, 1] While prevention of the causing factors remains the key strategy for curtailing these diseases, major progress and advances have been achieved in the early detection and therapy. Beside a combination of chemo- and radiotherapies as one of the most common strategies, hormonal and targeted therapy have emerged as promising treatments of malignancies. While chemo- and radiotherapy aims for treatment of rapidly dividing cells with cytotoxic drugs, damage of DNA and local heat, it often causes severe collateral damage in normal tissue by missing stringent discrimination between malignant and normal cells, often leading to side effects and onset of later diseases.[5, 6] Targeted therapies can circumvent those drawbacks by targeting specific molecular differences between normal and cancer cells.[6, 7] Yet, proper and effective targets for a great variety of cancers still need to be evaluated in order to treat malignancies that are yet resistant to traditional targeted therapies, highlighting the importance for further binding molecules of promising tumor targets that exhibit cellular protein expression, meet specific requirements, maximize effectiveness, minimize off-target toxicities, and provide an opportunity for a therapeutic effect. The receptor tyrosine kinase-like orphan receptor one (ROR1) represents a novel putative target that exhibits a crucial role in tumor progression and metastasis. Their unique expression profile further allows for potential treatment with minimal residual disease and therefore novel and potential curative approaches of a great variety of malignancies that are resistant to current tumor therapies.[8] Yet, only very few molecules have been isolated and characterised to specifically bind to the target with high affinities, limiting therefore its potential for further investigation of the biology of human ROR1 and therapies of aggressive malignancies and increasing the need for additional molecules with high affinity to human ROR1.[9, 10, 11]

## 1.1 Human ROR1

Human receptor tyrosine kinase-like orphan receptor 1 (hROR1) is a transmembrane protein within the receptor tyrosine kinase family that is highly conserved among species.[12] Its structure consists of an extracellular region including an immunoglobulin-like domain (Ig), followed by cysteine-rich frizzled domain (FZD) and a kringle domain (KRD), linked to the membrane via transmembrane domain. The intracellular region consists of a tyrosine kinase domain with weak to moderate kinase activity followed by two serine/threonine-rich domains and a proline rich domain, to be seen in figure 31.[13, 14, 15] In contrast to other related receptors, human ROR1 possesses multiple N-glycosylation sites. Posttranslational modification at these sites are considered as necessary for the trafficking and function of the receptor. [16] Many investigations and experiments have been performed in order to elucidate the function of human ROR1. Yet, the definite ligand and involved signalling pathways are still unknown and knowledge of the key biological function is still incomplete.[17, 18]

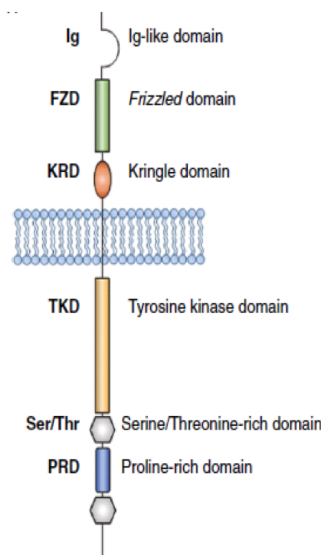


Figure 1.1: Structure of human ROR1. Receptor consisting of three extracellular domains, including Immunoglobulin domain (Ig), Frizzled domain (FZD) and Kringle domain (KRD), transmembrane domain and four intracellular domains including Tyrosine kinase domain (TKD), two Serine/Threonine rich domains (Ser/Thr) and a Proline rich domain (PRD). Adapted from N. Borchering et al. [17]

Besides the missing knowledge about key biological functions, human ROR1 is considered to play an essential role in embryonic patterning and neurogenesis, underpinned by its high degree of conservation among species and its strong expression profiles during development.[19, 20] In early stages of fetal development the receptor ROR1 is highly expressed in a great variety of tissues from all three germ lines, including neural crest cells, head mesenchyme, specialised sense organs, lung, skeletal and urogenital tissues. Knockdown of the receptor ultimately led to aberrant development of neural tissue and respiratory dysfunction within 24 hours after birth.[21, 22] Further studies revealed retarded growth, severe skeletal defects, urogenital and female infertility in ROR1-deficient mice. These findings highlight the receptor as a crucial factor for normal development.[22,

23]

In contrast to other receptor tyrosine kinases and its biological role, human ROR1 is only detectable in embryonic tissue and fetal development, while being absent within most mature tissues. Only low levels of ROR1 are expressed in adipose tissue and in even lesser degree in pancreas, the lung, a subset of intermediate B cells and undifferentiated ES cells.[10, 13] Unlike normal mature tissue, ROR1 seems to be highly expressed in cancer such as blood and solid malignancies. Especially B-cell chronic lymphocytic leukaemia cells, and a variety of haematological malignancies, such as non-Hodkin lymphomas and myeloid malignancies, show a high level of expression for human ROR1. The receptor is further observed in a large variety of solid malignancies such as ovarian, lymphoma, skin, lung, colorectal, neuroblastoma, testicular, uterine, prostate and adrenal cancers, pointing out its high correlation with malignancies and its progression.[24, 25, 26, 27]

While the exact role of human ROR1 in various cancers is still to be elucidated, several functions and interactions have been proposed by different *in vivo* studies. In case of blood malignancies an increased expression pattern in B-cell chronic lymphocytic leukemia (CLL), acute lymphocytic leukemia (ALL) and non-Hodkin lymphoma was identified, while being undetectable in peripheral blood mononuclear cells in cancer patients and healthy donors, revealing its potential role as biomarker and prognostic indicator. [28, 29] Yet, the exact role of human ROR1 within these malignancies remains still unsolved. A constitutive phosphorylation of STAT3, a known hallmark of CLL, was shown to bind several sites on the ROR1 promoter, inducing its expression in a IL-6- and STAT3-dependent manner. Further binding of Wnt5A to the receptor induced activation of NF- $\kappa$ B in HEK293 cells.[30, 31] Another study demonstrated that human ROR1 extensively contributes to leukemogenesis and binds to T-cell leukemia one (TCL-1), a known co-activator of AKT. Further, it has been described that ROR1 acts as a scaffold for the pAKT signalling pathway.[32] Studies in solid malignancies revealed its role as a pseudokinase, binding Wnt5A. Acting as a common node of kinase phosphorylation, it activates subsequent pathways, including EGFR potentiation, activation of c-Src, casein kinase1 $\epsilon$  and ultimate phosphorylation of AKT and CREB.[33, 34, 35] A recent study further showed that human ROR1 sustains crucial prosurvival signalling in lung adenocarcinoma, acting as a scaffold for the formation of cavin-1 and caveolin-1 and in subsequent result in formation and sustaining of caveolae. The prosurvival signalling towards AKT remains as a consequences sustained, highlighting its role as a potential approach for improved treatment of this yet devastating disease.[36]

Several antibodies and binding molecules, targeting human ROR1, have been generated in order to elucidate its functions and providing new potential therapies. Several antibodies induced internalisation of the receptor, and in some cases a very weak complement-dependent cytotoxicity (CDC) and antibody dependent cellular cytotoxicity (ADCC) could be observed upon binding on CLL and MCL cell lines. [11, 28] In further approaches over 70 antibodies were generated by immunisation of mice, resulting in binders covering all three extracellular domains of human ROR1. One of those antibodies, binding an epitope located between Ig and FZD, showed a direct cytotoxicity on ROR1 expressing leukemia cells *in vitro*. It further could decrease the levels of phosphorylated AKT and decrease the number of primary CLL cells.[37, 38] A further study showed that two mouse antibodies, D10 and 4A5, could bind at two distinct non-overlapping epitopes on the receptor. Antibody 4A5 showed a strong binding to the target with an almost 8-fold higher affinity than the respective binder D10. Still the effects on ROR1 expressing cells were negligible. In contrast, antibody D10 could induce rapid down-modulation of ROR1  $\times$  TCL-1 engrafted leukemia cells *in vitro* and reduce the expression of pAKT. Other studies revealed that D10 could inhibit ROR1<sup>+</sup> breast cancer metastasis *in vivo*.

The fact that D10 could, in contrast to 4A5, inhibit cancer cells, even though binding with 8-fold lower affinity, led to the conclusion that the activity of each antibody might be influenced by the respective epitope region on human ROR1.[32, 39] Yet, the low density of the receptor on the cell surface with an estimated  $10^3$  to  $10^4$  molecules on the surface represents a 10-100 fold lower expression than conventional targets of antibody therapies, making an effective targeting of ROR1 with binders challenging, due to strong affinities required.[11] An approach to overcome the limitation of low target density, a T-cell chimeric antigen receptor (CAR) specific for human ROR1 was further generated, that could retarget T-cell-mediated cytotoxicity against ROR1-positive tumor cells.[10]

Table 1.1: Existing binders which target human ROR1. Summary of the location of the epitope on the extracellular domains of receptor, affinity, ADCC, CDC, effect of inducing apoptosis, effective induced internalisation of receptor and inhibition of cancer cell growth. Ig: Immunoglobulin Domain; FZD: Frizzled Domain; KRD: Kringled Domain; ND: Not Determined. Adapted from Rebagay et al. [8].

Antibody	Epitope	Affinity ( $K_D$ )	ADCC	CDC	Apoptosis	Internal.	Inhibition
3B8 (IgM)	Ig	ND	ND	No	Yes	ND	ND
1C11 (IgM)	FZD	ND	ND	No	Yes	ND	ND
1D8 (IgG1)	FZD	ND	ND	Yes	Yes	ND	ND
4A7 (IgG1)	KRD	ND	Yes	Yes	Yes	ND	ND
4C10 (IgM)	KRD	ND	ND	No	Yes	ND	ND
R11 (IgG1)	KRD	0.19 nM	No	No	No	Strong	ND
R12 (IgG1)	Ig/FZD	0.11 nM	Yes	No	No	Modest	ND
Y31 (IgG1)	FZD/KRD	0.71 nM	No	No	No	Strong	ND
UC D10 (IgG)	Ig/FZD	41 nM	ND	Yes	Yes	ND	Yes

Combining the results of treatment with specific antibodies, ROR1 appears to be an excellent target for development of novel therapies for patients with disease related to this receptor and resistant to classical therapeutic approaches. Its restricted expression on tumor cells, its role as an important factor in regulation of apoptosis, its association with more aggressive disease and suggested role in epithelial-mesenchymal transition (EMT) make this receptor an ideal druggable target for malignancies that are of today resistant to classic therapies.[40, 8] The identification of only very few molecules binding to ROR1 and inducing apoptosis plus the low antigen density on the cell surface, which further limits the capability for efficient antibody-dependent cell-mediated cytotoxicity (ADCC) and complement dependent cytotoxicity (CDC), highlights the need for alternative strategies, such as highly potent toxin immunoconjugates, radio-immunoconjugates, bispecific binders or viral retargeting. Yet, antibodies contain some technical limitations when it comes to stability, folding, aggregation propensity and rapid evolvability of those molecules and variants they confer. When using antibodies in more ambitious formats, such as fusions, the limitations in their biophysical properties become even more apparent, ultimately increasing the need for alternative scaffolds. [41, 42, 43]

## 1.2 Alternative Protein Scaffolds

As of today, antibodies are the most successful class of binding molecules for biomedical science and application. Their key role in the immune defense of animals make them excellent binders for the application in living systems. Antibodies usually possess extraordinary specificity to the target and the ability to bind with high affinities in an efficient manner. Exhibiting a remarkable diversity, they can bind a great number of different molecules, ranging from peptides to proteins, sugars and small molecules. Furthermore, antibodies possess key functional properties, such as the ability to mediate antibody-dependent cell-mediated cytotoxicity (ADCC) and complement-dependent cytotoxicity (CDC), with further excellent half-life, due to their favorable size and binding of the neonatal Fc receptor that prevents degradation and excretion. Their key success was initially owed to its availability by immunisation. Approximately 16 years ago the immune system was the only source for binders with selected specificity, making it the only available binder with directed specificity towards targets.[44, 45, 46] However, until today remarkable progress has been achieved and specific binders can be generated by either using the immune system or synthetic libraries in combination with subsequent selection technologies.[47, 48, 49, 50, 51, 52] Nevertheless, several drawbacks become apparent in the application of antibodies. Its very large size, complex composition of four polypeptide chains, essential glycosylation pattern and presence of multiple relevant disulfide bonds require an eukaryotic expression system and cautious handling when it comes to the design and production of novel binders. This often involves the necessity of intensive optimisation processes, making the development and production of this class of biomolecules laborious and costly.[53, 54, 44]

One strategy to overcome those drawbacks was the development of antibody fragments. By the design and development of Ig fragments it was for the first time possible to produce and manipulate biomolecular binders in a prokaryotic expression system, boosting the field of antibody engineering in both discovery and biological drug development.[55, 56, 57] A dominant example of such antibody fragments are Fv fragments, comprised of the variable regions from both immunoglobulin chains. Yet, the limited stability of such constructs, due to non-covalent forces only, led to the introduction of a stabilising disulfide bond (dsFv) that resulted in poor expression yields.[58] By linking the two variable domains via short flexible peptide (scFv), the introduction of a disulfide bond could be avoided and the complex stabilised.[59, 58] Still, major drawbacks became apparent such as the necessary linkage of the N-terminus, resulting in possible conformational changes and sterical hindrance in the event of binding. Further drawbacks, such as lower folding efficacy upon expression in *E. coli* and the tendency to form oligomers and aggregates confined its success for biopharmaceutical application.[60] A more robust antibody variant represents the Fab fragment. A well defined protein comprised of an entire light chain paired with the variable and CH1 domain of the heavy chain. However, the short plasma half-life, due to smaller size and missing endosomal recycling, as well as less efficient tissue penetration limits its clinical application. Those drawbacks were tried to be overcome by a variety of modifications such as PEGylation or the generation of Fc fragments with introduced complement determining regions (CDR), retaining a prolonged half-life and partial effector functions.[61, 62] A class of smaller antibody fragments, so called domain antibodies or Nanobodies, comprised of a single variable domain from heavy chain antibodies, evolved as a further putative variant (Figure 1.2). Other than IgG-derived single V<sub>H</sub> fragments with exposed hydrophobic surfaces, such camelid V<sub>H</sub> domains overcame the problem of high aggregation propensity by a soluble form of the variable domain, enabling its application as a fusion protein.[57, 63] Still, antibodies and their respective derivatives contain some unsolved technical limita-

tions when it comes to stability, folding, aggregation propensity and rapid evolvability of those molecules and variants they confer. When using antibodies in more ambitious formats, such as fusions, the limitations in their biophysical properties become even more apparent.[41, 42] This increases the demand for alternative molecular scaffolds in order to enable additional innovative therapeutic approaches and investigations.

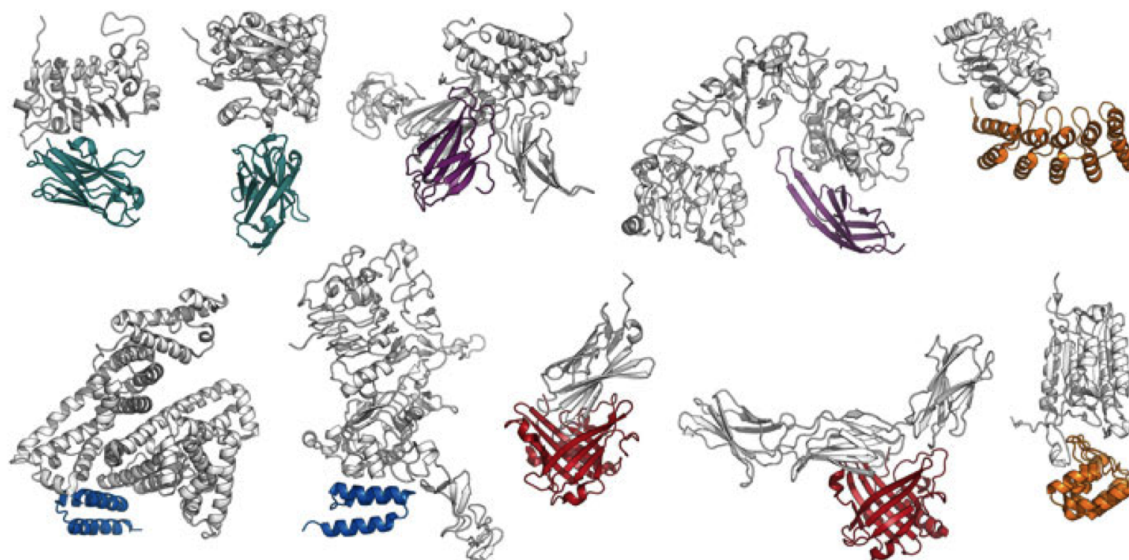


Figure 1.2: Structural comparison between alternative protein scaffolds. Each scaffold in complex with a biomedically relevant protein. Green: Nanobodies in complex with a EGFR fragment and ricin. Violet: Adnectins in complex with IL23 heterodimer and the EGFR extracellular region. Orange: DARPins in complex with a HER2 fragment and caspase 3. Blue: Affibodies in complex with albumin and the HER2 extracellular region. Red: Anticalins in complex with the CTLA-4 extracellular domain and ED-B. Adapted from A. Rosenberg et al. [44]

Enhanced by the need for novel alternative molecular scaffolds for therapeutic approaches and novel investigative strategies, a large effort was made in the past two decades to elucidate novel and potential binding scaffolds. As of today, more than 50 different protein scaffold have been proposed with emphasis on small single-chain proteins that possess high thermodynamic stability, lack of required posttranslational modifications and are missing free cysteines.[46, 64, 65] Due to the high technical demands on proteins for biopharmaceutical development and applications, only four scaffolds out of this great variety of constructs were finally able to mature beyond initial model case studies. These four protein scaffolds, Adnectins, Affibodies, Anticalins and DARPins constitute the most advanced approaches in this field and are of today the only alternative scaffold considered to yield products with a commercial value.[66, 44]

### *Adnectins*

One of the more promising classes of alternative proteins are Adnectins. Very similar designs have also been called Monobodies and Centyrins. A fibronectin type III domain (FN3), comprised of a 10 kDa autonomous domain that was first found in the abundant extracellular matrix proteins fibronectin and tenascin, as well as in a variety of multido-

main cell adhesion proteins. As one of the first alternative protein scaffolds investigated for its potential as binding protein, it shows a high structural similarity to the fold of Nanobodies, consisting of a framework of  $\beta$ -sheets and three exposed loops similar to the complement determining regions of antibodies. Unlike antibody domains, Adnectins lack a central disulfide bond between the  $\beta$ -sheet sandwich like structure, circumventing a key structural drawback of Nanobodies.[67, 68] By randomisation and length variation of the respective loops of Anticalins, libraries were created that allowed the successful generation of high affinity binder of various targets, including affinities in the sub-nanomolar range.[69, 70] The first binder of this class entering a clinical study, Pegdinetanib inhibiting the vascular endothelial growth factor receptor 2, yet led to the formation of anti-drug antibodies in the majority of patients. This effect and the circumstance that FN3 does not occur in the body arose concerns about potential immunological responses in humans upon administration. Nevertheless, the immune response of patients seemed to be directed against the engineered binding loops without cross reactivity with the wildtype FN3 scaffold.[71, 72] This finding led to a novel Adnectin design with the aim to eliminate immunogenic effects, including a redesign of the  $\beta$ -strand B, subsequent BC-loop and  $\beta$ -strand C.[73] Since then, another Adnectins, BMS-986089, successfully entered clinical studies [74] and several binder are in preclinical development including FGF21-AdPKE, a fusion protein between fibroblast growth factor 21 and Adnectin pharmacokinetic enhancer [75], and BMS-938790, a potent inhibitor of the inflammatory cytokine IL-23 (figure 1.2, highlighted in violet). [76]

### *Affibodies*

Another class of promising protein scaffolds are Affibodies, a protein that was derived from the IgG1 binding domain of protein A, found on the cell surface of *Staphylococcus aureus*. Its scaffold consist of a three  $\alpha$ -helix bundle without the presence of disulfide bonds. By random mutagenesis of the first two  $\alpha$ -helixes, considered to be involved in binding of the Fc part of antibodies, combinatorial phage display libraries were generated. Based on these libraries, binders for the detection, purification and targeting of biomedical relevant proteins were achieved.[77, 78] Its small size further opens advantages, such as rapid tissue penetration, fast renal plasma clearance or solid phase-synthesis of the peptide, permitting as a consequence a site-specific incorporation of potential chemical functionalities. These advantages make this scaffold an ideal candidate for molecular imaging. Nevertheless, Affibodies tend to have a less pronounced thermodynamic stability, resulting in e.g. molten globule structures. This effect might be caused by the extensive mutagenesis of structural relevant elements for the introduction of binding sites.[79, 80] As of today, several successful imaging approaches could be conducted with labeled Affibodies, targeting predominantly HER2.[81, 82, 83] Further studies successfully applied labeled Affibodies targeting other important members such as members of the transmembrane receptor tyrosine-kinase family, EGFR and PDGF-R $\beta$  (Figure 1.2, highlighted in blue).[84, 85]

### *Anticalins*

Other than Affibodies, Anticalins are derived from lipocalins, a family of compact and soluble  $\beta$ -barrel proteins. They are abundant in different organisms, including vertebrate species, and are naturally involved in binding of small molecules such as fluorescein, benzylbutyl phthalate or digoxigenin.[46] Lipocalins show a highly conserved structure that consists of eight antiparallel  $\beta$ -strands forming a cup-shaped structure with a hydrophobic densely packed core. The bottom of the  $\beta$ -barrel is closed by short loops. At

the top, four sets of loops form an entrance to a ligand pocket, exhibiting a large variation in sequence among species.[86, 87] Its high abundance in human blood plasma and hypervariable loops, similar to CDRs of antibodies, and its possible expression and modification in *E. coli* make this class of proteins promising binders for potential biomedical application. By combinatorial protein design and individual randomisation of the loop sequences, binders with high affinities and specificities towards prescribed targets could be generated, resulting in a large set of functionally active binding proteins against medically relevant targets for *in vivo* imaging strategies.[88, 89, 90] PRS-050, a PEGylated Anticalin blocking VEGF-A, was the first of its kind reaching a clinical trial. This study demonstrated a high tolerability of the Anticalin and exhibited no immune response upon administration over several days, showing promising results for future applications of Anticalins for biomedical purposes.[91] Ever since a great variety of applications have been studied in mouse models, including payload delivery and imaging approaches (Figure 1.2, highlighted in red).[92, 93, 94]

### *Repeat Proteins*

Repeat proteins constitute one of the most abundant forms of natural protein classes that are specialised in binding. As such they are found in all phyla, occurring in both intra- and extracellular environment, they are involved in a great diversity of biological processes, including the innate immunity, cell cycle control, apoptosis, differentiation, vesicular trafficking or transcriptional regulation.[95, 96] Other than the aforementioned scaffolds, repeat proteins are not limited by the size of the binding scaffold. Its key feature lies in its repeating structural units, which can be stacked together and form an elongated protein with continuous binding surface that can be varied in length, resulting in a protein with a potentially varying target-binding surface and high stability.[97, 98] As of today, many protein repeat families exist, differing in both structure and function. Overall three major structural types can be distinguished. Those of  $\beta$ -structure, including  $\beta$ -propellers and  $\beta$ -trefoils, the type of  $\alpha$ -structure, including armadillo repeats and TPR-like repeats, and mixed  $\alpha/\beta$ -structure, including leucine-rich and ankyrin proteins.[95, 99, 100, 101, 102] Several of these scaffolds have been successfully engineered by consensus design for targeted binding and libraries of different repeat proteins have been created, including DARPins, TPRs,  $\alpha$ REPs and ARMs.[103] As of today, DARPins constitute one of the most promising alternative binding scaffolds out of these repeat proteins and are discussed in more detail in the following subsection.[104]

## **1.2.1 Designed Ankyrin Repeat Proteins**

Ankyrin Repeat Proteins are built from tightly packed repeats of usually 33 amino acids. Each repeat unit comprises a  $\beta$ -loop followed by two antiparallel  $\alpha$ -helices that are connected by a short loop. The repeats are combined to a whole protein consisting usually of four to six repeat units and forming a right-handed solenoid structure with a large solvent-accessible surface that forms a groove-like binding surface.[41, 105, 98] Based a consensus strategy, an iterative process of sequence and structural analysis was performed by Binz et al., leading to libraries of Designed Ankyrin Repeat Proteins (DARPins) with fixed and variable positions. Each DARPIn consists of repeat units that exhibits fixed framework residues that are considered to be structurally important and six variable, non-conserved and surface exposed residues that can be engaged in binding. Thus, the theoretical diversity for libraries comprised of DARPins with three module binders is  $3.8 \times 10^{23}$ .[106] The respective repeat units are hold together by hydrophobic interaction in the core of the repeat protein. In order to shield the hydrophobic core from the surface,

N- and C- terminal capping repeats were designed that present a hydrophilic surface exposed to the solvent and therefore stabilising the protein.[106] The C-capping repeat was subsequently further improved in case of thermodynamic stability, due to tighter packing of the repeat unit against internal repeats.[107, 108] The resulting structure of a whole DARPIn, consisting of three internal repeat units, can be seen in Figure 1.3.

As such DARPins show remarkable properties. They can be expressed in high quantities of up to 200 mg/l in *E. coli*, showing on average excellent soluble monomeric behaviour and very high resistance in case of thermodynamic stability, which increases with length of the protein. Expression and purification is thus straightforward, and for laboratory use, IMAC purification is the standard method used, leading to very pure protein in a single purification step.[109] Further studies showed that DARPins consisting of three or more internal repeat units were resistant to boiling or guanidine hydrochloride, highlighting the extraordinary stability of these proteins.[104, 110, 108] Another specific feature of DARPins is their self-compatibility, that allows assembling in any order and therefore, in combination with its high thermodynamic stability, a great structural freedom and potential.[106] From such potential libraries a great variety of DARPins with high affinities were generated, using predominantly ribosome display selection. Efficiently targeting biomedically relevant targets, such as HIV gp120, EpCAM, amyloid- $\beta$  peptide, VEGF-A or HER2 DARPins, revealed their high potential for biomedical applications.[111, 112, 113, 114, 115] Such DARPins have been used in a variety of applications. Their ability to be expressed and function in an intracellular environment makes them an ideal basis for the creation of biosensors, enabling investigation in key cellular protein functions such as of mitogen-activated protein kinase, extracellular signal-regulated kinase or c-Jun N-terminal kinase-1.[116, 117, 118, 104] As DARPins can be created in a very robust and wide series of fusion proteins and conjugates, they are further well suited for the potential application of new diagnostic detection systems. This is especially the case in immunohistochemistry, where very high affinity and specificity is often crucial. One such example are DARPins with picomolar affinities to HER2, showing similar sensitivity and significantly higher specificity than an FDA-approved antibody.[119]

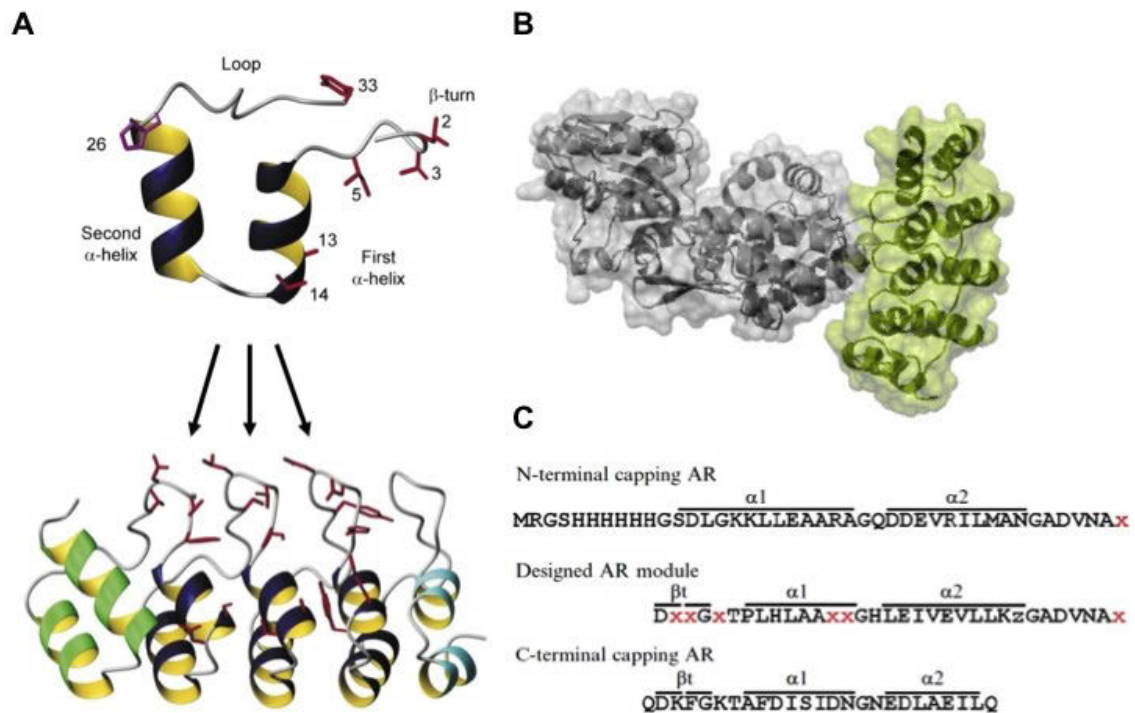


Figure 1.3: Structure of DARPins. (A) Middle Ankyrin Repeat module, consisting of two  $\alpha$ -helices and a  $\beta$ -turn, with potential interaction residues shown in red. Interaction residues are located in the  $\beta$ -turn and the concave shape of the L-shaped repeat module. A partly randomized framework residue is shown in magenta. Hydrophobic framework residues (not shown) are pointing into the core of repeat modules. A number of middle modules are combined and flanked by a specialised N- and C-terminal capping repeat that shield the hydrophobic core of middle repeat modules. (B) Crystal structure of a DARPin in complex with Maltose Binding Protein. All three randomised repeat modules are involved in binding, with 9 out of 18 randomised interaction residues being involved. (C) Sequence of the N-terminal capping repeat, designed internal repeat module, and the C-terminal capping repeat. Red 'x' indicates a randomised position. 'z' indicates any of the amino acids asparagine, histidine or tyrosine. Adapted from Binz et al. [106, 109]

In other approaches DARPins were successfully developed for tumour targeting. Due to their small size and (15 - 18 kDa) and high affinities, DARPins can rapidly penetrate into the tumour tissue and bind tightly to the respective surface molecules. Small unbound DARPins were furthermore cleared from the blood extremely rapidly, such that very high tumour to blood ratios (60:1) could be measured. [120, 121, 122] Based on their advantageous properties for tumour targeting, several 'naked' DARPins for the selective killing of tumor cells could be generated, including DARPins targeting relevant targets such as HER2, trapping and inactivating HER2-HER2 homodimers.[123, 124] Furthermore, DARPins could be successfully used as a delivery vehicle in tumour therapy. DARPins usually lack Cys and Met, allowing for efficient and safe coupling of the protein with respective conjugates. Based on these advantages, anti-EpCAM DARPins with several different conjugates have been generated, including a fusion toxin with ETA and delivery of a small interfering RNA.[125, 126] In another approach DARPins could be

successfully generated for viral retargeting. Bispecific adapters were generated, with DARPins binding to the fiber knob of adenovirus serotype 5 like a trimeric clamp and fused with a DARPin binding to a cell surface receptor of choice, allowing for stable and specific viral retargeting. Based on these constructs, delivery of a transgene in a HER2-, EGFR-, or EpCAM-dependent manner to tumour cell lines was achieved. Furthermore, DARPins coupled to Lentiviral vectors could successfully be generated and conferred specific retargeting to Her2-positive cells.[127, 128, 129, 130]

The superior properties of DARPins, with high expression yields, very high stability, flexibility in size, its ease of modification, evolvability and successful application in a great variety of alternative strategies make DARPins an ideal alternative protein platform for the development of alternative biomedical applications and investigation. Their low risk of immunogenic response, as seen in clinical studies, further proposes promising characteristics for putative applications in humans, making this scaffold an ideal candidate for the generation of monovalent constructs that bind human ROR1 with high affinity and enable further alternative strategies in the treatment and investigation of malignancies that are related to this receptor.[131, 132]

### 1.3 Ribosome Display

Over many generations, iterated mutation and natural selection during biological evolution provided solutions for challenges that organisms faced in the natural world. Yet, not all features that evolved from natural selection overlap with properties of specific biomolecules sought by humans. In order to gain access to favoured phenotypes, artificial selection strategies were established.[133] One of the key required features for a successful artificial directed evolution is the linkage of genotype (nucleotide sequence) and phenotype (properties). This requirement is accomplished by compartmentalisation or the direct physical linkage of both factors. During the last decades a great variety of strategies in order to combine those parameters were developed, including *in vivo* selection technologies, such as two-hybrid [134], phage [135], bacterial [136], yeast display [51] and mammalian display [137]. Yet, selection technologies that involve microbial cells exhibit a major drawback in respect of diversity. The diversity reached in practice after transformation strongly depends on the host system and on the effort that is made to transform the cells. This drawback becomes especially apparent when dealing with library diversities of more than  $10^{11}$ . [138] One possibility to overcome this problem are *in vitro* selection technologies, where the library size itself represents the limiting factor of diversity. Here again a great variety of selection technologies were established ranging from mRNA [139] and ribosome display [140] to more recently developed methods such as *in vitro* compartmentalisation or SNAP technology.[141, 142] One of the most powerful and best established *in vitro* selection technologies for affinity maturation constitutes ribosome display. Its great advantage lies in its possibility to combine selection with controllable PCR-based randomisation techniques, enabling as a result a true Darwinian evolution process that would be confined by a solely selection from an existing constant library.[138]

Ribosome display is based on stalled ribosomal complexes containing the nascent polypeptides and respective mRNA, therefore effectively linking genotype and phenotype during the selection process. For this purpose a library of interest is ligated into a vector containing features necessary for a successful selection, including a T7 promoter that allows for efficient transcription *in vitro*, a Shine-Dalgarno sequence that facilitates ribosome binding, a stem loop regions at the 5'- and 3'-end, respectively, that protect the transcribed mRNA from RNase degradation and a *tolA* spacer sequence that allows the protein to exit the ribosomal tunnel and fold in a correct way. Unlike most natural mRNA sequences, constructs for ribosome display exhibit no stop codon. As a result the nascent protein chain is not released from the ribosome complex but remains connected, effectively linking the expressed protein chain with its respective mRNA sequence via the ribosome complex.[140] The methodology of ribosome display selection technology is summarised in Figure 1.4. A DNA cassette, containing the library of interest and required features, is transcribed *in vitro*. The resulting mRNA strand is subsequently translated *in vitro*, using a cell-free translation, that runs to the end of mRNA strand and complexes the protein of interest with its respective mRNA strand and the ribosome. Due to the absence of a stop codon, the last codon can not be recognised by release factors that would hydrolyse the ester bond between the translated protein and the last tRNA. As a consequence the large and the small ribosome subunits are not separated by the ribosome recycling factor and elongation factor G. In order to minimize the risk of spontaneous hydrolysis of the ester bond between protein and tRNA,  $Mg^{2+}$  is added to the mix, condensing the ribosome complex and making it more difficult for the tRNA to dissociate.[138, 143, 144] Furthermore, tmRNA needs to be titrated out by addition of antisense oligonucleotide, which would rescue such stalled ribosome complexes and lead to regular termination and recycling of the ribosome and degradation of the protein.[140, 145] After successful

translation the ternary complexes are exposed to target molecules in a subsequent panning step and unbound proteins are washed away. In this step the target is either free in solution, and later captured by e.g. magnetic beads, or immobilised on plates. The way the library is exposed to the target will ultimately determine the selection outcome.[138] In order to remove unspecific binder that target constituents of the panning environment, a prepanning step can be performed, by exposing the ternary complexes to a panning environment without target of interest.[146, 109] After selection on the target, mRNA is released from the ribosome complex by addition of EDTA. This step does not require dissociation of the protein from the target and is therefore independent from its affinities. Upon release and purification, the mRNA needs to be reverse-transcribed into DNA. This step can appear to be technically demanding, since under stringent panning conditions, very few fragile molecules are isolated from the subsequent step and are under constant threat of degradation by RNase. As a consequence, careful handling of mRNA under constant cooling is required. The obtained cDNA is then amplified by PCR and subsequently again incorporated into pRDV for further rounds of selection or cloned into expression vectors for subsequent screening and characterisation.[138]

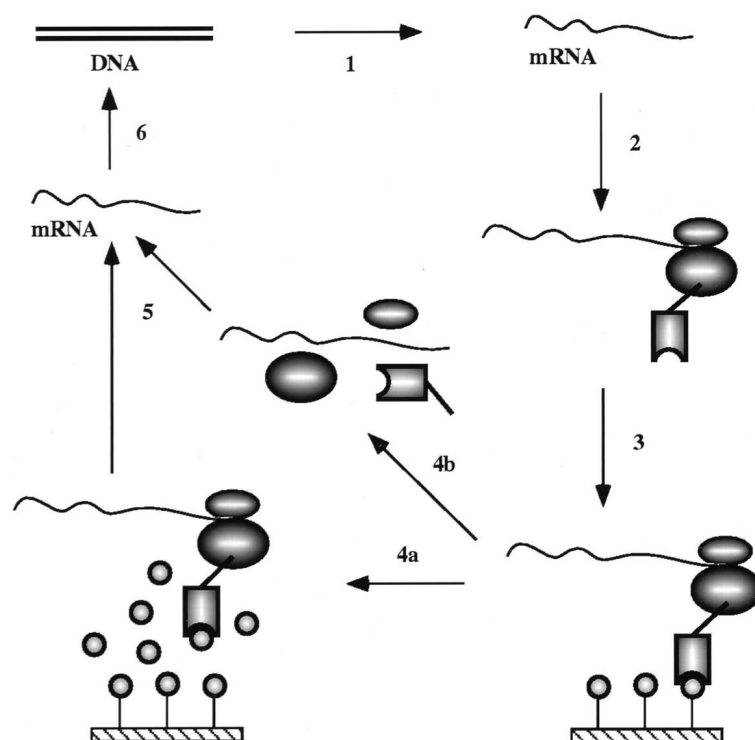


Figure 1.4: Overview of ribosome display selection. A DNA library, coding for binding proteins, is ligated into the ribosome display vector pRDV, resulting in a genetic fusion of protein with *tolA* spacer and a 5'-terminal promoter and translation initiation region. The construct is amplified using PCR, resulting in the final linear DNA fragment which is used for ribosome display. (1) *In vitro* transcription yields the mRNA. (2) After translation the ribosome complex remains at the end of mRNA strand and does not release the translated and folded protein, due to a missing stop codon. (3) The ribosome-mRNA-protein complex is used for affinity selection on immobilised or soluble target. (4a/b) After washing, the mRNA of bound complex is recovered by addition of EDTA, leading to dissociation of the complex, or by elution of the whole complex with antigen. (5, 6) Subsequently, recovered mRNA is reverse transcribed and amplified by PCR. The resulting PCR products, representing the selected pools of binders, can be used for the next cycle of ribosome display selection or cloned into expression vectors and analysed. Adapted from Hanes et al.[140]

#### *Off-rate selection*

The selection for binders with low to mid-nanomolar affinity can usually be accomplished by normal panning experiments, where binders are enriched from libraries by exposing them to antigen and eliminating unbound or weakly binders in subsequent washing steps. However, in iterative affinity maturation of binders with already low nanomolar affinity, more efficient strategies are needed, such as off-rate selection.[147, 148, 149] Studies have shown that under normal conditions the association rate constant of protein-protein interactions does not exceed a value of  $5 \times 10^6 \text{ M}^{-1}\text{s}^{-1}$ , making the off-rate the key parameter for the maturation of high affinities.[150] In order to select for binders with improved off-rate a large excess of competing antigen is added to the reaction after panning, capturing as a consequence the vast majority of the binding molecules

that dissociate from the target of interest. The excess of competitor further prevents re-binding of the immobilised or biotinylated target, ultimately enriching for binder with the slowest off-rates. [149, 151]

## 1.4 Current state of research

Many investigations and experiments have been performed in order to elucidate the function of human ROR1 in the development of fetal tissue and its role in the onset and progression of malignancies.[39, 24, 9, 152, 18, 17, 32, 153, 36, 21, 154, 155]

Yet, the vast majority of experiments was performed using mouse models by knock-down of ROR1 and associated genes. The absence of potential binders limits therefore potential investigations and therapies of respective malignancies, associated with this receptor. Thomas Kipps et al. developed first binder of human ROR1 in form of two antibodies D10 and 4A5.[37] While binding of 4A5 had only marginal effects on tumor tissues, D10 could inhibit breast cancer metastasis *in vivo* and further down-modulate ROR1 and pAKT, ultimately inhibiting leukemia cells in mice and highlighting the importance of further excellent binder of human ROR1.[39, 32] Still, antibodies contain some technical limitations when it comes to stability, folding, aggregation propensity and rapid evolvability of those molecules and variants they confer. When using antibodies in more ambitious formats, such as fusions, the limitations in their biophysical properties become even more apparent.[41, 42, 43] Other than antibodies, Designed Ankyrin Repeat Proteins (DARPs) are well suited for more ambitious purposes. Their stable and yet adaptable structure, possibility to create hetero-oligomers of various geometries, small molecular weight, evolvability and ease of production make them suitable tools for therapeutic applications and investigation of malignancies. Furthermore, the introduction of unique cysteines allows site-specific modification and conjugation with various effector moieties.[106, 109, 103, 112]

Based on three distinct libraries, initial ribosome display selection for DARPs binding human ROR1 was performed by Dreier et al. (unpublished). N2C Library consists of two internal randomised repeat units, and N3C consisting of three internal randomised repeat units as described by Binz et al. [106]. The third Library is based on the N3C fold, but in addition contains stabilised C-Caps for putative tighter packing and containing additionally a mixture of randomised and non-randomised sequences.[109, 107, 156] Each library was individually matured over four rounds of ribosome display selection with increasing stringency within each round. In order to maintain a degree of diversity, the first round was performed with low stringency. In the last round of selection a competition was performed, using 455-fold excess of competitor for off-rate selection. Characterisation of evolved and ELISA-screened DARPs revealed an increased tendency for oligomerisation (Stringhini and Dreier, unpublished). Therefore, a suitable screening strategy was still required in order to decrease the avidity effect of oligomerised DARPs in classical screening assays, such as crude extract ELISA, with which clones with excellent biophysical properties such as monomeric behaviour could be identified.

round	1st	2nd	3rd	4th
target	250 nM	100 nM	20 nM	2 nM
washing	6 x 2'	2 x 2'	2 x 2'	2 x 2'
		5', 10'	6 x 10'	6 x 10'
		5', 10'		
competition	na	na	na	455 x

Figure 1.5: Conditions for ribosome display selection for DARPins binding human ROR1. Each selection round is indicated with the amount of target used for panning step, duration and number of cycles for washing steps and amount of unbiotinylated competitor used for off-rate selection. Adapted from Dreier et al. (unpublished)

## 1.5 Aim of the thesis

The human receptor tyrosine kinase like orphan receptor 1 (human ROR1) is more and more recognised as an emerging tumour marker and putative candidate for targeted therapy. However, up to date only very few molecules have been identified that show high affinity to ROR1 and display a favourable effect in tumour cell eradication.

The aim of the project was to isolate and characterise novel binders to human ROR1. In course of this aim, DARPins binding human ROR1 should be identified from the output of ribosome display selections of 3 DARPIn libraries against the extracellular domain of human ROR1. Identified putative binders should be tested for required characteristics such as excellent biophysical properties, specificity, high affinity, ability to bind the target on cells and epitope regions distinguished by epitope binning using SPR with competition of binders. In addition, interesting binders not displaying unique pM affinities are sought to be improved using maturation. The ultimate goal was to generate a panel of high-affinity binders with monomeric behaviour, high stability, targeting different epitopes on human ROR1 thus, to study the receptor function and biology on the cellular level and opening putative alternative therapeutic strategies of cancers related to this receptor.

# Chapter 2

## Material and Methods

### 2.1 Material

#### 2.1.1 Buffer

All buffers and solutions used during experimental procedures were prepared using milliQ-H<sub>2</sub>O derived from Purelab Option filter system. All buffers used for experiments were freshly prepared prior use or diluted from respective stock solutions. Stock solutions were prepared and sterile filtered through a membrane filter with pore size of 0.22  $\mu\text{m}$  prior storage. Buffer used for analytical size exclusion chromatography, SEC-MALS, determination of kinetics and epitope binning were all fresh prepared, sterile filtered using membrane filter with pore size of 0.22  $\mu\text{m}$  and degassed for 3 h under vacuum and constant steering. All buffers prepared for ribosome display selection were prepared in a separate RNA-free environment. During the whole preparation RNase-free environment was ensured by cautious handling of the reagents and intensive cleaning of surfaces and surrounding materials. All stock solutions were sterile filter through a membrane with pore size of 0.22  $\mu\text{m}$ . Only RNase-free consumables and devices were used during preparation. The pH of all buffers was adjusted at 25 °C. The pH of buffers used for ribosome display selection was adjusted at 4 °C. The pH off all buffer was adjusted with HCl if not stated other.

Table 2.1: Buffer used for gel-electrophoresis

Buffer	Composition	pH
TAE	40 mM Tris 20 mM AcOH 1 mM Na <sub>2</sub> ·EDTA·(H <sub>2</sub> O) <sub>2</sub>	
6X DNA Loading Dye	60% (v/v) glycerol 60 mM Tris-HCl 60 mM EDTA 4.4 mM bromophenol blue 4.4 mM xylene cyanol	7.4

Table 2.2: Buffer used for cloning

Buffer	Composition	pH
10 × CutSmart buffer (B7204S) (New England Biolabs)	500 mM Potassium acetate 200 mM Tris-acetate 100 mM Magnesium acetate 100 µg/ml BSA	7.8
10 × T4 Ligase buffer (Fermentas)	500 mM Tris-HCl 100 mM MgCl <sub>2</sub> 10 mM ATP 100 mM DTT	7.5
10 × ThermoPol Reaction buffer (New England Biolabs)	200 mM Tris-HCl 100 mM (NH <sub>4</sub> ) <sub>2</sub> SO <sub>4</sub> 100 mM KCl 20 mM MgSO <sub>4</sub> 1.0% Triton X-100	8.8
5 × Herculase II Reaction Buffer (Agilent)	200 mM Tris-HCl 500 mM KCl	8.4
10 × Platinum Taq high fidelity PCR buffer (Thermofisher)	600 mM Tris-SO <sub>4</sub> 180 mM (NH <sub>4</sub> ) <sub>2</sub> SO <sub>4</sub>	8.9

Table 2.3: Buffer used for Ribosome Display selection

Buffer	Composition	pH
TBS	50 mM Tris 150 mM NaCl	7.4
TBS-T	50 mM Tris 150 mM NaCl 0.05% (v/v) Tween20	7.4
TBS-TB	50 mM Tris 150 mM NaCl 0.05% (v/v) Tween20 0.5% (w/v) BSA	7.4
WBT	50 mM Tris 150 mM NaCl 50 mM Mg(OAc) <sub>2</sub> 0.05% (v/v) Tween-20 0.5% (w/v) BSA 2.0 mg/ml Heparin (added just before use)	7.4 (adjusted with AcOH)
EB	50 mM Tris 150 mM NaCl 25 mM EDTA	7.4

Table 2.4: Lysis buffer used for preparation of crude extracts

Component	Concentration	pH
Tris-Cl	250 mM	8.0
NaCl	250 mM	
MgCl <sub>2</sub>	50 mM	
Lysozyme	50 mg/ml	
OTG	100 mg/ml	
Nuclease	100 U/ml	

Table 2.5: Buffer used for Homogenous Time Resolved Fluorescence

Buffer	Composition	pH
PBS-BSA 0.5%	137 mM NaCl 2.7 mM KCl 10 mM Na <sub>2</sub> HPO <sub>4</sub> 2 mM KH <sub>2</sub> PO <sub>4</sub> 0.5% (w/v) BSA	7.4
PBS-BSA 0.2%	137 mM NaCl 2.7 mM KCl 10 mM Na <sub>2</sub> HPO <sub>4</sub> 2 mM KH <sub>2</sub> PO <sub>4</sub> 0.2% (w/v) BSA	7.4

Table 2.6: Buffer used for crude extract ELISA

Buffer	Composition	pH
PBS	8 mM Na <sub>2</sub> HPO <sub>4</sub> ·(H <sub>2</sub> O) <sub>2</sub> 1.5 mM KH <sub>2</sub> PO <sub>4</sub> 3 mM KCl 137 mM NaCl	7.4
PBS-T	8 mM Na <sub>2</sub> HPO <sub>4</sub> ·(H <sub>2</sub> O) <sub>2</sub> 1.5 mM KH <sub>2</sub> PO <sub>4</sub> 3 mM KCl 137 mM NaCl 0.1% (v/v) Tween20	7.4
PBS-TB	8 mM Na <sub>2</sub> HPO <sub>4</sub> ·(H <sub>2</sub> O) <sub>2</sub> 1.5 mM KH <sub>2</sub> PO <sub>4</sub> 3 mM KCl 137 mM NaCl 0.1% (v/v) Tween20 0.2% (w/v) BSA	7.4
pNPP buffer	50 mM NaHCO <sub>3</sub> 50 mM MgCl <sub>2</sub> ·(H <sub>2</sub> O) <sub>6</sub>	
pNPP stock	1 M di-sodium 4-nitrophenyl phosphate	
pNPP solution	3 mM pNPP in pNPP buffer	

Table 2.7: Buffer used for cell lysis and protein purification

Buffer	Composition	pH
TBS	50 mM Tris-HCl 400 mM NaCl	7.4
TBS <sub>400</sub> , lysozyme	50 mM Tris-HCl 400 mM NaCl 1 mg/ml lysozyme	7.4
TBS adjusting buffer	50 mM Tris-HCl 400 mM NaCl 100 mM Imidazole 50% (v/v) Glycerol	7.4
TBS-W	50 mM Tris-HCl 400 mM NaCl 20 mM Imidazol 10% (v/v) Glycerol	7.4
TBS-E	50 mM Tris-HCl 400 mM NaCl 250 mM Imidazol 10% (v/v) Glycerol	7.4
TBS-W high salt	50 mM Tris-HCl 1 M NaCl 20 mM Imidazol	7.4
TBS-W low salt	50 mM Tris-HCl 50 mM NaCl 20 mM Imidazol	7.4
1 × PBS	8 mM Na <sub>2</sub> HPO <sub>4</sub> ·(H <sub>2</sub> O) <sub>2</sub> 1.5 mM KH <sub>2</sub> PO <sub>4</sub> 3 mM KCl 137 mM NaCl	7.4

Table 2.8: Buffers used for SDS-PAGE

Buffer	Composition	pH
4 × stacking buffer	0.5 M Tris 0.4% (w/v) SDS	6.8
4 × resolving buffer	1.5 M Tris 0.4% (w/v) SDS	8.8
Running buffer	25 mM Tris 192 mM Glycine 0.1% (w/v) SDS	8.3
5 × loading buffer	175 mM Tris-HCl 50% (v/v) Glycerol 10% (w/v) SDS 0.15% (w/v) bromophenol blue 5% (v/v) β-mercaptoethanol	6.8
Staining solution	0.1% (w/v) Coomassie Brilliant blue 10% (v/v) acetic acid 20% (v/v) ethanol	
Destaining solution	20% (v/v) ethanol 10% (v/v) acetic acid	

Table 2.9: Buffers used for qualitative ELISA

Buffer	Composition	pH
PBS	8 mM Na <sub>2</sub> HPO <sub>4</sub> ·(H <sub>2</sub> O) <sub>2</sub> 1.5 mM KH <sub>2</sub> PO <sub>4</sub> 3 mM KCl 137 mM NaCl	7.4
PBS-T	8 mM Na <sub>2</sub> HPO <sub>4</sub> ·(H <sub>2</sub> O) <sub>2</sub> 1.5 mM KH <sub>2</sub> PO <sub>4</sub> 3 mM KCl 137 mM NaCl 0.1% (v/v) Tween20	7.4
PBS-TB	8 mM Na <sub>2</sub> HPO <sub>4</sub> ·(H <sub>2</sub> O) <sub>2</sub> 1.5 mM KH <sub>2</sub> PO <sub>4</sub> 3 mM KCl 137 mM NaCl 0.1% (v/v) Tween20 0.2% (w/v) BSA	7.4
pNPP buffer	50 mM NaHCO <sub>3</sub> 50 mM MgCl <sub>2</sub> ·(H <sub>2</sub> O) <sub>6</sub>	
pNPP stock	1 M di-sodium 4-nitrophenyl phosphate	
pNPP solution	3 mM pNPP in pNPP buffer	

Table 2.10: Buffers used for FACS

Buffer	Composition	pH
FACS buffer	8 mM Na <sub>2</sub> HPO <sub>4</sub> ·(H <sub>2</sub> O) <sub>2</sub> 1.5 mM KH <sub>2</sub> PO <sub>4</sub> 3 mM KCl 137 mM NaCl 0.1% (w/v) BSA 0.1% (w/v) NaN <sub>3</sub>	7.4

Table 2.11: Buffers used for SPR

Buffer	Composition	pH
Running buffer	8 mM Na <sub>2</sub> HPO <sub>4</sub> ·(H <sub>2</sub> O) <sub>2</sub> 1.5 mM KH <sub>2</sub> PO <sub>4</sub> 3 mM KCl 137 mM NaCl 0.005% (v/v) Tween20	7.4
Regeneration buffer	1 M Glycine	2.0

## 2.1.2 Reagents for Ribosome Display selection

Table 2.12: Reagents used for selection

Reagent	Comment
<i>Saccharomyces cerevisiae</i> RNA (Fluka)	25 µg/µl in milliQ-H <sub>2</sub> O
Neutravidin (ThermoFisher)	1.2mg/ml (20 µM) in TBS
Streptavidin-coated MyOne T1 magnetic beads (Invitrogen)	20 µl
Biotinylated Target	

Table 2.13: Reagents used for clean up of mRNA after *in vitro* transcription

Reagent	Concentration
LiCl	6 M
NaOAc	3 M
EtOH	100% (v/v) 70% (v/v) in in milliQ-H <sub>2</sub> O
DNAseI (Roche)	10 U/µl

Table 2.14: Primer used for reverse transcription, PCR and cloning

Reagent	Sequence
Primer, 100 µM in milliQ-H <sub>2</sub> O (Microsynth)	
EWT5s	5'-TTCCTCCATGGGTATGAGAGGATCG-3'
WTC4	5'-TTTGGGAAGCTTTTGCAGGATTCAGC-3'
T7B	5'-ATACGAAATTAATACGACTCACTATAG GGAGACCACAACGG-3'
tolAk	5'-CCGCACACCAGTAAGGTGTGCGGTTT CAGTTGCCGCTTCTTTCT-3'

Table 2.15: Reagents used for reverse transcription, PCR and cloning

Reagent	Concentration
AffinityScrip™ Multiple Temp. Rev. Transcriptase (Stratagene)	50 U/mL
10 × AffinityScrip™ RT buffer (Agilent)	
DTT	100 mM
RNasin Ribonuclease Inhibitor (Promega)	40 U/μl
Vent DNA Polymerase (New England Biolabs)	2 U/μl
Platinum Taq DNA Polymerase (Invitrogen)	5 U/μl
dNTP (Eurogentec)	5 mM each
Nucleotide analog dPTP (Jena Biosciences)	100 μM
Nucleotide analog 8-oxo-dGTP (Jena Biosciences)	100 μM
DMSO	(Fluka)
Restriction endonuclease <i>Bam</i> HI (New England Biolabs, R3136)	20 U/μl
Restriction endonuclease <i>Hind</i> III (New England Biolabs, R3104)	20 U/μl
Restriction endonuclease <i>Nco</i> I (New England Biolabs, R0193)	10 U/μl
T4 DNA ligase (Fermentas)	5 U/μl

Table 2.16: Reagents used for *in vitro* transcription

Reagent	Concentration
T7 RNA polymerase (Fermentas)	20 U/μl
RNasin Ribonuclease Inhibitor (Promega)	40 U/μl
DTT	100 mM in milliQ-H <sub>2</sub> O
50 mM NTP mix (Sigma-Aldrich)	
	50 mM adenosine 5'-triphosphate
	50 mM uridine 5'-triphosphate
	50 mM guanosine 5'-triphosphate
	50 mM cytidine 5'-triphosphate
5 × homemade RNA polymerase buffer	
	1 M HEPES
	150 mM magnesium acetate
	10 mM spermidine
	200 mM DTT
	(pH 7.6)

Table 2.17: Reagents used for *in vitro* translation

Reagent	Concentration
Protein disulfide isomerase (Sigma-Aldrich)	22 $\mu$ M
Heparin (Sigma-Aldrich)	200 mg/ml, non-filtered
L-Methionine (Sigma-Aldrich)	200 mM, non-filtered
STOP mix	1 ml WBT buffer
	0.5% (w/v) BSA
	12.5 ml Heparin

S30 Extract and PremixZ were provided and prepared by Birgit Dreier according to B. Dreier and A. Plückthun, 2012 [157]

### 2.1.3 Plasmid Vectors

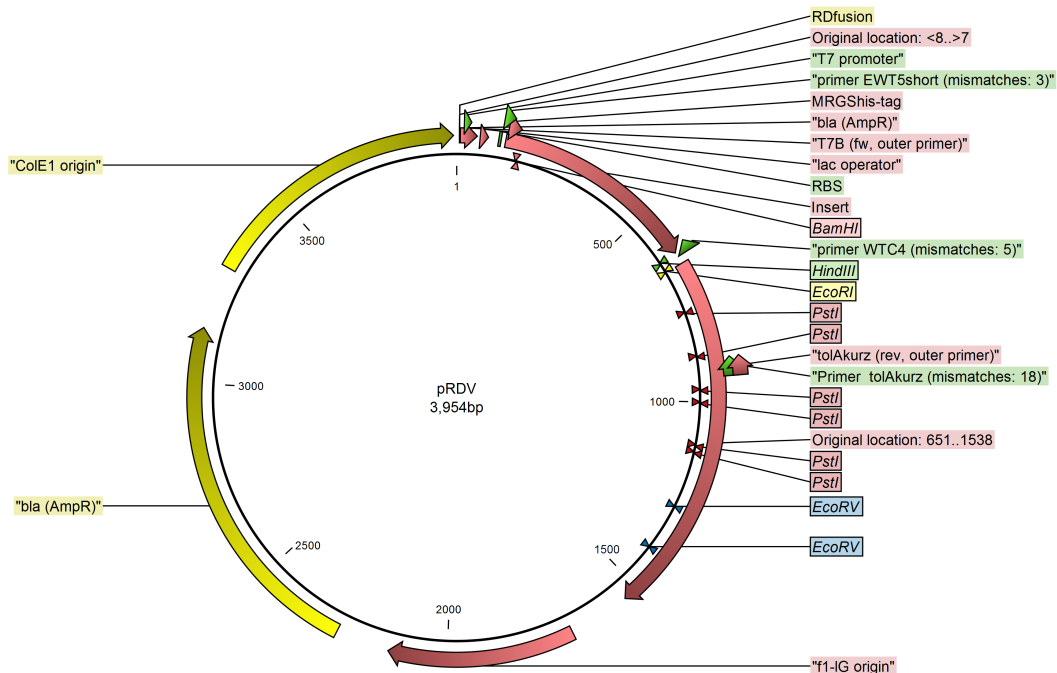


Figure 2.1: Vector pRDV used for Ribosome Display selection. Vector elements: This vector contains T7 promoter, ribosome binding site, 5' and 3' stem loop regions, annealing regions for the inner primer EWT5s, a spacer region from an unstructured region from the *E. coli* protein tolA, FLAG Tag and a gene coding for  $\beta$ -lactamase.

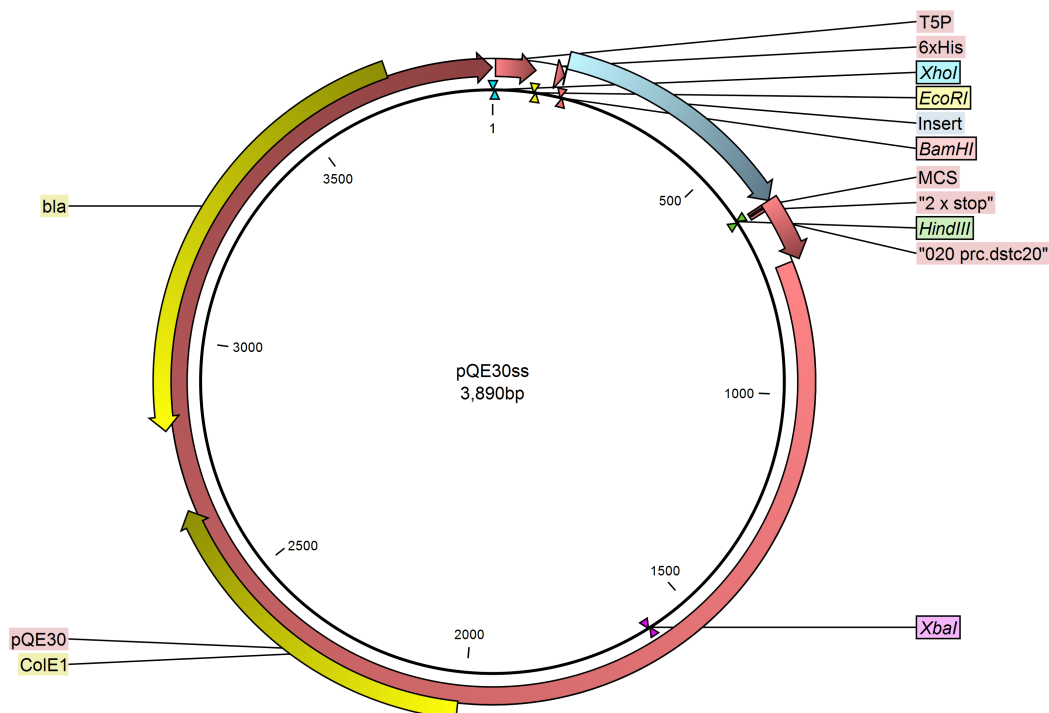


Figure 2.2: Vector pQE30ss used for expression of DARPins in *E.coli* XL1blue. Vector elements: This vector contains ColE1 origin of replication, bacteriophage T5 promoter, ribosome binding site RBSII, N-terminal MRGS(His)<sub>6</sub>, 2 × C-terminal stop codon, two transcriptional terminators  $t_0$  and T1, Amp<sup>R</sup> gene and  $\beta$ -lactamase coding sequence for selection.

## 2.1.4 Strains

Table 2.18: Strains

Strain	Genotype
<i>Escherichia coli</i> XL1blue, (Stratagene)	<i>recA1 endA1 gyrA96 thi-1 hsdR17 supE44</i> <i>relA1 lac [F' proAB lacI<sup>q</sup> Z<math>\Delta</math>M15 Tn10 (Tet<sup>r</sup>)]</i>

## 2.1.5 Media

All media were prepared using ddH<sub>2</sub>O and sterilised using autoclave at 121 °C, 103 kPa for 60 min. Media indicated as '+Amp' in Chapter 2.2 contain 100  $\mu$ g/ml Ampicillin, sterile filtered through 0.22  $\mu$ m pore membrane and added after sterilisation of medium.

Table 2.19: Media

Media	Component	Quantity
LB (Luria Broth)	Tryptone	10 g/l
	Yeast Extract	5 g/l
	NaCl	10 g/l
LB Agar	Tryptone	10 g/l
	Yeast Extract	5 g/l
	NaCl	10 g/l
	Agarose	15 g/l
2 × TY	Tryptone	16 g/l
	Yeast Extract	10 g/l
	NaCl	5 g/l
TB	Tryptone	11.8 g/l
	Yeast extract	23.6 g/l
	Glycerol 100%	0.4% (v/v)
TB salt	K <sub>2</sub> HPO <sub>4</sub>	9.4
	KH <sub>2</sub> PO <sub>4</sub>	2.2
Induction medium	TB/10% TB salt	2.85 ml
	1 M IPTG	150 µl (0.5 mM final)
	100 mg/ml ampicillin	3 µl (100 µg/ml final)

## 2.1.6 DNA and Protein Standards

Table 2.20: DNA and Protein Marker

Marker	Size range
SmartLadder (Eurogentec)	200-10'000 bp
SmartLadderSF (Eurogentec)	100-1'000 bp
PageRuler Prestained Protein Ladder (ThermoScientific)	10-170 kDa

Table 2.21: Molecular weight standard for SEC

Component	Mol. weight
Cytochrome c from horse heart, (Sigma-Aldrich, Cat. Nr. C7150, 10 mg/vial)	12.4 kDa
Carbonic Anhydrase from bovine erythrocytes, (Sigma-Aldrich, Cat. Nr. C7025, 15 mg/vial)	29 kDa
Albumin, bovine serum, (Sigma-Aldrich, Cat. Nr. A8631, 50 mg/vial) (contains 0.3% dithiothreitol)	66 kDa
$\beta$ -Amylase from sweet potato, (Sigma-Aldrich, Cat. Nr. A8781, 15 mg/vial) (contains 15% NaCl, 4% glucose, 1% dithiothreitol)	200 kDa

### 2.1.7 Antibodies

Table 2.22: Antibodies

Antibody	Source	Company	Use
anti RGS(His)4 IgG1	Mouse	Qiagen, No. 34650	1 <sup>st</sup> antibody for ELISA
anti-mouse IgG, AP conjugate	Goat	Sigma, No. A3562	2 <sup>nd</sup> antibody for ELISA
anti (His)5 IgG1, Alexa Fluor 488 conjugate	Mouse	Qiagen, No. 35310	FACS

### 2.1.8 Cell lines

Table 2.23: Cell lines

Cell line	Species	Company
Flp-In <sup>TM</sup> -CHO	Hamster	Thermofisher, R75807

## 2.1.9 Chemicals

Table 2.24: Chemicals

Chemical	Grade
HEPES (4-(2-Hydroxyethyl)-1-piperazineethanesulfonic acid), Applichem	
Acetic acid, Fluka	≥ 99.9%
Acetonitrile, Scharlau	≥ 99.9%
Agarose, Eurogentec	
Ammonium peroxosulfate (APS), Merck	≥ 98%
Bacto™ Tryptone, Becton Dickinson	
Bacto™ Yeast Extract, Becton Dickinson	
Bromophenol blue, Merck	
Calcium chloride dihydrate (CaCl <sub>2</sub> ·(H <sub>2</sub> O) <sub>2</sub> ), Fluka	≥ 99.5%
Coomassie Brilliant Blue R-250	
Dimethylsulfoxide (DMSO), Merck	
Dithiothreitol (DTT), Promega	
Ethanol (EtOH), Fluka	≥ 99.8%
Ethidium bromide (EtBr), Sigma	
Ethylenediaminetetraacetic acid (EDTA), Fluka	≥ 99%
D(+)-Glucose monohydrate, Merck	
Glycerol, Sigma	≥ 99%
Glycine, Eurobio	
Hydrochloric acid (HCl) 32% (v/v), Riedel-de Haën	
Imidazole, Sigma	≥ 99.8%
Isopropyl-β-D-1-thiogalactopyranoside (IPTG), Biosolve	≥ 99%
Lysozyme, Merck	
Magnesium chloride hexahydrate (MgCl <sub>2</sub> ·(H <sub>2</sub> O) <sub>6</sub> ), Fluka	≥ 99%
Magnesium sulfate heptahydrate (MgSO <sub>4</sub> ·(H <sub>2</sub> O) <sub>7</sub> ), Sigma	≥ 99.5%
Methanol (MeOH), Fluka	≥ 99%
N,N,N',N'-Tetramethylethylenediamine (TEMED), Sigma	≥ 99%
Non-fat milk powder, Migros	
p-Nitrophenyl phosphate di-sodium salt hexahydrate (pNPP), Fluka	
Potassium chloride (KCl), Fluka	≥ 99.5%
Potassium dihydrogen phosphate dihydrate (KH <sub>2</sub> PO <sub>4</sub> ·(H <sub>2</sub> O) <sub>2</sub> ), Fluka	≥ 99.5%
Potassium hydroxide (KOH), Sigma	
Select Agar, Invitrogen	
Sodium azide (NaN <sub>3</sub> ), Sigma	
Sodium chloride (NaCl), Fluka	≥ 99.5%
Sodium dodecyl sulfate (SDS), Sigma	≥ 99%
Sodium hydrogen carbonate (NaHCO <sub>3</sub> ), Merck	≥ 99.5%
Sodium hydroxide (NaOH), Fluka	≥ 97%
Sodium phosphate Dibasic (HNa <sub>2</sub> PO <sub>4</sub> ), Fluka	≥ 97%
2-Amino-2-hydroxymethyl-propane-1,3-diol (Tris), Serva	
Tween20, Fluka	
β-Mercaptoethanol, Sigma	

## 2.1.10 Instruments

Table 2.25: Instruments

Instrument	Company
AG104 Precision Balance	MettlerToledo
Äkta Micro Chromatography System	GE Healthcare
Argon Gas	PanGas
Basic 96 Gradient TProfessional Thermocycler	Biometra
Binder –80 °C Freezer	Binder
DI-25 Basic Dispenser	Yellowline
ELX 405 Select CW Plate Washer	BioTek
Fiberlite F13-14x50 Rotor	Thermo Scientific Sorvall
GENE GENIUS Bio Imaging System	Syngene
HTS 7000 Plus Bio Assay Reader	Perkin Elmer
ISF-1-W KuehnerShaker	Kuehner Switzerland
KingFisher™ Flex Purification System	Thermo Fischer Scientific Inc.
LabTherm 37 °C constant shaker	Kuehner Switzerland
LabTherm LT-X shaker	Kuehner Switzerland
Laminar Flow Bench	Gelaire
Liebherr ProfiLine Fridge, 4 °C	Liebherr
Liebherr ProfiLine Freezer, –20 °C	Liebherr
Liquidator 96-200	Rainin
Megafuge 1.0R	Hereaus
MicroFlo Select Dispenser MFS	BioTek
Microwave	Intertronic
Mini-PROTEAN Tetra Handcast System	Bio-Rad
MiniDAWN™ Treos	Wyatt Technologies
Model 102c Sonifier	Branson
NanoDrop ND-1000 Spectrophotometer	Thermo Fischer Scientific Inc.
Novaspec III – Visible Spectrometer	Amersham Biosciences
Optilab rEX™	Wyatt Technologies
ELGA OptionR-15 Water Purification	VWS GmbH
pH720 WtW-Series pH-meter	inoLab
PM4000 Balance	MettlerToledo
ProteOn XPR36	Bio-Rad Laboratories
Sonifier 250	Branson
Sorvall Evolution RC Centrifuge	Thermo Scientific Sorvall
Sorvall Instruments GS-3 Rotor	Thermo Scientific Sorvall
Sorvall RC-50 Plus Centrifuge	Thermo Scientific Sorvall
Tabletop Centrifuge 5430	Eppendorf
Thermomixer Comfort	Eppendorf
TiMix Control TH15 Plate Mixer	Edmund Buehler
UV-Vis Spectrometer, No. 8453	Agilent
UV Transilluminator	MWG-Biotech UVP
Vac-Man Laboratory Vaccum Manifold	Promega
Varioklav 25 T Steam Sterilizer	HP Labortechnik AG
Varioklav 135 S Steam Sterilizer	HP Labortechnik AG

## 2.1.11 Devices

Table 2.26: Kits

Kit	Company
QIAquick® Miniprep-Kit	Qiagen
QIAquick® Gel-Extraction-Kit	Qiagen
PureYield Plasmid Midiprep System	Promega

Table 2.27: Filter

Filter	Company
MF-Millipore 47mm 0.22 µm membrane filter	Millipore
Stericup-GP Filter Units 0.22 µm, PES	Millipore
Filtropur syringe filters sterile 0.20 µm, PES	Sarstedt AG

Table 2.28: Columns

Column	Company
Superdex 200 Increase 5/150 GL, (V = 3.004 ml, No. 28990945)	GE Healthcare
Superdex 200 10/300 GL, (V = 24 ml, No. 17517501)	GE Healthcare

Table 2.29: SPR Chips

Chip	Company	Chip-ID
ProteOn NLC Sensor Chip	Bio-Rad	NLCJ5F30KO1
ProteOn NLC Sensor Chip	Bio-Rad	NLCJ5F31IO1
ProteOn NLC Sensor Chip	Bio-Rad	NLCJ5F20KO1

Table 2.30: Devices for buffer exchange

Device	Company
Slide-A-Lyzer Mini Dialysis Device 0.5 ml	Thermo Fischer Scientific Inc.
PD-10 Desalting Column, (Sephadex™ G-25 Medium, 8.3 ml)	GE Healthcare

Table 2.31: Other devices

Device	Company
1.5 ml Microtubes, FTTP	Trefflab
15 ml sterile Polypropylene Round-Bottom Tubes	BD-Falcon
15 ml sterile PP Tubes	Sarstedt
Centrifuge Bottles 500 ml	Nalgene
Combitips Plus 0.01 ml	Eppendorf
Combitips Plus 0.2 ml	Eppendorf
Combitips Plus 1 ml	Eppendorf
Combitips Plus 5 ml	Eppendorf
Multiply- $\mu$ Strip Pro 8-Strip PCR Tubes	Sarstedt
Ni-NTA Superflow	Qiagen
Nunc Immunoplate F96 MaxiSorp	Thermo Fischer Scientific Inc.
Parafilm	Sigma-Aldrich
Petri Dish 92x16 mm	Sarstedt
Sterile Pipette Tip 2 ml	Greiner bio-one
Sterile Pipette Tip 5 ml	Greiner bio-one
Sterile Pipette Tip 15 ml	Greiner bio-one
Sterile Pipette Tip 25 ml	Greiner bio-one
Sterile Pipette Tip 50 ml	Greiner bio-one

## 2.2 Methods

### 2.2.1 Methods in Molecular Biology

#### Preparation of competent cells

The preparation of competent cells was essentially performed according to H. Inoue et al., 1990 [158].

A single clone of *E. coli* XL1 Blue was inoculated in 15 ml  $2 \times$  YT medium for overnight culture. The next morning 12.5 ml of overnight culture was transferred into 250 ml of  $2 \times$  YT medium and grown at 25 °C until an OD<sub>600</sub> of 0.6 to 0.7 was reached. The cells were chilled on ice immediately for 15 min and harvested at  $3000 \times g$  for 10 min at 4 °C, by using a Sorvall Evolution RC centrifuge (Thermo Scientific Sorvall). The resulting cell pellet was resuspended in 80 ml ice cold TB buffer and chilled on ice for 10 min. The cells were again centrifuged at  $3000 \times g$  for 10 min at 4 °C, resuspended in 20 ml ice cold TB buffer and 1.5 ml of 100% (v/v) DMSO added. The cells were chilled on ice for 10 min, dispensed into sterile Eppendorf tubes in 100  $\mu$ l aliquots and flash frozen in liquid nitrogen. The frozen cells were stored at -80 °C until use.

The transfection efficiency was tested using a dilution series of 1.0 ng, 0.1 ng, 0.01 ng and 0.001 ng of pQE30ss-off7 plasmid DNA. The dilutions of plasmid DNA were mixed with 100  $\mu$ l of competent cells and chilled on ice for 30 min. A heat shock was performed at 42 °C for 45 sec, the cells gently resuspended in 900  $\mu$ l of  $2 \times$  YT medium and grown under shaking at 37 °C for 1 h. Subsequently, the cells were plated on 1.5% (w/v) agar LB plates, containing 1% (w/v) glucose and 100  $\mu$ g/ml ampicillin, and incubated overnight at 37 °C. The next morning the number of colonies was counted on each plate and the transformation efficiency determined to  $2.4 \times 10^7$  cfu/ $\mu$ g DNA.

### DNA digestion using restriction endonucleases

For DNA digestion restriction sites of *Bam*HI and *Hind*III were used. These sites allowed isolation of the nucleotide sequence encoding for DARPin only, without additional histidine tag. For restriction reaction a mix as described in Table 2.32 was prepared. Subsequently the mix was incubated at 37 °C for one hour and the resulting fragment of interest isolated and purified using gel-electrophoresis and purification according to quick start protocol QIAquick Gel extraction kit (No 28704, July 2015). Restriction digest and purification of vector pRDV was performed in identical procedure as of vector pQE30ss containing clones of interest.

Table 2.32: Restriction reaction mix using *Bam*HI and *Hind*III

Component	Volume
<i>Bam</i> HI	1 µl (20 U)
<i>Hind</i> III	1 µl (20 U)
10 × CutSmart reaction buffer	6 µl
Purified Vector including clone	12 µg
Add to 60 µl using milliQH <sub>2</sub> O	

### Ligation and transformation

For ligation of the clone fragments into digested vector, vectors were mixed in approximate equimolar amount and a reaction mix prepared according to Table 2.44. The mix was subsequently incubated at room temperature for one hour. As negative control a reaction mix without insert was prepared and as well incubated at room temperature for one hour.

Table 2.33: Ligation reaction mix of clones and pRDV

Component	Volume
Vector	0.2 µg
Insert	0.8 µg
10 × T4 ligase reaction buffer	2 µl
T4 DNA ligase	0.5 µl (2.5 U)
Add to 20 µl using milliQH <sub>2</sub> O	

Subsequently 20 µl of ligation reaction mix according to Table 2.44 was mixed with 100 µl of competent *E. coli* cells by gently resuspending and chilled on ice for 20 min. Heat shock was subsequently performed at 42 °C for 45 sec. The cells were gently resuspended in pre-chilled 500 µl 2 × YT-medium and incubated on shaker at 37 °C for 0.5 h. After initial incubation 150 µl of culture were plated on LB+Amp plates and incubated at 37 °C overnight.

Three colonies were picked and incubated in 5 ml LB+Amp each at 37 °C on shaker overnight. In addition the picked clones were transferred on a new Agar-plate (LB+Amp) and incubated at 37 °C, overnight as well. After incubation the cells were harvested at 4000 × g, 5 min, 4 °C. The isolation and purification of plasmids were then performed according to the protocol of Qiagen Plasmid Mini-Prep. After purification, the derived

plasmid concentration was measured for each sample using nanodrop. The derived plasmids were analyzed for positive ligations and transformation of vector and insert by enzyme restriction enzymes using *HindIII* and *BamHI*. The reaction mix was prepared as stated in Table 2.32 and incubated at 37 °C for one hour in an incubator. Subsequently, the derived fragments analyzed using gelelectrophoresis and sent for Sanger sequencing.

### Introduction of additional diversity

The introduction of additional diversity in the amino acid sequence of parental clones was performed by introduction of random mutations. Using dNTP analogues dPTP and 8-oxo-dGTP. For that purpose error prone PCR was performed with different mutational loads using different concentrations of the dNTP analogues. (3  $\mu$ M and 9  $\mu$ M of dNTP analogues) (see Table 2.34). To avoid unspecific amplification a hot start was performed at the beginning of the PCR reaction, using thermocycler MWG Biotech Inc. Primus 25. The cycling parameters were applied as stated in Table 2.35.

Table 2.34: epPCR reaction mix

Component	Concentration
pRDV-DARPin template	55 nM
dNTP mix	250 $\mu$ M
8-oxo-dGTP	3 $\mu$ M or 9 $\mu$ M
dPTP	3 $\mu$ M or $\mu$ M
T7B fwd primer	1 $\mu$ M
tolAk rev primer	1 $\mu$ M
10 $\times$ polymerase buffer	1 $\times$
MgCl <sub>2</sub>	1.5 mM
Platinum Taq DNA polymerase	2 U
Add to 50 $\mu$ l using milliQH <sub>2</sub> O	

Table 2.35: Cycling parameters of epPCR of selected clones in pRDV

Cycle number	Denaturation	Annealing	Polymerisation
1	3 min at 95 °C		
2 - 26	30 s at 95 °C	30 s at 55 °C	1 min at 72 °C
27			5 min at 72 °C
Store at 8 °C			

For analysis of PCR product 5  $\mu$ L of reaction product was mixed with 1  $\mu$ L 6  $\times$  loading buffer and the fragments separated using gel-electrophoresis. The resulting fragment pattern was visualized using EtBr and UVP UV Transiluminator. The visualised bands were subsequently quantified using ImageJ Software.

## 2.2.2 Ribosome Display selection

In order to improve the affinity of in this work characterised DARPins binding to non-dominant epitope regions of human ROR1 a fifth and sixth round of ribosome display

selection using off-rate selection, followed by an additional round of selection with low stringency. This experiment mainly performed according to Ribosome Display Protocol, B. Dreier and A. Plückthun, 2012 [157]. For that purpose DARPinS characterised from round 3 and 4 of previous selections were either grouped in pools, if they shared a high sequence similarity and/or the same epitope region, or a single clone was used for the introduction of diversity. This strategy should avoid a bias in the process of the affinity maturation selection. Therefore, the DARPinS B7w and D7w as well as G3w, A3w and A2b were pooled together due to similarity in sequence and epitope regions, resulting in six pools that ran through selection individually (Table 2.36). In case of the first and the fifth pool DARPinS, evolved from the respective clones, were pooled in equimolar amounts, estimated by densitometry analysis using ImageJ software analysis of band intensities derived from gel-electrophoresis of the respective PCR products.

Table 2.36: Pools for off-rate selection with respective parental clones.

Pool 1	Pool 2	Pool 3	Pool 4	Pool 5	Pool 6	Pool 7
G3w	E5w	A11b	C2w	B7w	F4w*	D1w
A3w				D7w		
A2b						

\*The DNA sequence of parental clone F4 and putative decendants was not retrievable after the selections.

The derived PCR fragments were subsequently *in vitro* transcribed. For the reaction a mix according to Table 2.37 was prepared and PCR products added according to pools as stated in Table 2.36. The mix was then incubated for three hours at 37 °C.

Table 2.37: Reaction mix for *in vitro* transcription of PCR products

Component	Amount
5 × T7 polymerase buffer	20.0 µl
NTPs (final concentration 7 mM each)	14.0 µl
T7 RNA polymerase	4.0 µl (80 U)
RNasin	2.0 µl
PCR product	22.5 µl
Add to 100 µl using milliQ-H <sub>2</sub> O	

In order to remove all impurities from the reaction the obtained RNA was purified using gel filtration. All samples were pretreated by DNaseI adding 2 µl of DNaseI solution (2 U final) and 5 µl of 10 × dilution buffer (1 × final) to 43.0 µl transcription reaction and incubated at room temperature for 15 min. Illustra MicroSpin G-50 columns were re-suspended by vortexing, the bottom of the cap broke open, placed into a 1.5 ml collection tube and the material packed by centrifugation at 735 × g for one minute. The gel filtration tube was transferred into a fresh collection tube, 50 µl from the transcription reaction applied and again centrifuged at 735 × g for one minute. Aliquots of purified RNA were immediately flash frozen in liquid nitrogen and stored at −80 °C. The concentration of purified RNA was determined by OD<sub>260 nm</sub> of a 1:100 dilution.

For *in vitro* translation a reaction mix as shown in Table 2.38 was set up. During preparation of the mix all components and reagents were constantly chilled on ice.

Table 2.38: Reaction mix for *in vitro* translation of RNA products

Component	Amount/Volume
Methionine (200 mM)	2.0 $\mu$ l
PremixZ	41.0 $\mu$ l
<i>In vitro</i> -transcribed RNA	10 $\mu$ g total
S30 extract	50.0 $\mu$ l
Add to 110 $\mu$ l using milliQ-H <sub>2</sub> O	

The reaction mix was carefully pipetted up and down to mix and incubated at 37 °C for 10 min. After incubation the reaction was stopped by addition of 440  $\mu$ l ice cold stop mix and gentle pipetting up and down to mix. The stopped reaction was centrifuged at 20,000  $\times$  g, 4 °C for 5 minutes. Subsequently 500  $\mu$ l of supernatant were transferred into a fresh tube and chilled on ice.

### Selection

The selection was performed using the Kingfisher Flex Purification System. The selection steps of the different independent pools were performed in parallel. All wells used during the selection steps, except of wells containing WBT, were previously blocked using BSA and the whole procedure performed at 4 °C.

To remove ribosomal complexes that bound unspecifically a preselection on BSA blocked magnetic beads was performed, calling this initial step 'prepanning'. In course of this step translated DARPIn-ribosome complexes were transferred into BSA blocked 96 well plate. Twenty microl of magnetic beads were resuspended and washed in 750  $\mu$ l TBS, and blocked with BSA for 3 h and 35 min. Subsequently, the beads were washed with 1000  $\mu$ l WBT for 2 h 35 min. The streptavidin coated magnetic beads, provided for the panning step, were blocked in 750  $\mu$ l TBS-B for 3 h 35 min and subsequently collected and washed for 2 h 35 min in 1000  $\mu$ l WBT. Blocked magnetic beads without target were incubated with 500  $\mu$ l of ribosome complexes for 35 min as pre-panning step. the blocked magnetic beads were collected by a magnet and discarded. Magnetic beads with immobilised target at a concentration of 100 pM for the fifth round and of 50 nM for the sixth round respectively (Table 2.39) were transferred into the tubes containing supernatant and were incubated with prepanned ribosomal complexes for 32 min as the panning step. In case of round 5 a subsequently 10<sup>4</sup>-fold excess of unbiotinylated target was added to the solution as competitor for off-rate selection according to table 2.39 and incubated for 2 h 3 min, capturing ribosome complexes that dissociated from biotinylated target. For of both selection rounds the beads including target and bound DARPins were subsequently washed 3 times with 1000  $\mu$ l WBT for 10 min, followed by a washing step in 1000  $\mu$ l WBT for 20 min and a washing step in 1000  $\mu$ l WBT for 30 min. Ribosome complexes were finally eluted from target-coated magnetic beads in 150  $\mu$ l EB including *S. cerevisiae* RNA (50  $\mu$ g/ml final) for 15 min. The magnetic beads were subsequently collected and discarded. The solution was transferred into 400  $\mu$ l lysis buffer. The mix was briefly vortexed and stored on ice.

Table 2.39: Summary of differences in selection conditions performed in round 5 and 6 of ribosome display selection. NA: Not Applied

Selection round	Biot. target	Panning	Unbiot. target	Off-rate competition
5	0.1 nM	32 min	1000 nM	123 min
6	50 nM	32 min	NA	NA

*RNA purification*

For recovery of eluted RNA the lysis buffer - eluate mixture was applied on a column from High Pure RNA isolation kit and centrifuged at  $8,000 \times g$  for 1 min. The flow through was discarded and 100  $\mu$ l of diluted DNaseI (1.8 U/ $\mu$ l) added onto the column filter in order to avoid amplification of non-selected DNA templates. The mix was incubated for 15 min at room temperature and subsequently washed with 500  $\mu$ l wash buffer 1, using centrifugation at  $8,000 \times g$  for 1 min. The flow through was again discarded. The washing step was repeated with wash buffer 2 and the flow through again discarded. Hundred  $\mu$ l of wash buffer 2 was added, the column centrifuged at  $13,000 \times g$  for 2 min to remove residual EtOH. Fifty  $\mu$ l elution buffer was then added to the filter and the column incubated for 2 min before centrifugation at  $8,000 \times g$  for 1 min and the flow through collected in a fresh 1.5 ml RNase-free tube. The eluted RNA solutions were aliquoted, immediately flash frozen in liquid nitrogen and stored at  $-80^\circ\text{C}$ .

*RT-PCR*

For reverse transcription of DARPin-encoding mRNA 12.5  $\mu$ l of eluted RNA was transferred into a fresh 1.5 ml RNase-free tube, denatured at  $70^\circ\text{C}$  for 10 min and subsequently chilled on ice. A reaction mix as presented in Table 2.40 was prepared under constant cooling on ice and 7.75  $\mu$ l of mix added to 12.25  $\mu$ l denatured RNA. The mix was incubated at  $50^\circ\text{C}$  for 1 h. Subsequently, 5  $\mu$ l was aliquoted for further use as template for PCR using the inner primer WTC4 and EWT5s and chilled on ice. The rest of transcribed cDNA was frozen in liquid nitrogen and stored at  $-20^\circ\text{C}$ .

Table 2.40: Reaction mix for transcription of DARPin-encoding RNA

Component	Amount
WTC4 primer	0.25 $\mu$ l (1.25 $\mu$ M final)
dNTPs	0.5 $\mu$ l (125 $\mu$ M final each)
RNasin	0.5 $\mu$ l (20 U total)
AffinityScript <sup>TM</sup>	
Multiple Temperature Reverse Transcriptase	0.5 $\mu$ l (25 U total)
10 $\times$ AffinityScript buffer	2.0 $\mu$ l
DTT	2.0 $\mu$ l (10 mM final)
milliQ-H <sub>2</sub> O	2.0 $\mu$ l

Next the cDNA was amplified using PCR according to Table 2.41. As negative control the same reaction mix was prepared and the template cDNA substituted with milliQH<sub>2</sub>O in order to test for unspecific amplification during the reaction. For PCR reaction the PCR tubes containing reaction mix were transferred into a thermocycler. To further avoid

unspecific amplification a hot start was performed at the beginning of the PCR reaction. The cycling parameters were applied as stated in table 2.42.

Table 2.41: Reaction mix for amplification of cDNA coding for selected DARPins

Component	Amount/Volume
cDNA	5.0 $\mu$ l
5 $\times$ Herculase II reaction buffer	10.0 $\mu$ l
dNTPs	2.0 $\mu$ l (200 $\mu$ M each)
DMSO	2.5 $\mu$ l (5% final)
WTC4 primer	0.5 $\mu$ l (1 $\mu$ M final)
EWT5s primer	0.5 $\mu$ l (1 $\mu$ M final)
Herculase II fusion DNA polymerase	0.5 $\mu$ l
Add to 50.0 $\mu$ l using milliQ-H <sub>2</sub> O	

Table 2.42: Cycling parameters for amplification of cDNA coding for selected DARPins

Cycle number	Denaturation	Annealing	Polymerisation
1	3 min at 95 °C		
2 - 41	30 s at 95 °C	30 s at 55 °C	1 min at 72 °C
42	5 min at 72 °C		
Store at 8 °C			

For analysis of the PCR products 5  $\mu$ L of reaction product was mixed with 1  $\mu$ l 6  $\times$  loading buffer and the fragments separated using gel-electrophoresis. The resulting fragment pattern was visualized using EtBr and UVP UV Transiluminator. Subsequently, 45  $\mu$ l of PCR product was purified using gel-electrophoresis and purification according to quick start protocol QIAquick Gel extraction kit (No 28704, July.2015). The purified DNA fragments were finally stored at  $-20$  °C until subclonng either into pRDV or pQE30ss.

#### *Subcloning into pRDV*

In order to prepare new template containing all necessary elements for the next round of selectino, the purified PCR products were digested with restriction endonucleases according to Table 2.43. The reaction was incubated at 37 °C for one hour and the resulting fragment of interest. Restriction digest and purification of vector pRDV was performed in an identical procedure as of PCR products containing selected clones (Table 2.2.1).

Table 2.43: Restriction reaction mix using *Bam*HI and *Hind*III

Component	Volume
<i>Bam</i> HI	1 $\mu$ l (20 U)
<i>Hind</i> III	1 $\mu$ l (20 U)
10 $\times$ CutSmart reaction buffer	6 $\mu$ l
Purified PCR product	40 $\mu$ l
Add to 60 $\mu$ l using milliQH <sub>2</sub> O	

For ligation of the DNA fragments encoding for DARPin sequence into digested vector pRDV, insert and vector were mixed in approximate equimolar amount and a reaction mix prepared according to Table 2.44. As negative control a reaction mix without insert was prepared. The reactions were incubated at room temperature for one hour.

Table 2.44: Ligation reaction mix of clones and pRDV

Component	Volume
pRDV	1 $\mu$ l
Insert	4 $\mu$ l
10 $\times$ T4 ligase reaction buffer	2 $\mu$ l
T4 DNA ligase	0.5 $\mu$ l (2.5 U)
Add to 20 $\mu$ l using milliQH <sub>2</sub> O	

After the sixth round of ribosome display selection the evolved DARPins were sub-cloned into the expression vector pQE30ss according to section 2.2.1 and 2.2.1.

## 2.2.3 Microbiology

### Preparation of cryostocks

A single clone was picked from an agar plate, inoculated in 5 ml 2  $\times$  YT + Amp medium and incubated overnight under constant shaking at 37 °C. The next day, 500  $\mu$ l of cell culture were transferred into 500  $\mu$ l of 50% (w/v) glycerol in a cryo vial or well of a 96-well plate. Subsequently, the cells were frozen in liquid nitrogen and stored at -80 °C.

### Preparation of crude extract

Cells were picked from cryostocks and transferred into each 1 ml LB/Glu<sub>1</sub>%/Amp provided in 96 well plates, sealed with a breathable seal and incubated O/N at 37 °C, 330 rpm in the Edmund Bühler Shaker. The following day 10  $\mu$ l of each overnight culture was transferred into fresh 90  $\mu$ l medium and incubated for 1 h at 37 °C, 330 rpm in Edmund Bühler shaker. Subsequently the expression was induced by addition of 10  $\mu$ l LB/Glu<sub>1</sub>%/Amp + IPTG 5 mM (0.5 mM final). The cultures were incubated for further 4 h at 37 °C, 330 rpm in Edmund Bühler shaker.

After incubation the cells were lysed by addition of 13  $\mu$ l lysis buffer (Table 2.4) per well. The plates were incubated for 2 minutes on an orbital shaker at 900 rpm and subsequently incubated at RT for 1 h for further lysis without shaking. Finally the plates were sealed with an aluminum seal and stored at -20 °C until performance of HTRF or ELISA.

## 2.2.4 Methods in Biochemistry

### Homogenous Time Resolved Fluorescence

The screening of clones using homogenous time resolved fluorescence was performed according to the HTRF protocol, version CE-screen 1.1 (2014-04-02), Sub-protocol 1, HTBS-Facility, Dept. of Biochemistry, University of Zurich.

For screening of promising binders after ribosome display selection incubation of crude extract of *E. coli* expressing DARPins (FLAG-tagged) in a 10<sup>-3</sup> dilution with 8 nM biotinylated target hROR1 ECD was performed. The binding was detected using anti-FLAG-d2 (HTRF acceptor) antibody and Streptavidin-Terbium cryptate (HTRF donor).

For blocking of the plates 20  $\mu\text{l}$  of blocking buffer was added to each well of the 384 well plate and incubated for 1 h at room temperature (RT). The crude extracts on 96 well plates were thawed at room temperature for approximately 1.5 h. Subsequently the blocking buffer in the plate was discarded over a sink and beaten dry on a stack of paper towels. The plate was then washed twice with 20  $\mu\text{l}$  PBS/BSA 0.2% for each well and dried at room temperature. The thawed crude extracts were diluted to 1:250 in PBS/BSA 0.2% in a series of steps and the reagent working stocks diluted at two times the final concentration in PBS/BSA 0.2%. Both were subsequently stored on ice. The reaction components were added in the order of 5  $\mu\text{l}$  target, 5  $\mu\text{l}$  pre-diluted crude extract and 10  $\mu\text{l}$  reagent working stock to each well. The plate was sealed with aluminium seal and incubated for 2 h at room temperature on a Heidolph Titramax 1000 shaker at 750 rpm. The seal was removed and the plate measured at parameters as listed in table 2.45.

Table 2.45: Measuring parameters of HTRF

Excitation filter	UV2 (TRF) 340
1st Emission filter (Channel 1)	APC 665
2nd Emission filter (Channel 2)	Cy5 620
Measurement height	11 mm
Time between flashes	2000 $\mu\text{s}$
Number of flashes	150

## ELISA

### *Crude extract ELISA*

For coating of each well of a MaxiSorb 384 well plate with Neutravidin 20  $\mu\text{l}$  of 66 nM Neutravidin in  $1 \times$  PBS, pH 7.4 was transferred into each well using a microflow dispenser. Subsequently, the plates were sealed and incubated overnight at 4  $^{\circ}\text{C}$ . The next day residual Neutravidin was discarded and the plates beaten dry on a stack of paper towels. The wells were blocked by addition of 45  $\mu\text{l}$  PBS<sub>T</sub>/BSA 0.5% per well, sealed and incubated for 1 h at room temperature under constant shaking at 900 rpm. Each well was washed three times with 120  $\mu\text{l}$  PBS<sub>T</sub>, pH 7.4 using a plate washer and target immobilised by addition of 20  $\mu\text{l}$  of 100 nM biotinylated hROR1 in PBS<sub>T</sub>/BSA 0.1%, pH 7.4 per well using a dispenser. Subsequently the plates were sealed and incubated at room temperature for 1 h at 900 rpm. After 1 h each well was washed three times with 120  $\mu\text{l}$  PBS<sub>T</sub>, pH 7.4 using a plate washer and DARPin added by addition of 20  $\mu\text{l}$  of a  $1:5 \cdot 10^3$  dilution of DARPins in crude extract (diluted in PBS<sub>T</sub>/BSA 0.1%, pH 7.4) using a liquidator. For binding reaction the plates were again sealed and incubated at room temperature for 1 h under constant orbital shaking at 900 rpm. Subsequently the wells were washed three times with 120  $\mu\text{l}$  PBS<sub>T</sub>, pH 7.4 using a plate washer and the primary antibody added by 20  $\mu\text{l}$  of a  $1:5 \cdot 10^3$  dilution of mouse anti RGS(His)4 antibody in PBS<sub>T</sub>/BSA 0.1%, pH 7.4 per well (0.02  $\mu\text{g}/\text{ml}$  final). The plates were again sealed and incubated for 1 h at room temperature. Subsequently the wells were washed three times with 120  $\mu\text{l}$  PBS<sub>T</sub>, pH 7.4 using a plate washer and the secondary antibody added by 20  $\mu\text{l}$  of a  $1:3 \cdot 10^4$  dilution of mouse anti RGS(His)4 antibody in PBS<sub>T</sub>/BSA 0.1%, pH 7.4 per well. After incubation for another hour at room temperature each well was washed four times with 120  $\mu\text{l}$  PBS<sub>T</sub>, pH 7.4 using a plate washer. For color reaction 20  $\mu\text{l}$  of 3 mM pNPP substrate was added per well using a dispenser and  $\Delta\text{OD}$  ( $\lambda_{405 \text{ nm}} - \lambda_{540 \text{ nm}}$ ) measured after 10, 20, 30, 60 and 120 min respectively using the Synergy 2 multi mode reader. The obtained data was analysed

using the BioTek Gen5 data analysis software and Microsoft Excel professional plus 2013.

### *Qualitative ELISA*

A Nunc MaxiSorp® flat-bottom 96 well plate (eBioscience) was coated with 100  $\mu$ l of 66 nM Streptavidin in 1  $\times$  PBS per well and incubated at 4 °C O/N. Subsequently the wells were washed two times with PBS and blocked with 100  $\mu$ l of PBS-T/0.5% BSA and incubated at room temperature (RT) for 1 h. The wells were washed two times with PBS-T and target protein immobilized by addition of 100  $\mu$ l target in PBS-TB per well and incubation for 1 h at RT. The wells were again washed three times with PBS-T and 100  $\mu$ l DARPIn in PBS-TB added per well and incubated for 1 h at RT with orbital shaking at 900 rpm. Subsequently the plate was washed three times with PBS-T and 100  $\mu$ l of a 1:5000 dilution of the 1<sup>st</sup> antibody (see Table 2.22) in PBS-TB added per well. The plate was again incubated for 1 h at RT without orbital shaking and subsequently washed three times with PBS-T. Hundred  $\mu$ l of a 1:10'000 dilution of 2<sup>nd</sup> antibody (see Table 2.22) in PBS-TB was added per well and the plate incubated for 1 h at RT w/o orbital shaking. The plate was again washed four times with PBS-T and 100  $\mu$ l of pNPP substrate solution added to each well. The plate was then sealed and incubated for 0.5 h at 37 °C and the signal measured at  $\lambda$ = 405 nm. Subsequently the plate was again incubated for 0.5 h and the signal measured at  $\lambda$ = 405 nm. For the third measure the plate was again incubated at 37 °C and the signal measured after 1.5 h. The final measure was performed at  $\lambda$ = 405 nm after 2 h of overall incubation time.

### **Sequence Analysis**

Sanger sequencing of selected clones was performed by GATC Biotech using Supremerun 96 sequencing and Standard Sanger sequencing. For sequencing using Supremerun 96 each selected clone was transferred from the expression cryostock (Preparation of Cryostocks) to a defined well on the sequencing plate. Subsequently the plate was incubated for 2 h at 37 °C prior sending to GATC Biotech according to GATC protocol. For sequencing using standard Sanger sequencing, each sample was diluted according to sample requirements given by GATC and respective primer added to each sample.

Analysis of the derived sequences including translation to protein, sequence alignments and calculation of a prediction of biophysical properties of protein was performed using CLC software (Qiagen).

### **Expression of DARPins**

Positive clones binding to human ROR1 ECD were picked from cryostock 96 well plate, inoculated in 5 ml of LB/Glu<sub>1</sub>%/Amp and incubated O/N at 37 °C, 220 rpm. 5 ml of O/N culture were transferred into fresh 200 ml of LB/Glu<sub>1</sub>%/Amp and cells grown in 1l shake flasks at 37 °C, 215 rpm, until an OD<sub>600</sub> between 0.70 and 0.80 was reached. Subsequently, the expression was induced by addition of 50  $\mu$ l 500 nM IPTG (500  $\mu$ M final), and cells incubated at 37 °C, 215 rpm for further 5 h. The cells were harvested by centrifugation at 3000  $\times$  g in 50 ml Falcon tubes, the supernatant discarded, the remaining cell pellet frozen in liquid nitrogen and stored at -20 °C until cell lysis the next day.

### **Cell Lysis**

*Cell Lysis in 96 well format*

The cell pellets were thawed at RT for about 20 min and subsequently 0.4 ml cell lysis B buffer added to each well, and the thawed pellets resuspended by gently pipetting up and down. The plate was resealed and incubated for 10 min at RT under shaking at 750 rpm. Subsequently the plate was incubated for another 30 min at RT without shaking. Finally the plates were centrifuged at  $3200 \times g$  for 10 min at  $4^\circ\text{C}$  to remove cell debris.

### *Cell Lysis in 50 ml Falcon tubes*

5 mL of TBS<sub>400</sub>, Lysozyme was added to appr. 0.8 g cell pellet and cells resuspended thoroughly using a 5 ml Pipette and transferred into a 50 ml falcon tube. Subsequently 1.5 ml TBS Adjusting buffer (5 $\times$ ) was added and the cells ruptured by sonification using the home-constructed HTBS-F sonicator with a single step of sonication at 70 duty cycles, output control five and 150 pulses under continuous cooling to  $4^\circ\text{C}$ . Subsequently the lysate was centrifuged at  $15000 \times g$ ,  $4^\circ\text{C}$  for 20 min for removal of cell debris.

## **Protein Purification**

### *Affinity Chromatography in 96 well format*

For purification of the expressed DARPins the seal of a His MultiTrap FF Spin Plate (GE Healthcare, 28-4009-90) were removed and the plate placed on top of a 96 well collection plate. For equilibration the plate was once centrifuged at  $500 \times g$  for three minutes to remove the storage solution of 20% Ethanol and subsequently washed once with 400  $\mu\text{l}$  sterile UHP and two times with equilibration buffer. A maximum of 390  $\mu\text{l}$  of lysate was transferred into each corresponding well on the purification plate and incubated for 3 min at room temperature. Subsequently, the plate was centrifuged at  $100 \times g$  for 3 min. The plates were then washed four times with 400  $\mu\text{l}$  wash buffer and centrifuged at  $500 \times g$  for 3 min each. The purification plate was finally placed on a new 96 well collection plate and 180  $\mu\text{l}$  of elution buffer added to each well. The plate was then incubated for 5 min at room temperature and subsequently centrifuged at 500 rpm for 3 min. The elution step was repeated again with fresh 180  $\mu\text{l}$  elution buffer. Finally, the concentration of protein was measured in each well using nanodrop at OD<sub>280</sub> and the plate was subsequently sealed with aluminium seal and stored at  $-20^\circ\text{C}$  until further use.

### *Affinity Chromatography using benchtop column*

For purification of the expressed DARPins a single step of ion metal affinity chromatography using Ni-NTA Superflow (Quiagen, 30450) was performed. Using a benchtop gravity driven column, the matrix was overloaded with Protein fused to either a (His)6 or (His)8 tag, respectively, by applying more protein than the theoretical binding capacity of the used resin.

The residual 1 CV 20% (v/v) EtOH was removed from the Ni-NTA columns containing 1 ml resin by washing with 10 ml milliQ-H<sub>2</sub>O. After the columns were equilibrated with 2 ml TBS-W, the supernatant of the cell lysate was applied on the column. The washing step was performed by washing with 20 column volumes (20 ml) TBS<sub>W</sub>, 20 CV (20 ml) TBS<sub>W, high salt</sub>, 20 CV (20 ml) TBS<sub>W, low salt</sub> and a final wash using 10 CV (10 ml) of TBS. Subsequently 300  $\mu\text{l}$  of elution buffer was added and the flow through was discarded. For elution of protein a final amount of 2.5 ml elution buffer was added and the eluted protein solution collected. Subsequently, the protein was quantified using Nanodrop at OD<sub>280</sub> and the respective extinction coefficient, as calculated from the respective amino acid composition using CLCbio Software (Quiagen).

After elution the column was regenerated for reuse by washing the resin with 10 CV milliQ-H<sub>2</sub>O, 2 CV of 6 M GdmCl, 10 CV milliQ-H<sub>2</sub>O, 2 CV 0.5 M NaOH, 10 CV milliQ-H<sub>2</sub>O, 2 CV 0.1 M EDTA, 10 CV milliQ-H<sub>2</sub>O, 2 CV NiSO<sub>4</sub>·H<sub>2</sub>O and 20 CV milliQ-H<sub>2</sub>O. Subsequently, the columns were stored in 2 CV 20% EtOH at 4 °C until reuse for purification.

### *Buffer exchange*

For removal of cytotoxic Imidazol from DARPin purified in 96 well format, all samples were dialysed against 1 × PBS, pH 7.4. The elution fraction of the IMAC containing the purified protein was transferred into 0.5 ml dialysis device and samples were dialysed against 2 l of 1 × PBS at 4 °C for 4 h. Subsequently, the buffer was exchanged for fresh 1 × PBS and the DARPins dialysed at 4 °C for three days under constant steering. After purification the molar concentration of each sample was determined, by measuring the absorption at  $\lambda = 280$  nm, using the respective molecular weight and extinction coefficient, derived from the protein sequences.

The buffer exchange of DARPin solution, purified using benchtop column, was performed according to PD10 desalting Column, Gravity Protocol, GE Healthcare. For preparation of the PD10 column the top cap was removed, the storage solution was poured off and the sealed end was cut using a scissor. The column was subsequently equilibrated by 25 ml of 1 × PBS, pH 7.4. Two ml of purified DARPin was applied. After the sample entered the packed bed completely another 0.5 ml of 1 × PBS, pH 7.4 were added for volume adjustment. The flow through was discarded. Subsequently the columns were placed over 15 ml falcon tubes and the DARPins eluted by addition of 3.5 ml 1 × PBS, pH 7.4.

### **SDS-PAGE and Coomassie Staining**

To test for an efficient purification, an SDS-PAGE was performed with 5 µg purified DARPin each in 1 × protein loading buffer. Prior loading on the gel all samples were heated to 95 °C for 6 minutes using a thermomixer. The proteins separated by 140 V for 45 min (55 mA initial and 35 mA final). The gels were transferred into each 25 mL of Coomassie staining solution, pre-heated to 90 °C in a microwave, and incubated on a shaker for 20 min. After incubation, the staining solution was discarded and the gels washed twice with dH<sub>2</sub>O. For de-staining, 25 ml of destaining solution was added to each gel, a pulp placed in the corner of the dish, again heated in the microwave and incubated on a shaker overnight at room temperature. The next day the pulp and acetic acid were discarded and the gels washed with dH<sub>2</sub>O. Subsequently both gels were scanned using an office flat bed scanner (Canon).

### **Size Exclusion Chromatography (SEC)**

Prior to analysis via size exclusion chromatography the DARPin solutions were filtered. The DARPin solutions were transferred onto a 0.22 µm filter plate into each corresponding well and centrifuged for 10 min at 1,500 rpm in a Sorvall RC-50 Plus centrifuge (Thermofisher). The column Superdex 200 Increase (GE Healthcare) was equilibrated with 1 × PBS pH 7.4 equilibration buffer at a flow rate of 0.4 ml/min until constant conductivity of eluate was reached. Fifty µl of sample was injected manually using a 200 µl syringe. Between each loading step the syringe was washed three times with each milliQ-H<sub>2</sub>O and ethanol. The OD at wavelength 230, 260 and 280 was recorded. The loop was loaded manually by starting program at a given flow rate of 0.4 ml/min and 9 °C at a defined pressure limit of 4.8 MPa. For each run isocratic elution was performed using 1 × PBS

pH7.4 as running buffer. At the end of analysis, system and column were washed with equilibration buffer until constant signal of conductivity and stored in 20% (v/v) ethanol.

### Multi Angle Light Scattering

For determination of oligomeric DARPins using size exclusion chromatography coupled to multi angle light scattering detection (SEC-MALS) all samples were filtered through filters with 0.22  $\mu\text{m}$  pore size and stored at 4  $^{\circ}\text{C}$  until separation and analysis of sample.  $1 \times \text{PBS}$ , pH 7.4 and milliQ- $\text{H}_2\text{O}$  were filtered through sterile filter with pore size of 0.22  $\mu\text{m}$  and degassed for three hours under vacuum and constant steering.

In order to obtain a stable baseline and continuous flow the system was equilibrated using milliQ- $\text{H}_2\text{O}$  for several hours and the flow cells washed until a the baseline of both detectors were stable. The whole procedure was repeated with running buffer  $1 \times \text{PBS}$ , pH 7.4 until a stable baseline was achieved. In order to avoid slight variation in refractive index by buffer exchange, the same running buffer was used for the measurement of all samples. Approximatley 30 min prior start of the first run the laser was turned on in order to let it warm up. Subsequently, the parameters of separation and measurement were set (Table 2.46). For  $1 \times \text{PBS}$  as running buffer a refractive index of solvent of 1.3396 was defined. For refractive index increment for protein needed for calculation of molecular mass a  $\frac{dn}{dc}$  of 0.185 was defined. The detectors of laser light beam of multi angle light scattering detector miniDAWN TREOS (Wyatt Technology) were positioned at 45 $^{\circ}$ , 90 $^{\circ}$  and 135 $^{\circ}$  angle respectively. For calculation of protein concentration the RI detector Optilab-rEX (Wyatt Technology) was used. As method for calculation of data point Zimm equation was applied according to  $M_W = \frac{K \cdot c}{R}$ , where K is a constant dependent on the polarizability relative to the solvent, c is the solute concentration and R is the excess Rayleigh ratio of the solution as a function of scattering light and concentration.

All samples were injected with an injection volume of 50  $\mu\text{l}$  at a protein concentration of approximately 50  $\mu\text{M}$  using the autosampler. Before and after measurement of all samples, bovine serum albumin, representing molecular weight standard (66.5 kDa) was run as sample. Proteins were first separated via size exclusion chromatography using a Superdex 200 column and subsequently detected using UV detection, multi angle light scattering detection and refractive index detector coupled online to the separation column. All runs were performed at a constant flow rate of 0.500 ml/min for 60 min.

Table 2.46: Method and parameters of SEC-MALS

Flow rate [ml·min <sup>-1</sup> ]	0.500
Injected Volume [μl]	50.0
Sample conc. [μM]	50.0
Sample dn/dc [ml·g <sup>-1</sup> ]	0.185
Sample UV ext. coef. [mg·ml <sup>-1</sup> ·cm <sup>-1</sup> ]	0.667 for BSA
Buffer refractive index (658.9 nm)	1.3396
miniDAWN wavelength [nm]	658.9
miniDAWN calibration const. [V <sup>-1</sup> ·cm <sup>-1</sup> ]	4.857·10 <sup>-5</sup>
Optilab wavelength [nm]	685.0
Optilab Temp. [°C]	25.0
dRI calibration constant [RIU/pixel]	3.5207·10 <sup>-5</sup>
Inject to collection delay [ml]	0
Known parameters	dn/dc and AUX cc
Detector fit method	Zimm ( $\frac{K \cdot c}{R}$ )
Angles of LS detectors	45°, 90°, 135°

In order to determine the interdetector delay volumes signals obtained from bovine serum albumin were aligned to the light scattering signal at 90°. The detectors were normalised with the monomeric peak of bovine serum albumin with a defined radius of 3 nm. The method for BSA was then applied to all samples. For evaluation of the light scattering measurement baselines were defined by setting the baseline of all obtained signals individually. Peak areas of each sample were selected individually for the calculation of the molar mass of the defined areas. The molar masses, polydispersity and relative mass accumulation was calculated using the ASTRA 6.1.5 Software.

After the measurement the whole system was equilibrated to milliQ-H<sub>2</sub>O. The flow cell of the LS detector was sonicated using the sonifier COMET. The system was equilibrated to 20% EtOH for storage.

### Cell Binding (FACS)

The cell line stably expressing human ROR1 using CHO FlpIn cell line (Thermofisher), was established by Dreier et al. (unpublished). Cells were grown in DMEM (F12 Nutrient-Mix for CHO), including 10% (v/v) FCS (Amimed), at 37 °C and 5% (v/v) CO<sub>2</sub> to a number of approximately  $8.8 \times 10^6$  per plate by using two 100 mm dishes, resulting in  $1.7 \times 10^7$  cells for the experiment. For FACS the cells were treated with trypsin and briefly incubated at 37°C. The trypsin was inhibited with 10 ml of medium, harvested by centrifugation at 0.8 rcf for 5 min and gently resuspended in 10 ml FACS buffer. The cells were then washed once with another 10 ml FACS buffer, gently resuspended and chilled on ice. The cells were subsequently aliquoted into 1 ml, centrifuged at 0.8 rcf for 2 min and resuspended in 100 μl FACS buffer incl. 100 nM DAPI. The cells were incubated for 1 h on ice, with vortex every 15 to 20 min and subsequently centrifuged at 0.8 rcf. The supernatant was discarded and the cells washed two times with 500 μl FACS buffer. The cells were then resuspended in 100 μl of 1 μg/ml antibody solution (Table 2.22) in FACS buffer, shielded with aluminum foil and incubated for 1 h on ice. During incubation the cells were vortexed every 15 to 20 min. Subsequently the cells were washed two times with 500 μl FACS buffer, finally resuspended in 1 ml FACS buffer, shielded with aluminium foil and stored on ice until analysis.

### Affinity Determination (SPR)

For determination of the binding kinetics of selected DARPins to the extracellular domain of human ROR1 surface plasmon resonance (SPR) was performed using ProteOn XPR36. For analysis 5 l running buffer of  $1 \times$  PBS, pH 7.4 was prepared and 0.005% (w/v) Tween20 added in order to minimize adsorption of the protein to the microfluidics tubing and MCM channels. The buffer was filtered through sterile filter with a pore size of 0.22  $\mu\text{m}$  and subsequently degassed under vacuum and constant stirring for approximately three hours. In order to avoid slight changes in background signals all samples were analysed with the identical buffer without exchange during the measure of samples.

For priming the system a maintenance chip was inserted into the ProteOn XPR36 protein interaction array system (Biorad) and the running buffer flushed through the whole system in order to eliminate potential air bubbles and avoid a signal drift resulting from the slow change in refractive index during the transition between buffers. For immobilisation of target a neutravidin layer attached to a GLC chip (NLC chip) was used for binding of biotinylated ligand molecules. The maintenance chip was replaced and the NLC sensor chip conditioned using running buffer at a flow rate of 30  $\mu\text{l}/\text{min}$ . Subsequently the chip was initialized using air initialization and the sensor chip temperature set at 25  $^{\circ}\text{C}$ .

For immobilisation of target 5 nM of biotinylated human ROR1 extracellular domain was applied on two lanes (L5 and L6) of the chip with 150  $\mu\text{l}$ , a contact time of 300 s and a flow rate of 30  $\mu\text{l}$  until a response signal of approximately 210 RU was reached. In case of samples evolved from the fourth pool of ribosome display selection round six, the chip surface was saturated with target, resulting in a response signal of approximately 900 RU. After immobilisation of target the chip was equilibrated with running buffer until a constant signal was achieved.

All samples containing DARPins were either diluted to 10, 20 or 30 nM as the respective highest concentration and further diluted in 1:3 dilution steps. The protein samples were transferred into a 96 deep-well plate and positioned in an autosampler, cooled to 4  $^{\circ}\text{C}$ . The experimental protocol was created using the software ProteOn Manager 3.1.0.6. For each binding analysis 300  $\mu\text{l}$  of diluted DARPin solution were applied on the chip at a constant flow rate of 60  $\mu\text{l}/\text{min}$ , with running buffer only applied on the sixth lane as reference signal. Subsequently, dissociation was measured for 2700 s applying running buffer only at the same flow rate. Between each measured sample a single regeneration step was applied using 30  $\mu\text{l}$  of 1 M glycine, pH 2.0 at a flow rate of 60  $\mu\text{l}/\text{min}$ . A summary of the protocol for sample measurement can be seen in Table 2.47.

Table 2.47: Method and parameters of SPR

Flow rate [ $\text{ml}\cdot\text{min}^{-1}$ ]	60
Injected Volume [ $\mu\text{l}$ ]	300
Flow stabilisation	20
Dissociation [s]	2700
Temperature chip [ $^{\circ}\text{C}$ ]	4
Temperature sample plate [ $^{\circ}\text{C}$ ]	25
Regeneration	30 $\mu\text{l}$ , 60 $\mu\text{l}/\text{min}$
Target response [RU]	210 and 900

For analysis and calculation of binding kinetics from data as obtained from SPR the software ProteOn Manager 3.1.0.6 was used. Measured interspots were lined up with the interaction data. The injection and baseline was aligned, artefacts removed and a double

reference performed using 'blank reference'. For fitting of the measured binding curves both binding signals were used and a globular fit applied. For calculation of the binding constants a 1:1 langmuir model was applied. In rare cases a heterogenous ligand model was used for calculation of the binding kinetics.

### Epitope Binning

Epitope Binning using SPR was performed essentially as described in Section 2.2.4. All samples containing DARPin were diluted to 500 nM in 400  $\mu\text{l}$  and transferred into a 96 well plate and positioned in an autosampler, cooled to 4  $^{\circ}\text{C}$ . The experimental protocol was created using the software ProteOn Manager 3.1.0.6. In first step the epitope was masked by 180  $\mu\text{l}$  of the first clone at a concentration of 500 nM and a flow rate of 60  $\mu\text{l}/\text{min}$ . Subsequently, the first and the second DARPin at a concentration of each 500 nM was applied with 180  $\mu\text{l}$  at a flow rate of  $\mu\text{l}/\text{min}$ . Finally a dissociation of 180 s was performed. In order to ensure saturation by the first DARPin a self competition was performed, masking an epitope with the first DARPin at 500 nM and applying subsequently the same DARPin with a concentration of 1  $\mu\text{M}$ . Running buffer only was applied on the sixth lane as reference signal. Between each measured sample a single step of regeneration was performed using 30  $\mu\text{l}$  of 1 M glycine, pH 2.0 at a flow rate of 60  $\mu\text{l}/\text{min}$ . A summary of the protocol for sample measurement can be seen in Table 2.48.

Table 2.48: Method and parameters of epitope binning

Flow rate [ $\text{ml}\cdot\text{min}^{-1}$ ]	60
Injected Volume [ $\mu\text{l}$ ]	180
Flow stabilisation	20
Dissociation [s]	180
Temperature chip [ $^{\circ}\text{C}$ ]	4
Temperature sample plate [ $^{\circ}\text{C}$ ]	25
Saturating DARPin [nM]	500
Competing DARPin [nM]	500
Self-comp. DARPin [nM]	1000
Regeneration	30 $\mu\text{l}$ , 60 $\mu\text{l}/\text{min}$
Target response [RU]	210

For analysis and calculation of binding kinetics from data as obtained from SPR the software ProteOn Manager 3.1.0.6 was used. Measured interspots were lined up with the interaction data. The injection and baseline was aligned, artefacts removed and a double reference performed using blank reference.

# Chapter 3

## Results

### 3.1 Characterisation of DARPins evolved from previous selections

Based on a previously performed ribosome display selection of three independent DARPIn libraries (Chapter 1.4), a screening for putative binders of human ROR1 and a subsequent full characterisation of promising clones was performed in order to obtain binders with less oligomerisation tendency. Previously, putative human ROR1 ECD binders were screened by ELISA and when analysed by SEC showed oligomerisation of a large number of clones. HTRF could be an alternative, since it may favour timely monomeric species and thus decrease the effect of higher avidity by dimerisation or oligomerisation.[159]

#### 3.1.1 Homogenous Time Resolved Fluorescence (HTRF)

HTRF is a FRET-based method that allows for time resolved, sensitive and robust detection of molecular interactions in small quantities. The binding signal is represented by the ratio of emitted light at 665 nm and 620 nm respectively. The close proximity of donor and acceptor, indicating the binding of target by ligand, leads to a shift of signal intensity at 620 nm towards 665 nm wavelength and therefore an increase in the ratio of the respective signals.[160]

#### Screening of DARPins from selection round 3

Due to the high sensitivity of HTRF, all samples were measured in a 1:10,000 dilution of crude extract. All negative controls, consisting of a measurement setup with reagents only, a setup with target only without DARPins and a setup with MBP binding DARPIn off7 [109] with the biotinylated target MBP, showed similar data points at a wavelength of 665 nm wavelength and 620 nm, with respective ratios of intensities at 665 nm and 620 nm ranging between 0.148 and 0.141. This represents a rather low ratio and therefore a low interference of signal from the background can be expected, provided that actual signals are significantly high. Still, at very high dilutions of 1:10,000 the difference between ratios obtained from the negative controls and ratios obtained from DARPins binding the target human ROR1 ECD can be rather small. Therefore, only clones that exhibit a signal ratio significantly higher than the respective ratio obtained from the negative controls will be considered full.

To test for background signal and specificity of the assay a setup with reagents only without target or binding reagent being added was measured. In this assay a low ratio of signals obtained at 665 nm and 620 nm of around 0.141 was measured, which confirmed

that no unspecific binding by reagents used in the basic assay composition occurred. The negative control using target but no DARPins resulted in a signal ratio of about 0.148, showing a signal very similar to the negative control of reagents only and confirmed that no unspecific binding of reagents to the target occurs. The third negative control, including the DARPin off7 specifically binding Maltose Binding Protein (MBP), but in the absence of MBP as target, resulted in a signal ratio of about 0.148, therefore showing a similar signal as the first and second negative control, confirming no unspecific binding of DARPins to the extracellular domain of human ROR1.

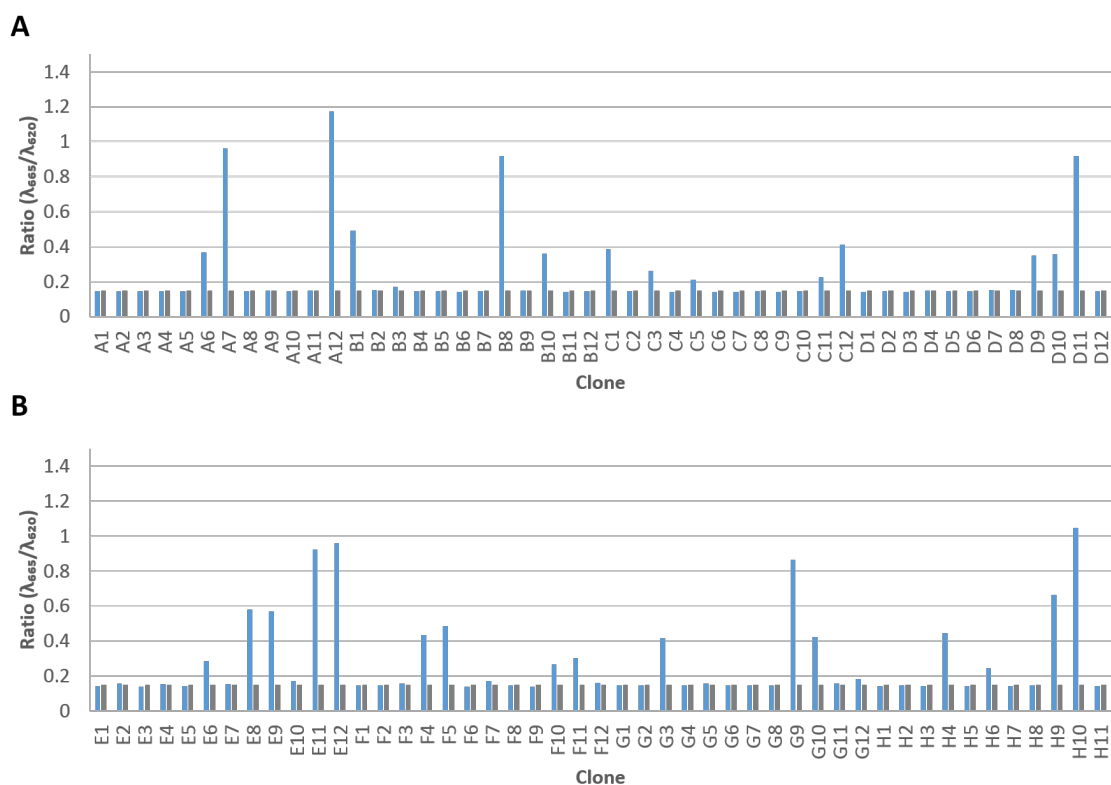


Figure 3.1: Homogenous Time Resolved Fluorescence of clones from the naive library N2C obtained after the third selection round against human ROR1 ECD using ribosome display. Signal plotted as the ratio of detected counts at 665 nm over detected counts at 620, measured in 1:10,000 dilution of crude extract. Blue: measured signal of setup including DARPin, Gray: negative control using reagents only. A: clone A1 - D12, B: clone E1 - H11. The name of each clone refers to its position on the respective expression plate

As shown in Figure 3.1, DARPins from the naive library containing N2C DARPins [106], that were obtained from the third selection round by using ribosome display, showed a clear ratio between counts at 665 nm and 620 nm, respectively, over background. A clear shift towards 665 nm and therefore binding to the extracellular domains of human ROR1 could be suspected. A significant number of clones show only a marginal increase in signal ratio compared to the signal of background at a dilution of 1:10,000 ranging from 0.14 to 0.19. About a third of the analysed clones showed a signal significantly higher than the background, ranging from a signal ratio of 0.40 to 1.2.

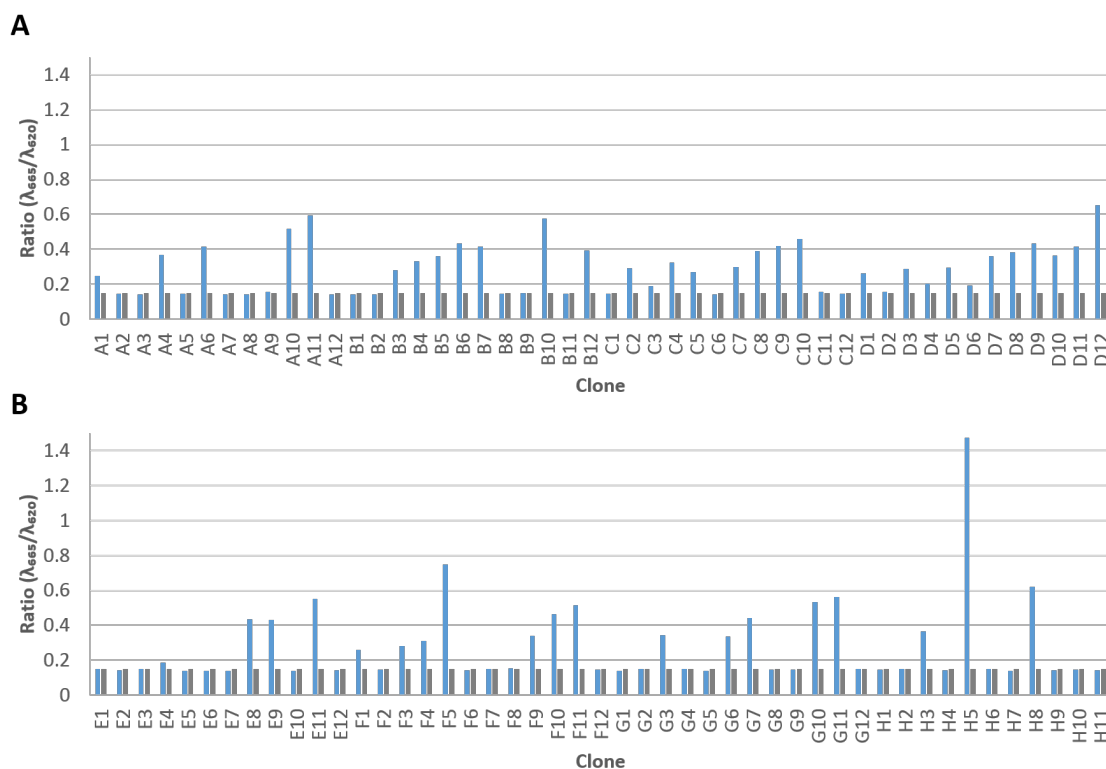


Figure 3.2: Homogenous Time Resolved Fluorescence of clones from the naive library N3C obtained after the third selection round against human ROR1 ECD using ribosome display. Signal plotted as the ratio of detected counts at 665 nm over detected counts at 620, measured in 1:10,000 dilution. Blue: measured signal of setup including DARPin, Gray: negative control using reagents only. A: clone A1 - D12, B: clone E1 - H11. The name of each clone refers to its position on the respective expression plate

Similarly, clones selected from the naive library containing N3C DARPins [106], that were obtained from the third selection round by using ribosome display, showed a clear increased ratio between counts at 665 nm and 620 nm, respectively, over background to be seen in Figure 3.2, indicating a binding of the extracellular domains of human ROR1.

Clones from the library containing N3C DARPins showed signals that were significantly over background, resulting in 48% of analysed clones that showed a significant signal of binding to human ROR1 ECD. These clones are ranging in signal ratios from 0.20 to 1.45. About 52% of the analysed clones showed only a marginal or no increased ratio of signals compared to the measured negative control.

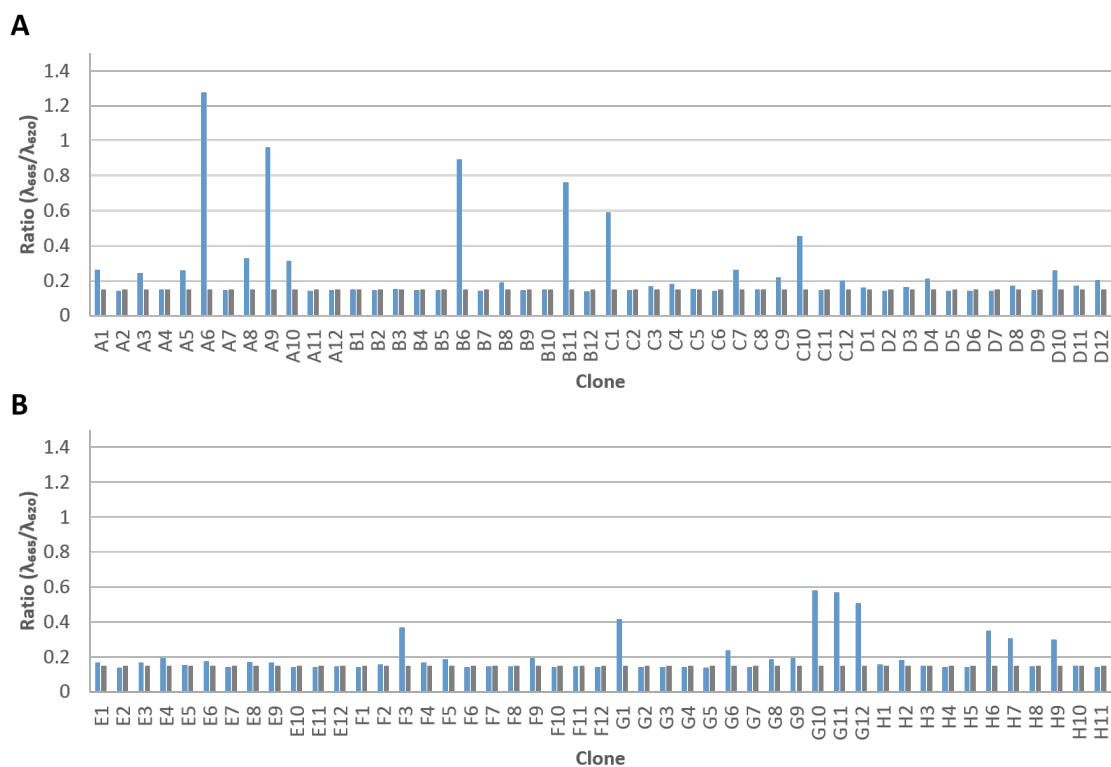


Figure 3.3: Homogenous Time Resolved Fluorescence of clones from the naive library r+nr obtained after the third selection round against human ROR1 ECD using ribosome display. Signal plotted as the ratio of detected counts at 665 nm over detected counts at 620, measured in 1:10,000 dilution. Blue: measured signal of setup including DARPin, Gray: negative control using reagents only. A: clone A1 - D12, B: clone E1 - H11. The name of each clone refers to its position on the respective expression plate

Figure 3.3 shows that DARPins derived from the library where N3C DARPins with stabilised Ccap [109] and N3C DARPins with either randomised and non-randomised capping repeats [106] were mixed in equimolar amounts (r+nr) from the third selection round showed distinct increased signals ratios above background. About 23% of clones analysed from library r+nr from selection round 3 showed a significantly higher signal than the negative controls and therefore significant binding to the extracellular domains of human ROR1. The ratio of counts at 665 nm to 620 nm, equivalent to the proximity of target and ligand, in case of the analysed positive clones of r+nr from the third round was between 0.20 and 1.30. About 77% of analysed clones showed only marginal or no signal over background.

#### Screening of DARPins from selection round 4

All negative controls, consisting of a measurement setup with reagents only, a setup with target only without DARPins and a setup with target and the MBP binding control DARPin off7, showed a similar ratio of counts at 665 nm wavelength to counts at 620 nm ranging between 0.151 and 0.143. Similar to the negative controls of the HTRF screening of DARPins from the third selection round this represents a rather low ratio and therefore a low interference of signal from the background can be expected. Still, at

very high dilutions of 1:10,000 the difference between ratios obtained from the negative controls and ratios obtained from DARPs binding the target human ROR1 ECD can be rather small. Therefore only clones that show a distinct signal over background will be followed further.

An obtained signal of 665 nm to 620 nm of around 0.143 in the measurement setup, where only reagents but no target or DARPs were added, confirmed no unspecific binding by reagents used in the basic assay composition. The negative control using target but no DARPs resulted in a signal ratio of about 0.148, showing a signal very similar to the negative control of reagents only and confirming that no unspecific binding of reagents to the target occurs. The third negative control, including the DARPin off7 specifically binding Maltose-Binding-Protein, resulted in a signal ratio of about 0.151. Therefore showing a similar signal as the first and second negative control and confirming no unspecific binding of DARPs to the extracellular domain of human ROR1.

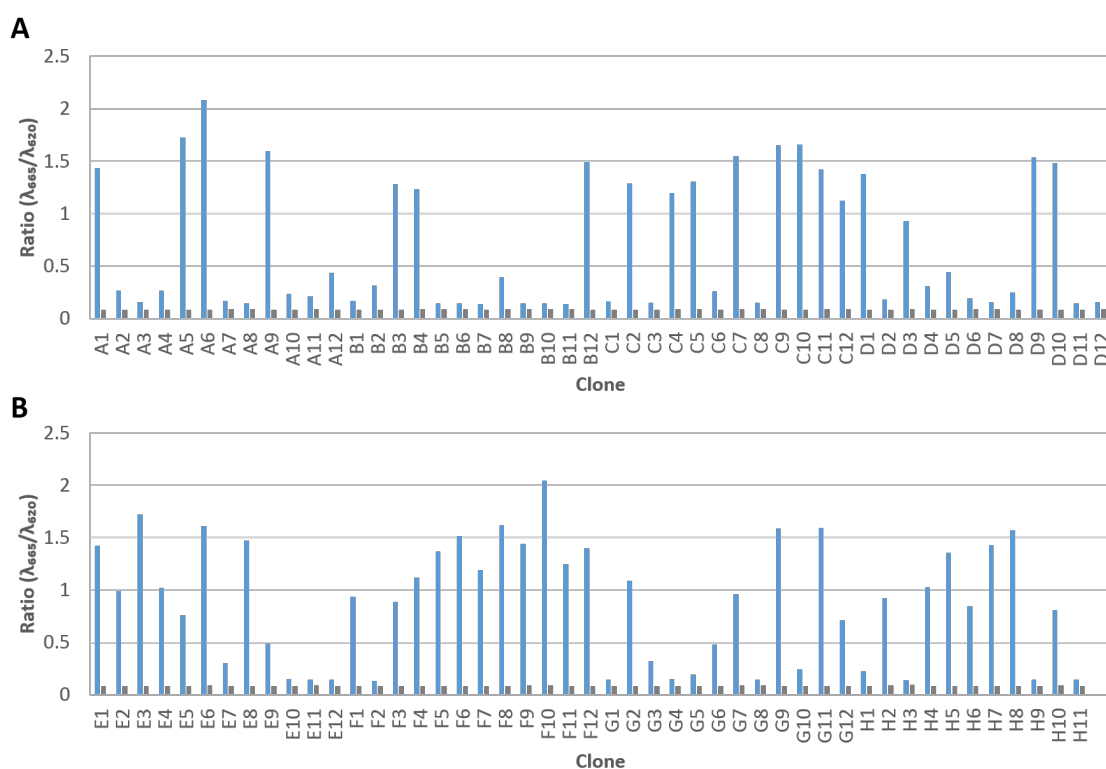


Figure 3.4: Homogenous Time Resolved Fluorescence of clones from the naive library N2C obtained after the fourth selection round against human ROR1 ECD using ribosome display. Signal plotted as the ratio of detected counts at 665 nm over detected counts at 620, measured in 1:10,000 dilution. Blue: measured signal of setup including DARPin, Gray: negative control using reagents only. A: clone A1 - D12, B: clone E1 - H11. The name of each clone refers to its position on the respective expression plate

As seen in Figure 3.4, DARPs from the naive library containing N2C DARPs [106], that were obtained from the fourth selection round by using ribosome display, showed a clear increased ratio between signals at a wavelength of 665 nm and 620 nm, respectively, over background. This indicated a shift towards 665 nm and therefore binding to the extracellular domains of human ROR1. All analysed clones that evolved from the

fourth selection round showed a clear signal over background, with more than 42% of all analysed clones showing signal ratios higher than 1.0. The highest signal was obtained at a signal ratio of 2.2. Only 32% of analysed clones showed a signal lower than 0.25. The rest of DARPin of N2C from selection round four exhibited a ratio between 0.2 and 1.0.

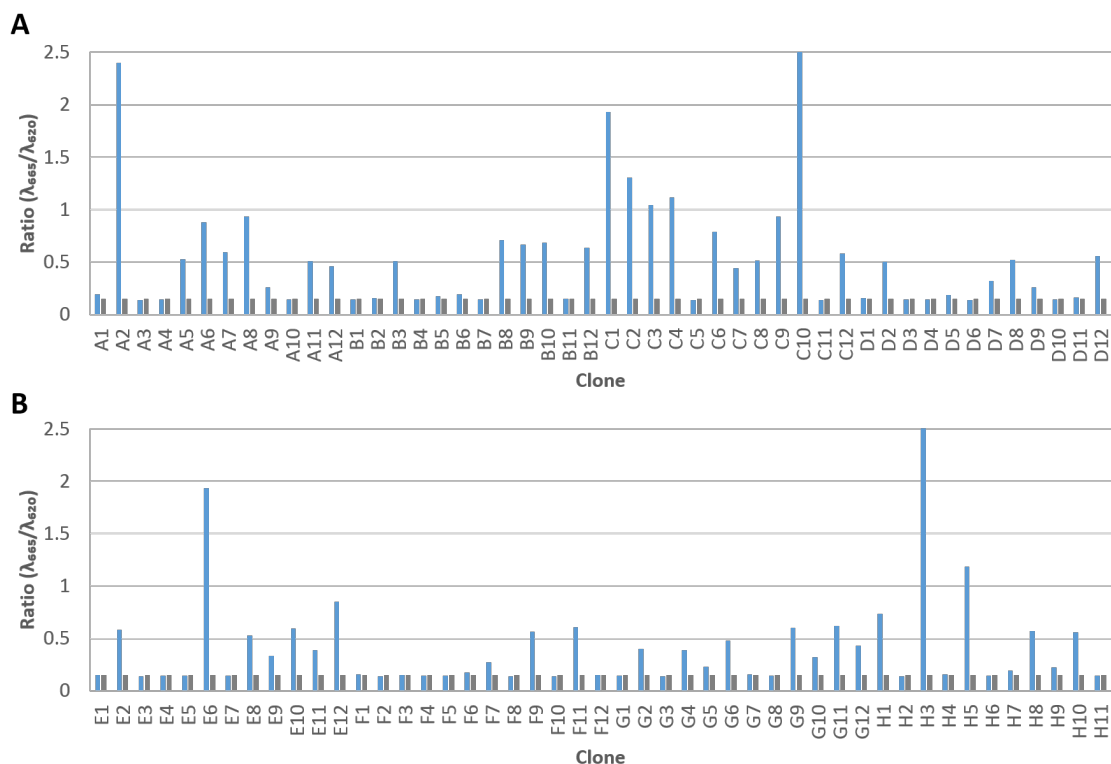


Figure 3.5: Homogenous Time Resolved Fluorescence of clones from the naive library N3C obtained after the fourth selection round against human ROR1 ECD using ribosome display. Signal plotted as the ratio of detected counts at 665 nm over detected counts at 620, measured in 1:10,000 dilution. Blue: measured signal of setup including DARPin, Gray: negative control using reagents only. A: clone A1 - D12, B: clone E1 - H11. The name of each clone refers to its position on the respective expression plate

Clones from the naive library containing N3C DARPins [106] that were obtained from the fourth selection round by using ribosome display, showed a clear ratio between counts at 665 nm and 620 nm, respectively, over background to be seen in Figure 3.5, indicating a binding of the extracellular domains of human ROR1, with 67% of analysed DARPins showing a signal that is significantly higher than background. Only 9% of clones showed a signal ratio than was higher than 1.0, with a maximum in ratio at about 3.1. All other positive clones are ranging in signal ratios of 0.25 to 0.95.

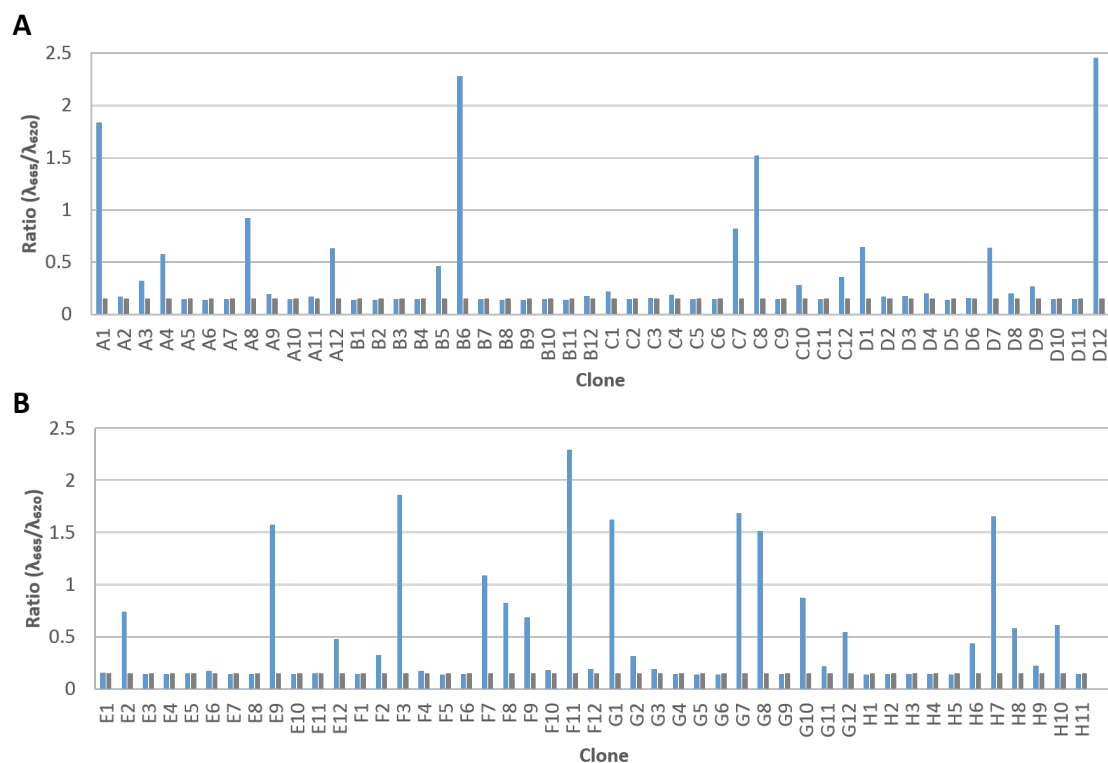


Figure 3.6: Homogenous Time Resolved Fluorescence of clones from the naive library r+nr obtained after the fourth selection round against human ROR1 ECD using ribosome display. Signal plotted as the ratio of detected counts at 665 nm over detected counts at 620, measured in 1:10,000 dilution. Blue: measured signal of setup including DARPin, Gray: negative control using reagents only. A: clone A1 - D12, B: clone E1 - H11. The name of each clone refers to its position on the respective expression plate

Figure 3.3 shows that DARPins derived from the library where N3C DARPins with stabilised Ccap [109] and N3C DARPins with either randomised and non-randomised capping repeats [106] were mixed in equimolar amount (r+nr) from the third selection round showed distinct signals ratios above background. Ratios of counts towards a signal at 665 nm could be observed that were significantly higher than the background, indicating a binding of the target human ROR1 ECD. About 50% of the analysed clones showed a distinct signal ratio over background. About 13% of the analysed clones showed signal ratios that were higher than 1.0, including a highest measured ratio of signals at 2.45.

Within analysed clones from both selection rounds (round 3 and 4) a significant number of clones that showed a signal over background could be identified. Notably, DARPins that evolved from the fourth round showed on average 5- to 10-fold higher signals than DARPins that evolved from the third round. Sixty clones that showed the highest signal ratios and were considered to putatively bind human ROR1 were further analysed by Sanger sequencing, in order to identify the sequence of the putative binder as well as to evaluate its similarities and putative conclusions towards distinct families and properties. Further clones that represented cys-containing DARPins and identical sequences were eliminated from further characterisation.

### 3.1.2 Sequence Analysis

After DARPins that putatively bound human ROR1 were identified using HTRE, sequences of 60 clones that showed the highest signals were analysed using Sanger sequencing.

About 18 analysed clones possessed one or more cysteines in its sequence. These clones were therefore excluded from further characterisation and analysis. Only 2 sequences showed identical amino acid sequence and therefore one was excluded from the pool of candidates. Within the alignment of all obtained sequences distinct families related to a certain selection round and libraries could be seen (Figure 3.7). While at position 75 almost all DARPins evolved from library N2C exhibited basic residues, the majority of DARPins evolved from library N3C and r+nr contained the hydrophilic residues Serine or Threonine at the respective position. At position 145 DARPins evolved from N2C tended to show the hydrophobic residues Valine and Isoleucine, while the majority of DARPins evolved from N3C and r+nr exhibited the aromatic residue Tryptophan. In case of position 189 clones that evolved from the third selection round exhibited the small residue Alanine while clones that evolved from the fourth round contained primarily the hydrophilic amino acid Serine. After excluding all unfavourable sequences, 32 out of 60 sequenced clones remained for further analysis and characterisation, including the binding of target on the cell. For the following characterisation of the remaining clones, all DARPins needed to be expressed and purified in the following step.



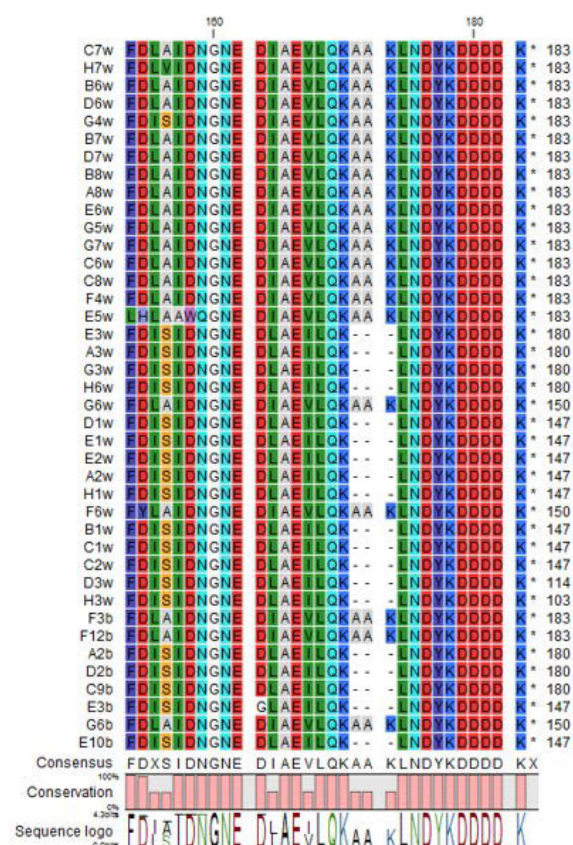


Figure 3.7: Sequence analysis of screened clones selected from ribosome display selection round three and four. Nucleotide sequences were derived by Sanger sequencing. All sequences were translated to protein sequence *in silico* and aligned using CLC software (clcbio). All sequences containing Cys or showing identical sequence were deleted from the graph. The selected DARPin's are listed in order according to its similarity of sequence. The first three characters of each DARPin's ID refers to its respective position on the sequenced plate. On each bottom of the graph the consensus amino acid, its conservation and appearing amino acids are presented for each position

### 3.1.3 Expression and Purification of DARPins

Each clone was expressed in 200 ml culture using shake flasks and induction of expression for 5 h with 500  $\mu$ M IPTG. Expressed DARPins were purified using IMAC with washing steps of 20 CV TBS-W, 20CV TBS-W high salt, 20 CV TBS-W low salt and 10 CV TBS-W as well as a subsequent buffer exchange to 1  $\times$  PBS pH 7.4 using PD10 columns. All DARPins that were considered for further characterisation after sequence analysis were analysed using SDS-PAGE in order to assess purity. DARPins were separated on a SDS-PAGE and stained with Coomassie Brilliant Blue.

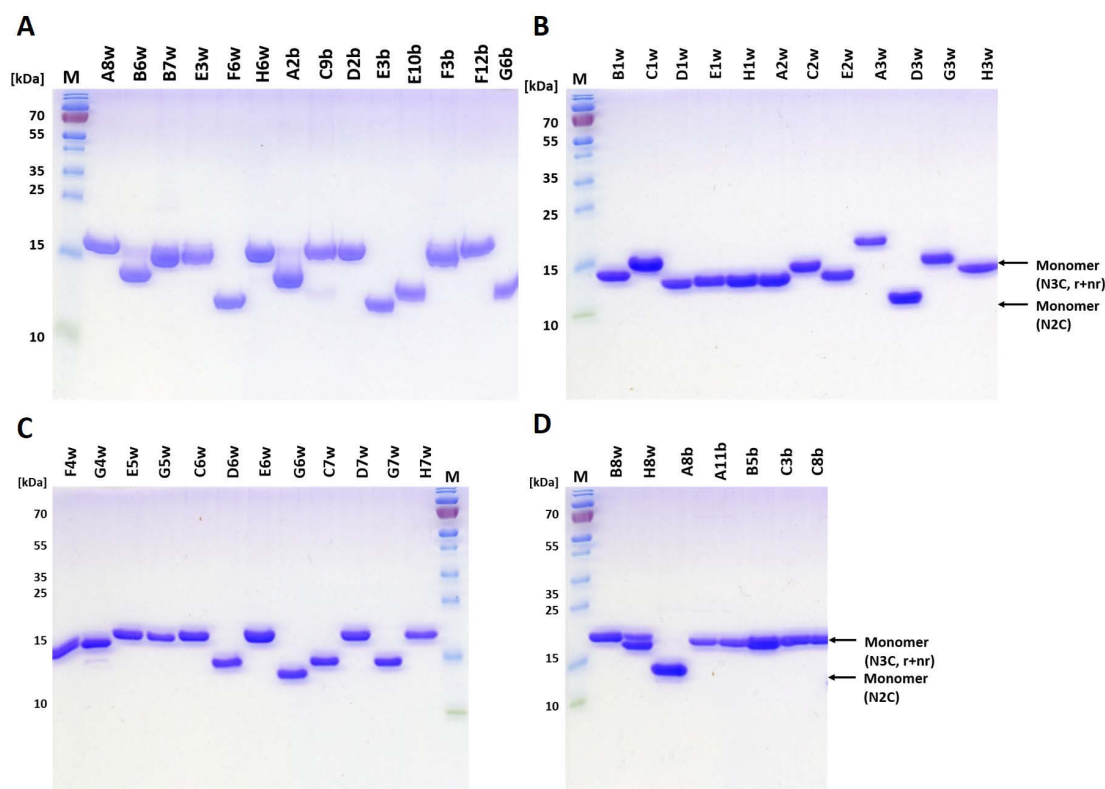


Figure 3.8: SDS-PAGE of purified DARPins. Eight  $\mu\text{g}$  protein loaded on a 15% SDS-PAGE and stained using Coomassie blue. M - Molecular Weight Standard, PageRuler 180 – 10 kDa. Purified DARPins derived from ribosome display selection round three and four (A) Clones A8w to G6b (B) Clones B1w to H3w (C) Clones F4w to H7w (D) Clones B8w to C8b.

In Figure 3.8 the expressed and purified DARPins evolved from ribosome display selection can be seen. In each lane only DARPins at its expected size range could be seen without further impurities, suggesting a successful expression and a purity of  $> 98\%$  of the respective DARPins. The purified DARPins were then used to characterise their biophysical properties regarding to their oligomeric behaviour by using size exclusion chromatography. The protein concentration was determined by measuring  $\text{OD}_{280}$ . All clones yielded several milligrams of pure protein, ranging from 8.5 mg to 37.8 mg DARPin per 200 ml culture.

### 3.1.4 Analytical Size Exclusion Chromatography (SEC)

For characterisation of the biophysical properties of DARPins regarding their oligomeric behaviour, analytical size exclusion chromatography of DARPins was performed.

All samples were analysed after purification and buffer exchange to  $1 \times \text{PBS}$ , pH 7.4. In addition, 13 clones that evolved from a previous ribosome display selection for DARPins binding human ROR1 and that represented the most promising candidates in terms of monomeric behaviour (B. Dreier, unpublished), were again analysed using SEC and considered for further characterisation.

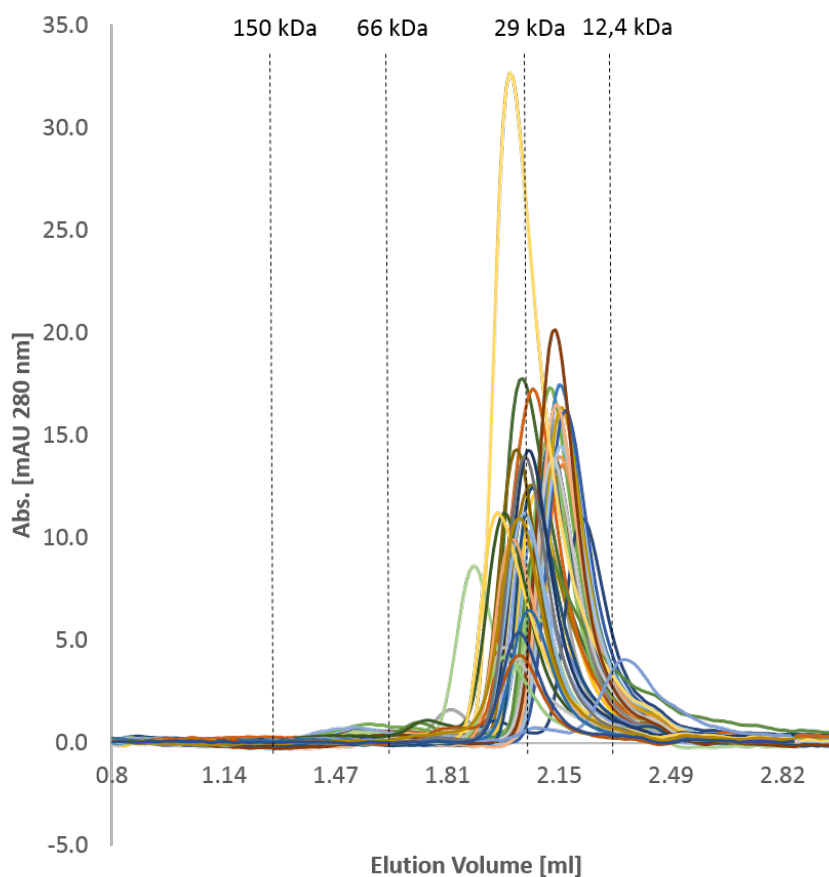


Figure 3.9: Analytical SEC of DARPins evolved from round three and four of ribosome display selection. Curves represent the elution profile of each single clone as detected using absorbance at 280 nm, after purification and removal of Imidazole by buffer exchange. For each run 50  $\mu$ l of a 10  $\mu$ M protein-solution was loaded onto a Superdex 200 increase column with 1  $\times$  PBS pH 7.4 at a flow rate of 0.4 ml/min using an ÄKTAmicro chromatography system. All curves plotted as Abs. [mAU 280 nm] vs. elution volume [ml]. The elution profile of the MW standard (150 kDa, 66 kDa, 29 kDa and 12.4 kDa) is represented by dashed black vertical lines.

Figure 3.9 shows the summary of analytical size exclusion chromatography of selected DARPins, evolved from the third and fourth round of ribosome display selection after removal of imidazole by buffer exchange to 1  $\times$  PBS, pH 7.4. All 45 clones analysed in Figure 3.9 represent the most promising candidates, regarding a monomeric elution profile.

It can be seen that the vast majority of the analysed DARPins from ribosome display selection round 3 and 4 showed an elution profile at  $OD_{280}$  that was characteristic for monomers. Only 6 out of 46 analysed clones (C1w, D3w, G7w, B7w, E10b and C9b) showed a slight tendency for a second peak at the approximate size of 30 to 40 kDa, which would represent the potential size of DARPin dimers. A single clone (B5b) eluted in a profile that was characteristic for dimers, to be seen as a second peak at the approximate size of a dimeric N3C DARPin. The signal intensity of this first eluting peak seemed to be larger than the second peak, which was considered to represent monomeric DARPins, suggesting a strong tendency for dimerisation.

About 84.4% of analysed clones showed promising elution profiles typical for monomeric DARPins.

Table 3.1: DARPins evolved from ribosome display selection round 3 and 4 that were analysed by SEC in absence of imidazole. Tag indicates respective Tags of the DARPIn when analysed. EV: Elution Volume at respective peak maximum.

Clone	Tag	EV [ml]	Clone	Tag	EV [ml]
A8w	(His) <sub>6</sub>	2.19	C1w	(His) <sub>8</sub> , FLAG	2.11
E3w	(His) <sub>6</sub>	2.21	E2w	(His) <sub>8</sub> , FLAG	2.13
A2b*	(His) <sub>6</sub>	2.13	G4w	(His) <sub>8</sub> , FLAG	2.15
E3b*	(His) <sub>6</sub>	2.22	G6w	(His) <sub>8</sub> , FLAG	2.14
F12b*	(His) <sub>6</sub>	2.20	H8w	(His) <sub>8</sub> , FLAG	2.13
B6w	(His) <sub>6</sub>	2.22	D1w	(His) <sub>8</sub> , FLAG	2.14
B7w	(His) <sub>6</sub>	2.15	A2w	(His) <sub>8</sub> , FLAG	2.12
C9b*	(His) <sub>6</sub>	2.50	A3w	(His) <sub>8</sub> , FLAG	2.06
H6w	(His) <sub>6</sub>	2.15	H3w	(His) <sub>8</sub> , FLAG	2.08
F6w	(His) <sub>6</sub>	2.17	E5w	(His) <sub>8</sub> , FLAG	2.08
D2b*	(His) <sub>6</sub>	2.15	D6w	(His) <sub>8</sub> , FLAG	2.15
E10b*	(His) <sub>6</sub>	2.20	C7w	(His) <sub>8</sub> , FLAG	2.16
F3b*	(His) <sub>6</sub>	2.21	H7w	(His) <sub>8</sub> , FLAG	2.15
G6b*	(His) <sub>6</sub>	2.19	A8b*	(His) <sub>8</sub> , FLAG	2.00
B1w	(His) <sub>8</sub> , FLAG	2.16	C3b*	(His) <sub>8</sub> , FLAG	2.07
H1w	(His) <sub>8</sub> , FLAG	2.12	G3w	(His) <sub>8</sub> , FLAG	2.04
C6w	(His) <sub>8</sub> , FLAG	2.12	G7w	(His) <sub>8</sub> , FLAG	2.09
B5b*	(His) <sub>8</sub> , FLAG	1.89	E1w	(His) <sub>8</sub> , FLAG	2.13
C2w	(His) <sub>8</sub> , FLAG	2.14	D3w	(His) <sub>8</sub> , FLAG	2.22
F4w	(His) <sub>8</sub> , FLAG	2.15	G5w	(His) <sub>8</sub> , FLAG	2.11
E6w	(His) <sub>8</sub> , FLAG	2.07	D7w	(His) <sub>8</sub> , FLAG	2.17
B8w	(His) <sub>8</sub> , FLAG	2.14	A11b*	(His) <sub>8</sub> , FLAG	2.05
C8b*	(His) <sub>8</sub> , FLAG	2.14			

\*Clones identified from ribosome display by ELISA  
(B. Dreier, unpublished)

In order to confirm the actual molar mass of eluting DARPins, all DARPins as analysed by SEC were further be characterised by size exclusion chromatography coupled to multi-angle light scattering.

### 3.1.5 Multi Angle Light Scattering (MALS)

To confirm the results obtained by SEC alone, SEC coupled to MALS was performed. The detection with multi-angle light scattering should allow to determine the absolute molecular mass of the DARPins. For this purpose all DARPins as analysed in Figure 3.9 were analysed using SEC-MALS. For each run 50  $\mu$ l of a 50  $\mu$ M protein-solution was loaded onto a Superdex 200 column with 1  $\times$  PBS pH 7.4 at a flow rate of 0.5 ml/min and the eluting protein detected by UV detection at OD<sub>280</sub>, followed by static light scattering and refractive index detection on line.

In Table 3.2 the summary of SEC-MALS for the characterisation of biophysical properties regarding monomeric behaviour of DARPins that were analysed previously by SEC only (Figure 3.9) can be seen. The elution profile of each clone was detected by UV and the respective molecular weight of each peak calculated using the Zimm equation. The chromatograms and determined absolute molecular masses of DARPins can be found in the Appendix 5.

As to be seen in Table 3.2, the vast majority of selected clones appeared to be monomeric, to be seen by the identified molecular weight of eluting protein as expected by previous size exclusion chromatography with UV detection, representing 98% to 100% of the eluting mass. These measured molecular masses coincide with the expected masses calculated from the respective amino acid sequences using CLC software (clcbio). Only 3 out of 45 DARPins (B7w, C1w and C9b) eluted with a significant mass fraction of 12.4%, 10.2% and 10.3% indicating dimers, suggesting a high tendency for oligomerisation in these cases. Another clone F12b showed a small fraction of 4.2% that was eluting with the respective weight of dimers, which could be a small tendency towards dimerisation in case of this DARPIn. Furthermore, clone A11b showed a tendency for potential aggregation with a fraction of 3.6%, suggesting a tendency for aggregation with this DARPIn. This effect could be caused by a remaining cysteine within its sequence as determined by Sanger sequencing.

All eluting peaks of analysed DARPins showed a polydispersity factor between 1.00 and 1.02. This confirmed that a single protein species eluted in each peak, and an accurate calculation of molecular weight was possible. It can be seen in Table 3.2 that the reference sample BSA showed peaks with the expected masses and mass fraction of the total eluting mass. This confirmed the correct and calibration of the SEC-MALS analysis.

The results of SEC-MALS suggested that 90% of all analysed DARPins eluted as monomers only, leading to the conclusion that the vast majority of DARPins showed excellent biophysical properties in terms of monomeric behaviour.

Table 3.2: Summary of SEC-MALS for the characterisation of biophysical properties regarding monomeric behaviour of DARPinS that evolved from ribosome display selection round 3 and 4. Mw refers to molecular weight as determined by MALS while theoretical Mw refers to the molecular weight expected from the sequence. Mass fraction shows the accumulated mass as represented by the analysed peak.

Clone	theoretical	Peak 1		Peak 2	
	Mw [kDa]	Mw [kDa]	Mass fraction [%]	Mw [kDa]	Mass fraction [%]
BSA	66.5	64.4	87.6	126.5	10.3
A2b*	18.2	20.2	100	-	-
A8w	19.8	17.7	100	-	-
B6w	18.6	17.8	100	-	-
B7w	18.4	17.9	87.6	32.1	12.4
C9b*	18.3	17.4	89.7	13.5	10.3
D2b*	18.3	18.0	100	-	-
E3b*	14.6	14.2	100	-	-
E3w	18.3	17.6	100	-	-
E10b*	14.7	16.9	100	-	-
F3b*	18.4	17.7	97.9	29.5	2.1
F6w	14.9	18.7	100	-	-
F12b*	18.6	18.1	95.8	40.7	4.2
G6b*	15.0	14.5	100	-	-
H6w	18.3	21.9	100	-	-
A2w	15.9	17.5	98.3	53.2	0.8
A3w	19.4	21.4	100	-	-
A8b*	18.4	22.1	100	-	-
A11b*	16.0	20.2	96.4	148.8	3.6
B1w	16.0	15.6	98.7	58.1	1.3
B5b*	19.9	21.7	98.4	82.7	1.6
B8w	19.8	19.0	98.9	56.1	1.1
C1w	15.9	15.3	89.8	44.1	10.2
C2w	16.0	15.6	98.7	28.7	1.3
C3b*	19.8	21.4	100	-	-
C6w	19.9	19.2	98.3	39.6	1.7
C7w	19.8	19.1	100	-	-
C8b*	16.2	15.5	96.4	41.1	3.6
D1w	16.0	17.6	98.1	60.9	0.9
D3w	12.6	12.4	96.2	34.9	3.8
D6w	19.7	19.2	100	-	-
D7w	19.7	18.9	100	-	-
E1w	16.0	17.7	96.4	63.4	1.7
E2w	16.0	18.1	95.1	65	2.7
E5w	19.6	18.9	98.0	46.0	2.0
E6w	19.7	20.4	99.2	50.2	0.8
F4w	19.8	19.5	96.3	45.7	3.7
G3w	19.5	21.2	100	-	-
G4w	19.8	19.2	100	-	-
G5w	19.6	19.4	100	-	-
G6w	16.8	15.6	98.2	39.6	1.8
G7w	19.9	28.3	96.5	90.8	3.5
H1w	16.0	17.5	98.1	78.4	1.9
H3w	11.1	19.0	100	-	-
H7w	19.8	19.5	100	-	-
H8w	19.8	19.0	98.6	28.4	1.4

\*Clones identified from ribosome display by ELISA  
(B. Dreier, unpublished)

### 3.1.6 Qualitative ELISA

In order to test the specific binding of the purified DARPins to the target human ROR1 ECD a qualitative ELISA of 45 of the initially 570 clones was performed.

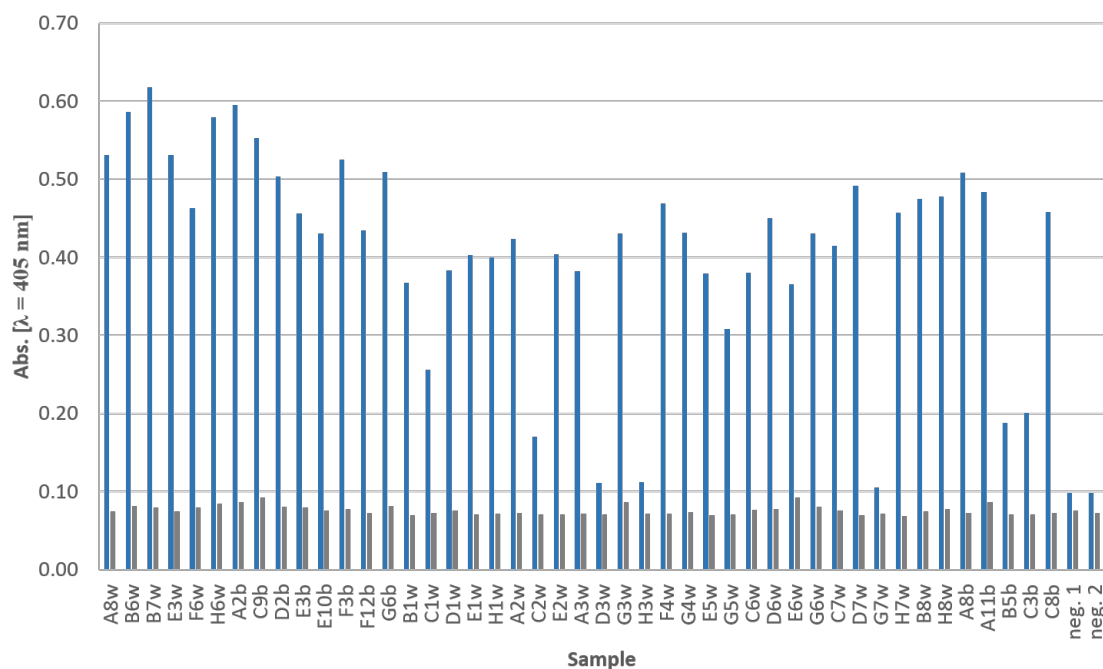


Figure 3.10: ELISA to test binding of purified DARPins to the human ROR1 ECD. A qualitative ELISA was used to analyse the binding of DARPins to the protein human ROR1 ECD. Hundred  $\mu\text{l}$  of 100 nM target was immobilised via Streptavidin after 1.0 h in each well. Hundred  $\mu\text{l}$  of 100 nM DARPIn was incubated for 1.5 h. Bound DARPins were detected using anti MRGS-His<sub>4</sub> antibody + secondary antibody coupled to AP. After addition of pNPP as substrate OD<sub>405</sub> was determined. The absorption at 405 nm was plotted on y-axis. Blue: Absorption of the respective DARPins. Gray: Negative control without target. Neg.1 refers to the negative control where no primary antibody was used. Neg. 2 refers to the negative control where no DARPIn was used.

As can be seen in Figure 3.10, the results of the qualitative ELISA for binding of human ROR1 were plotted as signal obtained after one hour of incubation with substrate, as represented by absorbance at  $\lambda = 405$  nm on the y-axis.

The majority DARPins were able to bind to the immobilised protein human ROR1 ECD. On average an absorption of 0.43 after 1.5 h of incubation was measured. Almost all clones reached an absorption that was significantly higher than the background signal, suggesting a promising specific binding of the target by the selected clones, with B7w, a putative dimer, showing the strongest measured signal of 0.62. Only three DARPins, D3w, H3w and G7w, exhibited a signal that was only marginally higher than the background, suggesting a very weak or even an absence of binding to the target human ROR1.

The negative control with missing primary antibody, shown as 'neg.1' on the right panel of the x-axis, showed an absorption that is equivalent to the background signal. With increased incubation time, the signal remained constantly low, confirming the specific binding of the secondary antibody, to the primary antibody (Table 2.22). The negative control where no DARPins were applied, shown as 'neg.2' on the right panel of the

x-axis, showed an absorption that is again equivalent to the background signal. With increased incubation time, the signal remained in the range of background, confirming the specific binding of the primary antibody to the DARPin. This ensured no false positives by the detection system. Furthermore, the specificity of DARPins for the target human ROR1 was tested by control samples without target for each analysed clone. Again the negative control showed a constantly low signal over time in case of every analysed clone. These signals confirmed that no off-target binding of the analysed DARPins occurred.

About 93% of all analysed DARPins exhibited ELISA signals that suggested specific binding to the target human ROR1 ECD as purified protein. Only 3 out of 46 clones showed signals that were only marginally higher than the background, suggesting a weak binding to the target.

### 3.1.7 Cell Binding

In order to assess binding of DARPins to the target human ROR1 ECD not only to the recombinant purified protein, but also for binding on the cell surface, fluorescent activated cell sorting was performed with CHO cells that were stably expressing human ROR1 (Dreier, unpublished). Initially CHO/ROR1 cells were tested for ROR1 expression using an anti-ROR1 Ab and secondary Ab coupled to Alexa488. As negative controls a second DARPin (E2-5) [106] that is not able to bind the target human ROR1 ECD was used (Table 3.12). The intensity of fluorescent signal, equivalent to intensity of binding, was plotted against percent of maximum cell count for each sample. Approximately 100,000 cells per sample were analysed.

Table 3.3: Setup of samples and control samples

---

Sample	CHO/ROR1 + DARPin + mAb anti DARPin-AlexaFluor88
293ctrl	CHO + DARPin + mAb anti DARPin-AlexaFluor88
CHOAbonly	CHO/ROR1 + mAb anti DARPin-AlexaFluor88
CHOctrl	CHO
ROR1Abonly	CHO/ROR1 + mAb anti DARPin-AlexaFluor88
ROR1ctrl	CHO/ROR1

---

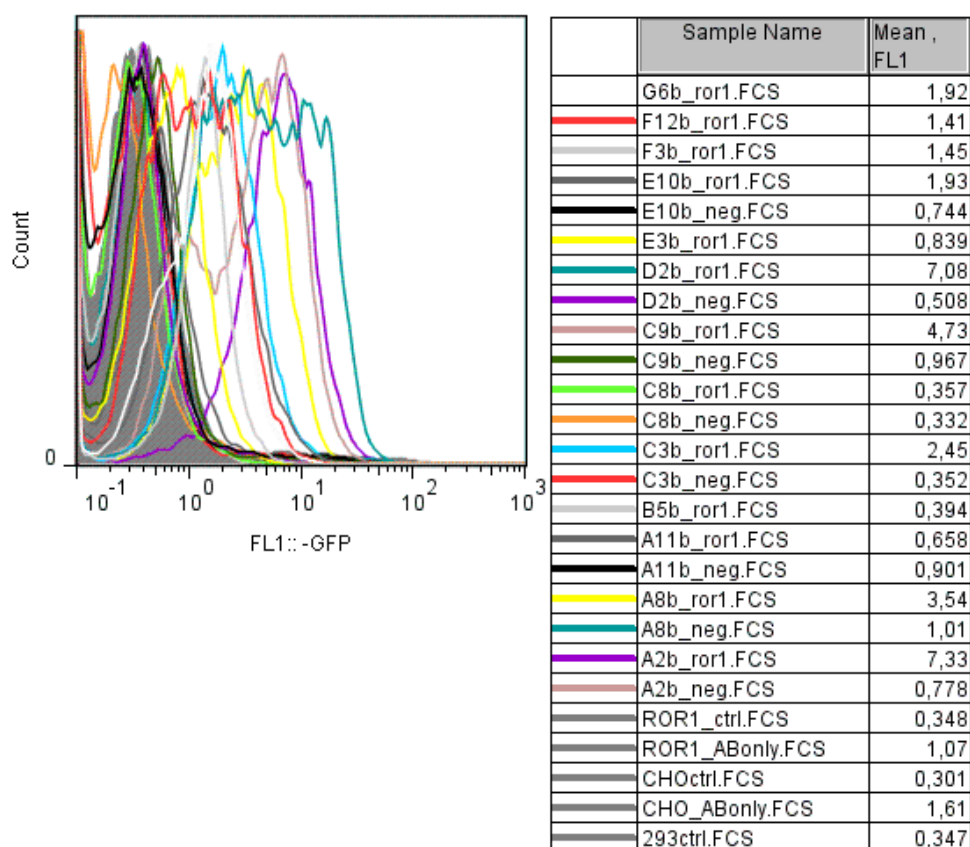


Figure 3.11: Summary of test for cell binding of DARPins evolved from initial ribosome display selection round three and four as performed by B. Dreier. Flow cytometry was used to analyse the binding of DARPins to the target human ROR1 expressed on the cell surface of CHO FlpIn cells. The intensity of fluorescent signal is plotted against cell count of each sample. Mean,FL1 represents the mean fluorescence intensity of the individual samples. Sample 293ctrl, CHOABonly, CHOctrl, ROR1ABonly and ROR1ctrl refer to the negative controls. The name affix neg refers to signal obtained on ROR1 negative cells. The name affix ror1 refers to signal obtained from CHO/ROR1 cells. Fluorescence observed for all controls are highlighted as grey area.

As shown in Figure 3.11 all negative controls showed a fluorescent signal intensity below  $10^0$ , representing no unspecific binding.. All samples tested on ROR1-negative CHO cells exhibited signal intensities below  $10^0$ . ROR1 positive cells that were tested without DARPins showed as well very low signal intensities. This led to the conclusion that both cell lines and antibody conjugated to AlexaFluor488 were suited for the assay, since no unspecific binding signal could be expected. This led to the conclusion that the assay was suited for assessing the binding of DARPins to the target hROR1, expressed on CHO cells. All DARPins, that were tested, exhibited fluorescent signal intensities higher than the respective background on ROR1 negative cells or on CHO/ROR1 cells incubated with antibody only. The obtained signal intensities were in a range between 1 and

10. This suggested binding of the DARPins to the human ROR1 on the cell surface.

After the initial characterisation and set up of the FACS conditions additional DARPins were only tested for binding using CHO/hROR1 cells.

Table 3.4: Setup of samples and control samples

Sample	Cells + DARPIn + mAb anti DARPIn-AlexaFluor88
Pos. ctrl.	Cells + mAb mouse anti hROR1 + mAb anti mouse AlexaFluor88
Neg. ctrl. 1	Cells + E2-5 + mAb anti DARPIn-AlexaFluor88
Neg. ctrl. 2	Cells + mAb anti DARPIn-AlexaFluor88
Neg. ctrl. 3	Cells + mAb anti mouse AlexaFluor88

As seen in Figure 3.12 the majority of the 32 analysed DARPins exhibited a medium to strong binding of target on CHO cells, ranging from fluorescent intensities of 1, which represented medium binding, to up to 10, which was equal to a strong binding of target on the cells. In case of 3 out of 32 analysed clones (D3w, H3w, G7w) no detectable binding occurred. This was consistent with the results of ELISA with purified and dialysed DARPins, where clones H3w, D3w and G7w showed no binding. Two clones (B1w, C1w) exhibited only weak binding. Five clones (G3w, F6w, H6w, B7w and B8w) appeared to bind in a strong intensity, that was similar to the tested positive control. However, the strong binding signal of the B7w might be explained by its partial presence as dimer.

In the case of the negative control E2-5 it can be seen that no binding occurred during the performance of FACS. Furthermore, both negative controls of secondary antibodies did not show a fluorescent signal, which indicated that no binding occurred. The positive control was detected with a fluorescent intensity of about 10, which represented a strong ability of the antibody to bind to the cell surface.

About 93% of all analysed DARPins exhibited fluorescent signals that suggested specific binding to the target human ROR1 ECD on the cell surface of CHO cells. Only 3 out of 46 clones showed signals that were only marginally higher than the background, suggesting a weak or missing binding to the target. A ranking of the MFI can be seen in Table 3.5.

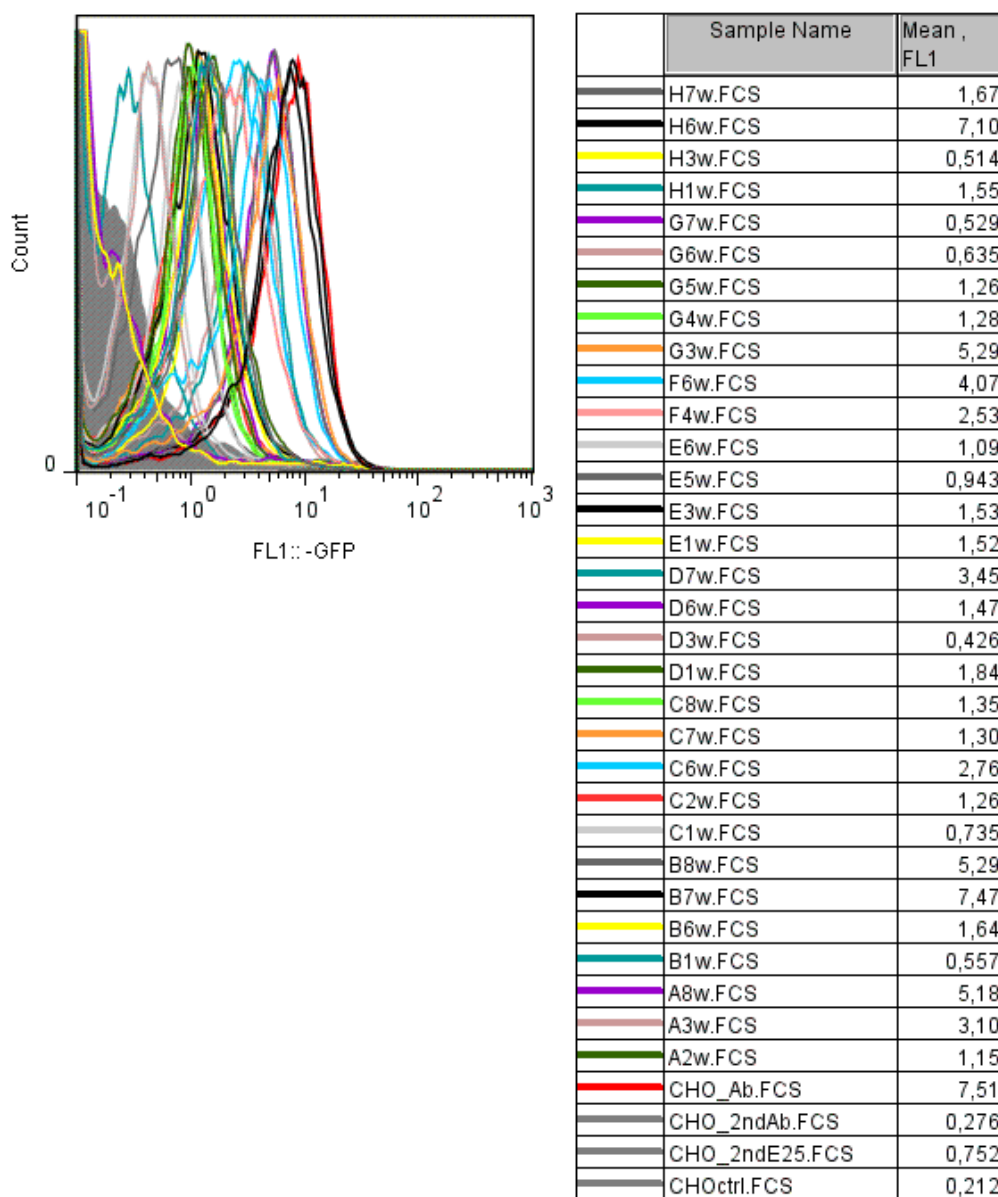


Figure 3.12: Summary of test for cell binding of DARPins evolved from ribosome display selection round three and four. Flow cytometry used to analyse the binding of DARPins on target, human ROR1, expressed on cell surface of CHO cells. Intensity of fluorescent signal plotted against percent of max. Mean,FL1 represents the mean fluorescence intensity of the individual samples. cell count of each sample. Sample CHO-E25 refers to the negative control. CHO-2ndE25 and CHO-2ndAb to samples with the secondary antibody only, representing the negative controls for 2nd antibodies. CHO-Ab represents the positive control. Fluorescence observed for all controls are highlighted as grey area.

Table 3.5: Clones tested for cell binding and ranked according to the measured Mean Fluorescent Intensity (MFI)

Clone	MFI	Clone	MFI	Clone	MFI
B7w	7.82	E10b	1.80	C2w	1.12
H6w	7.33	D1w	1.66	G5w	1.12
A2b	7.33	G6b	1.65	A2w	1.03
D2b	7.08	H7w	1.64	E6w	0.94
B8w	5.43	B6w	1.58	E3b	0.78
G3w	5.43	H1w	1.48	E5w	0.77
A8w	5.37	E1w	1.37	A11b	0.59
C9b	4.51	F3b	1.37	C1w	0.57
F6w	4.15	E3w	1.35	G6w	0.50
D7w	3.47	E2w	1.34	B1w	0.38
A8b	3.41	F12b	1.33	B5b	0.35
A3w	3.06	D6w	1.32	C8b	0.31
C6w	2.64	C8w	1.16	G7w	0.29
F4w	2.41	C7w	1.14	H3w	0.27
C3b	2.28	G4w	1.14	D3w	0.24

### 3.1.8 Affinity Determination

In order to determine the affinity of selected DARPins to the ECD of human ROR1, Surface Plasmon Resonance (SPR) using the ProteOn XPR36 system was performed. The experimental setup is described in Chapter Material and Methods 2.2.4. Purified DARPins samples were applied on a NA chip, where 200 RU of the human ROR1 ECD was immobilised and analysed at a constant flow rate of 60  $\mu\text{l}/\text{min}$ . Association was performed for 300 s. Subsequently, dissociation was measured for 2700 s. Between each measured sample a single regeneration step was applied using 30  $\mu\text{l}$  of 1 M glycine, pH 2.0. Based on the resulting signals the on- and off-rate constants were determined and the respective  $K_D$  calculated. The resulting graphs and calculated constants can be found in Appendix 5.

Table 3.6: Summary of binding kinetics of DARPins evolved round 3 and 4 of ribosome display selection. The constants of on-rate [ $k_{\text{on}}$ ] and off-rate [ $k_{\text{off}}$ ] were calculated from the respective binding curve as determined by surface plasmon resonance. Both constants presented with the respective standard deviation were obtained from fitting of measured curves. Dissociation constants [ $K_{\text{D}}$ ] were calculated from the obtained constants.

Clone	$k_{\text{on}}$ [ $\text{M}^{-1} \text{s}^{-1}$ ]	$k_{\text{off}}$ [ $\text{s}^{-1}$ ]	$K_{\text{D}}$ [nM]
D1w	$2.37 \times 10^6 \pm 3.67 \times 10^4$	$8.06 \times 10^{-3} \pm 6.79 \times 10^{-5}$	3.40
A3w	$4.92 \times 10^6 \pm 6.18 \times 10^4$	$2.54 \times 10^{-2} \pm 2.18 \times 10^{-4}$	5.17
E3w	$9.11 \times 10^4 \pm 1.75 \times 10^3$	$4.52 \times 10^{-5} \pm 5.77 \times 10^{-7}$	0.50
G3w	$3.01 \times 10^6 \pm 2.99 \times 10^4$	$1.93 \times 10^{-2} \pm 1.14 \times 10^{-4}$	6.43
H6w	$2.81 \times 10^6 \pm 5.43 \times 10^3$	$2.33 \times 10^{-4} \pm 1.23 \times 10^{-6}$	0.08
A2b	$3.40 \times 10^6 \pm 4.48 \times 10^4$	$2.03 \times 10^{-2} \pm 1.66 \times 10^{-4}$	5.99
A8b	$8.44 \times 10^6 \pm 1.23 \times 10^5$	$8.46 \times 10^{-3} \pm 7.39 \times 10^{-5}$	1.00
C9b	$7.14 \times 10^5 \pm 3.29 \times 10^2$	$9.22 \times 10^{-5} \pm 8.55 \times 10^{-7}$	0.13
D2b	$6.48 \times 10^5 \pm 1.36 \times 10^3$	$2.36 \times 10^{-4} \pm 7.15 \times 10^{-7}$	0.37
E3b	$8.70 \times 10^5 \pm 3.92 \times 10^3$	$1.12 \times 10^{-3} \pm 2.45 \times 10^{-6}$	1.28
E10b	$1.53 \times 10^6 \pm 8.73 \times 10^3$	$9.38 \times 10^{-3} \pm 3.38 \times 10^{-5}$	6.12
A11b	$1.25 \times 10^6 \pm 1.05 \times 10^4$	$5.02 \times 10^{-3} \pm 2.30 \times 10^{-5}$	4.03
A8b	$8.44 \times 10^6 \pm 1.23 \times 10^5$	$8.46 \times 10^{-3} \pm 7.39 \times 10^{-5}$	1.00
C8b	$1.11 \times 10^7 \pm 4.12 \times 10^5$	$5.21 \times 10^{-3} \pm 1.85 \times 10^{-4}$	0.47
F4w	$2.42 \times 10^6 \pm 5.99 \times 10^3$	$2.11 \times 10^{-4} \pm 3.65 \times 10^{-6}$	0.09
E5w	$2.24 \times 10^6 \pm 9.25 \times 10^3$	$1.45 \times 10^{-4} \pm 3.37 \times 10^{-6}$	0.06
B6w	$5.24 \times 10^5 \pm 5.90 \times 10^3$	$4.88 \times 10^{-4} \pm 5.02 \times 10^{-6}$	0.93
D6w	$1.01 \times 10^7 \pm 1.52 \times 10^5$	$8.99 \times 10^{-3} \pm 9.91 \times 10^{-5}$	0.89
E6w	$6.67 \times 10^6 \pm 8.53 \times 10^4$	$1.21 \times 10^{-2} \pm 1.13 \times 10^{-4}$	1.82
B7w	$3.97 \times 10^6 \pm 1.16 \times 10^5$	$3.01 \times 10^{-2} \pm 6.14 \times 10^{-4}$	7.58
C7w	$6.36 \times 10^6 \pm 8.25 \times 10^4$	$8.49 \times 10^{-3} \pm 8.13 \times 10^{-5}$	1.33
D7w	$4.14 \times 10^6 \pm 4.04 \times 10^4$	$6.11 \times 10^{-3} \pm 6.20 \times 10^{-5}$	1.47
B8w	$4.64 \times 10^6 \pm 2.46 \times 10^5$	$1.44 \times 10^{-3} \pm 9.32 \times 10^{-5}$	0.31
C8w	$6.67 \times 10^6 \pm 3.77 \times 10^4$	$2.79 \times 10^{-4} \pm 3.77 \times 10^{-6}$	0.04
F3b	$5.72 \times 10^5 \pm 8.86 \times 10^2$	$2.24 \times 10^{-5} \pm 2.47 \times 10^{-7}$	0.04
F12b	$4.00 \times 10^5 \pm 1.29 \times 10^3$	$1.79 \times 10^{-4} \pm 4.06 \times 10^{-7}$	0.45
C3b	$1.10 \times 10^7 \pm 3.00 \times 10^5$	$1.87 \times 10^{-2} \pm 3.97 \times 10^{-4}$	1.70

Table 3.7: Summary of binding kinetics of DARPins evolved round 3 and 4 of ribosome display selection. The constants of on-rate [ $k_{\text{on}}$ ] and off-rate [ $k_{\text{off}}$ ] were calculated from the respective binding curve as determined by surface plasmon resonance using heterogenous ligand fit. Both constants presented with the respective standard deviation were obtained from fitting of measured curves. Binding affinity [ $K_D$ ] was calculated from the obtained constants.

Clone	$k_{\text{on}}$ [ $\text{M}^{-1} \text{s}^{-1}$ ]	$k_{\text{off}}$ [ $\text{s}^{-1}$ ]	$K_D$ [nM]
B1w*	$1.54 \times 10^6 \pm 8.57 \times 10^3$	$5.78 \times 10^{-4} \pm 5.31 \times 10^{-6}$	0.37
	$8.72 \times 10^6 \pm 9.97 \times 10^4$	$1.98 \times 10^{-2} \pm 1.80 \times 10^{-4}$	2.27
C1w*	$4.23 \times 10^6 \pm 1.44 \times 10^5$	$1.59 \times 10^{-2} \pm 4.39 \times 10^{-4}$	3.75
	$5.02 \times 10^6 \pm 2.21 \times 10^4$	$1.85 \times 10^{-4} \pm 3.70 \times 10^{-6}$	0.04
E1w*	$1.05 \times 10^7 \pm 1.47 \times 10^5$	$1.53 \times 10^{-2} \pm 1.63 \times 10^{-4}$	1.46
	$3.03 \times 10^6 \pm 1.30 \times 10^4$	$3.98 \times 10^{-4} \pm 2.70 \times 10^{-6}$	0.13
H1w*	$1.38 \times 10^7 \pm 1.70 \times 10^5$	$1.44 \times 10^{-2} \pm 1.29 \times 10^{-4}$	1.04
	$4.67 \times 10^6 \pm 2.02 \times 10^4$	$3.89 \times 10^{-4} \pm 2.01 \times 10^{-6}$	0.08
A2w*	$1.53 \times 10^7 \pm 2.48 \times 10^5$	$1.52 \times 10^{-2} \pm 1.92 \times 10^{-4}$	0.99
	$5.74 \times 10^6 \pm 3.11 \times 10^4$	$5.61 \times 10^{-4} \pm 4.86 \times 10^{-6}$	0.98
C2w*	$1.15 \times 10^6 \pm 1.07 \times 10^5$	$1.75 \times 10^{-1} \pm 6.76 \times 10^{-3}$	153.00
	$2.72 \times 10^0 \pm 2.43 \times 10^{-2}$	$9.66 \times 10^{-4} \pm 2.12 \times 10^{-5}$	3550
E2w*	$1.12 \times 10^7 \pm 1.31 \times 10^5$	$1.28 \times 10^{-2} \pm 1.10 \times 10^{-4}$	1.14
	$4.44 \times 10^6 \pm 1.87 \times 10^4$	$4.53 \times 10^{-4} \pm 2.25 \times 10^{-6}$	0.10
G6w*	$9.84 \times 10^6 \pm 1.15 \times 10^5$	$9.72 \times 10^{-3} \pm 8.47 \times 10^{-5}$	0.99
	$3.12 \times 10^6 \pm 9.59 \times 10^3$	$3.55 \times 10^{-4} \pm 2.04 \times 10^{-6}$	0.11
G4w*	$5.44 \times 10^6 \pm 6.29 \times 10^4$	$7.20 \times 10^{-3} \pm 5.92 \times 10^{-5}$	1.32
	$1.15 \times 10^6 \pm 2.58 \times 10^3$	$1.89 \times 10^{-4} \pm 1.16 \times 10^{-6}$	0.17
G5w*	$5.57 \times 10^5 \pm 1.68 \times 10^3$	$1.73 \times 10^{-4} \pm 1.57 \times 10^{-6}$	0.31
	$4.04 \times 10^6 \pm 5.07 \times 10^4$	$8.75 \times 10^{-3} \pm 7.82 \times 10^{-5}$	2.16
C6w*	$3.26 \times 10^6 \pm 8.68 \times 10^3$	$1.73 \times 10^{-4} \pm 2.31 \times 10^{-6}$	0.05
	$1.20 \times 10^7 \pm 2.28 \times 10^5$	$6.23 \times 10^{-3} \pm 2.02 \times 10^{-5}$	0.52
H7w*	$7.05 \times 10^6 \pm 9.03 \times 10^4$	$6.40 \times 10^{-3} \pm 6.16 \times 10^{-5}$	0.91
	$1.79 \times 10^6 \pm 3.44 \times 10^3$	$1.87 \times 10^{-4} \pm 1.42 \times 10^{-6}$	0.10

\*Constants obtained by heterogenous ligand fit.

Table 3.6 and 3.7 show the kinetics of DARPins that evolved from ribosome display selection round three and four. These clones showed on average a strong to very strong affinity to the ECD of human ROR1. Several selected DARPins showed a very strong affinity in the sub-nanomolar range. Four of the selected DARPins (F3b, C8w, E5w and H6w) showed a very strong affinity in the double-digit picomolar range of 40 pM to 90 pM. These clones represented the strongest binders within this group, exhibiting an affinity of 40 pM, 40 pM, 50 pM and 90 pM to the ECD of human ROR1, respectively. The fraction of N2C DARPins that bound with sub-nanomolar affinity to human ROR1 ECD was 25%. The fraction of clones evolved from the library N3C that showed an affinity in the sub-nanomolar range was at 45%. The fraction of clones evolved from the library r+nr that showed an affinity in the sub-nanomolar range was about 64%.

An appropriate fit using 1:1 binding model of the measured binding curves was possible with the majority of measured samples, as can be seen by relatively low standard deviations of the on- and off-rate constants as determined using fit to a 1:1 binding model. This confirmed a monovalent one to one binding of the target by the majority of measured

DARPin. In case of 12 analysed samples a heterogenous ligand fit was applied. The analysed DARPins exhibited on average very high affinities in the sub-nanomolar range to the target human ROR1 ECD. The weakest binders showed affinities in the single- or double-digit nanomolar range. In case of a single DARPin (C2w) a weak affinity of  $K_{D1} = 153$  nM was determined. In order to further distinguish different epitope regions on human ROR1 that are targeted by the respective DARPins, an epitope binning using competitive SPR was performed.

### 3.1.9 Epitope Binning

In order to distinguish different binding regions of selected DARPins on the ECD of human ROR1, competition surface plasmon resonance was performed. Each DARPin was tested against all other clones pairwise by evaluating blocking of each other's binding to the respective epitope region. For this purpose a competitive blocking profile was created by saturation of one epitope by one DARPin and binning of the second DARPin against the respective first DARPin, allowing no binding on the same or overlapping proximity of the epitope region. If an increase in binding signal by the second DARPin occurs, the two clones are considered to bind on different, non-overlapping epitope regions. If no increase in binding signal can be detected, the two competing clones bind on epitopes that are similar or in overlapping proximity.

Figure 3.13 shows a node plot presenting the summary of the competitive blocking profile of each DARPin to all other DARPins binding human ROR1 that have been selected and characterised. The blocking profile, as created by competition surface plasmon resonance, shows the different epitope regions bound by the selected clones. Each red dot represents a clone, selected and characterised from ribosome display selection, that was binned against all other clones. Grey lines connecting two dots indicate a blocking of each other's binding to the target if binned against each other, revealing binding on epitopes that are similar or in overlapping proximity. Missing of grey connecting lines between two dots represent unblocked binding of the second clone to the target if binned against each other, indicating binding of different epitope regions.

The overall binning profile shows three epitope regions targeted by selected binders evolved from round three and four of ribosome display selection. As can be seen, the vast majority of 79% of selected DARPins from selection round three and four bind to an identical epitope or a region that lie in very close or overlapping proximity to each other. The binding of this region by more than 79% of selected clones reveals a very dominant region with a strong evolutionary tendency towards this binding area. As can be seen by the node plot all clones binding the dominant region are connected with every other DARPin within this group, showing that every clone was able to block binding of the respective other clones, suggesting a well defined small epitope region that was favoured by directed evolution.

Beside the very dominant binding area a second set of clones can be distinguished, binding a second region. 16% of the selected DARPins bind this epitope region, revealing a second, less dominant, binding region. As well as for the dominant region all clones binding this area are connected with every other DARPin within this group, suggesting again binding of well defined small epitope regions that lie in overlapping proximity to each other. Five clones bound at the interface of region one and two, suggesting a close proximity of the two respective epitope regions.

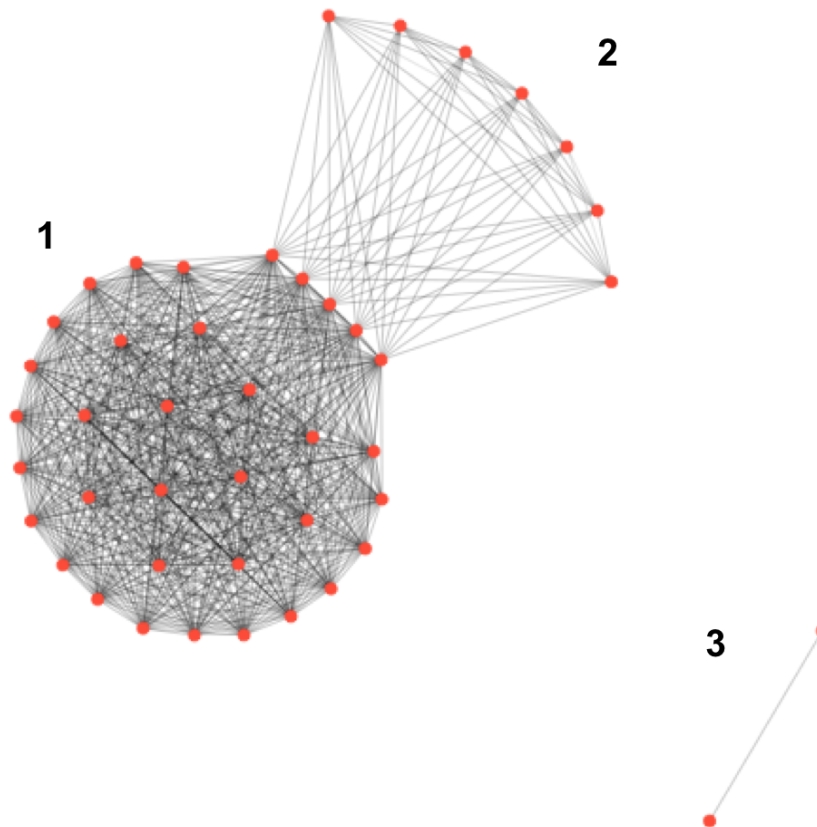


Figure 3.13: Summary of results of epitope binning on extracellular domain of human ROR1. The node plot shows different epitope regions bound by selected and characterised DARPins. Each red dot represents the respective DARPin binned. Grey connecting lines represent missing binding when binned against respective DARPin, representing binding of the same epitope region. Missing grey line between dots indicate binding on different epitope region. Number 1, 2 and 3 indicate the three regions targeted.

As of Figure 3.13 a third very rare epitope region, bound by only 5% of the selected DARPins, can be seen, representing a rather unfavoured unique binding area during directed evolution. Other than region one and two, this identified epitope showed no binder with overlapping binding of other regions, revealing a distinct binding region that is targeted by the two clones. Again as well as for the other two unique regions both clones binding this area are connected with each other, suggesting again binding of well defined small epitope regions that lie in overlapping proximity to each other. Notably, both clones binding this area evolved from the N2C library, while for epitope 1 and 2 binders from the libraries N2C, N3C and r+nr were found. A summary of the epitope regions for the tested DARPins is depicted in Table 3.8.

Table 3.8: Summary of epitope binning of DARPins evolved from previous selection. Epitope region targeted by respective clone indicated by number 1-3, as shown in Fig. 3.13.

Clone	Epitope Region	Clone	Epitope Region
B1w	1	G7w	1/2
C1w	1	H7w	1
E1w	1	B8w	1/2
H1w	1	H8w	1
A2w	1	A8b	1/2
E2w	1	C3b	1
F3b	1	A8w	1
B6w	1	E3w	1
F6w	1	H6w	1
C9b	1	D2b	1
E3b	1	E10b	1
F12b	1	G6b	1
G4w	1	A3w	2
G5w	1	G3w	2
C6w	1/2	E5w	2
D6w	1	D7w	2
E6w	1	A11b	2
G6w	1	B7w	2
C7w	1	A2b	2
D7w	1	D1w	3
C8b	1/2	C2w	3
H3w	1		

While binders of the epitope region 1 showed a high affinity in the pM range, DARPins that bound to the epitope regions 2 and 3 exhibited significantly lower affinities in the nM range. In order to increase the affinity towards these two further binding regions additional diversity was introduced and subsequent selection for improved off-rates using ribosome display selection was performed.

## 3.2 Affinity maturation of DARPins binding to the human ROR1 ECD

Based on the characterisation of DARPins evolved from the initial selection, binders with high affinity and good biophysical properties could be identified. These have been mapped by competitive SPR to bind three distinct epitope regions on the ECD of human ROR1. While the vast majority of approximately 29 clones bind to a dominant epitope region, 9 binders to different and distinguishable epitopes were identified. These usually had affinities between 3.4 and 7.6 nM with the exception of C2w, that exhibited a  $K_D$  of > 100 nM. In order to increase the affinity towards these two further binding regions additional diversity was introduced and subsequent selection for improved off-rates using ribosome display selection was performed. Clones, binding non-dominant epitope regions on human ROR1, were used as templates for introduction of additional diversity by random mutagenesis, using nucleotide analogues. The generated single clones or pools of clones were then selected independently for decreased off-rates from human ROR1 ECD by addition of a competitor target. Subsequently enrichment for specific binders was performed by an additional low stringency selection without competitor.

### 3.2.1 Introduction of Additional Diversity

For introduction of additional diversity all clones, as seen in Table 3.9 that have been mapped by competitive SPR (Table 3.8) to bind a distinguishable epitope region other than the most dominant epitope 1 on the ECD of human ROR1 and that showed good biophysical properties, as determined by SEC (see Figure 3.9), were chosen for further affinity maturation.

Table 3.9: DARPins subcloned for ribosome display selection round five and six.  
\* Clone F4w was not retrievable after selection

Clone	Epitope region	Library	Pool	$K_D$ [nM]
G3w	2	N3C	1	6.43
A3w	2	N3C	1	5.17
A2b	2	N3C	1	5.99
E5w	2	r+nr	2	0.06
A11b	2	N3C	3	4.03
C2w	3	N2C	4	153/3550
D7w	2	r+nr	5	1.47
B7w	2	r+nr	5	7.58
*F4w	2	r+nr	6	0.09
D1w	3	N2C	7	3.40

The introduction of additional diversity in the amino acid sequence of parental clones was performed by introduction of random mutations, using dNTP analogues dPTP and 8-oxo-dGTP. The gels presented in Figure 3.14 show the products of error-prone PCR with different dNTP analog concentrations, stained with ethidium bromide and exposed to UV light at 312 nm.

In lane UHP 3  $\mu$ M and UHP 9  $\mu$ M where no template DNA was added no DNA fragments could be detected. Only at very small fragment sizes a weak fluorescent signal

could be seen, representing the respective primers, added to the reaction mix. This confirmed that no unspecific amplification of DNA occurred during the polymerase chain reaction. In case of both reactions, using 3  $\mu\text{M}$  and 9  $\mu\text{M}$  of dPTP and 8-oxo-dGTP, respectively, a clear signal of stained DNA fragments could be observed for every template DNA. These fragments migrated similarly to fragments with about 930 bp length in case of clones evolved from the libraries N3C and r+nr and similarly to fragments with about 830 bp length in case of clones evolved from the library N2C, indicating the successful amplification of template DNA under presence of the respective concentrations of dNTP analogs.

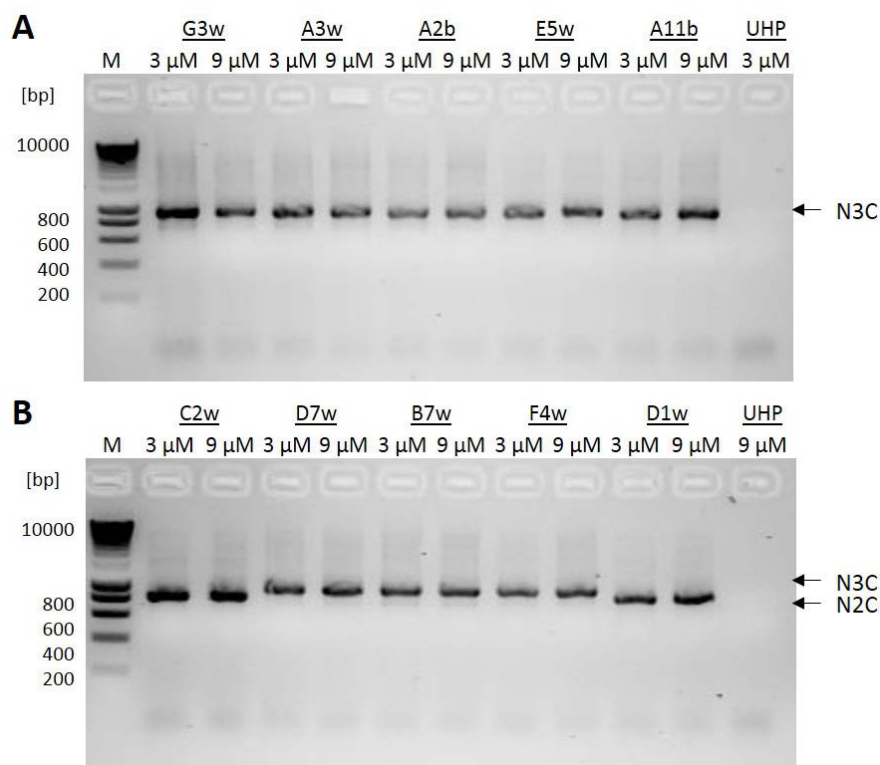


Figure 3.14: DNA products of error-prone PCR separated on a 1.5% agarose gel. (A) Clones G3w, A3w, A2b, E5w and A11b. (B) Clones C2w, D7w, B7w, F4w and D1w. M: Smart-Ladder DNA MW-1700-10, 3  $\mu\text{M}$ : epPCR reaction using 3  $\mu\text{M}$  dNTP analogs in addition to dNTP mix, 9  $\mu\text{M}$ : epPCR reaction using 9  $\mu\text{M}$  dNTP analogs in addition to dNTP mix. UHP: Negative control, using same reaction mix with 3  $\mu\text{M}$  dNTP analog but no template DNA. All products, controls and standard were visualised by intercalating ethidium bromide exposed to UV light at 312 nm wavelength.

In order to assess the mutational load, Sanger sequencing of selected clones derived from epPCR was performed. A mutational load of three mutations on average in the amino acid sequence with products derived from reactions with 3  $\mu\text{M}$  dNTP analogues was detected, as observed by sequence alignment. Products from epPCR reactions that contained 9  $\mu\text{M}$  dNTP analogues showed on average four mutations in the amino acid sequences.

After introduction of additional diversity, the respective products of clones G3w, A3w and A2b as well as of the clones D7w and B7w were pooled together due to high similar-

ities in respective sequences, affinities and biophysical properties.

### 3.2.2 Ribosome Display selection - Round 5

As Ribosome Display selection round five an off-rate selection was performed for decreased off-rates of DARPin binding human ROR1 ECD. Each clone was incubated with target bound to magnetic beads, and subsequently exposed to a  $10^4$  fold excess of non-biotinylated human ROR1 ECD for selection of DARPins with improved binding kinetics. DARPins were each panned against target and magnetic beads coated with streptavidin only as negative control.

In Fig. 3.15 the derived DNA products of the off-rate selection are shown. (A) Shows the DNA products of the PCR with the inner primer WTC4, annealing to the sequence encoding the C-terminus of the DARPin sequence, and EWT5, a pRDV specific primer binding to the RBS and beginning of the (His)<sub>6</sub> tag. In the non-template control (UHP) no DNA fragments could be seen. Only at very small fragment sizes a weak fluorescent signal could be seen, representing the respective primers, added to the reaction mix. This confirmed that no unspecific amplification of DNA occurred during polymerase chain reaction. In case of all pools a single band at the approximate size of 477 bp in case of clones evolved from the library N3C and r+nr as well as the approximate size of 369 bp in case of clones evolved from the library N2C could be seen, representing the expected sizes of DARPins selected from round five. This confirmed the successful amplification of clones after this very stringent panning step. In Figure 3.15 (A) it can be seen that the respective band intensity of the positive samples increases only marginally compared to the respective negative control where no biotinylated target was used during the panning step. This may represent a high amount of background binders, partially enriched by the stringent conditions applied in the off-rate selection. In all pools (P1, P3, P4 and P7) a successful amplification of clones could be seen with marginal increased intensity compared to its respective negative controls. This was not surprising since very stringent conditions for selection were chosen which only few clones might fulfill. Due to a high cycle number of 40, background signals are very likely to be amplified.

Since clones that evolved from the library r+nr differed in their capping repeats, the primers WTC4 and EWT5 were not applicable. As a result the primer Dif4 and Dir2 that bound outside of the capping repeats were used for amplification. In Figure 3.15 (B) DNA products of the PCR with primer Dif4 and Dir2 used for final amplification are shown. Again the PCR negative control, indicated as UHP, showed no DNA fragments, confirming that no unspecific amplification of DNA occurred during the polymerase chain reaction. With all pools a single band at the approximate size of 477 bp could be seen, representing the expected size of DARPins selected from round five. This confirmed the successful amplification of clones after this very stringent panning step. Unlike Figure 3.15 (A), a clearly stronger signal of band intensity in case of the positive samples could be seen compared to the respective negative control, considered with background binders only, representing an enrichment and higher amount of specific binders from this selection round in case of the pools P2, P5 and P6.

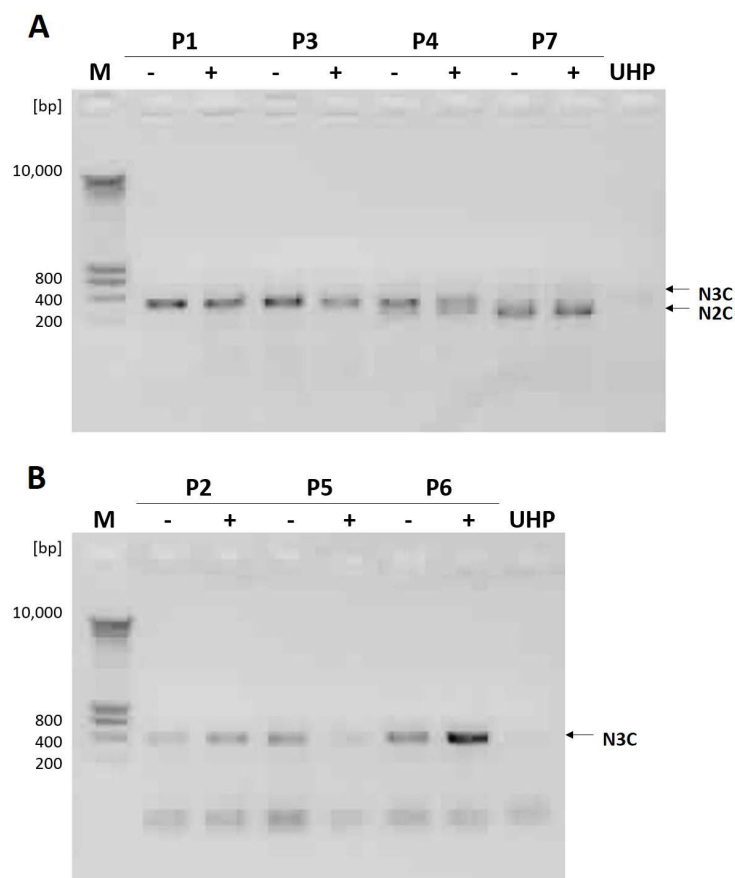


Figure 3.15: Agarose gel-electrophoresis of DNA products of RT-PCR products from selection round 5. Five  $\mu$ l of PCR reaction mix loaded each. M: Smart-Ladder DNA MW-1700-10. (-): Specificity control, PCR product of RT from selection with DARPins panned without target bound to magnetic beads. UHP: Negative control, using same PCR reaction mix without template DNA. (+): PCR products of RT from selection with DARPins panned against target. (A) PCR products of RT from selection round 5 using primer WTC4 and EWT5. (B) PCR products of RT from selection round 5 using primer Dif4 and Dir2. Left axis indicates the respective fragment length of DNA ladder in base pairs. All products, controls and standard were visualised by intercalating ethidium bromide exposed to UV light at 312 nm wavelength.

### 3.2.3 Ribosome Display selection - Round 6

In Ribosome Display selection round six a rescue round for enrichment of specific binders of human ROR1 ECD was performed. After pre-panning, each clone was incubated with biotinylated target immobilised via streptavidin to magnetic beads, and no competitor applied. DARPins were panned against target and against magnetic beads only as negative control.

In Figure 3.16 the derived DNA products of the off-rate selection are shown. (A) Shows the DNA products of the PCR with primer WTC4 and EWT5 used for final amplification using 30 cycles. In the non-template control (UHP) no DNA fragments could be seen. Only at very small fragment sizes a weak fluorescent signal could be seen, repre-

senting the respective primers, added to the reaction mix. This confirmed that no unspecific amplification of DNA occurred during polymerase chain reaction. In case of all pools a single band at the approximate size of 477 bp and in case of P4 and P7 of 369 bp could be seen in the respective positive sample, representing the expected size of DARPin selected from round six. This confirmed the successful isolation of remaining clones from the pre-panning and panning step.

In Figure 3.16 (A) it can be seen that the respective band intensity of the positive samples increases only marginally compared to the respective negative control where no biotinylated target was used during the panning step in case of pool number one. This may represent a higher amount of background binders being present in the pool. In case of pool number three a clearly stronger band intensity and therefore enrichment of specific binders could be seen compared to the respective negative control. Pool number four showed a stronger band intensity compared to the respective negative control at the expected size of about 369 bp, showing an enrichment of specific binders within this pool during the rescue round. A second rather weak band at 477 bp could be seen in the negative sample, and may be explained by a small cross-contamination from the neighbouring sample. Pool number seven showed a strong single band at approximately 369 bp. In case of the respective negative control a shift towards about 477 bp could be seen. This may have originated from a cross-contamination from another pool. Since no band at 477 bp in the positive sample occurred, an enrichment of specific binders evolved from pool seven could be expected.

Since clones that evolved from the library r+nr differed in their capping repeats, the primers WTC4 and EWT5 were again not applicable. As a result the primer Dif4 and Dir2 that bound outside of the capping repeats were used for amplification. In Figure 3.16 (B) DNA products of the PCR with primer Dif4 and Dir2 used for final amplification are shown. Again the PCR negative control, indicated as UHP, showed no DNA fragments, confirming that no unspecific amplification of DNA occurred during polymerase chain reaction. Within all pools a single band at the approximate size of 477 bp could be seen, representing the expected size of DARPin selected from round six. This confirmed the successful amplification of clones from the selection round. Compared to 3.16 (A) a clearly stronger band intensity in case of the positive samples could be seen within all pools. In case of pool number two and six no signal in the lane of negative sample could be seen, suggesting a strong eradication of background binders during the rescue round. In the negative control of pool number five a very weak band at 477 bp could be seen. Due to the very weak signal compared to the respective positive sample only very small number of remaining unspecific binders could be expected within the pool, suggesting a successful enrichment of specific binders of human ROR1 ECD during the sixth round of ribosome display selection.

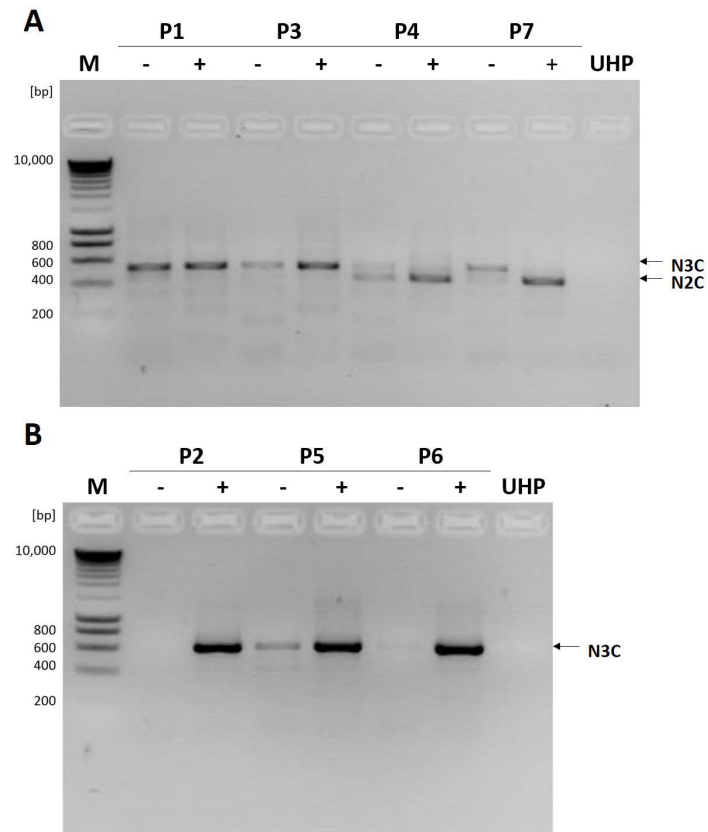


Figure 3.16: Agarose gel-electrophoresis of DNA products of PCR of RT products from selection round 6. 5  $\mu$ l of PCR reaction mix loaded each. M: Smart-Ladder DNA MW-1700-10. (-): Specificity control, PCR product of RT from selection with DARPins panned without target bound to magnetic beads. UHP: Negative control, using same PCR reaction mix without template DNA. (+): PCR products of RT from selection with DARPins panned against target. (A) PCR products of RT from selection round 6 using primer WTC4 and EWT5. (B) PCR products of RT from selection round 6 using primer Dif4 and Dir2. Left axis indicates the respective fragment length of DNA ladder in base pairs. All products, controls and standard were visualised by intercalating ethidium bromide exposed to UV light at 312 nm wavelength.

### 3.3 Characterisation of DARPins evolved from affinity maturation

Based on the final ribosome display selection for improved off-rates (Chapter 3.2) of DARPins that were mapped by competitive SPR to bind less dominant epitope regions on human ROR1 ECD, a screening for putative binder to human ROR1 and a subsequent characterisation of promising clones was performed.

#### 3.3.1 Crude extract ELISA

Crude extract ELISA is a solid-phase enzyme based immunoassay that allows for sensitive and robust detection of molecular interactions in small quantities and complex matrix such as cell lysate. Other than FRET-based methods this assay allows for signal intensities that are less dependent of the location of epitopes on the target.

DNA was cloned into the expression vector pQE30ss using *Bam*HI/*Hind*III. Single clones were picked and inoculated in 1 ml cultures in 96 well plates and expressed as described in Material and Methods 2. After expression the cell pellet was lysed using 13  $\mu$ l lysis buffer, as described in Table 2.4, and diluted with PBS<sub>T</sub>/BSA 0.1%. Due to the high sensitivity of the assay all samples were measured in a 1:5,000 dilution, which could potentially allow a better discrimination regarding affinity. 47 clones were analysed per pool. For detection of putative binders a primary antibody targeting a (His)<sub>4</sub> sequence on the DARPins' Histidin-Tag and a secondary antibody conjugated to alkaline phosphatase targeting the primary antibody was used (See Chapter 2, Table 2.22).

Crude lysate ELISA for the screening of putative candidates from the off-rate and subsequent specificity selection (sixth round of selection) showed distinct signal intensities that were equivalent to binding signals obtained by its respective parental clones. The binding signals are represented by the difference in absorption at 405 nm wavelength and 540 nm. Absorption at 540 nm was used to measure unspecific signals and to correct for respective errors. The difference in absorption at 405 nm wavelength is proportional to the amount of peroxidase immobilised, which is further approximately equimolar to the amount of ligand bound to target in the respective well.

#### Screening of DARPins from selection round 6

To test for the specificity of obtained signals in this assay several negative controls were measured. The negative control of each sample, containing reagents and DARPins only, showed a constantly low signal of about 0.015, confirming that no unspecific binding of DARPins to other than the target occurred. The negative control, containing target, DARPins and all reagents except of the first antibody (mAb1), binding the His-tag of DARPins, showed as well a low signal of around 0.016, confirming the specificity of mAb1. The second negative control, containing target, DARPins and all reagents except of the secondary antibody (indicated as mAb2) showed a similar signal as the first antibody, confirming the specificity of the second antibody to the respective mAb1.

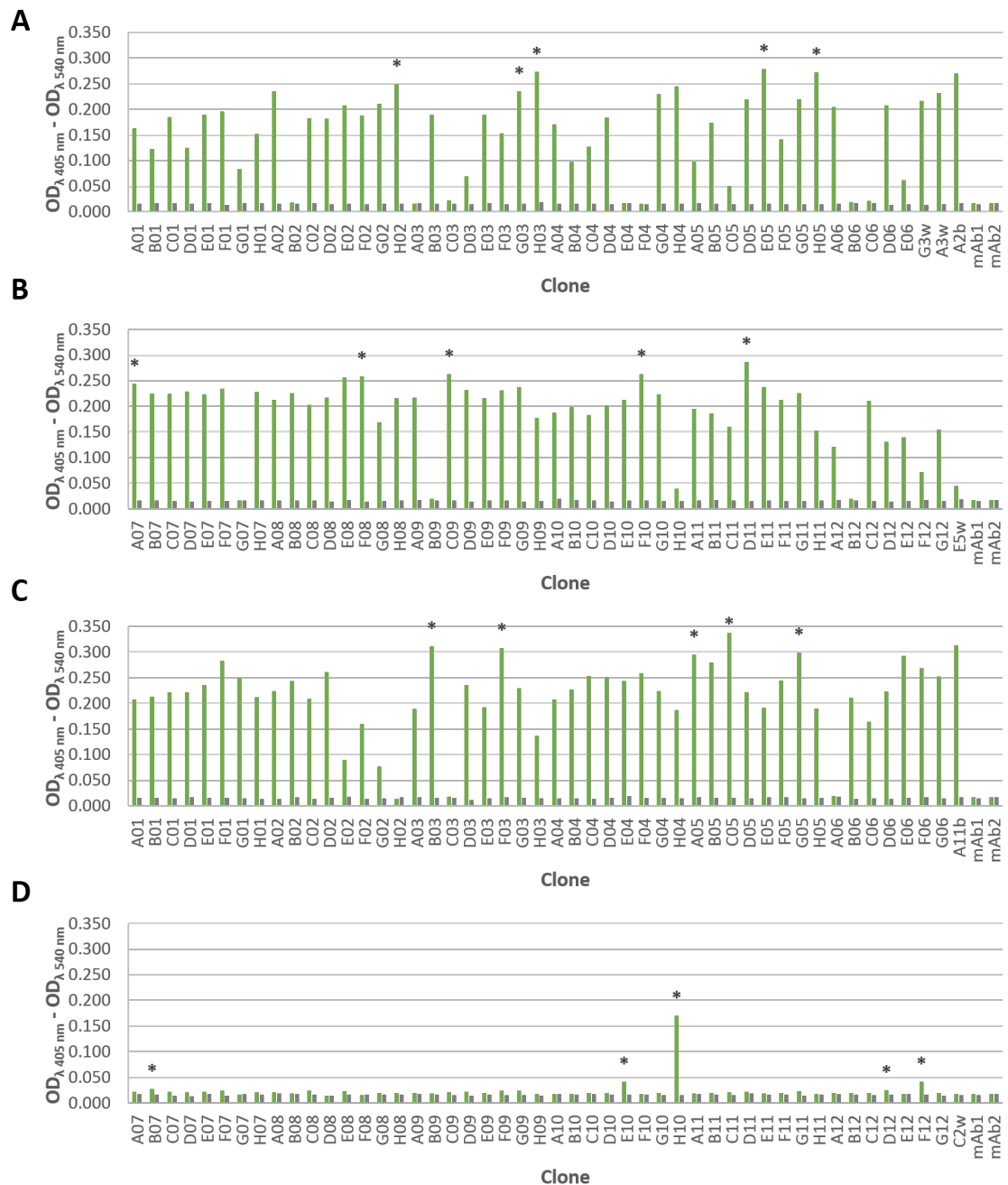


Figure 3.17: Crude extract ELISA of clones evolved from off-rate selection. Signal plotted as the difference in absorption at 405 nm and 540 nm wavelength. All samples were measured and plotted in a 1:5,000 dilution. Green: measured absorption of samples including target human ROR1 ECD and respective DARPin. Gray: negative control using reagents and DARPins only. (A) Clones evolved from P1 (44 clones). (B) Clones evolved from P2 (45 clones). (C) Clones evolved from P3 (45 clones). (D) Clones evolved from P4 (45 clones). mAb1: negative control using target and first antibody only. mAb2: negative control using target and second antibody only. The name of each clone refers to its position on the respective expression plate. Clones that were selected for further sequence analysis are highlighted with \*.

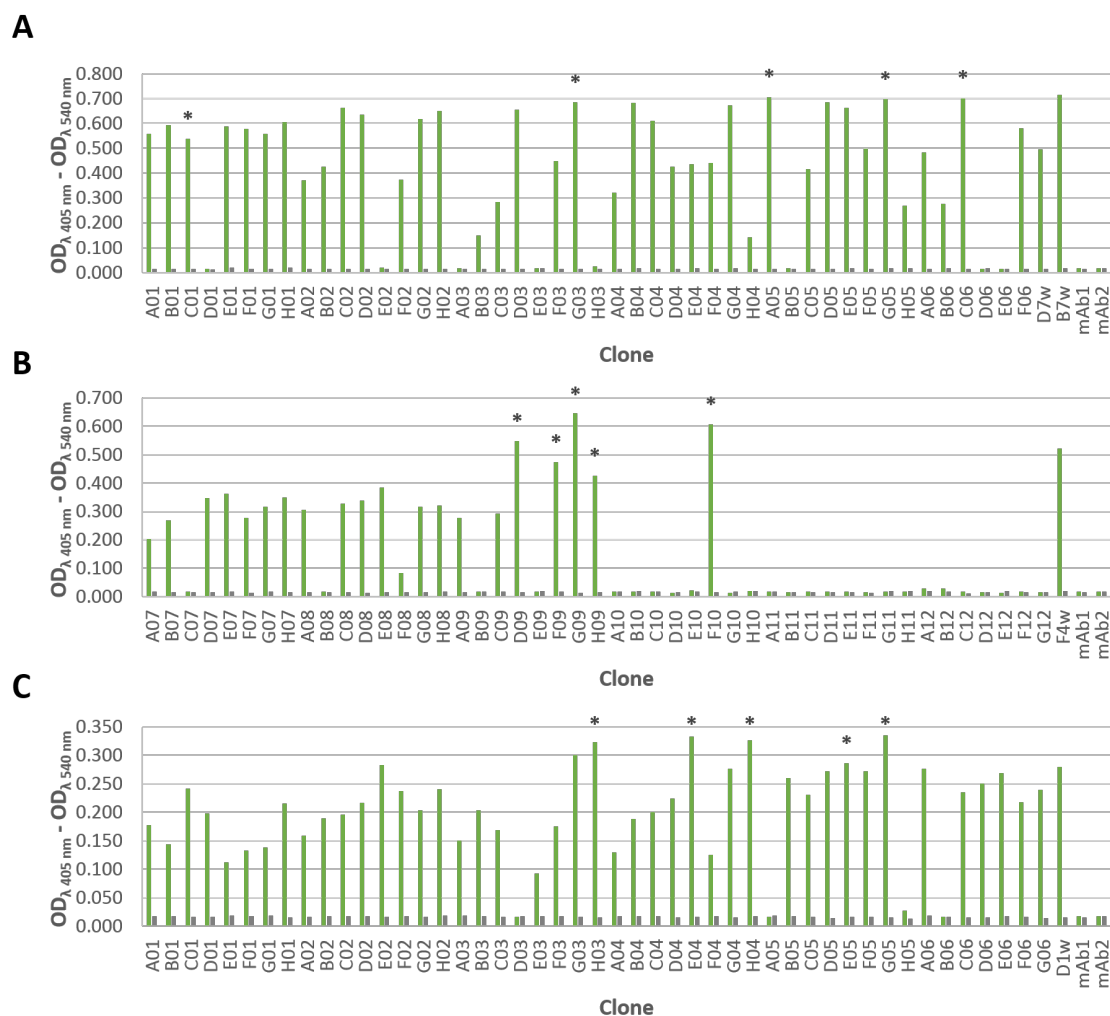


Figure 3.18: Crude extract ELISA of clones evolved from off-rate selection. Signal plotted as the difference in absorption at 405 nm and 540 nm wavelength. All samples were measured and plotted in a 1:5,000 dilution. Green: measured absorption of samples including target human ROR1 ECD and respective DARPin. Gray: negative control using reagents and DARPins only. (A) Clones evolved from P5 (44 clones). (B) Clones evolved from P6 (45 clones). (C) Clones evolved from P7 (45 clones). mAb1: negative control using target and first antibody only. mAb2: negative control using target and second antibody only. The name of each clone refers to its position on the respective expression plate. Clones that were selected for further sequence analysis are highlighted with \*.

Figure 3.17 shows the results of the crude extract ELISA for the screening for putative binder of human ROR1 ECD, that evolved from the sixth round of ribosome display selection. (A) Shows the results of the screening of clones evolved from the first pool (P1) derived from the sixth round of ribosome display selection. The parental clones derived from the first pool, indicated as G3w, A3w and A2b on the right panel of Figure 3.17, showed a distinct increase in signal compared to the respective negative controls where target was omitted. The signal intensities ranged between 0.220 and 0.270. The parental clone A2b, that showed the lowest affinity of parental DARPins as determined by SPR (Section 3.1.8) showed the highest signal with 0.270. Almost all selected clones

evolved from the first pool of off-rate selection, showed a signal significantly higher than background, indicating the specific binding of human ROR1 ECD. Only six clones of the analysed pool showed no or only marginal signals over background. About 87% of analysed clones showed a specific binding to the target in crude lysate. Among the positive clones a signal intensity of about 0.170 on average was detected. 31% of the analysed DARPins showed a signal that was similar to the parental clones, exhibiting difference in absorption between 0.220 and 0.270. Three clones revealed higher signals than any of the respective parental clones, ranging from 0.272 to 0.275.

(B) shows the results of the screening of clones evolved from the second pool (P2). The parental clone of the derived pool number two, indicated as E5w on the right panel of Figure 3.17 (B), showed a distinct signal intensity compared to the respective negative control without target, exhibiting a difference in absorption of about 0.045. Almost all selected clones evolved from the second pool of off-rate selection showed a signal that was significantly higher than the background, indicating the specific binding of human ROR1 ECD. Only three clones of the second pool showed no or only marginal signal over background, resulting in about 93% of analysed clones that showed a specific binding to the target in crude lysate. Among the positive clones a signal intensity of about 0.190 on average was detected. All positive clones showed a signal that was higher than the measured parental clone E5w. The highest signal was measured with about 0.280, being about six times higher than the signal derived from E5w. The average and range of signals of the positive clones is similar to the signals of parental clones from the first pool.

As of Figure 3.17 (C), clones evolved from the third pool (P3) showed distinct signals. The parental clone of the third pool, indicated as A11b on the right panel of Figure 3.17, showed a distinct increase in signal compared to the respective negative control with missing target, exhibiting a measured difference in absorption of about 0.320. Except of three DARPins, all selected clones from the third pool of off-rate selection, showed a signal significantly higher than the background, indicating the binding of human ROR1 ECD. The other three clones of the analysed pool showed no or only marginal signal over background, resulting in about 93% of analysed clones that showed a positive binding to the target in crude lysate. On average a signal intensity of about 0.200 was detected among clones that showed a signal higher than background. The highest signal was measured with about 0.340. Only the clone with highest measured absorption showed a signal that was higher than the parental clone A11b.

Figure 3.17 (D) shows the results of the screening of clones evolved from the fourth pool (P4). The parental clone, indicated as C2w on the right panel of Figure 3.17, showed only a marginally increased signal compared to the respective negative control, where target was omitted, with a measured difference in absorption of about 0.018. The vast majority of selected clones from the fourth pool of off-rate selection showed a signal that was similar to the measured absorption of the respective parental clone, exhibiting signals that were only marginally higher than the background, indicating a similar binding affinity of human ROR1 ECD as C2w in crude lysate. About 67% of the analysed clones showed a slightly higher difference in positive signal than the respective parental clone. The highest absorption was measured with H08 that exhibited a signal of about 0.170, which was about 10-fold higher than the signal derived from C2w. The clones E10 and F12 showed signals that were 2.0 to 2.5 times higher than the respective parental clone.

As of Figure 3.18 (A), clones that evolved from the fifth pool (P5) of the sixth round of ribosome display showed distinct signals of binding. The parental clones of the derived pool number five, indicated as D7w and B7w on Figure 3.18, showed a significantly increased signal compared to the respective negative control with missing target. The parental clone D7w resulted in a difference of absorption of about 0.495. For B7w an absorption of about 0.710 was measured. About 82% of analysed DARPins evolved

from the fifth pool of off-rate selection showed a signal that was higher than the background, indicating the binding of human ROR1 ECD in crude lysate. Only eight clones of the analysed pool showed no or only marginal signal over background. On average a signal intensity of about 0.450 was detected among clones that showed a signal higher than background. The highest signal was measured with a difference in absorption of about 0.705. 23 clones showed a signal higher than the parental clone D7w. In contrast to D7w no DARPins with an absorption signal that was higher than the parental clone B7w could be seen.

Figure 3.18 (B) shows the results of the screening of DARPins that evolved from the sixth pool (P6) of the sixth round of ribosome display selection. The parental clone of the derived pool number two, indicated as F4w on 3.18, showed a distinct increase in signal compared to the respective negative control with missing target, with a measured signal of about 0.280. Almost all selected clones evolved from the second pool of off-rate selection exhibited a signal that was higher than the background, indicating a binding of the target human ROR1 ECD. Only three clones of the analysed pool showed no or only marginal signal over background, resulting in about 93% of analysed clones that were considered as specific binder of the target in crude lysate. Among the positive clones a signal intensity of about 0.200 on average was detected. The highest signal was measured with a an absorption of about 0.335. Seven clones from the analysed pool six of off-rate selection showed a signal that was higher than the respective parental clone F4w.

As of Figure 3.18 (C), DARPins that evolved from the seventh pool (P7) of the sixth round of ribosome display selection showed distinct signals that were higher than the background. The parental clone of the derived pool number seven, indicated as D1w on Figure 3.18, showed a significantly increased signal compared to the respective negative control with missing target. The parental clone D1w showed an absorption of about 0.515. About 44% of analysed DARPins, evolved from the seventh pool of off-rate selection, showed a signal significantly higher than the background, indicating the binding of human ROR1 ECD in crude lysate. About 56% of the screened clones showed no or only marginal signal over background. On average a signal intensity of about 0.310 was detected among positive clones that showed a signal higher than background. The highest signal was measured with a difference in absorption of about 0.625. A signal that was 1.2 times higher than the respective parental clone. Only three clones showed a signal higher than the parental clone D1w.

Within analysed clones from the sixth round of ribosome display selection a significant number of clones that showed a signal over background could be identified. Five clones of each pool that showed the highest signals within each pool (highlighted as '\*') were further analysed by Sanger sequencing, in order to identify the sequence of the putative binder as well as to evaluate its similarities and putative conclusions towards distinct sequence families and properties.

### 3.3.2 Sequence Analysis

DARPins after the final round of ribosome display selection that putatively bound human ROR1 were identified using ELISA, sequences of the 5 most promising clones of each pool that showed the highest signals were analysed using Sanger sequencing.

In Figure 3.19 the sequence alignment of DARPins evolved from pool P1 is shown. P1H2 appeared to be a double clone and was therefore not included in the alignment. Almost all clones differed only in a one or two residues in its sequence. This new diversity mainly occurred in positions of framework residues, with two clones (P1G3 and P1H3)

showing the identical sequence. Furthermore, all clones seemed to originate from the parental clone G3w, suggesting a certain evolutionary advantage towards the sequence of this clone. Furthermore, the parental clone A2b has the identical sequence as clone G3w.

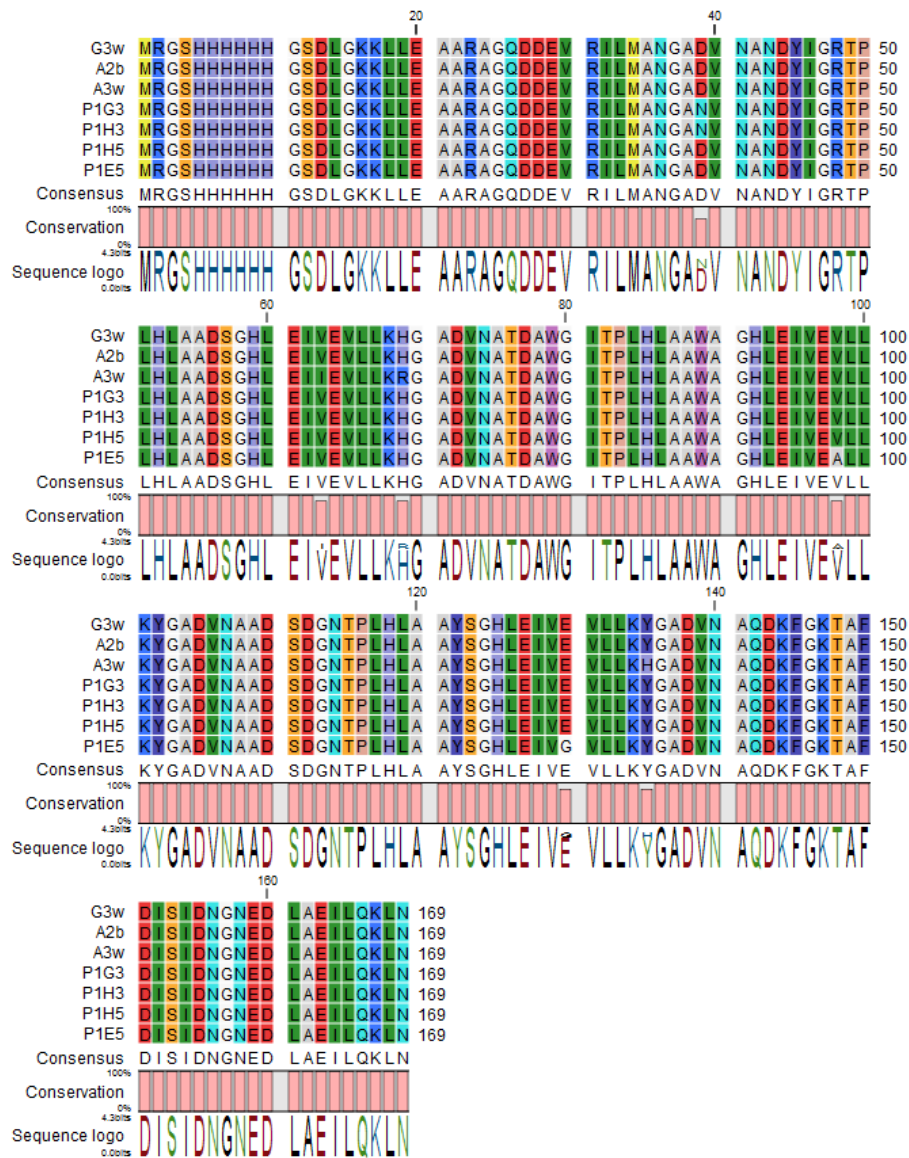


Figure 3.19: Sequence analysis of screened clones selected from from pool P1. G3w, A3w and A2b represent the respective parental clones. Nucleotide sequences were derived by Sanger sequencing. All sequences were translated to protein sequence *in silico* and aligned using CLC software. Clones are listed according to its similarity. Each letter within the the amino acid sequence represents the respective single-letter amino acid code. This applies as well to Figure 3.20, 3.21, 3.22, 3.23, 3.24 and 3.25.

In case of DARPins evolved from pool P2 of ribosome display selection round six no sequence diversity could be found. P2F10 appeared to be a double clone and was therefore not included in the alignment. As of figure 3.20 all DARPins selected and screened from this round showed the identical sequence. Alignment with all other pools revealed

a sequence identity with G3w, which represents a parental clone from the first pool. A possible explanation could be a contamination by this DARPin during the off-rate selection and further favouring of this clone due to its preferential binding in advance of all other clones during the panning procedure.

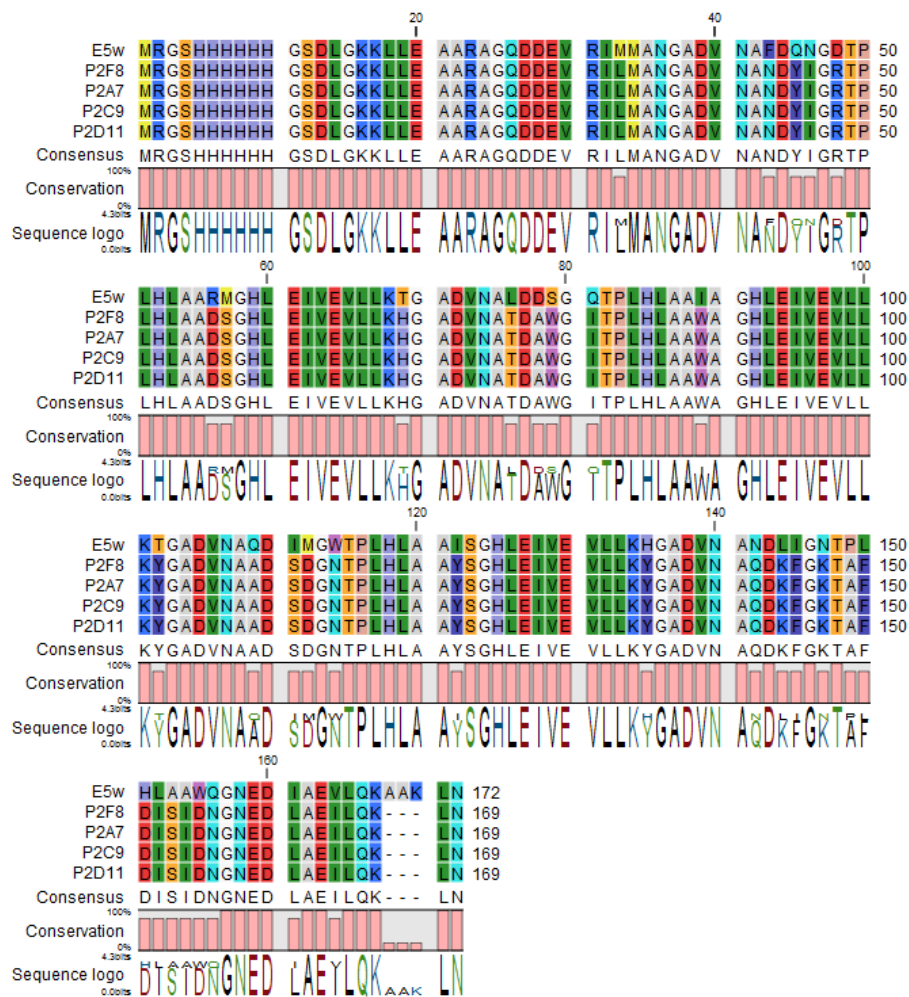


Figure 3.20: Sequence analysis of screened clones selected from pool P2. E5w represents the respective parental clone.

Figure 3.21 shows the sequence alignment of clones evolved from pool P3, starting from the clone A11b, which contained a cystein at position 80. Almost all clones differed only in a one or two amino acids in its sequence. Only clone P3B3 showed a greater diversity, with four residues deviating from other DARPins. P3C5 and P3F3 exhibited an identical sequence to its parental clone A11b. All selected DARPins retained a cystein at position 80, which could have a potential effect on the biophysical properties of the selected clones, e.g. leading to dimerisation.

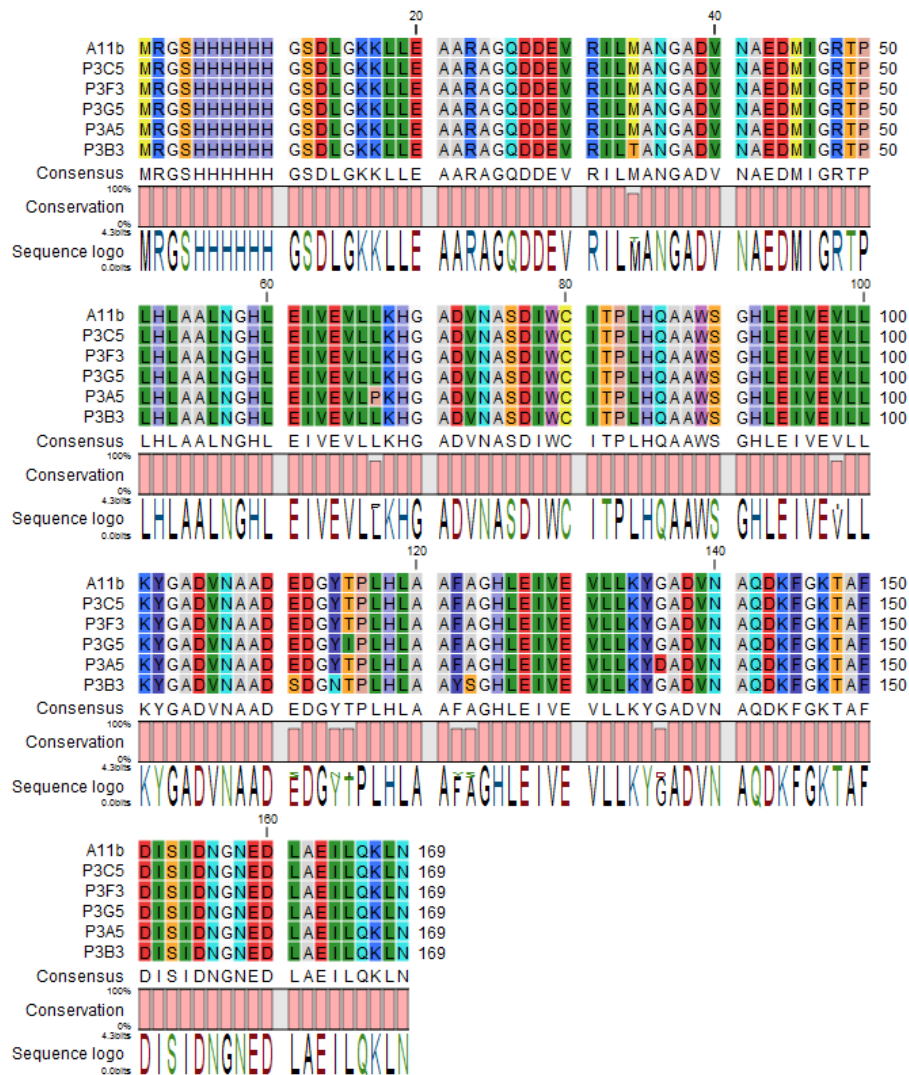


Figure 3.21: Sequence analysis of screened clones selected from pool P3. A11b represents the respective parental clone.

In Figure 3.22 the sequence alignment of DARPins evolved from pool P4 using clone C2w is shown. Almost all clones differ only in one or two residues in its sequence. In case of P4E10, P4D12 and P4F12 only one residue each was substituted compared to the parental clone C2w. Clone P4E10 exhibited a V96A mutation, clone P4F12 deviated with A87T and clone P4D12 showed a mutation at T49A. In case of P4H10 two mutations, V96A and A87T, occurred. One selected clone, P4B7, exhibited an identical sequence with the parental clone C2w.

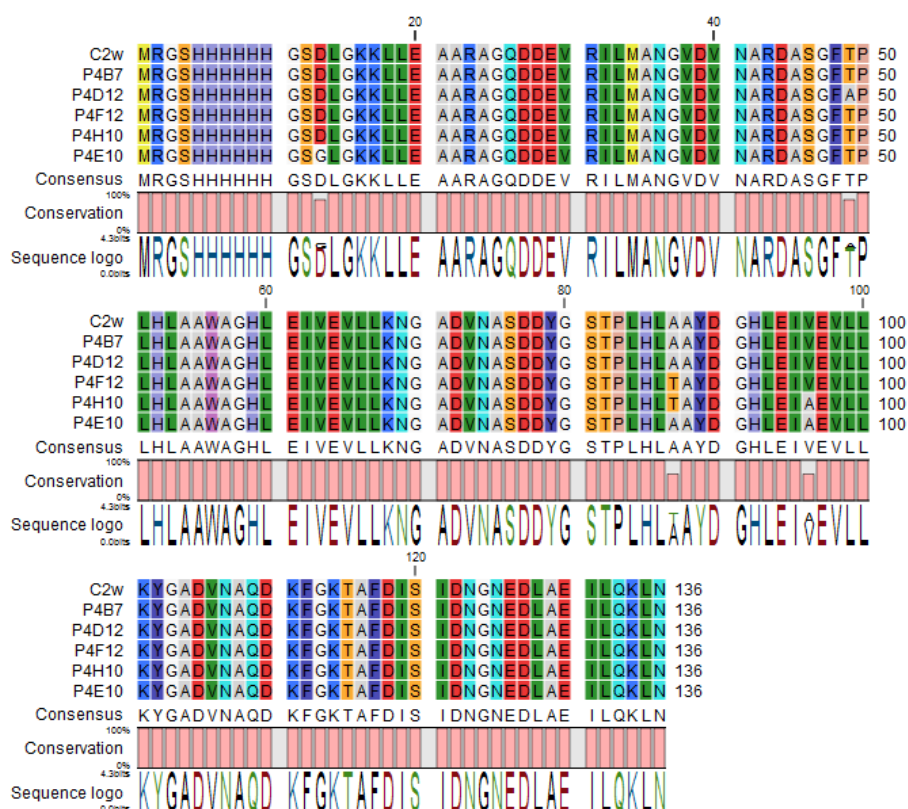


Figure 3.22: Sequence analysis of screened clones selected from pool P4. C2w represents the respective parental clone.

Figure 3.23 shows the alignment of sequences derived from pool P5 using the clones B7w and D7w. It can be seen that all clones selected from this pool had a strong sequence similarity with the parental clone B7w, exhibiting a lower  $K_D$  of 7.58 nM than the clone D7w with a  $K_D$  of 1.47 nM. Almost all clones showed only two or three mutations of residues in its sequence compared to B7w, suggesting a tendency towards this sequence. When compared to clones binding the dominant epitope region a great similarity with F3b, which exhibited a far lower  $K_D$  of 0.04 nM, could be seen. The sequences of B7w and F3b deviate by only one residue, suggesting a strong evolutionary trend towards the sequence of F3b due to strong similarity to the parental clone B7w and higher affinity. The clone P5G3 exhibited a single mutation of V105. P5C6 showed two mutation with N36D and V105D. P5A5 exhibited a mutation according to S43P and V105D. The clone P5C1 showed the exchange of three residues with V30A, L77P and V105D. P5G5 showed two mutations of A54T and V105D.

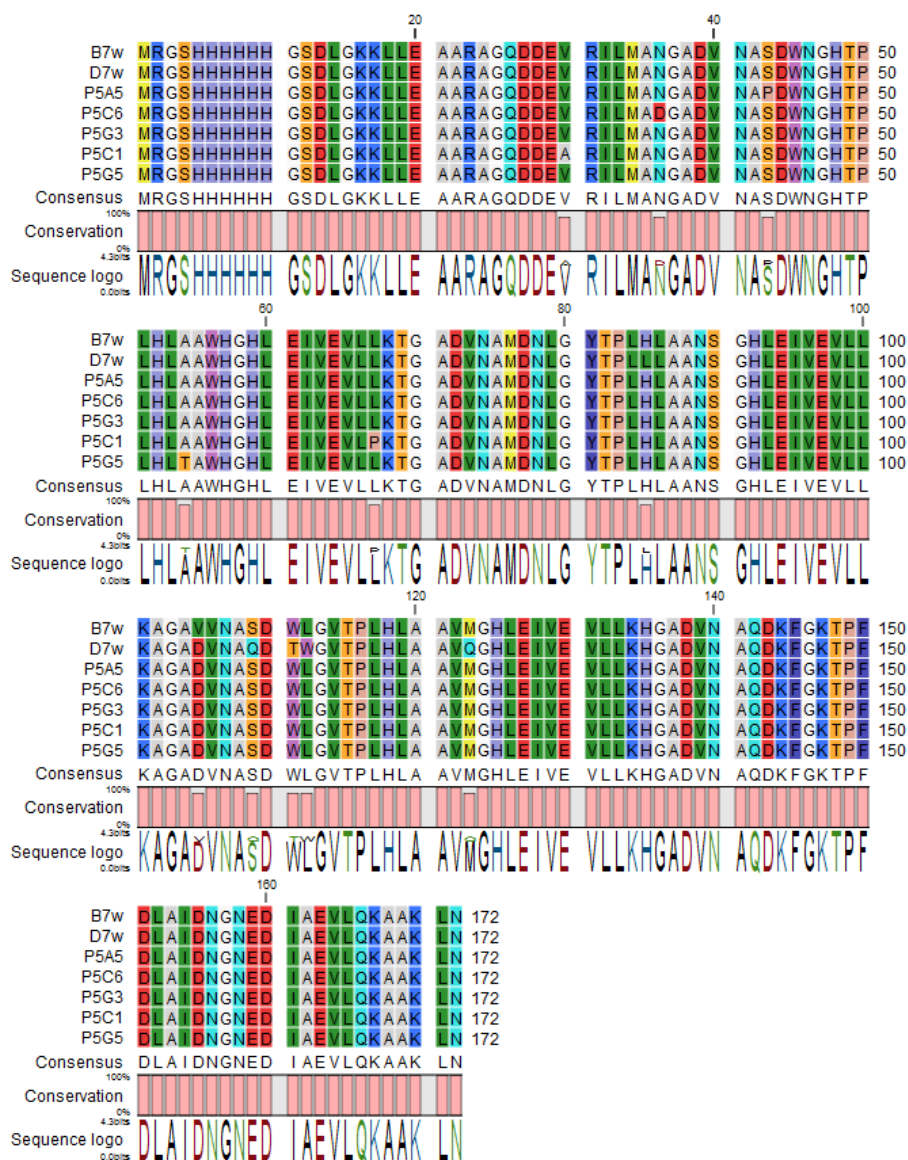


Figure 3.23: Sequence analysis of screened clones selected from pool P5. D7w and B7w represent the respective parental clones.

In Figure 3.24, the sequence alignment of DARPinS evolved from pool P6 based on clone F4w can be seen. Three clones appeared to be double clones and were therefore not included in the alignment. The sequences of the two remaining clones, P6G9 and P6H9, had no sequence similarity with the parental clone F4w. P6G9 deviated with 14 residues compared to its parental clone. The selected clone P6H9 showed 20 mutations compared to its parental clone. When aligned with all other clones a sequence identity of P6H9 with G3w could be observed. This might could be explained by a contamination during the off-rate selection. Furthermore, no sequence identity of F4w with sequence data obtained by previous sequencing of F4w could be seen. Due to this mismatch with previous sequencing results a definite identity of F4w with respect to its sequence and biophysical properties was not possible and this pool, as a consequence, excluded from further characterisation.

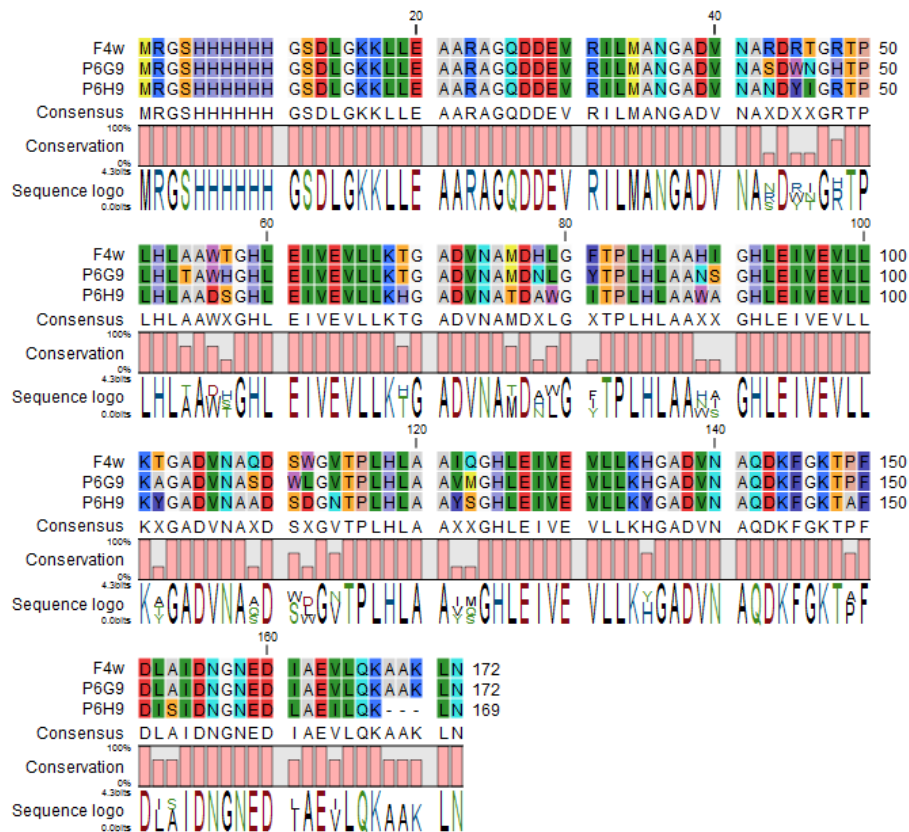


Figure 3.24: Sequence analysis of screened clones selected from pool P6. F4w represents the respective parental clone.

As shown in Figure 3.25, the alignment of sequences of clones evolved from pool P7 using the clone D1w revealed a strong sequence similarity. P7E4 appeared to be a double clone and was therefore not included in the alignment. While P7E5 being identical with the parental clone D1w, all other clones showed only a single mutation. Clone P7H3 deviated with F117L while clone P7H4 exhibited a A24V mutation and clone P7G5 showed two exchanged residues with A35T and A128T with respect to its parental clone D1w.

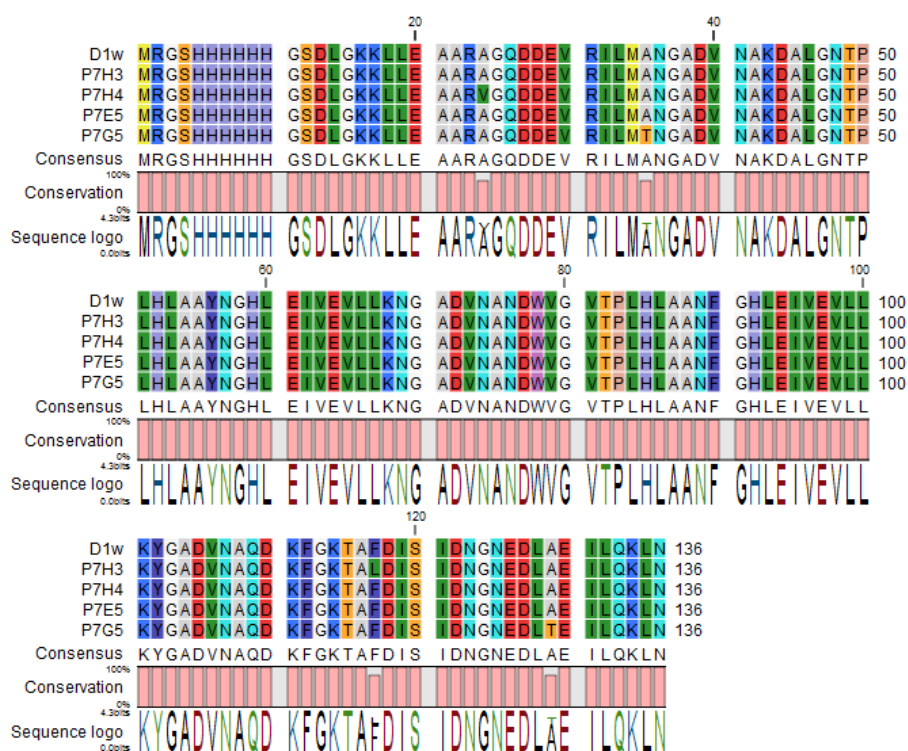


Figure 3.25: Sequence analysis of screened clones selected from pool P7. D1w represents the respective parental clone.

All DARPins that exhibited an identical sequence or appeared to be double clones were excluded from further characterisation. While a sequence diversity of on average 4 to 5 amino acid was introduced prior to selection, a decrease in diversity to 1 to 3 residues on average was observed, suggesting strong evolutionary trends towards the existing clones that were used for further affinity maturation. All 18 DARPins that did not appear to be a double clone or had an identical sequence to another clone were further expressed, purified and characterised for their oligomeric behaviour, using size exclusion chromatography, affinity, using SPR, and cell binding.

### 3.3.3 Expression and Purification of DARPins

Each DARPIn was expressed in 50 ml culture using shake flasks and induction with 500  $\mu$ M IPTG for 5 h and purified using IMAC with washing steps of 20 CV TBS-W, 20CV TBS-W high salt, 20 CV TBS-W low salt and 10 CV TBS-W as well as a subsequent buffer exchange to  $1 \times$  PBS, pH 7.4 using PD10 columns. The protein concentration was determined by using the  $OD_{280}$ . DARPins were analysed using SDS-PAGE and stained with Coomassie in order to assess the purity.

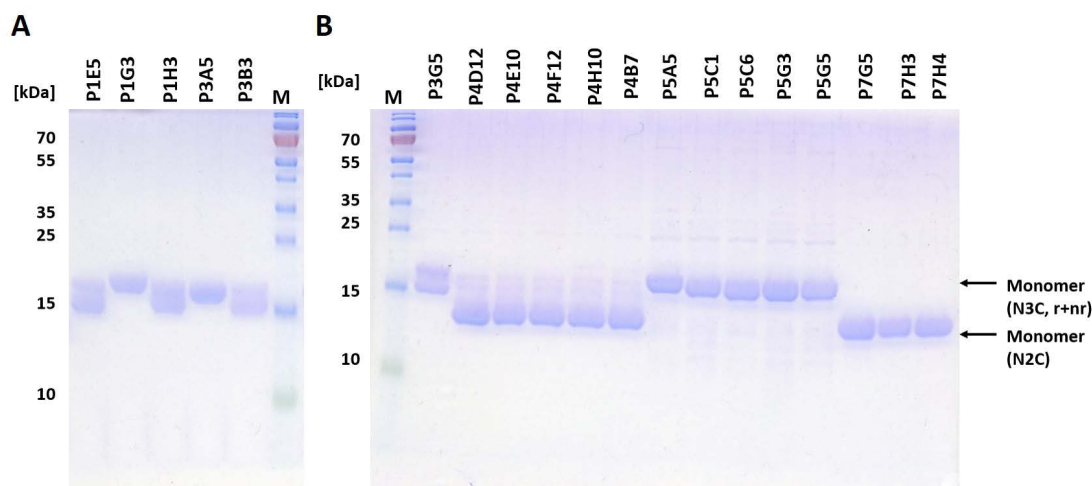


Figure 3.26: SDS-PAGE of purified DARPins. Five  $\mu\text{g}$  protein per sample were loaded on a 15% SDS-PAGE and stained using Coomassie blue. M - Molecular Weight Standard, PageRuler 180 – 10 kDa. Clones derived from off-rate selection (A) Clones from first and third pool purified (B) Clones from third, fourth, fifth and seventh pool purified.

As of Figure 3.26 the expressed and purified DARPins evolved from off-rate selection can be seen. The separated samples, loaded after incubation at  $96^\circ\text{C}$  for 6 min in  $1 \times$  Laemmli buffer, could be seen in each respective lane. In each lane DARPins at their expected size range could be seen. Purified DARPins showed a purity of  $> 95\%$ . All clones yielded several milligrams of protein produced during expression, ranging from 1.4 mg to 6.4 mg DARPin per 50 ml culture. The purified DARPins were then used to characterise their biophysical properties regarding to their oligomeric behaviour by using size exclusion chromatography.

### 3.3.4 Analytical Size Exclusion Chromatography (SEC)

For characterisation of the biophysical properties of DARPins regarding to their oligomeric behaviour, analytical size exclusion chromatography of DARPins selected after sequence analysis was performed to assess their tendency for aggregation and oligomerisation.

All DARPins were analysed after purification and removal of Imidazole by buffer exchange. All were analysed according to the respective pools as to be seen in Table 3.10. All parental clones were again analysed by SEC for comparability of the individual elution profiles.

Table 3.10: DARPins evolved from the sixth round of selection and characterised by SEC

Clone	Pool	Clone	Pool
P1E5	1	P4H10	4
P1G3	1	P5A5	5
P1H3	1	P5C1	5
P3A5	3	P5C6	5
P3B3	3	P5G3	5
P3G5	3	P5G5	5
P4D12	4	P7G5	7
P4E10	4	P7H3	7
P4F12	4	P7H4	7

Figure 3.27 shows the summary of the analytical size exclusion chromatography of selected clones evolved from the final affinity maturation.

(A) shows the first pool (P1) of the sixth round of ribosome display selection. All analysed DARPins showed a similar elution profile. As well as of the parental clones, G3w, A3w and A2b, no additional shoulder, drift or tailing of the peak could be seen with these DARPins.

(B) shows the summary of the analytical size exclusion chromatography of selected clones from pool number three (P3) evolved from the sixth round of ribosome display selection. All DARPins eluted primarily in a single peak at the expected size of monomeric DARPIn. In addition an increased signal between 50 kDa and 160 kDa can be seen, suggesting a partial aggregation of the respective DARPins.

(C) shows the summary of the analytical size exclusion chromatography of selected clones from pool number four (P4) evolved from the sixth round of ribosome display selection. All analysed DARPins, evolved from this pool, exhibited an almost identical elution profile to its respective parental clone C2w. As well as of the parental clone, no significant additional shoulder, drift or tailing of the peak could be seen with these DARPins.

(D) shows the summary of the analytical size exclusion chromatography of selected clones evolved from the fifth pool (P5) of off-rate selection. All analysed clones, evolved from this pool, showed an almost identical elution profile to the two parental clones B7w and D7w, eluting in a single peak at the respective size of a monomeric DARPIn consisting of five repeat units.

(E) shows the elution profiles of the analytical size exclusion chromatography of selected clones from pool number seven (P7) evolved from the sixth round of ribosome display selection. All analysed DARPins eluted in a single peak at the respective size of a single DARPIn consisting of four repeats units, without drift or tailing. In contrast to the elution profile of D1w, two out of three analysed clones showed an additional shoulder next to the main peak.

The vast majority of analysed DARPins maintained the same characteristic elution profile as its respective parental clones.

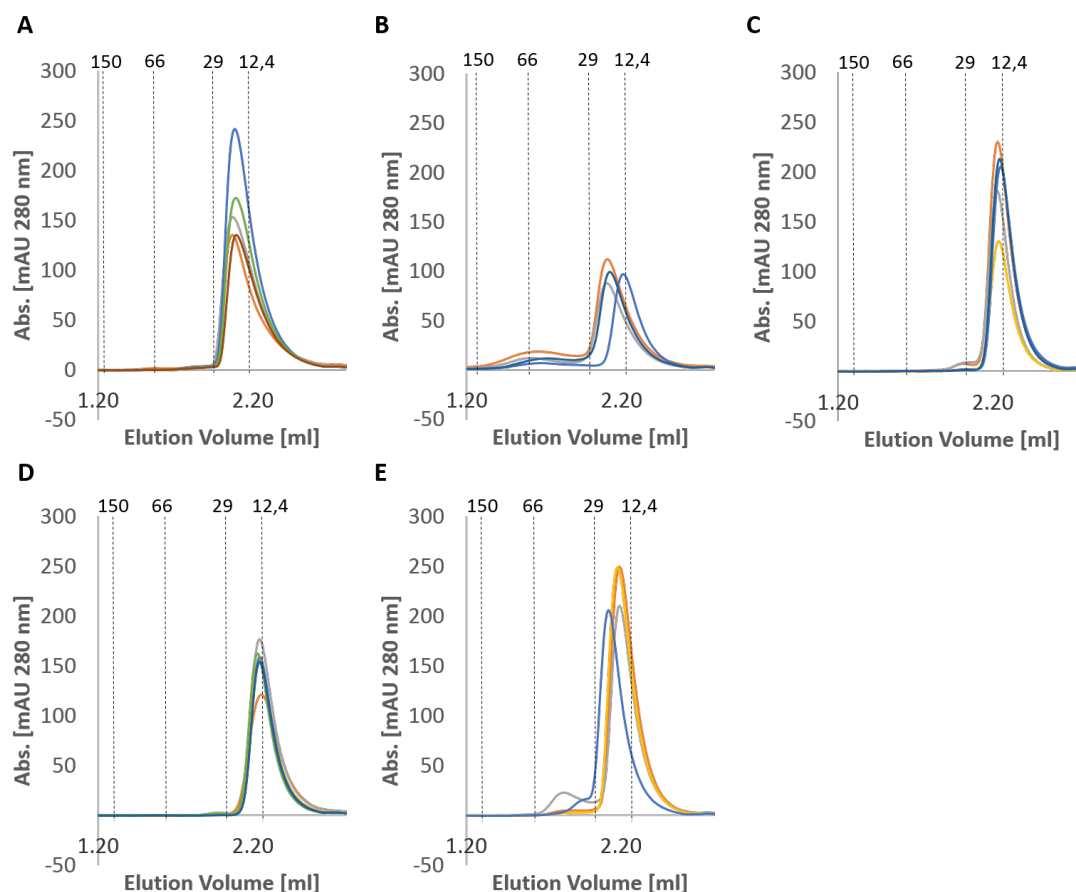


Figure 3.27: Analytical SEC of DARPins from the first pool evolved from round six of ribosome display selection. [A] DARPins evolved from pool P1. The parental clones are indicated as orange (G3w), light gray (A3w) and yellow (A2b) line. [B] DARPins evolved from pool P3. The parental clone is indicated as orange line (A11b). [C] DARPins evolved from pool P4. The parental clone is indicated in orange (C2w). [D] DARPins evolved from pool P5. The parental clones are indicated as orange (D7w) and gray (B7w). [E] DARPins evolved from pool P7. The parental clone is indicated in orange (D1w). Curves represent the elution profile of each single clone at  $OD_{280}$ , after purification and removal of imidazole by buffer exchange. For each run 50  $\mu$ l of a 10  $\mu$ M protein-solution was loaded onto a Superdex 200 column with  $1 \times$  PBS pH 7.4 at a flow rate of 0.4 ml/min. All curves plotted as Abs. [mAU 280 nm] vs. elution volume [ml]. The elution profile of MW standard (150 kDa, 66 kDa, 29 kDa and 12.4 kDa) is represented by dashed black vertical lines.

### 3.3.5 Multi Angle Light Scattering (MALS)

To confirm the results obtained by SEC alone, SEC coupled to MALS was performed. With multi angle light scattering one can determine the actual molecular mass of the protein in their eluting peak independent of their elution profile. For this purpose all DARPins as analysed in Section 3.3.4 were analysed using SEC-MALS. For each run 50  $\mu$ l of a 50  $\mu$ M protein-solution was loaded onto a Superdex 200 column with  $1 \times$  PBS pH 7.4 at a flow rate of 0.5 ml/min and the eluting protein detected by UV detection at  $OD_{280}$ ,

followed by static light scattering and refractive index detection on line.

Table 3.11: Summary of SEC coupled to multi angle light scattering of DARPins evolved from ribosome display selection round six. Mw refers to molecular weight as determined by MALS while theoretical Mw refers to the molecular weight expected from the sequence. Mass fraction shows the accumulated mass as represented by the analysed peak. BSA: Bovine Serum Albumin, representing molecular weight standard (66.5 kDa).

Clone	theoretical	Peak 1		Peak 2	
	Mw [kDa]	Mw [kDa]	Mass fraction [%]	Mw [kDa]	Mass fraction [%]
BSA	66.5	65.5	79.3	131.6	17.1
P1E5	18.1	19.8	100	-	-
P1G3	18.2	20.1	100	-	-
P1H2	18.2	18.9	86.5	36.4	13.5
P3A5	18.4	19.2	94.3	146.5	5.7
P3B3	18.3	17.9	93.9	52.5	2.8
P3G5	18.3	19.2	94.2	106.8	5.5
P4D12	14.7	14.3	100	-	-
P4E10	14.6	14.2	100	-	-
P4F12	14.8	14.1	100	-	-
P4H10	14.7	14.4	100	-	-
P5A5	18.5	17.8	99.0	37.3	1.0
P5C1	18.5	18.0	100	-	-
P5C6	18.4	18.1	99.1	52.2	0.9
P5G3	18.5	17.8	97.2	35.6	2.8
P5G5	18.4	17.9	99.1	25.4	0.9
P7G5	14.7	15.4	86.8	51.8	13.2
P7H3	14.6	16.2	98.8	39.9	1.2
P7H4	14.7	21.3	96.7	50.0	3.3

In Table 3.11 the summary of SEC- MALS for the characterisation of biophysical properties of DARPins selected from selection round six is shown. The detailed elution profiles and detected masses of all DARPins can be found under Supplementary Data. All DARPins included a N-terminal RGS(His)<sub>6</sub> tag. For creating a summary of SEC-MALS, only the calculated molecular mass of eluting protein and its respective mass fraction are presented in the table. The elution profile of each clone was detected by UV<sub>280</sub> and the respective molecular weight of each peak calculated using the Zimm equation.

The vast majority of selected clones appeared to be monomeric, to be seen by the identified molecular weight of eluting monomeric DARPIn, representing 98% to 100% of the eluting mass. These measured molecular masses coincide with the expected masses calculated from the respective amino acid sequences using CLC software (Qiagen). In most cases the second peak that eluted exhibit a molecular mass that was similar to the expected mass of a dimeric DARPIn. DARPins that evolved from the first, fourth and fifth pool were primarily monomeric only, or exhibited only a small fraction of dimeric DARPins. In case of DARPins evolved from the third pool a slight propensity for aggregation could be seen in almost all samples, with mass fractions showing molecular masses greater than 100 kDa. The seventh pool exhibited significant fractions of molecular masses that were similar to dimeric DARPins, proposing a slight trend towards dimerisation of clones that evolved from this pool. All other DARPins showed only a minor or marginal fraction of oligomerised DARPins and can therefore be seen as DARPins with promising monomeric behaviour.

It can be seen in Table (3.2 that the reference sample BSA showed peaks with the expected masses and mass fraction, confirming the suitability and calibration of the SEC-MALS analysis. All eluting peaks of analysed DARPins showed a polydispersity factor between 1.00 and 1.02. This confirms that a single species of protein eluted within each peak.

The results of SEC-MALS suggested that the vast majority of analysed DARPins eluted as monomers only, leading to the conclusion that these DARPins exhibited excellent biophysical properties in terms of monomeric behaviour.

### 3.3.6 Cell Binding

In order to assess binding of DARPins to the target not only as recombinant purified protein immobilised on a surface, but for binding to the target human ROR1 expressed on the cell surface, flow cytometry was performed with CHO cells that were stably expressing human ROR1. Initially CHO/ROR1 cells were tested for ROR1 expression using an anti ROR1 Ab and secondary Ab coupled to Alexa488. For negative controls DARPIn (E2-5) that is not able to bind to the target human ROR1 ECD was used (Table 3.12). Furthermore, secondary antibodies without DARPIn were tested as negative controls. The intensity of the fluorescent signal, equivalent to intensity of binding, was plotted against percent of maximum cell count for each sample. (Figure 3.28 A)

Table 3.12: Setup of samples and control samples

Sample	Cells + DARPIn + 2 <sup>nd</sup> mAb anti DARPIn-AlexaFluor88
Pos. ctrl.	Cells + mAb mouse anti hROR1 + 2 <sup>nd</sup> mAb anti mouse AlexaFluor88
Neg. ctrl. 1	Cells + E2-5 + 2 <sup>nd</sup> mAb anti DARPIn-AlexaFluor88
Neg. ctrl. 2	Cells + 2 <sup>nd</sup> mAb anti DARPIn-AlexaFluor88
Neg. ctrl. 3	Cells + 2 <sup>nd</sup> mAb anti mouse AlexaFluor88

In Figure 3.28 the results of a test for cell binding of DARPins evolved from ribosome display selection round six can be seen.

As of Figure 3.28 (A), all negative controls showed a constantly low signal of no binding. This can be seen as a fluorescent signal intensity below  $10^0$ . All samples tested on ROR1 negative CHO cells exhibited signal intensities below  $10^0$ . ROR1 positive cells that were tested without DARPins showed as well very low signal intensities. This led to the conclusion that both cell lines and antibody conjugated to AlexaFluor488 were suited for the assay, since no unspecific binding was observed. Furthermore, the positive control using an anti-ROR1 antibody exhibited a distinguishable signal compared to the negative controls. This led to the conclusion that the assay was suited for assessing the binding of DARPins to the target hROR1, expressed on CHO cells.

As of Figure 3.28 (B), DARPins that evolved from the off-rate selection showed on average good binding signals on cell surface that were comparable or even higher than the respective positive control consisting of the respective parental clone. All DARPins that evolved from the first pool bound to the cell surface. When compared with the positive control, all three clones showed an almost 1.5 times higher mean fluorescence intensity than the respective antibody, suggesting a promising binding of the target on the cell surface. Yet, compared with the three parental clones G3w and A3w no substantial improvement of cell binding could be seen after the off-rate selection within this pool.

DARPin that evolved from the third pool showed a similar fluorescence intensity compared to the respective positive control as well as a similar signal intensity as its respective parental clone A11b. P3B3 revealed a slightly higher affinity to the cell surface than compared to other evolved DARPins and a slight improvement compared to its parental clone A11b.

In case of DARPins that evolved from the fourth pool of the final off-rate selection the parental clone C2w showed, as expected, only a very weak binding signal to the cell surface, with a measured mean fluorescent intensity being only slightly over background. Yet, all selected and analysed DARPins that evolved from this pool showed fluorescent intensities that were substantially higher than its respective parental clone C2w and higher than the positive control. The two clones P4E10 and P4F12 deviating from its parental clone only by one mutation, V96A and A87T respectively, exhibited a 25 to 30 fold higher fluorescent intensity than C2w and a higher binding signal than the respective antibody. Notably, clone P4H10, that comprised both mutations V96A and A87T, showed the highest improvement of cell binding after the final off-rate selection. The fluorescence signal was approximately 50-fold higher than of its parental clone and almost 2.5 times higher than of the comparable antibody, representing the strongest signal of cell binding being measured.

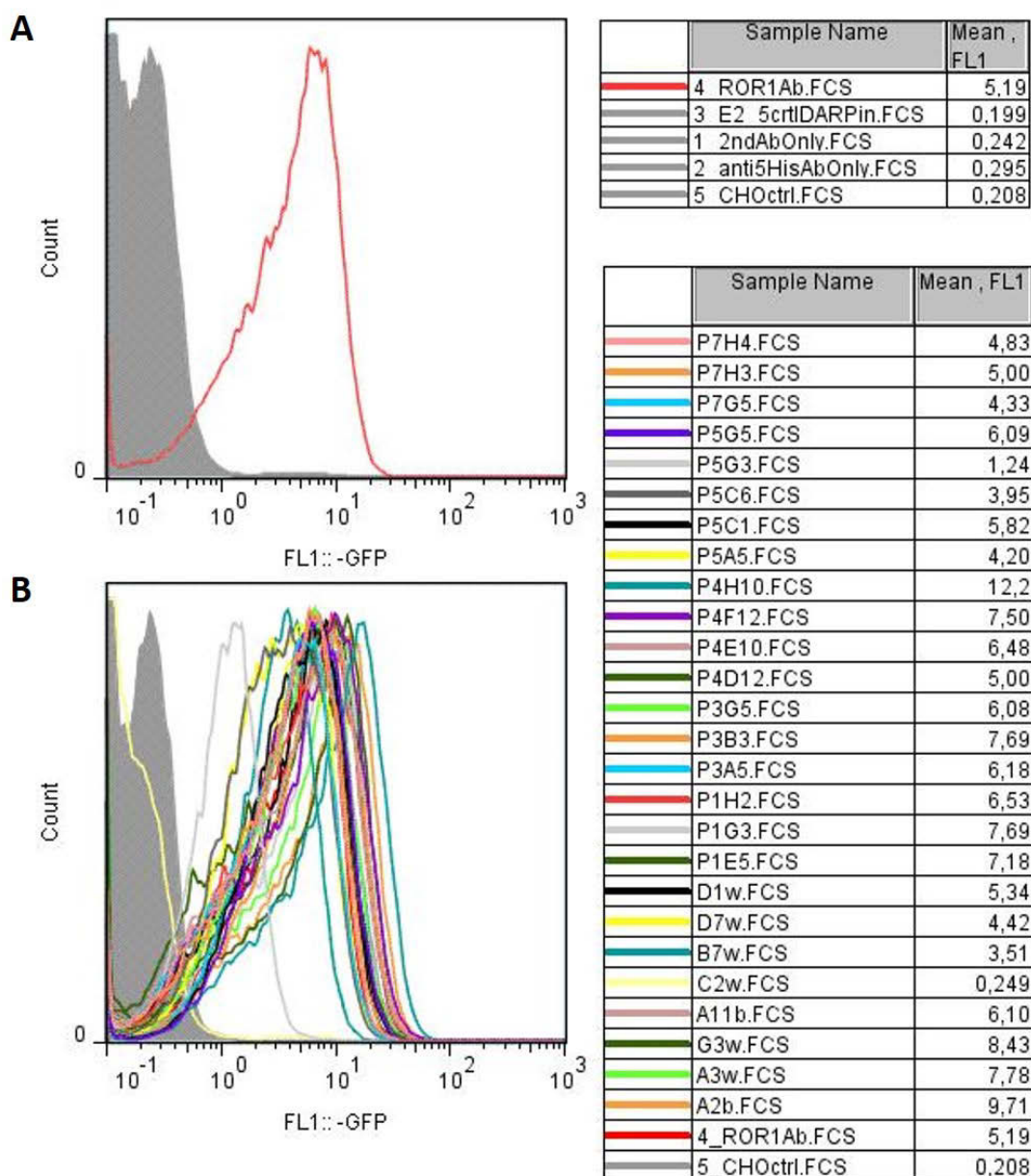


Figure 3.28: Summary to test for cell binding of DARPins evolved from ribosome display selection round six. Flow cytometry was used to analyse the binding of DARPins on the target, human ROR1, expressed on the cell surface of CHO cells. Intensity of fluorescent signal plotted against percent of max. cell count of each sample. Mean,FL1 represents the mean fluorescence intensity of the individual samples. (A) Negative and positive controls. Sample CHO-E25 refers to the negative control. CHO-2ndE25 and CHO-2ndAb to samples with the secondary antibody only, representing the negative controls for 2nd antibodies. CHO-Ab represents the positive control using an anti-ROR1 antibody. (B) DARPins evolved from off-rate selection.

DARPins evolved from pool number five of ribosome display selection round six showed binding of human ROR1 on the cell surface comparable or only slightly lower than the respective parental clones D7w and B7w. The measured fluorescence intensity

of the two clones P5C1 and P5G5 revealed a binding affinity to the cell surface that was higher than of both parental clones, B7w and D7w, and slightly higher than of the respective positive control, representing an improved cell binding after the final rounds of ribosome display selection. One clone P5G3 exhibited only a very weak binding with a mean fluorescent intensity being significantly lower than of its parental clones and the antibody.

DARPin that evolved from the seventh pool of off-rate selection revealed a good binding of cell surface, comparable to the positive control. Still, all clones showed a similar or slightly lower fluorescence intensity than of its parental clone D1w, confirming no substantial improvement of this pool after the final rounds of ribosome display selection in case of cell binding.

Table 3.13: Clones tested for cell binding and ranked according to the measured Mean Fluorescence Intensity (MFI)

Clone	MFI	Clone	MFI	Clone	MFI
P4H10	12.20	P3A5	6.18	E5w	4.44
G3w	8.43	A11b	6.10	D7w	4.42
A3w	7.78	P5G5	6.09	P7G5	4.33
P1G3	7.69	P3G5	6.08	P5A5	4.20
P3B3	7.69	P5C1	5.82	P5C6	3.95
P4F12	7.50	D1w	5.34	B7w	3.51
P1E5	7.18	P4D12	5.00	P5G3	1.24
P1H2	6.53	P7H3	5.00	C2w	0.25
P4E10	6.48	P7H4	4.83		

The vast majority of analysed DARPins exhibited excellent binding signals to the cell surface of human ROR1 expressing CHO cells, with fluorescence signals being similar or even higher than the respective positive control, using an anti-ROR1 antibody. Yet, the majority of DARPins exhibited binding signals that were similar to its respective parental clones. Only in case of DARPins that evolved from the fourth pool of off-rate selection, a substantial improvement in cell binding could be achieved compared to its respective parental clone C2w.

### 3.3.7 Affinity Determination

In order to determine the affinity of DARPins to the extracellular domains of human ROR1, Surface Plasmon Resonance (SPR) based on the ProteOn XPR36 system was performed. The experimental setup is described in Chapter Material and Methods 2.2.4. Purified DARPin samples were applied on a NA chip, where 200 RU of the human ROR1 ECD was immobilised, at a constant flow rate of 60  $\mu\text{l}/\text{min}$ . Association was performed for 300 s. Subsequently, dissociation was measured for 2700 s. Between each measured sample a single regeneration step was applied using 30  $\mu\text{l}$  of 1 M glycine, pH 2.0. Based on the resulting signals the on- and off-rate constants were determined and the respective  $K_D$  was calculated. The resulting graphs and calculated constants can be found in the Appendix 5.

Table 3.14: Summary of binding Kinetics of DARPins evolved from final off-rate selection (Ribosome Display Selection round 6). The constants of on-rate [ $k_{\text{on}}$ ] and off-rate [ $k_{\text{off}}$ ] calculated from the respective binding curve as determined by surface plasmon resonance. Both constants are presented with the respective standard deviation obtained from fitting of measured curves. Dissociation constants [ $K_{\text{D}}$ ] were calculated from the obtained constants.

Clone	$k_{\text{on}}$ [ $\text{M}^{-1} \text{s}^{-1}$ ]	$k_{\text{off}}$ [ $\text{s}^{-1}$ ]	$K_{\text{D}}$ [nM]
G3w	$3.01 \times 10^6 \pm 2.99 \times 10^4$	$1.93 \times 10^{-2} \pm 1.14 \times 10^{-4}$	6.43
A3w	$4.92 \times 10^6 \pm 6.18 \times 10^4$	$2.54 \times 10^{-2} \pm 2.18 \times 10^{-4}$	5.17
A11b	$1.25 \times 10^6 \pm 1.05 \times 10^4$	$5.02 \times 10^{-3} \pm 2.30 \times 10^{-5}$	4.03
C2w*	$1.15 \times 10^6 \pm 1.07 \times 10^5$	$1.75 \times 10^{-1} \pm 6.76 \times 10^{-3}$	153.00
	$2.72 \times 10^0 \pm 2.43 \times 10^{-2}$	$9.66 \times 10^{-4} \pm 2.12 \times 10^{-5}$	3550
B7w	$3.97 \times 10^6 \pm 1.16 \times 10^5$	$3.01 \times 10^{-2} \pm 6.14 \times 10^{-4}$	7.58
D7w	$4.14 \times 10^6 \pm 4.04 \times 10^4$	$6.11 \times 10^{-3} \pm 6.20 \times 10^{-5}$	1.47
D1w	$2.37 \times 10^6 \pm 3.67 \times 10^4$	$8.06 \times 10^{-3} \pm 6.79 \times 10^{-5}$	3.40
P1E5	$3.97 \times 10^6 \pm 4.22 \times 10^4$	$1.65 \times 10^{-2} \pm 1.12 \times 10^{-4}$	4.15
P1G3	$3.04 \times 10^6 \pm 5.05 \times 10^4$	$1.29 \times 10^{-2} \pm 1.27 \times 10^{-4}$	4.25
P1H2	$3.21 \times 10^6 \pm 3.83 \times 10^4$	$1.52 \times 10^{-2} \pm 1.09 \times 10^{-4}$	4.72
P3A5	$1.64 \times 10^6 \pm 1.26 \times 10^4$	$4.41 \times 10^{-3} \pm 1.67 \times 10^{-5}$	2.69
P4D12	$1.41 \times 10^6 \pm 4.11 \times 10^4$	$6.28 \times 10^{-2} \pm 1.12 \times 10^{-3}$	44.50
P4E10	$1.53 \times 10^6 \pm 2.78 \times 10^4$	$4.15 \times 10^{-2} \pm 4.99 \times 10^{-4}$	27.00
P4F12	$1.31 \times 10^6 \pm 3.08 \times 10^4$	$5.28 \times 10^{-2} \pm 7.54 \times 10^{-4}$	40.30
P4H10	$2.40 \times 10^6 \pm 1.90 \times 10^{11}$	$4.07 \times 10^{-2} \pm 1.56 \times 10^3$	16.90
P5A5	$1.36 \times 10^6 \pm 2.07 \times 10^3$	$6.35 \times 10^{-5} \pm 1.00 \times 10^{-6}$	0.05
P5C1	$1.60 \times 10^6 \pm 1.64 \times 10^2$	$1.21 \times 10^{-4} \pm 1.18 \times 10^{-6}$	0.08
P5C6	$1.72 \times 10^6 \pm 2.76 \times 10^3$	$6.41 \times 10^{-5} \pm 8.86 \times 10^{-7}$	0.04
P5G3	$2.36 \times 10^6 \pm 3.69 \times 10^3$	$6.68 \times 10^{-5} \pm 1.00 \times 10^{-6}$	0.03
P5G5	$1.79 \times 10^6 \pm 2.69 \times 10^3$	$8.69 \times 10^{-5} \pm 8.52 \times 10^{-7}$	0.05
P7G5	$1.04 \times 10^6 \pm 7.05 \times 10^3$	$5.26 \times 10^{-3} \pm 1.57 \times 10^{-5}$	5.07
P7H3	$2.35 \times 10^6 \pm 1.18 \times 10^4$	$5.30 \times 10^{-3} \pm 1.48 \times 10^{-5}$	2.26
P7H4	$2.93 \times 10^6 \pm 1.41 \times 10^4$	$5.25 \times 10^{-3} \pm 3.44 \times 10^{-6}$	1.80

\*Constants obtained by heterogenous ligand fit.

In Table 3.14 the binding kinetics of DARPins that evolved from off-rate selection (ribosome display selection round six) can be seen. For a better overview, the binding constants of the respective parental clones are as well presented in the Table. An appropriate fit using 1:1 binding model of the measured binding curves was possible with all samples of DARPins that evolved from the off-rate selection, to be seen by relatively low standard deviations of the on- and off-rate constants as determined using fit to a 1:1 binding model. This confirmed a monovalent one to one binding of the target by the DARPins. All respective response curves as measured can be found under Supplementary Data. DARPins that derived from the first pool showed on average a  $K_{\text{D}}$  of 4.4 nM, an average that was only slightly higher than of its respective parental clones G3w and A3w, with determined affinities of 4.15 nM, 4.25 nM and 4.72 nM for P1E5, P1G3 and P1H2, respectively. Therefore, DARPins evolved from this pool exhibited only minor improvement of affinity. In case of DARPins evolved from the third pool of off-rate selection only a single clone with marginally improved affinity compared to its parental clone

A11b could be identified, showing a  $K_D$  of 2.69 nM. In case of DARPins evolved from the fourth pool an average affinity to human ROR1 ECD of 32.2 nM could be identified. The DARPins P4H10 and P4E10 represented the strongest binder with a  $K_D$  of 27.0 nM and 16.9 nM, respectively, representing a 9-fold and 6-fold improvement in affinity compared to its parental clone C2w, exhibiting a  $K_{D1}$  of 153.0 nM. DARPins evolved from the fifth pool showed a substantial improvement of affinity compared to its parental clones B7w and D7w, exhibiting on average a  $K_D$  of 50 pM. This improvement could be owed to the strong sequence similarity to the clone F3b, which exhibited a  $K_D$  of 0.04 nM and bound to the dominant epitope region one, rather than to B7w or D7w. However, due to the strong sequence similarity between B7w and F3b the strong sequence similarity of the evolved DARPins to F3b could be owed to an evolutionary pressure rather than contamination. Notably, all selected clones exhibited affinities in the double digit picomolar range. DARPins P5G3 and P5C6 represented the strongest binders within this group, with a  $K_D$  of 30 pM and 40 pM, respectively, leading to a 150-fold increase in affinity after round five and six of ribosome display selection. DARPins that evolved from the seventh pool of off-rate selection exhibited only a minor improvement of affinity compared to its parental clone D1w, with an average  $K_D$  of 3.07 nM compared to 3.40 nM of D1w. P7H4 represented the strongest binder within this pool exhibiting a  $K_D$  of 1.80 nM and a 1.9-fold improvement in affinity.

### 3.4 Summary of evolved DARPins

For an overview, the results of the properties of selected DARPins, that are considered for further experiments can be seen in Table 3.15. The table includes the results of characterisation of DARPins with signals of screening, SEC-MALS, qualitative ELISA, cell binding, binding kinetics and respective epitope. In Figure 3.29 an evolutionary tree based on the sequences of the selected DARPins can be seen.

A subset of 16 DARPins could be identified that were considered for further characterisation. All of those DARPins exhibited good monomeric behaviour as assessed by SEC and SEC-MALS. Six of those DARPins (F3b, E5w, P5G5, H6w, P5C1 and A8w) showed affinities in the sub-nanomolar range, while exhibiting medium to high mean fluorescent intensities, ranging from 1.24 to 7.33 in case of cell binding. Those DARPins bound primarily to the two overlapping epitope regions 1 and 2. DARPins that consist of only 2 internal repeat units (P4H10, P7H3, P4E10, D1w and C2w) exhibited medium to weak affinities in the single to triple digit nanomolar range, as measured by surface plasmon resonance, but showed, except of C2w, high mean fluorescent intensities of 5.00 to 12.2 in case of cell binding. Those DARPins bound primarily to the distinct third epitope region. All DARPins that exhibited affinities in the nanomolar range and bound to the two overlapping epitope regions 1 and 2 (G3w, D7w, P1G3, P1E5 and A3w), consisted of three internal repeat units and bound to the cell surface with medium to high mean fluorescence intensities of 4.42 to 9.71.

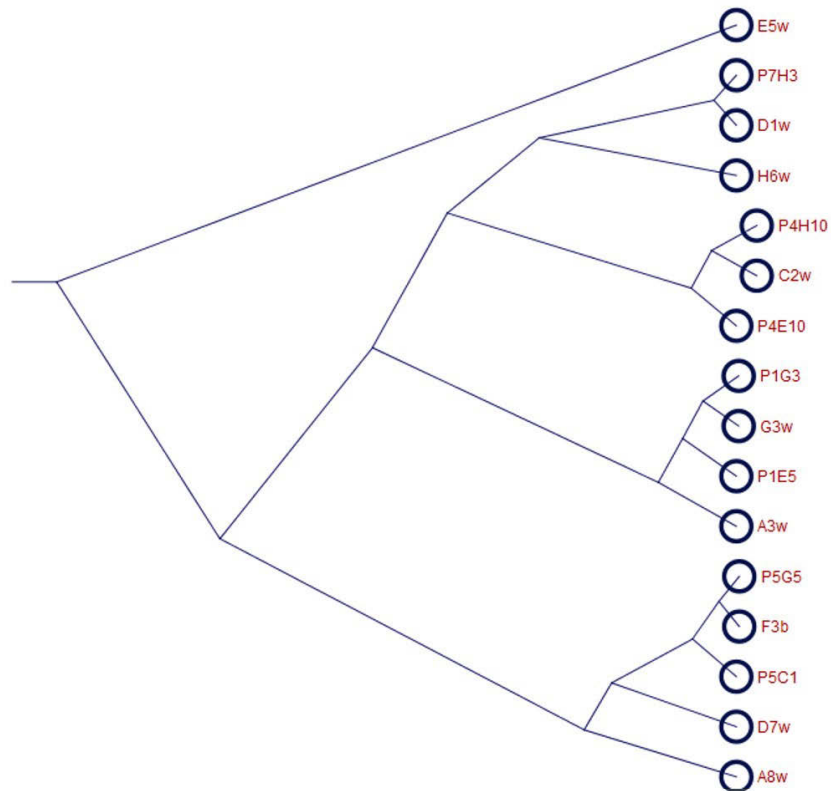


Figure 3.29: Evolutionary tree based on the sequences of evolved DARPins that are considered for further characterisation.

For future use of those DARPins for biological studies of human ROR1 and therapeutic strategies of related diseases, further characterisation of the evolved DARPins must be performed. Further characterisation would include an epitope mapping on truncations of the human ROR1 ECD in order to determine the exact domain region that is targeted by the respective DARPins. Further assays aim at elucidating a putative biological effect of the DARPins. To achieve this, apoptosis assays could be performed on human ROR1 addicted cancer cells, in order to study the effects of naked DARPins, targeting different epitope regions on the receptor.

Table 3.15: Summary of properties of evolved DARPins. Molecular mass is represented in kDa as calculated from the sequence. Extinction coefficient as calculated with software CLC (Qiagen). Monomer (+): DARPins present as monomer only as assessed by SEC and SEC-MALS. Affinity constant  $K_D$  as determined by using SPR. Cell binding indicated with mean fluorescent intensity as measured using flow cytometry. Epitope represents the respective binding region on human ROR1

Clone	Mol.Mass [kDa]	Ext. Coeff. [ $10^3$ ]	Monomer	$K_D$ [nM]	Cell binding [MFI]	Epitope
F3b	18.44	18.35	+	0.04	1.37	1
P4H10	14.65	9.53	+	16.9	12.2	3**
E5w	18.33	11.38	+	0.20	3.51	2
P7H3	14.65	8.25	+	2.3	5.00	3**
P5G5	18.47	18.35	+	0.05	1.24	2**
P4E10	14.65	9.53	+	27	7.5	3**
H6w	14.94	9.53	+	0.08	7.33	1
D1w	14.68	8.25	+	3.4	8.43	3
G3w	18.15	16.5	+	6.4	9.71	1
P5C1	18.39	18.35	+	0.08	5.82	2**
D7w	18.44	18.35	+	1.3	4.42	2
P1G3	18.15	16.5	+	4.3	7.69	2**
A8w	18.51	18.35	+	0.71	5.37	1
P1E5	18.05	16.5	+	4.2	7.18	2**
C2w	14.69	9.53	+	153* / 3550*	0.25	3
A3w	18.16	15.22	+	5.2	7.78	2

\*  $K_D$  obtained by heterogenous ligand fit

\*\* Epitope region as targeted by the respective parental clone

# Chapter 4

## Discussion

The human receptor tyrosine kinase like orphan receptor 1 (hROR1) represents a crucial factor for tumor progression in a great variety of blood and solid malignancies. [39] As such, hROR1 offers a novel and promising target for tumor therapy. The aim of this project was the selection and biophysical characterisation of Designed Ankyrin Repeat Proteins (DARPin), a novel class of binding molecules with favourable biophysical properties [41] that are specific for human ROR1.

### 4.1 Characterisation of DARPins evolved from previous selections

#### 4.1.1 Screening of selected clones

For screening of clones, evolved from the third and fourth round of ribosome display selection, a binding assay using Homogenous Time Resolved Fluorescence (HTRF) was performed, a fluorescence resonance energy transfer (FRET) based method that allowed for time resolved, sensitive and robust detection of molecular interactions in small quantities. Other than comparable methods, HTRF allows for detection in solution.

Screening of clones in crude extract for binding to the extracellular domains of human ROR1 by HTRF showed a clear shift in case of fluorescence at the acceptor wavelength with clones evolved from all three libraries, indicating a close proximity of the HTRF donor and acceptor, and therefore a binding of the target protein (Figures 3.1 to 3.6). Based on these signals, 60 putative binders were isolated from the different pools for further characterisation. Notably, DARPins that evolved from the fourth round of ribosome display selection showed on average a 10-fold higher ratio of signal over background than DARPins that evolved from the third round of selection, suggesting a substantial improvement of affinity during the fourth round. DARPins that consist of only 2 internal repeats (N2C) showed in general a lower binding intensity than comparable DARPins with 3 internal repeats (N3C). However, this difference appeared to be negligible after the fourth round of selection. Other than after screening using ELISA (see Chapter 1.4), a significant number of DARPins with good monomeric behaviour could be isolated.

#### 4.1.2 Sequence Analysis

About 30% of all DARPins that evolved from selection round 3 and 4, possessed one or more Cysteines in their sequence and were not considered for further characterisation,

since this residue increased the likelihood of dimerisation (see Figure 3.7). Only two clones exhibited an identical amino acid sequence, indicating that a high degree of diversity was still contained. Many clones showed only a slight difference in their sequence, deviating only by one or two residues, suggesting a certain trend towards narrowing in sequence diversity. Despite their high degree of similarity, no distinct families related to specific biophysical properties or binding behaviour could be seen, which could have revealed information about the influence of position-specific exchange of single amino acids.

### 4.1.3 Monomeric Behaviour

For a first critical assessment regarding the oligomeric behaviour of selected DARPins, analytical size exclusion chromatography was performed (Figure 3.9). Approximately 84.4% of all DARPins that evolved from ribosome display selection round three and four eluted as monomers only, which indicated a substantial improvement compared to previous selection and screening using ELISA (see chapter 1.4). This suggested HTRF as a promising screening platform for enhanced isolation of monomeric DARPins. In order to confirm the monomeric nature of the eluting peaks, these DARPins were further tested for their respective molecular weight using SEC coupled to MALS (Table 3.2). By using a combination of SEC-MALS all DARPins species present could be identified and their respective oligomeric state determined. The results of this characterisation confirmed the previously obtained data from SEC, showing that approximately 90% of all screened and characterised DARPins were present in their monomeric state only. These results suggested promising biophysical properties in terms monomeric behaviour for DARPins selected from round three and four.

### 4.1.4 Cell Binding

In order to assess binding of DARPins to the target human ROR1 ECD on the cell surface, flow cytometry was performed with CHO cells that were stably expressing human ROR1 (Figure 3.11 and 3.12). Almost all of 32 analysed DARPins exhibited a medium to strong binding to the target on CHO cells, with five clones (G3w, F6w, H6w, B7w, B8w) binding with similar or even higher intensity than the respective positive control using an anti-ROR1 antibody. This confirmed a successful binding of human ROR1 on cell surface by DARPins that evolved from round three and four of ribosome display selection. Only 5 out of 32 DARPins (D3w, H3w, G7w, B1w, C1w) exhibited weak binding signals on cell surface. The signal intensity of DARPins binding to cell surface seemed to be independent of the respective selection round. The affinity to cell surface seemed to be generally lower in case of DARPins that consisted of only two internal repeat units than of DARPins that exhibited three internal repeats (Figure 3.11 and 3.12).

### 4.1.5 Binding Kinetics

For the characterisation of the biophysical properties of selected DARPins in case of binding to the extracellular domain of human ROR1, Surface Plasmon Resonance (SPR) was performed. For this purpose target was immobilised on the chip via neutravidin-biotin interaction and the DARPins subsequently applied in solution. In case of all analysed DARPins, a stable measurement of binding and dissociation could be observed (see Table 3.6, 3.7 and Appendix 5). In most cases of the obtained data a 1:1 binding model was possible, confirmed by an unbiased distribution of the respective residuals, therefore confirming a 1:1 monovalent binding of target by the respective DARPins. The majority of

DARPin, evolved from ribosome display selection round 3 and 4, exhibited affinities in the sub-nanomolar range. These high affinities seemed to be independent of the initial library of clones, showing a similar mean  $K_D$  in case of DARPin evolved from all three pools. Only DARPin obtained from the library N2C, containing only two internal repeat units, exhibited a higher number of clones that bound in the double-digit nanomolar range or even lower affinities. The affinity of clones seemed to be dependent on the respective selection round. While DARPin that evolved from the third round of ribosome display selection exhibited a moderate to high affinity, DARPin that evolved from the fourth round, including an initial competition with moderate stringency, exhibited on average an up to 10-fold higher affinity, resulting in DARPin that bound to the human ROR1 ECD with very high affinities of up to 39 pM.

### 4.1.6 Epitope Regions

In order to distinguish different binding regions of selected DARPin on the extracellular domain of human ROR1, competitive surface plasmon resonance was performed. Each DARPin was tested against all other clones pairwise by evaluating blocking of each other's binding to the respective epitope region (Figure 3.13).

The respective binding pattern revealed 2 overlapping and a third distinct epitope region. One very dominant epitope region could be identified that was bound by approximately 79% of all characterised DARPin. Notably, DARPin that bound this region exhibited on average higher affinities towards the target, showing affinities in the sub-nanomolar range. This suggested a strong evolutionary trend and favouring of this particular epitope region. Another less dominant overlapping epitope region, bound by eight clones, could be identified, showing on average an affinity of single to double digit nanomolar range. Five clones were identified to bind at the interface of the two regions, suggesting a close proximity of these two epitope region. A third, least dominant but distinct, epitope region could further be identified, with only two binders targeting this region (Table 3.8). These two DARPin exhibited on average a weaker affinity in the lower and higher nanomolar range, respectively. Notably, both binders evolved from the library N2C and consisted only of two internal repeat units, suggesting a tendency towards smaller sizes or N2C conformation for accessibility of this binding region. Yet, in order to gain more detailed information about the exact location of the epitope region and its proximity to cell surface, in respect of both location and receptor conformation, further investigation would be necessary.

## 4.2 Ribosome Display selection

Ribosome display selection represents a powerful evolution method for generating high affinity binders and has been successfully applied to a variety of scaffolds, including single-chain Fv fragments of antibodies and alternative scaffolds, such as Designed Ankyrin Repeat Proteins.[140, 138, 149, 109] The selection for affinity maturation of DARPin with lower affinities and binding to the less dominant epitope regions 2 and 3 of human ROR1 ECD was exclusively performed in solution. Random mutations were introduced in single clones (Figure 3.14), yielding a mutational load of three to four mutations on average in its amino acid sequence. By separation of parental clones into respective pools prior selection, it was further possible to preserve the respective binding regions of DARPin on the target human ROR1, allowing therefore an equal chance for maturation a putative higher diversity in epitope regions.

The off-rate selection could be performed in a highly automated and reproducible way by using immobilisation via magnetic beads and KingFisher Flex system for steps

such as pre-panning, panning, washing and elution. This should allow a decreased risk of mRNA degradation and cross-contamination by the operator, during these highly sensitive steps. Despite the very low amount of target and high amount of competitor in a  $10^4$  excess, it was possible to isolate a sufficient amount of evolved clones for the amplification of DNA fragments (Figure 3.15). The amplification of DNA fragments originating from negative wells, where no target was applied, lead to the conclusion that unspecific binders were silently enriched during this stringent selection round and cross-contamination did occur. Even though a pre-panning step against constituents for enrichment of specific binders was performed prior selection step, a significant amount of unspecific binder seemed to have survived the off-rate selection. However, this result was not unexpected since low amount of target and great excess of competitor would lead to a strong decrease of specific binders that would survive the stringent panning conditions, making a strong amplification with 40 cycles necessary. As a result the amplification of background was increased. These results made a non-stringent selection round for enrichment of specific binders necessary.

In the subsequent non-stringent selection a significantly higher amount of specific binders could be observed on the analytical agarose gels of PCR products, while detecting only marginal signals in the respective positive controls (Figure 3.16). This enrichment was achieved by a non-stringent selection, using a higher amount of target (50 nM) in absence of competitor and later confirmed by screening using ELISA.

## 4.3 Characterisation of DARPins evolved from off-rate selection

### 4.3.1 Screening of selected clones

For screening of DARPins evolved from the sixth round of ribosome display selection a 384-well single clone, crude extract ELISA was performed. Other than for HTRE, screening using crude lysate ELISA allowed for a sensitive and robust detection of molecular interactions that was approximately independent of the location of epitope on the target. Therefore, a favouring of certain epitope regions due to their closer proximity to the detection system could be avoided. In case of all seven pools, evolved from the sixth round of selection, signals significantly higher than background signal could be detected, confirming the successful selection of specific binders after the final round of ribosome display selection (Figure 3.17 and 3.18). Based on these signals, a number of 35 promising binders could be isolated for further characterisation. Almost all analysed clones showed a signal that was similar or even higher than its respective parental clone. Only few signals were similar to signals of the respective negative controls without target, which led to the assumption that a successful enrichment of specific binder by the final round of ribosome display could be achieved. Only in case of pool number seven a higher number of signals, similar to background, were detected, suggesting a higher number of unspecific binders. In case of the fourth pool, the majority of evolved clones showed a signal that was only marginally higher than background and similar to the signal obtained from the respective parental clone. Due to the low binding signal of the respective parental clone C2w that was only marginal higher than the background, DARPins that exhibited similar signals could be assumed to be either binders with affinities similar to C2w or unspecific binders. The data obtained by ELISA and later by SPR suggest that the high dilution of 1:5,000 of crude extract for ELISA was sufficient to distinguish high affinity from very high affinity binders. Yet, in order to distinguish binders with lower affinities from unspecific binders, such as in pool 4, a lower dilution would have been

more suited. However, by selecting 5 binders with the highest signals within each pool, a sufficient number of promising binders of human ROR1 could be identified and later characterised.

### 4.3.2 Sequence Analysis

Despite the vast sequence diversity of clones derived from selection round three and four, a highly decreased diversity could be seen with DARPins that evolved from the final round of ribosome display selection (Figures 3.19 to 3.25). Almost all clones differed only in one or few residues, suggesting a possible restriction in further evolvability of clones in terms of affinity. Furthermore, new diversity within selected DARPins mainly occurred in positions of framework residues, indicating again a possible decreased evolvability of residues within the loops in terms of affinity. In case of pool P1, only four sequences could be isolated, due to a identified double clone in the fifth sequencing reaction (Figure 3.19). Two of the four sequences were identical. Furthermore, all DARPins from this pool seemed to have evolved from the parental clone G3w, suggesting an evolutionary preference of this clone. The sequence analysis of the second pool of off-rate selection revealed an identical sequence with G3w in case of all clones (Figure 3.20). A parental clone from pool number one was probably inserted by cross-contamination and that seemed to have out ruled all other clones during the stringent conditions of off-rate selection. In case of pool P3, all evolved DARPins maintained their cysteine within the sequence, suggesting a possible conditionality of this residue for binding of target (Figure 3.21). The unfavourable biophysical properties of these clones, nevertheless, led to the exclusion of these clones for further characterisation. Pool P4 exhibited as well only marginal sequence diversity (Figure 3.22). However, a single mutation at V96A and A87T respectively seemed to be sufficient to improve the binding of target on cells by approximately 30 fold. In case of a single clone that exhibited both mutations the cell binding could be improved by approximately 50-fold. Notably, all mutations were located in positions of framework residues. In case of pool P5, all clones seemed to have initially evolved from the parental clone B7w (Figure 3.23). Yet, when aligned with all other characterised clones a strong sequence similarity with F3b rather than B7w was apparent. This result could be owed to the strong sequence similarity of the two DARPins, deviating only in one residue. This strong similarity could have caused a trend towards F3b due to its very high affinity to the target. DARPins that evolved from Pool P6 were excluded from further characterisation due to mismatches in the sequence F4w in respect to previously obtained sequences of this parental clone (Figure 3.24). DARPins from pool 7 exhibited again a high degree of sequence similarity, including one identical clone (Figure 3.25).

In conclusion, a substantial improvement of affinity could be achieved in one pool (P4), where the parental clone C2w could be evolved from micromolar to double-digit nanomolar affinities.

### 4.3.3 Monomeric Behaviour

In case of DARPins that evolved from ribosome display selection round six, the good biophysical properties in case of monomeric behaviour could be maintained (Figure 3.27). These results could be observed even though ELISA was used as the respective screening platform and are probably owed to the strong sequence similarities with the respective parental clones. Approximately 74% of all DARPins eluted as monomers only. In case of pool 3, all evolved DARPins exhibited a tendency to aggregate, which was similar to its respective parental clone. This phenomenon could potentially be caused by a free cysteine residue present in all these sequences. Furthermore, in case of pool 6 and 7, a

fraction of one and three clones respectively showed a slight tendency for dimerisation. In order to confirm the monomeric nature of the eluting peaks, these clones were further tested for its respective molecular weight using SEC coupled to MALS (Table 3.11). The results of this characterisation confirmed the previously obtained data from SEC only, showing that approximately 74% of all screened and characterised DARPins that evolved from the last selection round were present as monomers only, suggesting good biophysical properties in terms of monomeric behaviour. The fact that a higher number of monomeric DARPins could be identified after screening based on ELISA might be explained by the high degree of sequence similarity of selected DARPins to its respective parental clones, which, with exception of pool number three, already constituted good biophysical stability in terms of monomeric behaviour.

#### 4.3.4 Cell Binding

In case of DARPins that evolved from off-rate selection, substantial improvement of cell binding could only be achieved in pool P4 based on the parental clone C2w. DARPins that evolved from pool P1, based on the parental clones G3w and A3w, P3, based on the parental clone A11b, and P7, based on the parental clone D1w, exhibited strong binding of target on cell surface comparable with the respective positive control, using an anti-ROR1 antibody (Figure 3.28). Yet, the majority of DARPins showed binding signals that were similar to the respective parental clones. Two clones, P5C1 and P5G5 that evolved from the fifth pool of final off-rate selection exhibited a strong binding of target on cells that was higher than the respective signal of both parental clones and slightly higher than of the positive control, suggesting an improved cell binding after the final rounds of ribosome display selection in case of two clones. Yet, a stronger similarity to the clone F3b rather than the expected and similar parental clone B7w could be seen during sequence analysis, suggesting an evolutionary trend towards this sequence and might explaining the strong increase in measured affinities, that were similar to F3b. In case of DARPins that evolved from the seventh pool of ribosome display selection, all DARPins characterised showed affinities similar to their parental clones, therefore exhibiting no improvement of binder evolved from the clone D1w. In contrast, DARPins that evolved from C2w in the fourth pool showed a substantial improvement in cell binding after the final round of selection. Despite the very weak binding of its parental clone C2w, an up to 25 to 30 fold improvement in cell binding could be achieved by the two DARPins P4E10 and P4F12. Notably, a single mutation, V96A and A87T respectively, within its framework residues seemed to be sufficient for an improved cell binding and affinity. A single clone, P4H10, that comprised both mutations, showed the strongest improvement of cell binding, with a 50-fold improvement of binding compared to its respective parental clone and a mean fluorescent intensity that was approximately 2.5-fold higher than the respective antibody, representing the strongest signal of cell binding of all selected clones and suggesting a superior binder of target on cells.

In conclusion, excellent binders on the cell surface on the third distinct epitope region with substantial improvement compared to its parental clone C2w could be obtained by the off-rate selection.

#### 4.3.5 Binding Kinetics

Clones that evolved from the two final rounds of ribosome display selection exhibited on average no or only a slight increase in affinity in case of pool P1, P3 and P7, and therefore no improvement of affinities within these pools (Figure 3.14). Other than these pools, a substantial improvement of affinity was observed with clones evolved from the

fifth pool, with P5G3 representing the strongest binder with an approximately 90-fold increase in affinity compared to its respective parental clones, B7w and D7w. As discussed in section 4.3.4, a stronger similarity to the clone F3b rather than the expected and similar parental clone B7w could be the reason for these highly improved affinities, suggesting a putative binding of the dominant epitope region, targeted by F3b, rather than the less dominant epitope region, targeted by B7w. In case of pool 4 an improvement of up to 10 fold could be achieved with clones binding the least-dominant epitope region. P4H10 represented the most promising binder with an obtained  $K_D$  of 16.9 nM. Unlike binders with very high affinities of up to 40 pM, clones evolved from this pool exhibited the strongest signals in case of cell binding while exhibiting the lowest affinities in only double-digit nanomolar range in case of SPR, suggesting a possible favoured accessibility of the targeted epitope on cell surface, compared to other epitope regions.

In conclusion, a successful selection and characterisation of DARPins with good biophysical properties and very high affinities to three epitope regions on human ROR1 could be achieved. These results show the strength of directed evolution for the generation of suitable binders and provides a set of promising binders that represent an excellent basis for alternative therapeutic strategies and investigations of malignancies that are related to human ROR1.

# Chapter 5

## Conclusion

The human receptor tyrosine kinase-like orphan receptor 1 (human ROR1) represents a crucial factor for tumor progression in a great variety of blood and solid malignancies. As such, human ROR1 offers a novel and promising target for tumor therapy. However, the low expression levels of human ROR1 on tumor cells limits the capability of antibodies for efficient antibody-dependent cell-mediated cytotoxicity (ADCC) and complement dependent cytotoxicity (CDC) and highlights the need for alternative therapeutic strategies.[8] The aim of this project was the generation and biophysical characterisation of Designed Ankyrin Repeat Proteins (DARPs), a novel class of binding molecules, specific for human ROR1, which would allow new to investigate receptor biology and alternative therapies of malignancies that are related to human ROR1.

A combination of directed evolution, the screening of a high number of clones and their intensive characterisation revealed to be a powerful strategy for the generation of DARPs binding to the human ROR1 ECD. Screening of single clones after 3 + 4 rounds of ribosome display selection using HTRF, measured in crude extract, and further characterisation, a set of DARPs that exhibited sub-nanomolar affinities of up to 39 pM were obtained. These DARPs also were capable to bind human ROR1 on cell surface, which could be grouped into three different epitope regions. The selection and characterisation of DARPs binding human ROR1 revealed a strong evolutionary trend towards a single epitope region that was targeted with very high affinities in the double-digit picomolar range, while very few others targeted a second overlapping and a third distinct epitope region with lower affinities. However, binders that targeted the third distinct region evolved all from the library N2C that consisted of two internal repeat units only and exhibited the highest signals in terms of binding the target on cells while showing the lowest measured affinities in the double- to triple-digit nanomolar range. This suggested a certain conditionality in terms of easier accessibility in case of this third, evolutionary rare epitope region. By further affinity maturation of DARPs that bound with lower affinities to less-dominant epitope regions, using a very stringent off-rate selection followed by a subsequent less-stringent selection, the affinity and binding on the cell surface could further be improved by up to 50-fold, representing 2.5-fold higher signals than a comparable anti-ROR1 antibody.

Future experiments will aim at the determination of the exact domain that is targeted by the respective DARPs. As an initial approach, ELISA or SPR against truncations of the human ROR1 ECD could be used. Furthermore, crystal structures of DARPs bound to the target could be obtained. To elucidate a potential biological effect of these here identified DARPs, these will be tested on ROR1 expressing tumour cells using a XTT assay. In addition, the DARPs targeting different epitope regions on the receptor will be used to shed more light on the individual roles of each extracellular domain to understand receptor biology.

It can be concluded that the successful selection and characterisation of DARPins with good biophysical properties and very high affinities to three epitope regions on human ROR1 showed the strengths of directed evolution for the generation of suitable binders. This approach led to a set of 16 promising binders that represent an excellent basis for alternative therapeutic strategies and investigations of malignancies that are related to human ROR1.

# References

- [1] J. Ferlay, I. Soerjomataram, R. Dikshit, S. Eser, C. Mathers, M. Rebelo, D. M. Parkin, D. Forman, and F. Bray, "Cancer incidence and mortality worldwide: sources, methods and major patterns in globocan 2012," *Int J Cancer*, vol. 136, pp. E359–E386, 2015.
- [2] D. Hanahan and R. A. Weinberg, "The hallmarks of cancer," *Cell*, vol. 100, pp. 57–70, 2000.
- [3] D. Hanahan and R. A. Weinberg, "Hallmarks of cancer: the next generation," *Cell*, vol. 144, pp. 646–674, 2011.
- [4] B. Stewart and C. P. Wild, "World cancer report 2014," *World*, 2016.
- [5] M. Lind, "Principles of cytotoxic chemotherapy," *Medicine*, vol. 39, pp. 711–716, 2011.
- [6] D. E. Gerber, "Targeted therapies: a new generation of cancer treatments," *Am Fam Physician*, vol. 77, pp. 311–319, 2008.
- [7] W. Tai, R. Mahato, and K. Cheng, "The role of her2 in cancer therapy and targeted drug delivery," *J Control Release*, vol. 146, pp. 264–275, 2010.
- [8] G. Rebagay, S. Yan, C. Liu, and N.-K. Cheung, "Ror1 and ror2 in human malignancies: potentials for targeted therapy," *Front Oncol*, vol. 2, p. 34, 2012.
- [9] S. Baskar, A. Wiestner, W. H. Wilson, I. Pastan, and C. Rader, "Targeting malignant b cells with an immunotoxin against ror1," *MAbs*, vol. 4, pp. 349–361, 2012.
- [10] M. Hudecek, T. M. Schmitt, S. Baskar, M. T. Lupo-Stanghellini, T. Nishida, T. N. Yamamoto, M. Bleakley, C. J. Turtle, W.-C. Chang, H. A. Greisman, *et al.*, "The b-cell tumor-associated antigen ror1 can be targeted with t cells modified to express a ror1-specific chimeric antigen receptor," *Blood*, vol. 116, pp. 4532–4541, 2010.
- [11] J. Yang, S. Baskar, K. Y. Kwong, M. G. Kennedy, A. Wiestner, and C. Rader, "Therapeutic potential and challenges of targeting receptor tyrosine kinase ror1 with monoclonal antibodies in b-cell malignancies," *PloS One*, vol. 6, p. e21018, 2011.
- [12] P. Masiakowski and R. D. Carroll, "A novel family of cell surface receptors with tyrosine kinase-like domain.," *J Biol Chem*, vol. 267, pp. 26181–26190, 1992.
- [13] M. Katoh and M. Katoh, "Identification and characterization of rat ror1 and ror2 genes in silico," *Int J Mol Med*, vol. 15, pp. 533–538, 2005.
- [14] J. L. Green, S. G. Kuntz, and P. W. Sternberg, "Ror receptor tyrosine kinases: orphans no more," *Trends Cell Biol*, vol. 18, pp. 536–544, 2008.

- [15] I. Oishi, S. Sugiyama, Z.-J. Liu, H. Yamamura, Y. Nishida, and Y. Minami, "A novel drosophila receptor tyrosine kinase expressed specifically in the nervous system unique structural features and implication in developmental signaling," *J Biol Chem*, vol. 272, pp. 11916–11923, 1997.
- [16] M. Kaucká, P. Krejčí, K. Plevová, Š. Pavlová, J. Procházková, P. Janovská, J. Valňohová, A. Kozubík, Š. Pospíšilová, and V. Bryja, "Post-translational modifications regulate signalling by *ror1*," *Acta Physiol*, vol. 203, pp. 351–362, 2011.
- [17] N. Borchering, D. Kusner, G.-H. Liu, and W. Zhang, "Ror1, an embryonic protein with an emerging role in cancer biology," *Protein Cell*, vol. 5, pp. 496–502, 2014.
- [18] M. Hojjat-Farsangi, A. Moshfegh, A. H. Daneshmanesh, A. S. Khan, E. Mikaelsson, A. Österborg, and H. Mellstedt, "The receptor tyrosine kinase *ror1*—an oncofetal antigen for targeted cancer therapy," in *Semin Cancer Biol*, vol. 29, pp. 21–31, Elsevier, 2014.
- [19] C. Wilson, D. Goberdhan, and H. Steller, "Dror, a potential neurotrophic receptor gene, encodes a drosophila homolog of the vertebrate *ror* family of *trk*-related receptor tyrosine kinases," *Proc Natl Acad Sci U S A*, vol. 90, pp. 7109–7113, 1993.
- [20] A. Yoda, I. Oishi, and Y. Minami, "Expression and function of the *ror*-family receptor tyrosine kinases during development: Lessons from genetic analyses of nematodes, mice, and humans," *J Recept Signal Transduct Res*, vol. 23, pp. 1–15, 2003.
- [21] R. Al-Shawi, S. V. Ashton, C. Underwood, and J. P. Simons, "Expression of the *ror1* and *ror2* receptor tyrosine kinase genes during mouse development," *Dev Genes Evol*, vol. 211, pp. 161–171, 2001.
- [22] M. Nomi, I. Oishi, S. Kani, H. Suzuki, T. Matsuda, A. Yoda, M. Kitamura, K. Itoh, S. Takeuchi, K. Takeda, *et al.*, "Loss of *mrer1* enhances the heart and skeletal abnormalities in *mrer2*-deficient mice: redundant and pleiotropic functions of *mrer1* and *mrer2* receptor tyrosine kinases," *Mol Cell Biol*, vol. 21, pp. 8329–8335, 2001.
- [23] N. Lyashenko, M. Weissenböck, A. Sharir, R. G. Erben, Y. Minami, and C. Hartmann, "Mice lacking the orphan receptor *ror1* have distinct skeletal abnormalities and are growth retarded," *Dev Dyn*, vol. 239, pp. 2266–2277, 2010.
- [24] S. Zhang, L. Chen, J. Wang-Rodriguez, L. Zhang, B. Cui, W. Frankel, R. Wu, and T. J. Kipps, "The onco-embryonic antigen *ror1* is expressed by a variety of human cancers," *Am J Pathol*, vol. 181, pp. 1903–1910, 2012.
- [25] A. H. DaneshManesh, E. Mikaelsson, M. Jeddi-Tehrani, A. A. Bayat, R. Ghods, M. Ostadkarampour, M. Akhondi, S. Lagercrantz, C. Larsson, A. Österborg, *et al.*, "Ror1, a cell surface receptor tyrosine kinase is expressed in chronic lymphocytic leukemia and may serve as a putative target for therapy," *Int J Cancer*, vol. 123, pp. 1190–1195, 2008.
- [26] M. Shabani, H. Asgarian-Omran, P. Vossough, R. A. Sharifian, M. Faranoush, S. Ghragozlou, J. Khoshnoodi, A. Roohi, M. Jeddi-Tehrani, H. Mellstedt, *et al.*, "Expression profile of orphan receptor tyrosine kinase (*ror1*) and wilms' tumor gene 1 (*wt1*) in different subsets of b-cell acute lymphoblastic leukemia," *Leuk Lymphoma*, vol. 49, pp. 1360–1367, 2008.

- [27] T. M. Wright, A. R. Brannon, J. D. Gordan, A. J. Mikels, C. Mitchell, S. Chen, I. Espinosa, M. van de Rijn, R. Pruthi, E. Wallen, *et al.*, "Ror2, a developmentally regulated kinase, promotes tumor growth potential in renal cell carcinoma," *Oncogene*, vol. 28, pp. 2513–2523, 2009.
- [28] A. H. Daneshmanesh, A. Porwit, M. Hojjat-Farsangi, M. Jeddi-Tehrani, K. P. Tamm, D. Grandér, S. Lehmann, S. Norin, F. Shokri, H. Rabbani, *et al.*, "Orphan receptor tyrosine kinases ror1 and ror2 in hematological malignancies," *Leuk Lymphoma*, vol. 54, pp. 843–850, 2013.
- [29] G. Barna, R. Mihalik, B. Timár, J. Tömböl, Z. Csende, A. Sebestyén, C. Bödör, B. Csernus, L. Reiniger, I. Peták, *et al.*, "Ror1 expression is not a unique marker of cll," *Hematol Oncol*, vol. 29, pp. 17–21, 2011.
- [30] P. Li, D. Harris, Z. Liu, J. Liu, M. Keating, and Z. Estrov, "Stat3 activates the receptor tyrosine kinase like orphan receptor-1 gene in chronic lymphocytic leukemia cells," *PloS One*, vol. 5, p. e11859, 2010.
- [31] T. Fukuda, L. Chen, T. Endo, L. Tang, D. Lu, J. E. Castro, G. F. Widhopf, L. Z. Rassenti, M. J. Cantwell, C. E. Prussak, *et al.*, "Antisera induced by infusions of autologous ad-cd154-leukemia b cells identify ror1 as an oncofetal antigen and receptor for wnt5a," *Proc Natl Acad Sci U S A*, vol. 105, pp. 3047–3052, 2008.
- [32] G. F. Widhopf, B. Cui, E. M. Ghia, L. Chen, K. Messer, Z. Shen, S. P. Briggs, C. M. Croce, and T. J. Kipps, "Ror1 can interact with tcl1 and enhance leukemogenesis in  $e\mu$ -tcl1 transgenic mice," *Proc Natl Acad Sci U S A*, vol. 111, pp. 793–798, 2014.
- [33] T. Yamaguchi, K. Yanagisawa, R. Sugiyama, Y. Hosono, Y. Shimada, C. Arima, S. Kato, S. Tomida, M. Suzuki, H. Osada, *et al.*, "Nkx2-1/titf1/ttf-1-induced ror1 is required to sustain egfr survival signaling in lung adenocarcinoma," *Cancer Cell*, vol. 21, pp. 348–361, 2012.
- [34] L. Grumolato, G. Liu, P. Mong, R. Mudbhary, R. Biswas, R. Arroyave, S. Vijayakumar, A. N. Economides, and S. A. Aaronson, "Canonical and noncanonical wnts use a common mechanism to activate completely unrelated coreceptors," *Genes Dev*, vol. 24, pp. 2517–2530, 2010.
- [35] S. Zhang, L. Chen, B. Cui, H.-Y. Chuang, J. Yu, J. Wang-Rodriguez, L. Tang, G. Chen, G. W. Basak, and T. J. Kipps, "Ror1 is expressed in human breast cancer and associated with enhanced tumor-cell growth," *PloS One*, vol. 7, p. e31127, 2012.
- [36] T. Yamaguchi, C. Lu, L. Ida, K. Yanagisawa, J. Usukura, J. Cheng, N. Hotta, Y. Shimada, H. Isomura, M. Suzuki, *et al.*, "Ror1 sustains caveolae and survival signalling as a scaffold of cavin-1 and caveolin-1," *Nat Commun*, vol. 7, 2016.
- [37] B. Cui, G. F. Widhopf, J. Yu, D. Martinez, E. Avery, S. Zhang, L. Chen, R. Wu, C. C. Wu, C. Prussak, *et al.*, "Targeting of chronic lymphocytic leukemia b cells with a novel monoclonal antibody to ror1," *Blood*, vol. 118, pp. 984–984, 2011.
- [38] A. Daneshmanesh, M. Hojjat-Farsangi, A. Khan, M. Jeddi-Tehrani, M. Akhondi, A. Bayat, R. Ghods, A. Mahmoudi, R. Hadavi, A. Österborg, *et al.*, "Monoclonal antibodies against ror1 induce apoptosis of chronic lymphocytic leukemia (cll) cells," *Leukemia*, vol. 26, pp. 1348–1355, 2012.

- [39] B. Cui, S. Zhang, L. Chen, J. Yu, G. F. Widhopf, J.-F. Fecteau, L. Z. Rassenti, and T. J. Kipps, "Targeting *ror1* inhibits epithelial–mesenchymal transition and metastasis," *Cancer Res*, vol. 73, pp. 3649–3660, 2013.
- [40] S. Asgharzadeh, R. Pique-Regi, R. Sposto, H. Wang, Y. Yang, H. Shimada, K. Matthay, J. Buckley, A. Ortega, and R. C. Seeger, "Prognostic significance of gene expression profiles of metastatic neuroblastomas lacking *mycn* gene amplification," *J Natl Cancer Inst*, vol. 98, pp. 1193–1203, 2006.
- [41] R. Tamaskovic, M. Simon, N. Stefan, M. Schwill, and A. Plückthun, "Designed ankyrin repeat proteins (darpins) from research to therapy," *Methods Enzymol*, vol. 503, pp. 101–134, 2012.
- [42] A. Wörn and A. Plückthun, "Stability engineering of antibody single-chain fv fragments," *J Mol Biol*, vol. 305, pp. 989–1010, 2001.
- [43] R. Glockshuber, T. Schmidt, and A. Plückthun, "The disulfide bonds in antibody variable domains: effects on stability, folding in vitro, and functional expression in *escherichia coli*," *Biochemistry*, vol. 31, pp. 1270–1279, 1992.
- [44] A. Rosenberg and B. Demeule, *Biobetters: Protein engineering to approach the curative*, vol. 19. Springer, 2015.
- [45] D. R. Burton and J. M. Woof, "Human antibody effector function," *Adv Immunol*, vol. 51, pp. 1–84, 1992.
- [46] H. K. Binz, P. Amstutz, and A. Plückthun, "Engineering novel binding proteins from nonimmunoglobulin domains," *Nat Biotechnol*, vol. 23, pp. 1257–1268, 2005.
- [47] G. Köhler and C. Milstein, "Continuous cultures of fused cells secreting antibody of predefined specificity," *Nature*, vol. 256, pp. 495–497, 1975.
- [48] J. Osbourn, M. Groves, and T. Vaughan, "From rodent reagents to human therapeutics using antibody guided selection," *Methods*, vol. 36, pp. 61–68, 2005.
- [49] C. R. Geyer, J. McCafferty, S. Dübel, A. R. Bradbury, and S. S. Sidhu, "Recombinant antibodies and in vitro selection technologies," *Methods Mol Biol*, pp. 11–32, 2012.
- [50] P. Amstutz, P. Forrer, C. Zahnd, and A. Plückthun, "In vitro display technologies: novel developments and applications," *Curr Opin Biotechnol*, vol. 12, pp. 400–405, 2001.
- [51] E. T. Boder and K. D. Wittrup, "Yeast surface display for screening combinatorial polypeptide libraries.," *Nat Biotechnol*, vol. 15, pp. 553–557, 1997.
- [52] W. R. Strohl and L. M. Strohl, *Therapeutic antibody engineering: current and future advances driving the strongest growth area in the pharmaceutical industry*. Elsevier, 2012.
- [53] D. E. Steinmeyer and E. L. McCormick, "The art of antibody process development," *Drug Discov Today*, vol. 13, pp. 613–618, 2008.
- [54] R. G. Werner, "Economic aspects of commercial manufacture of biopharmaceuticals," *J Biotechnol*, vol. 113, pp. 171–182, 2004.
- [55] A. Skerra and A. Plückthun, "Assembly of a functional immunoglobulin fv fragment in *escherichia coli*," *Science*, vol. 240, p. 1038, 1988.

- [56] A. Skerra, "Bacterial expression of immunoglobulin fragments," *Curr Opin Immunol*, vol. 5, pp. 256–262, 1993.
- [57] P. Holliger and P. J. Hudson, "Engineered antibody fragments and the rise of single domains," *Nat Biotechnol*, vol. 23, no. 9, pp. 1126–1136, 2005.
- [58] R. Glockshuber, M. Malia, I. Pfitzinger, and A. Plueckthun, "A comparison of strategies to stabilize immunoglobulin fv-fragments," *Biochemistry*, vol. 29, pp. 1362–1367, 1990.
- [59] J. S. Huston, D. Levinson, M. Mudgett-Hunter, M.-S. Tai, J. Novotný, M. N. Margolies, R. J. Ridge, R. E. Brucoleri, E. Haber, and R. Crea, "Protein engineering of antibody binding sites: recovery of specific activity in an anti-digoxin single-chain fv analogue produced in escherichia coli," *Proc Natl Acad Sci U S A*, vol. 85, pp. 5879–5883, 1988.
- [60] A. L. Nelson and J. M. Reichert, "Development trends for therapeutic antibody fragments," *Nat Biotechnol*, vol. 27, pp. 331–337, 2009.
- [61] G. Y. Melmed, S. R. Targan, U. Yasothan, D. Hanicq, and P. Kirkpatrick, "Certolizumab pegol," *Nat Rev Drug Discov*, vol. 7, pp. 641–642, 2008.
- [62] G. Wozniak-Knopp, S. Bartl, A. Bauer, M. Mostageer, M. Woisetschläger, B. Antes, K. Ettl, M. Kainer, G. Weberhofer, S. Wiederkum, *et al.*, "Introducing antigen-binding sites in structural loops of immunoglobulin constant domains: Fc fragments with engineered her2/neu-binding sites and antibody properties," *Protein Eng Des Sel*, vol. 23, pp. 289–297, 2010.
- [63] K. Conrath, C. Vincke, B. Stijlemans, J. Schymkowitz, K. Decanniere, L. Wyns, S. Muyldermans, and R. Loris, "Antigen binding and solubility effects upon the veneering of a camel vhh in framework-2 to mimic a vh," *J Mol Biol*, vol. 350, pp. 112–125, 2005.
- [64] A. Skerra, "Alternative non-antibody scaffolds for molecular recognition," *Curr Opin Biotechnol*, vol. 18, pp. 295–304, 2007.
- [65] T. Wurch, A. Pierré, and S. Depil, "Novel protein scaffolds as emerging therapeutic proteins: from discovery to clinical proof-of-concept," *Trends Biotechnol*, vol. 30, pp. 575–582, 2012.
- [66] M. Gebauer and A. Skerra, "Engineered protein scaffolds as next-generation antibody therapeutics," *Curr Opin Chem Biol*, vol. 13, pp. 245–255, 2009.
- [67] E. Hohenester and J. Engel, "Domain structure and organisation in extracellular matrix proteins," *Matrix Biol*, vol. 21, pp. 115–128, 2002.
- [68] A. Koide, C. W. Bailey, X. Huang, and S. Koide, "The fibronectin type iii domain as a scaffold for novel binding proteins," *J Mol Biol*, vol. 284, pp. 1141–1151, 1998.
- [69] B. J. Hackel, A. Kapila, and K. D. Wittrup, "Picomolar affinity fibronectin domains engineered utilizing loop length diversity, recursive mutagenesis, and loop shuffling," *J Mol Biol*, vol. 381, pp. 1238–1252, 2008.
- [70] B. J. Hackel and K. D. Wittrup, "The full amino acid repertoire is superior to serine/tyrosine for selection of high affinity immunoglobulin g binders from the fibronectin scaffold," *Protein Eng Des Sel*, p. gzp083, 2010.

- [71] L. Bloom and V. Calabro, "Fn3: a new protein scaffold reaches the clinic," *Drug Discov Today*, vol. 14, pp. 949–955, 2009.
- [72] A. W. Tolcher, C. J. Sweeney, K. Papadopoulos, A. Patnaik, E. G. Chiorean, A. C. Mita, K. Sankhala, E. Furfine, J. Gokemeijer, L. Iacono, *et al.*, "Phase i and pharmacokinetic study of ct-322 (bms-844203), a targeted adnectin inhibitor of vegfr-2 based on a domain of human fibronectin," *Clin Cancer Res*, vol. 17, pp. 363–371, 2011.
- [73] J. Davis, D. Lipovsek, and R. Camphausen, "Fibronectin binding domains with reduced immunogenicity," Feb. 1 2013. US Patent App. 13/757,668.
- [74] S. Cload, L. Engle, D. Lipovsek, M. Madireddi, G. C. Rakestraw, J. Swain, W. Zhao, H. Wei, A. P. Yamniuk, V. Ramamurthy, *et al.*, "Fibronectin based scaffold domain proteins that bind to myostatin," Oct. 7 2014. US Patent 8,853,154.
- [75] P.-C. Klöhn, U. Wuellner, N. Zizlsperger, Y. Zhou, D. Tavares, S. Berger, K. A. Zettlitz, G. Proetzel, M. Yong, R. H. Begent, *et al.*, "Ibc's 23rd annual antibody engineering, 10th annual antibody therapeutics international conferences and the 2012 annual meeting of the antibody society: December 3–6, 2012, san diego, ca," *MAbs*, vol. 5, pp. 178–201, 2013.
- [76] M. Gebauer and A. Skerra, "Alternative protein scaffolds as novel biotherapeutics," *Biobetters*, pp. 221–268, 2015.
- [77] K. Nord, E. Gunneriusson, J. Ringdahl, S. Ståhl, M. Uhlén, and P.-Å. Nygren, "Binding proteins selected from combinatorial libraries of an  $\alpha$ -helical bacterial receptor domain," *Nat Biotechnol*, vol. 15, pp. 772–777, 1997.
- [78] J. Löfblom, J. Feldwisch, V. Tolmachev, J. Carlsson, S. Ståhl, and F. Y. Frejd, "Affibody molecules: engineered proteins for therapeutic, diagnostic and biotechnological applications," *FEBS Lett*, vol. 584, pp. 2670–2680, 2010.
- [79] E. Wahlberg, C. Lendel, M. Helgstrand, P. Allard, V. Dincbas-Renqvist, A. Hedqvist, H. Berglund, P.-Å. Nygren, and T. Härd, "An affibody in complex with a target protein: structure and coupled folding," *Proc Natl Acad Sci U S A*, vol. 100, pp. 3185–3190, 2003.
- [80] W. Hoyer, C. Grönwall, A. Jonsson, S. Ståhl, and T. Härd, "Stabilization of a  $\beta$ -hairpin in monomeric alzheimer's amyloid- $\beta$  peptide inhibits amyloid formation," *Proc Natl Acad Sci U S A*, vol. 105, pp. 5099–5104, 2008.
- [81] R. P. Baum, V. Prasad, D. Müller, C. Schuchardt, A. Orlova, A. Wennborg, V. Tolmachev, and J. Feldwisch, "Molecular imaging of her2-expressing malignant tumors in breast cancer patients using synthetic 111in-or 68ga-labeled affibody molecules," *J Nucl Med*, vol. 51, pp. 892–897, 2010.
- [82] S. Ahlgren, A. Orlova, H. Wållberg, M. Hansson, M. Sandström, R. Lewsley, A. Wennborg, L. Abrahmsén, V. Tolmachev, and J. Feldwisch, "Targeting of her2-expressing tumors using 111in-aby-025, a second-generation affibody molecule with a fundamentally reengineered scaffold," *J Nucl Med*, vol. 51, pp. 1131–1138, 2010.
- [83] A. Orlova, A. Jonsson, D. Rosik, H. Lundqvist, M. Lindborg, L. Abrahmsen, C. Ekblad, F. Y. Frejd, and V. Tolmachev, "Site-specific radiometal labeling and improved biodistribution using aby-027, a novel her2-targeting affibody molecule–albumin-binding domain fusion protein," *J Nucl Med*, vol. 54, pp. 961–968, 2013.

- [84] V. Tolmachev, D. Rosik, H. Wällberg, A. Sjöberg, M. Sandström, M. Hansson, A. Wennborg, and A. Orlova, "Imaging of egfr expression in murine xenografts using site-specifically labelled anti-egfr in-111-dota-z (egfr: 2377) affibody molecule: aspect of the amount of injected tracer," *Eur J Nucl Med Mol Imaging*, vol. 36, pp. S251–S252, 2009.
- [85] J. Strand, Z. Varasteh, O. Eriksson, L. Abrahmsen, A. Orlova, and V. Tolmachev, "Gallium-68-labeled affibody molecule for pet imaging of pdgfr $\beta$  expression in vivo," *Mol Pharm*, vol. 11, pp. 3957–3964, 2014.
- [86] D. R. Flower, "The lipocalin protein family: structure and function," *Biochem J*, vol. 318, pp. 1–14, 1996.
- [87] A. Skerra, "'anticalins': a new class of engineered ligand-binding proteins with antibody-like properties," *J Biotechnol*, vol. 74, pp. 257–275, 2001.
- [88] M. Gebauer and A. Skerra, "7 anticalins: Small engineered binding proteins based on the lipocalin scaffold," *Methods Enzymol*, vol. 503, p. 157, 2012.
- [89] V. Albrecht, A. Richter, S. Pfeiffer, M. Gebauer, S. Lindner, E. Gieser, U. Schüller, C. Schichor, F. J. Gildehaus, P. Bartenstein, *et al.*, "Anticalins directed against the fibronectin extra domain b as diagnostic tracers for glioblastomas," *Int J Cancer*, vol. 138, pp. 1269–1280, 2016.
- [90] D. M. Pardoll, "The blockade of immune checkpoints in cancer immunotherapy," *Nat Rev Cancer*, vol. 12, pp. 252–264, 2012.
- [91] K. Mross, H. Richly, R. Fischer, D. Scharr, M. Büchert, A. Stern, H. Gille, L. P. Audoly, and M. E. Scheulen, "First-in-human phase i study of prs-050 (angiocal), an anticalin targeting and antagonizing vegf-a, in patients with advanced solid tumors," *PLoS One*, vol. 8, p. e83232, 2013.
- [92] A. G. T. van Scheltinga, M. N. Lub-de Hooge, M. J. Hinner, R. B. Verheijen, A. Allersdorfer, M. Hülsmeier, W. B. Nagengast, C. P. Schröder, J. G. Kosterink, E. G. de Vries, *et al.*, "In vivo visualization of met tumor expression and anticalin biodistribution with the met-specific anticalin 89zr-prs-110 pet tracer," *J Nucl Med*, vol. 55, pp. 665–671, 2014.
- [93] M. Steiner, K. Gutbrodt, N. Krall, and D. Neri, "Tumor-targeting antibody–anticalin fusion proteins for in vivo pretargeting applications," *Bioconjug Chem*, vol. 24, pp. 234–241, 2013.
- [94] A. M. Hohlbaum, S. Trentman, H. Gille, A. Allersdorfer, R. S. Belaiba, M. Huelsmeyer, J. Christian, T. Sandal, G. Matschiner, K. Jensen, *et al.*, "Discovery and preclinical characterization of a novel hepcidin antagonist with tunable pk/pd properties for the treatment of anemia in different patient populations," *Blood*, vol. 118, pp. 687–687, 2011.
- [95] M. A. Andrade, C. Perez-Iratxeta, and C. P. Ponting, "Protein repeats: structures, functions, and evolution," *J Struct Biol*, vol. 134, pp. 117–131, 2001.
- [96] P. Forrer, M. T. Stumpp, H. K. Binz, and A. Plückthun, "A novel strategy to design binding molecules harnessing the modular nature of repeat proteins," *FEBS Lett*, vol. 539, pp. 2–6, 2003.
- [97] M. R. Groves and D. Barford, "Topological characteristics of helical repeat protein," *Curr Opin Struct Biol*, vol. 9, pp. 383–389, 1999.

- [98] S. G. Sedgwick and S. J. Smerdon, "The ankyrin repeat: a diversity of interactions on a common structural framework," *Trends Biochem Sci*, vol. 24, pp. 311–316, 1999.
- [99] E. J. Neer, C. J. Schmidt, R. Nambudripad, and T. F. Smith, "The ancient regulatory-protein family of wd-repeat proteins.," *Nature*, vol. 371, p. 297, 1994.
- [100] M. Peifer, S. Berg, and A. B. Reynolds, "A repeating amino acid motif shared by proteins with diverse cellular roles," *Cell*, vol. 76, pp. 789–791, 1994.
- [101] B. Kobe and J. Deisenhofer, "The leucine-rich repeat: a versatile binding motif," *Trends Biochem Sci*, vol. 19, pp. 415–421, 1994.
- [102] S. E. Lux, K. M. John, and V. Bennett, "Analysis of cDNA for human erythrocyte ankyrin indicates a repeated structure with homology to tissue-differentiation and cell-cycle control proteins," *Nature*, 1990.
- [103] Y. L. Boersma and A. Plückthun, "Darpins and other repeat protein scaffolds: advances in engineering and applications," *Curr Opin Biotechnol*, vol. 22, pp. 849–857, 2011.
- [104] A. Plückthun, "Designed ankyrin repeat proteins (darpins): binding proteins for research, diagnostics, and therapy," *Annu Rev Pharmacol Toxicol*, vol. 55, pp. 489–511, 2015.
- [105] B. Kobe and A. V. Kajava, "When protein folding is simplified to protein coiling: the continuum of solenoid protein structures," *Trends Biochem Sci*, vol. 25, pp. 509–515, 2000.
- [106] H. K. Binz, M. T. Stumpp, P. Forrer, P. Amstutz, and A. Plückthun, "Designing repeat proteins: well-expressed, soluble and stable proteins from combinatorial libraries of consensus ankyrin repeat proteins," *J Mol Biol*, vol. 332, pp. 489–503, 2003.
- [107] G. Interlandi, S. K. Wetzel, G. Settanni, A. Plückthun, and A. Caflisch, "Characterization and further stabilization of designed ankyrin repeat proteins by combining molecular dynamics simulations and experiments," *J Mol Biol*, vol. 375, pp. 837–854, 2008.
- [108] S. K. Wetzel, C. Ewald, G. Settanni, S. Jurt, A. Plückthun, and O. Zerbe, "Residue-resolved stability of full-consensus ankyrin repeat proteins probed by nmr," *J Mol Biol*, vol. 402, pp. 241–258, 2010.
- [109] H. K. Binz, P. Amstutz, A. Kohl, M. T. Stumpp, C. Briand, P. Forrer, M. G. Grütter, and A. Plückthun, "High-affinity binders selected from designed ankyrin repeat protein libraries," *Nat Biotechnol*, vol. 22, pp. 575–582, 2004.
- [110] S. K. Wetzel, G. Settanni, M. Kenig, H. K. Binz, and A. Plückthun, "Folding and unfolding mechanism of highly stable full-consensus ankyrin repeat proteins," *J Mol Biol*, vol. 376, pp. 241–257, 2008.
- [111] A. Mann, N. Friedrich, A. Krarup, J. Weber, E. Stiegeler, B. Dreier, P. Pugach, M. Robbiani, T. Riedel, K. Moehle, *et al.*, "Conformation-dependent recognition of hiv gp120 by designed ankyrin repeat proteins provides access to novel hiv entry inhibitors," *J Virol*, vol. 87, pp. 5868–5881, 2013.

- [112] N. Stefan, P. Martin-Killias, S. Wyss-Stoeckle, A. Honegger, U. Zangemeister-Wittke, and A. Plückthun, "Darpins recognizing the tumor-associated antigen ep-cam selected by phage and ribosome display and engineered for multivalency," *J Mol Biol*, vol. 413, pp. 826–843, 2011.
- [113] M. Hanenberg, J. McAfoose, L. Kulic, T. Welt, F. Wirth, P. Parizek, L. Strobel, S. Cattepoel, C. Späni, R. Derungs, *et al.*, "Amyloid- $\beta$  peptide-specific darpins as a novel class of potential therapeutics for alzheimer disease," *J Biol Chem*, vol. 289, pp. 27080–27089, 2014.
- [114] A. Stahl, M. T. Stumpp, A. Schlegel, S. Ekawardhani, C. Lehrling, G. Martin, M. Gulotti-Georgieva, D. Villemagne, P. Forrer, H. T. Agostini, *et al.*, "Highly potent vegf-a-antagonistic darpins as anti-angiogenic agents for topical and intravitreal applications," *Angiogenesis*, vol. 16, pp. 101–111, 2013.
- [115] C. Zahnd, E. Wyler, J. M. Schwenk, D. Steiner, M. C. Lawrence, N. M. McKern, F. Pecorari, C. W. Ward, T. O. Joos, and A. Plückthun, "A designed ankyrin repeat protein evolved to picomolar affinity to her2," *J Mol Biol*, vol. 369, pp. 1015–1028, 2007.
- [116] L. Kummer, P. Parizek, P. Rube, B. Millgramm, A. Prinz, P. R. Mittl, M. Kaufholz, B. Zimmermann, F. W. Herberg, and A. Plückthun, "Structural and functional analysis of phosphorylation-specific binders of the kinase erk from designed ankyrin repeat protein libraries," *Proc Natl Acad Sci U S A*, vol. 109, pp. E2248–E2257, 2012.
- [117] P. Parizek, L. Kummer, P. Rube, A. Prinz, F. W. Herberg, and A. Plückthun, "Designed ankyrin repeat proteins (darpins) as novel isoform-specific intracellular inhibitors of c-jun n-terminal kinases," *ACS Chem Biol*, vol. 7, pp. 1356–1366, 2012.
- [118] L. Kummer, C.-W. Hsu, O. Dagliyan, C. MacNevin, M. Kaufholz, B. Zimmermann, N. V. Dokholyan, K. M. Hahn, and A. Plückthun, "Knowledge-based design of a biosensor to quantify localized erk activation in living cells," *Chem Biol*, vol. 20, pp. 847–856, 2013.
- [119] J.-P. Theurillat, B. Dreier, G. Nagy-Davidescu, B. Seifert, S. Behnke, U. Zürcher-Härdi, F. Ingold, A. Plückthun, and H. Moch, "Designed ankyrin repeat proteins: a novel tool for testing epidermal growth factor receptor 2 expression in breast cancer," *Mod Pathol*, vol. 23, pp. 1289–1297, 2010.
- [120] C. Zahnd, M. Kawe, M. T. Stumpp, C. de Pasquale, R. Tamaskovic, G. Nagy-Davidescu, B. Dreier, R. Schibli, H. K. Binz, R. Waibel, and A. Plückthun, "Efficient tumor targeting with high-affinity designed ankyrin repeat proteins: effects of affinity and molecular size," *Cancer Res*, vol. 70, pp. 1595–1605, 2010.
- [121] M. M. Schmidt and K. D. Wittrup, "A modeling analysis of the effects of molecular size and binding affinity on tumor targeting," *Mol Cancer Ther*, vol. 8, pp. 2861–2871, 2009.
- [122] G. M. Thurber, M. M. Schmidt, and K. D. Wittrup, "Antibody tumor penetration: transport opposed by systemic and antigen-mediated clearance," *Adv Drug Deliv Rev*, vol. 60, pp. 1421–1434, 2008.
- [123] C. Jost, J. Schilling, R. Tamaskovic, M. Schwill, A. Honegger, and A. Plückthun, "Structural basis for eliciting a cytotoxic effect in her2-overexpressing cancer cells via binding to the extracellular domain of her2," *Structure*, vol. 21, pp. 1979–1991, 2013.

- [124] R. Tamaskovic, M. Schwill, G. Nagy-Davidescu, C. Jost, D. C. Schaefer, W. P. Verdurmen, J. V. Schaefer, A. Honegger, and A. Plückthun, "Intermolecular biparatopic trapping of erbb2 prevents compensatory activation of pi3k/akt via ras-p110 crosstalk," *Nat Commun*, vol. 7, 2016.
- [125] P. Martin-Killias, N. Stefan, S. Rothschild, A. Plückthun, and U. Zangemeister-Wittke, "A novel fusion toxin derived from an epcam-specific designed ankyrin repeat protein has potent antitumor activity," *Clin Cancer Res*, vol. 17, pp. 100–110, 2011.
- [126] J. Winkler, P. Martin-Killias, A. Plückthun, and U. Zangemeister-Wittke, "Epcam-targeted delivery of nanocomplexed sirna to tumor cells with designed ankyrin repeat proteins," *Mol Cancer Ther*, vol. 8, pp. 2674–2683, 2009.
- [127] B. Dreier, G. Mikheeva, N. Belousova, P. Parizek, E. Boczek, I. Jelesarov, P. Forrer, A. Plückthun, and V. Krasnykh, "Her2-specific multivalent adapters confer designed tropism to adenovirus for gene targeting," *J Mol Biol*, vol. 405, pp. 410–426, 2011.
- [128] B. Dreier, A. Honegger, C. Hess, G. Nagy-Davidescu, P. R. Mittl, M. G. Grütter, N. Belousova, G. Mikheeva, V. Krasnykh, and A. Plückthun, "Development of a generic adenovirus delivery system based on structure-guided design of bispecific trimeric darpin adapters," *Proc Natl Acad Sci U S A*, vol. 110, pp. E869–E877, 2013.
- [129] R. C. Münch, M. D. Mühlebach, T. Schaser, S. Kneissl, C. Jost, A. Plückthun, K. Cichutek, and C. J. Buchholz, "Darpins: an efficient targeting domain for lentiviral vectors," *Mol Ther*, vol. 19, pp. 686–693, 2011.
- [130] K. Friedrich, J. R. Hanauer, S. Prüfer, R. C. Münch, I. Völker, C. Filippis, C. Jost, K.-M. Hanschmann, R. Cattaneo, K.-W. Peng, *et al.*, "Darpin-targeting of measles virus: unique bispecificity, effective oncolysis, and enhanced safety," *Mol Ther*, vol. 21, pp. 849–859, 2013.
- [131] S. Wolf, E. H. Souied, M. Mauget-Faysse, F. Devin, M. Patel, U. E. Wolf-Schnurrbusch, M. Stumpp, M. wet AMD study group, *et al.*, "Phase i mp0112 wet amd study: Results of a single escalating dose study with darpin® mp0112 in wet amd," *Invest Ophthalmol Vis Sci*, vol. 52, pp. 1655–1655, 2011.
- [132] E. H. Souied, F. Devin, M. Mauget-Fayssse, P. Kolář, U. Wolf-Schnurrbusch, C. Framme, D. Gaucher, G. Querques, M. T. Stumpp, S. Wolf, and M. S. Group, "Treatment of exudative age-related macular degeneration with a designed ankyrin repeat protein that binds vascular endothelial growth factor: a phase i/ii study," *Am J Ophthalmol*, vol. 158, pp. 724–732, 2014.
- [133] M. S. Packer and D. R. Liu, "Methods for the directed evolution of proteins," *Nat Rev Genet*, vol. 16, pp. 379–394, 2015.
- [134] G. Karimova, J. Pidoux, A. Ullmann, and D. Ladant, "A bacterial two-hybrid system based on a reconstituted signal transduction pathway," *Proc Natl Acad Sci U S A*, vol. 95, pp. 5752–5756, 1998.
- [135] G. P. Smith, "Filamentous fusion phage: novel expression vectors that display cloned antigens on the virion surface," *Science*, vol. 228, pp. 1315–1317, 1985.
- [136] J. A. Francisco, C. F. Earhart, and G. Georgiou, "Transport and anchoring of beta-lactamase to the external surface of escherichia coli," *Proc Natl Acad Sci U S A*, vol. 89, pp. 2713–2717, 1992.

- [137] R. R. Beerli, M. Bauer, R. B. Buser, M. Gwerder, S. Muntwiler, P. Maurer, P. Saudan, and M. F. Bachmann, "Isolation of human monoclonal antibodies by mammalian cell display," *Proc Natl Acad Sci U S A*, vol. 105, no. 38, pp. 14336–14341, 2008.
- [138] A. Plückthun, "Ribosome display: a perspective," *Methods Mol Biol*, pp. 3–28, 2012.
- [139] R. W. Roberts and J. W. Szostak, "Rna-peptide fusions for the in vitro selection of peptides and proteins," *Proc Natl Acad Sci U S A*, vol. 94, pp. 12297–12302, 1997.
- [140] J. Hanes and A. Plückthun, "In vitro selection and evolution of functional proteins by using ribosome display," *Proc Natl Acad Sci U S A*, vol. 94, pp. 4937–4942, 1997.
- [141] A. D. Griffiths and D. S. Tawfik, "Directed evolution of an extremely fast phosphotriesterase by in vitro compartmentalization," *EMBO J*, vol. 22, pp. 24–35, 2003.
- [142] M. Kaltenbach and F. Hollfelder, "Snap display: in vitro protein evolution in microdroplets," *Methods Mol Biol*, pp. 101–111, 2012.
- [143] L. Kisselev, M. Ehrenberg, and L. Frolova, "Termination of translation: interplay of mrna, rrnas and release factors?," *EMBO J*, vol. 22, pp. 175–182, 2003.
- [144] M. Y. Pavlov, A. Antoun, M. Lovmar, and M. Ehrenberg, "Complementary roles of initiation factor 1 and ribosome recycling factor in 70s ribosome splitting," *EMBO J*, vol. 27, pp. 1706–1717, 2008.
- [145] K. Cheng, N. Ivanova, S. H. Scheres, M. Y. Pavlov, J. M. Carazo, H. Hebert, M. Ehrenberg, and M. Lindahl, "tmrna· smpb complex mimics native aminoacyl-trnas in the a site of stalled ribosomes," *J Struct Biol*, vol. 169, pp. 342–348, 2010.
- [146] H. Yanagida, T. Matsuura, and T. Yomo, "Ribosome display for rapid protein evolution by consecutive rounds of mutation and selection," *Methods Mol Biol*, pp. 257–267, 2010.
- [147] J. Hanes, L. Jermutus, S. Weber-Bornhauser, H. R. Bosshard, and A. Plückthun, "Ribosome display efficiently selects and evolves high-affinity antibodies in vitro from immune libraries," *Proc Natl Acad Sci U S A*, vol. 95, pp. 14130–14135, 1998.
- [148] R. E. Hawkins, S. J. Russell, and G. Winter, "Selection of phage antibodies by binding affinity: mimicking affinity maturation," *J Mol Biol*, vol. 226, pp. 889–896, 1992.
- [149] C. Zahnd, S. Spinelli, B. Luginbühl, P. Amstutz, C. Cambillau, and A. Plückthun, "Directed in vitro evolution and crystallographic analysis of a peptide-binding single chain antibody fragment (scfv) with low picomolar affinity," *J Biol Chem*, vol. 279, pp. 18870–18877, 2004.
- [150] S. H. Northrup and H. P. Erickson, "Kinetics of protein-protein association explained by brownian dynamics computer simulation.," *Proc Natl Acad Sci U S A*, vol. 89, pp. 3338–3342, 1992.
- [151] C. Zahnd, C. A. Sarkar, and A. Plückthun, "Computational analysis of off-rate selection experiments to optimize affinity maturation by directed evolution," *Protein Eng Des Sel*, vol. 23, pp. 175–184, 2010.
- [152] N. B. Fernández, D. Lorenzo, M. E. Picco, G. Barbero, L. S. Dergan-Dylon, M. P. Marks, H. García-Rivello, L. Gimenez, V. Labovsky, L. Grumolato, *et al.*, "Ror1 contributes to melanoma cell growth and migration by regulating n-cadherin expression via the pi3k/akt pathway," *Mol Carcinog*, 2015.

- [153] C. Berger, D. Sommermeyer, M. Hudecek, M. Berger, A. Balakrishnan, P. J. Paszkiewicz, P. L. Kosasih, C. Rader, and S. R. Riddell, "Safety of targeting *ror1* in primates with chimeric antigen receptor–modified t cells," *Cancer Immunol Res*, vol. 3, pp. 206–216, 2015.
- [154] A. R. Afzal, A. Rajab, C. D. Fenske, M. Oldridge, N. Elanko, E. Ternes-Pereira, B. Tüysüz, V. A. Murday, M. A. Patton, A. O. Wilkie, *et al.*, "Recessive robinow syndrome, allelic to dominant brachydactyly type b, is caused by mutation of *ror2*," *Nat Genet*, vol. 25, pp. 419–422, 2000.
- [155] S. Takeuchi, K. Takeda, I. Oishi, M. Nomi, M. Ikeya, K. Itoh, S. Tamura, T. Ueda, T. Hatta, H. Otani, *et al.*, "Mouse *ror2* receptor tyrosine kinase is required for the heart development and limb formation," *Genes Cells*, vol. 5, pp. 71–78, 2000.
- [156] M. A. Kramer, S. K. Wetzel, A. Plückthun, P. R. Mittl, and M. G. Grütter, "Structural determinants for improved stability of designed ankyrin repeat proteins with a redesigned c-capping module," *J Mol Biol*, vol. 404, pp. 381–391, 2010.
- [157] B. Dreier and A. Plückthun, "Rapid selection of high-affinity binders using ribosome display," *Methods Mol Biol*, pp. 261–286, 2012.
- [158] H. Inoue, H. Nojima, and H. Okayama, "High efficiency transformation of *escherichia coli* with plasmids," *Gene*, vol. 96, pp. 23–28, 1990.
- [159] E. L. Cussler, *Diffusion: mass transfer in fluid systems*. Cambridge University Press, 2009.
- [160] F. Degorce, A. Card, S. Soh, E. Trinquet, G. P. Knapik, and B. Xie, "Htrf: a technology tailored for drug discovery—a review of theoretical aspects and recent applications," *Curr Chem Genomics*, vol. 3, 2009.

# Acknowledgement

I would like to thank Prof. Dr. Andreas Plückthun for giving me the great opportunity to work in his lab and giving me regular feedback and valuable discussions during my Master's thesis.

Further I want to emphasise a special thank to Dr. Birgit Dreier. Her supervision and neverlasting support throughout the whole project as well as her genuine interest in my development as a scientist made this project an exciting experience.

I would also like to thank Fabian Brandl for his valuable discussions and inputs, as well as Martina Zimmermann, Simon Hansen, Thomas Reinberg and Julia Thielicke for their technical support.

I further want to thank the whole group of Prof. Dr. Andreas Plückthun for their constant support and inputs during my stay in Zurich.

# List of Figures

1.1	Structure of human ROR1 . . . . .	2
1.2	Structural comparison between alternative protein scaffolds . . . . .	6
1.3	Structure of DARPins . . . . .	10
1.4	Overview of ribosome display selection . . . . .	14
1.5	Conditions for ribosome display selection for DARPins binding human ROR1 . . . . .	17
2.1	Vector pRDV . . . . .	28
2.2	Vector pQE30ss . . . . .	29
3.1	Homogenous Time Resolved Fluorescence of clones from the naive library N2C round 3 . . . . .	52
3.2	Homogenous Time Resolved Fluorescence of clones from the naive library N3C round 3 . . . . .	53
3.3	Homogenous Time Resolved Fluorescence of clones from the naive library r+nr round 3 . . . . .	54
3.4	Homogenous Time Resolved Fluorescence of clones from the naive library N2C round 4 . . . . .	55
3.5	Homogenous Time Resolved Fluorescence of clones from the naive library N3C round 4 . . . . .	56
3.6	Homogenous Time Resolved Fluorescence of clones from the naive library r+nr round 4 . . . . .	57
3.7	Sequence analysis of screened clones selected from ribosome display selection round three and four . . . . .	60
3.8	SDS-PAGE of purified DARPins . . . . .	61
3.9	Analytical SEC of DARPins evolved from round three and four of ribosome display selection . . . . .	62
3.10	ELISA to test binding of purified DARPins to the human ROR1 ECD . . . . .	66
3.11	Summary of test for cell binding of DARPins evolved from initial ribosome display selection round three and four . . . . .	68
3.12	Summary of test for cell binding of DARPins evolved from ribosome display selection round three and four . . . . .	70
3.13	Summary of results of epitope binning on extracellular domain of human ROR1 . . . . .	75
3.14	DNA products of error-prone PCR . . . . .	78
3.15	Agarose gel-electrophoresis of DNA products of RT-PCR products . . . . .	80
3.16	Agarose gel-electrophoresis of DNA products 2 of PCR of RT products . . . . .	82
3.17	Crude extract ELISA of clones evolved from off-rate selection (P1, P2, P3, P4) . . . . .	84
3.18	Crude extract ELISA of clones evolved from off-rate selection (P5, P6, P7) . . . . .	85
3.19	Sequence analysis of screened clones selected from pool P1 . . . . .	88
3.20	Sequence analysis of screened clones selected from pool P2 . . . . .	89

## LIST OF FIGURES

---

3.21	Sequence analysis of screened clones selected from pool P3 . . . . .	90
3.22	Sequence analysis of screened clones selected from pool P4 . . . . .	91
3.23	Sequence analysis of screened clones selected from pool P5 . . . . .	92
3.24	Sequence analysis of screened clones selected from pool P6 . . . . .	93
3.25	Sequence analysis of screened clones selected from pool P7 . . . . .	94
3.26	SDS-PAGE of purified DARPin . . . . .	95
3.27	Analytical SEC of DARPin from the first pool evolved from round six of ribosome display selection . . . . .	97
3.28	Summary to test for cell binding of DARPin evolved from ribosome display selection round six 1.1 . . . . .	101
3.29	Evolutionary tree of evolved DARPin . . . . .	105
1	Sequence A3w . . . . .	135
2	Sequence A8w . . . . .	135
3	Sequence C2w . . . . .	135
4	Sequence D1w . . . . .	135
5	Sequence D7w . . . . .	135
6	Sequence F3b . . . . .	136
7	Sequence G3w . . . . .	136
8	Sequence H6w . . . . .	136
9	Sequence P1E5 . . . . .	136
10	Sequence P1G3 . . . . .	136
11	Sequence P4E10 . . . . .	137
12	Sequence P4H10 . . . . .	137
13	Sequence P5C1 . . . . .	137
14	Sequence P5G5 . . . . .	137
15	Sequence P7H3 . . . . .	137
16	SEC-MALS (A2b, A2w, A3w, A8b, A8w, A11b, B1w, B5b) . . . . .	139
17	SEC-MALS (B6w, B7w, B8w, C1w, C2w, C3b, C6w, C7w) . . . . .	140
18	SEC-MALS (C8b, C9b, D1w, D2b, D3w, D6w, D7w, E1w) . . . . .	141
19	SEC-MALS (E2w, E3b, E3w, E5w, E6w, E10b, F3b, F4w) . . . . .	142
20	SEC-MALS (F6w, F12b, G3w, G4w, G5w, G6b, G6w, G7w) . . . . .	143
21	SEC-MALS (H1w, H3w, H6w, H7w, H8w, P1E5, P1G3, P1H3) . . . . .	144
22	SEC-MALS (P3A5, P3B3, P3G5, P4D12, P4E10, P4F12, P4H10, P5A5) . . . . .	145
23	SEC-MALS (P5C1, P5C6, P5G3, P5G5, P7G5, P7H3, P7H4) . . . . .	146
24	SPR (A2b, E10b, F4w, C9b, D2b, F3b, F12b, E3w) . . . . .	148
25	SPR (A8w, B6w, E3b, G6b, H6w, B7w) . . . . .	149
26	SPR (A2w, B1w, B5b, B8w, C1w, C6w, C7w, D6w) . . . . .	150
27	SPR (D7w, E1w, E2w, E6w, F4w, G4w, G5w, G6w) . . . . .	151
28	SPR (H1w, H7w) . . . . .	152
29	SPR (A11b, A3w, D1w, G3w, C2w, P1E5, P1G3, P1H2) . . . . .	153
30	SPR (P3A5, P3B3, P3G5, P4D12, P4E10, P4F12, P4H10, P5A5) . . . . .	154
31	SPR (P5C1, P5C6, P5G5, P5G3, P7G5, P7H3, P7H4) . . . . .	155

# List of Tables

1.1	Existing binders which target human ROR1 . . . . .	4
2.1	Buffer used for gel-electrophoresis . . . . .	19
2.2	Buffer used for cloning . . . . .	20
2.3	Buffer used for Ribosome Display selection . . . . .	21
2.4	Lysis buffer used for preparation of crude extracts . . . . .	21
2.5	Buffer used for Homogenous Time Resolved Fluorescence . . . . .	22
2.6	Buffer used for crude extract ELISA . . . . .	22
2.7	Buffer used for cell lysis and protein purification . . . . .	23
2.8	Buffers used for SDS-PAGE . . . . .	24
2.9	Buffers used for qualitative ELISA . . . . .	25
2.10	Buffers used for FACS . . . . .	25
2.11	Buffers used for SPR . . . . .	26
2.12	Reagents used for selection . . . . .	26
2.13	Reagents used for clean up of mRNA after <i>in vitro</i> transcription . . . . .	26
2.14	Primer used for reverse transcription, PCR and cloning . . . . .	26
2.15	Reagents used for reverse transcription, PCR and cloning . . . . .	27
2.16	Reagents used for <i>in vitro</i> transcription . . . . .	27
2.17	Reagents used for <i>in vitro</i> translation . . . . .	28
2.18	Strains . . . . .	29
2.19	Media . . . . .	30
2.20	DNA and Protein Marker . . . . .	30
2.21	Molecular weight standard for SEC . . . . .	31
2.22	Antibodies . . . . .	31
2.23	Cell lines . . . . .	31
2.24	Chemicals . . . . .	32
2.25	Instruments . . . . .	33
2.26	Kits . . . . .	34
2.27	Filter . . . . .	34
2.28	Columns . . . . .	34
2.29	SPR Chips . . . . .	34
2.30	Devices for buffer exchange . . . . .	34
2.31	Other devices . . . . .	35
2.32	Restriction reaction mix using <i>Bam</i> HI and <i>Hind</i> III . . . . .	36
2.33	Ligation reaction mix of clones and pRDV . . . . .	36
2.34	epPCR reaction mix . . . . .	37
2.35	Cycling parameters of epPCR of selected clones in pRDV . . . . .	37
2.36	Pools for off-rate selection with respective parental clones. . . . .	38
2.37	Reaction mix for <i>in vitro</i> transcription of PCR products . . . . .	38
2.38	Reaction mix for <i>in vitro</i> translation of RNA products . . . . .	39

2.39	Summary of differences in selection conditions performed in round 5 and 6 of ribosome display selection. NA: Not Applied . . . . .	40
2.40	Reaction mix for transcription of DARPIn-encoding RNA . . . . .	40
2.41	Reaction mix for amplification of cDNA coding for selected DARPins . . .	41
2.42	Cycling parameters for amplification of cDNA coding for selected DARPins	41
2.43	Restriction reaction mix using <i>Bam</i> HI and <i>Hind</i> III . . . . .	41
2.44	Ligation reaction mix of clones and pRDV . . . . .	42
2.45	Measuring parameters of HTRF . . . . .	43
2.46	Method and parameters of SEC-MALS . . . . .	48
2.47	Method and parameters of SPR . . . . .	49
2.48	Method and parameters of epitope binning . . . . .	50
3.1	DARPins round 3 and 4 analysed by SEC in absence of imidazole . . . . .	63
3.2	Summary SEC-MALS of DARPins evolved from ribosome display selection round three and four . . . . .	65
3.3	Setup of samples and control samples . . . . .	67
3.4	Setup of samples and control samples . . . . .	69
3.5	Clones tested for cell binding and ranked according to the measured Mean Fluorescent Intensity (MFI) . . . . .	71
3.6	Summary of binding kinetics of DARPins evolved round 3 and 4 of ribosome display selection . . . . .	72
3.7	Summary of binding kinetics of DARPins evolved round 3 and 4 of ribosome display selection . . . . .	73
3.8	Summary of epitope binning of DARPins . . . . .	76
3.9	DARPins subcloned for ribosome display selection round five and six. * Clone F4w was not retrievable after selection . . . . .	77
3.10	DARPins evolved from the sixth round of selection and characterised by SEC . . . . .	96
3.11	Summary of SEC-MALS of DARPins evolved from ribosome display selection round six . . . . .	98
3.12	Setup of samples and control samples . . . . .	99
3.13	Clones tested for cell binding and ranked according to the measured Mean Fluorescence Intensity (MFI) . . . . .	102
3.14	Summary of binding Kinetics of DARPins evolved from off-rate selection	103
3.15	Summary of properties of evolved DARPins . . . . .	106

# Appendices

# Appendix A

## Sequences

```

                20                40                60
MRGSHHHHHH GSDLGKKLLE AARAGQDDEV RILMANGADV NANDYIGRTP LHLAADSGHL
                80                100                120
E I I E V L L K R G A D V N A T D A W G I T P L H L A A W A G H L E I V E V L L K Y G A D V N A A D S D G N T P L H L A
                140                160
A Y S G H L E I V E V L L K H G A D V N A Q D K F G K T A F D I S I D N G N E D L A E I L Q K L N

```

Figure A.1: A3w

```

                20                40                60
MRGSHHHHHH GSDLGKKLLE AARAGQDDEV RILMANGADV DASDWNGHTP LHLAAWHGHL
                80                100                120
E I V D V L L K T G A D V N A M D N L G Y T P L H L A A N S G H L E I V E V L L K T G D D V N A D D W I G V T P L H L A
                140                160
A V L G H L E I V E V L L K H G A D V N A Q D K F G K T P F D L A I D N G N E D I A E V L Q K A A K L N

```

Figure A.2: A8w

```

                20                40                60
MRGSHHHHHH GSDLGKKLLE AARAGQDDEV RILMANGVDV NARDASGFTP LHLAAWAGHL
                80                100                120
E I V E V L L K N G A D V N A S D D Y G S T P L H L A A Y D G H L E I V E V L L K Y G A D V N A Q D K F G K T A F D I S
I D N G N E D L A E I L Q K L N

```

Figure A.3: C2w

```

                20                40                60
MRGSHHHHHH GSDLGKKLLE AARAGQDDEV RILMANGADV NAKDALGNTP LHLAAYNGHL
                80                100                120
E I V E V L L K N G A D V N A N D W V G V T P L H L A A N F G H L E I V E V L L K Y G A D V N A Q D K F G K T A F D I S
I D N G N E D L A E I L Q K L N

```

Figure A.4: D1w

```

                20                40                60
MRGSHHHHHH GSDLGKKLLE AARAGQDDEV RILMANGADV NASDWNGHTP LHLAAWHGHL
                80                100                120
E I V E V L L K T G A D V N A M D N L G Y T P L L L A A N S G H L E I V E V L L K A G A D V N A Q D T W G V T P L H L A
                140                160
A V Q G H L E I V E V L L K H G A D V N A Q D K F G K T P F D L A I D N G N E D I A E V L Q K A A K L N

```

Figure A.5: D7w

```

                20                40                60
                |                |                |
MRGSHHHHHH  GSDLGKKLLE  AARAGQDDEV  RILMANGADV  NASDWNGHTP  LHAAWHGHL
                80                100               120
E IVEVLLKTG  ADVNAMDNLG  YTPLHLAANS  GHLEIVEVLL  KAGADVNASD  WLGVTPLHLA
                140               160
AVMGHLEIVE  VLLKHGADV  AQDKFGKTPF  DLAI DNGNED  IAEVLQKAAK  LN
    
```

Figure A.6: F3b

```

                20                40                60
                |                |                |
MRGSHHHHHH  GSDLGKKLLE  AARAGQDDEV  RILMANGADV  NANDYIGRTP  LHLAADSGHL
                80                100               120
E IVEVLLKHG  ADVNATDAWG  I TPLHLAAWA  GHLEIVEVLL  KYGADVNAAD  SDGNTPLHLA
                140               160
AYSGHLEIVE  VLLKYGADV  AQDKFGKTAF  DISI DNGNED  LAEILQKLN
    
```

Figure A.7: G3w

```

                20                40                60
                |                |                |
MRGSHHHHHH  GSDLGKKLLE  AARAGQDDEV  RILMANGADV  NASDRYGRTP  LHAAFNGHL
                80                100               120
E IVEVLLKNG  ADVNAKDKIG  N TPLHLAANH  GHLEIVEVLL  KYGAVVNATD  WLGVTPLHLA
                140               160
AVFGHLEIVE  VLLKYGADV  AQDKFGKTAF  DISI DNGNED  LAEILQKLN
    
```

Figure A.8: H6w

```

                20                40                60
                |                |                |
MRGSHHHHHH  GSDLGKKLLE  AARAGQDDEV  RILMANGADV  NANDYIGRTP  LHLAADSGHL
                80                100               120
E IVEVLLKHG  ADVNATDAWG  I TPLHLAAWA  GHLEIVEALL  KYGADVNAAD  SDGNTPLHLA
                140               160
AYSGHLEIVG  VLLKYGADV  AQDKFGKTAF  DISI DNGNED  LAEILQKLN
    
```

Figure A.9: P1E5

```

                20                40                60
                |                |                |
MRGSHHHHHH  GSDLGKKLLE  AARAGQDDEV  RILMANGANV  NANDYIGRTP  LHLAADSGHL
                80                100               120
E IVEVLLKHG  ADVNATDAWG  I TPLHLAAWA  GHLEIVEVLL  KYGADVNAAD  SDGNTPLHLA
                140               160
AYSGHLEIVE  VLLKYGADV  AQDKFGKTAF  DISI DNGNED  LAEILQKLN
    
```

Figure A.10: P1G3

```

                20                40                60
                |                |                |
MRGSHHHHHH  GSDLGKKLLE  AARAGQDDEV  RILMANGVDV  NARDASGFTP  LHAAWAGHL
                80                100               120
                |                |                |
E IVEVLLKNG  ADVNASDDYG  STPLHLAAYD  GHLEIAEVLL  KYGADVNAQD  KFGKTAFDIS

IDNGNEDLAE  ILQKLN

```

Figure A.11: P4E10

```

                20                40                60
                |                |                |
MRGSHHHHHH  GSDLGKKLLE  AARAGQDDEV  RILMANGVDV  NARDASGFTP  LHAAWAGHL
                80                100               120
                |                |                |
E IVEVLLKNG  ADVNASDDYG  STPLHLTAYD  GHLEIAEVLL  KYGADVNAQD  KFGKTAFDIS

IDNGNEDLAE  ILQKLN

```

Figure A.12: P4H10

```

                20                40                60
                |                |                |
MRGSHHHHHH  GSDLGKKLLE  AARAGQDDEA  RILMANGADV  NASDWNGHTP  LHAAWHGHL
                80                100               120
                |                |                |
E IVEVLPKTG  ADVNAMDNLG  YTPLHLAANS  GHLEIVEVLL  KAGADVNASD  WLGVTPLHLA
                140               160
                |                |
AVMGHLEIVE  VLLKHGADV  AQDKFGKTPF  DLAI DNGNED  IAEVLQKAAK  LN

```

Figure A.13: P5C1

```

                20                40                60
                |                |                |
MRGSHHHHHH  GSDLGKKLLE  AARAGQDDEV  RILMANGADV  NASDWNGHTP  LHLTAWHGHL
                80                100               120
                |                |                |
E IVEVLLKTG  ADVNAMDNLG  YTPLHLAANS  GHLEIVEVLL  KAGADVNASD  WLGVTPLHLA
                140               160
                |                |
AVMGHLEIVE  VLLKHGADV  AQDKFGKTPF  DLAI DNGNED  IAEVLQKAAK  LN

```

Figure A.14: P5G5

```

                20                40                60
                |                |                |
MRGSHHHHHH  GSDLGKKLLE  AARAGQDDEV  RILMANGADV  NAKDALGNTP  LHAAAYNGHL
                80                100               120
                |                |                |
E IVEVLLKNG  ADVNANDWVG  VTPLHLAANF  GHLEIVEVLL  KYGADVNAQD  KFGKTALDIS

IDNGNEDLAE  ILQKLN

```

Figure A.15: P7H3

# **Appendix B**

## **SEC-MALS**

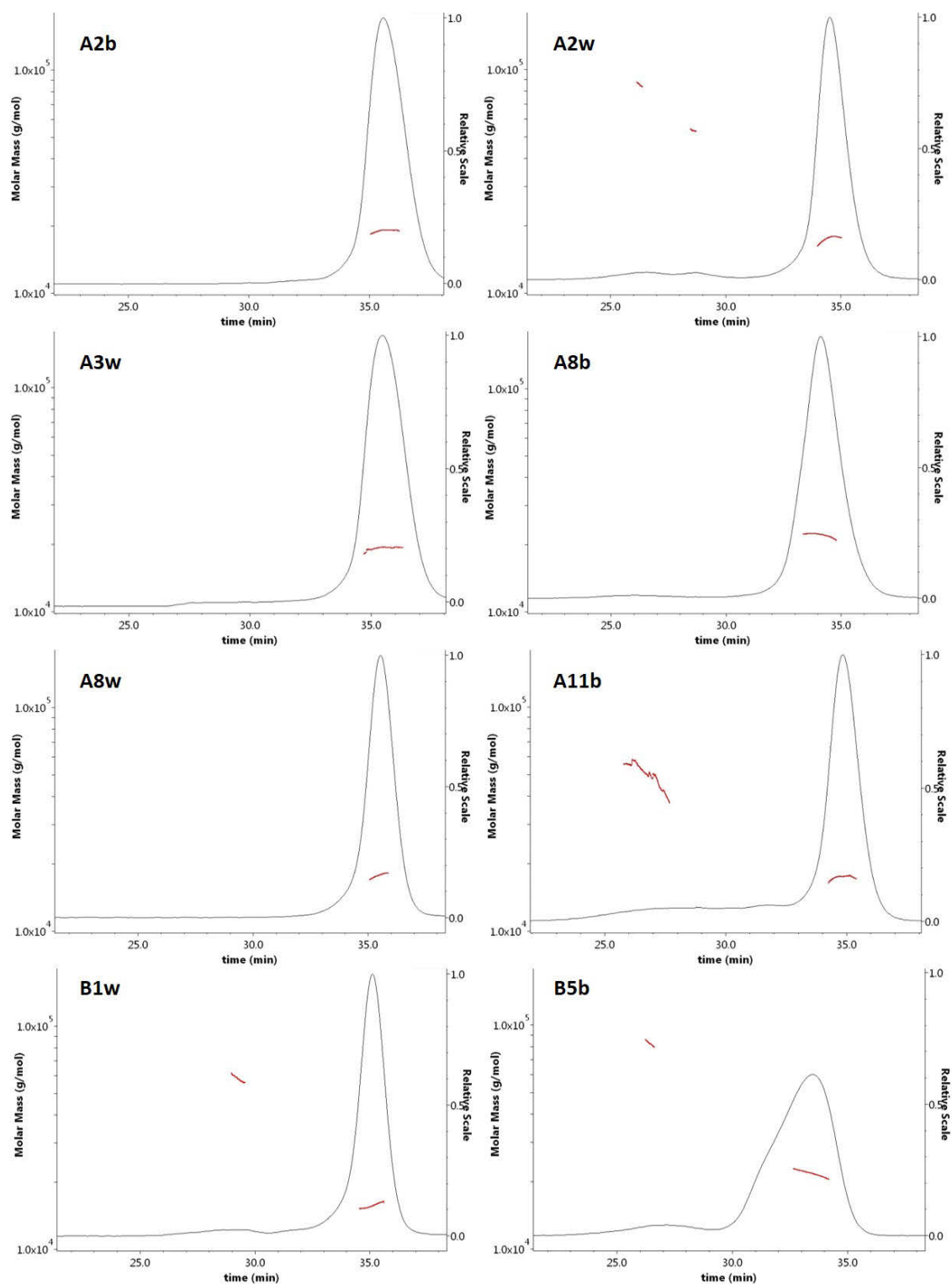


Figure B.1: SEC-MALS elution profiles of A2b, A2w, A3w, A8b, A8w, A11b, B1w and B5b. Left vertical axis: molar mass [g/mol] (indicated in red). Right vertical axis: UV absorbance at 280 nm (indicated in black). Bottom axis: Elution time [min].

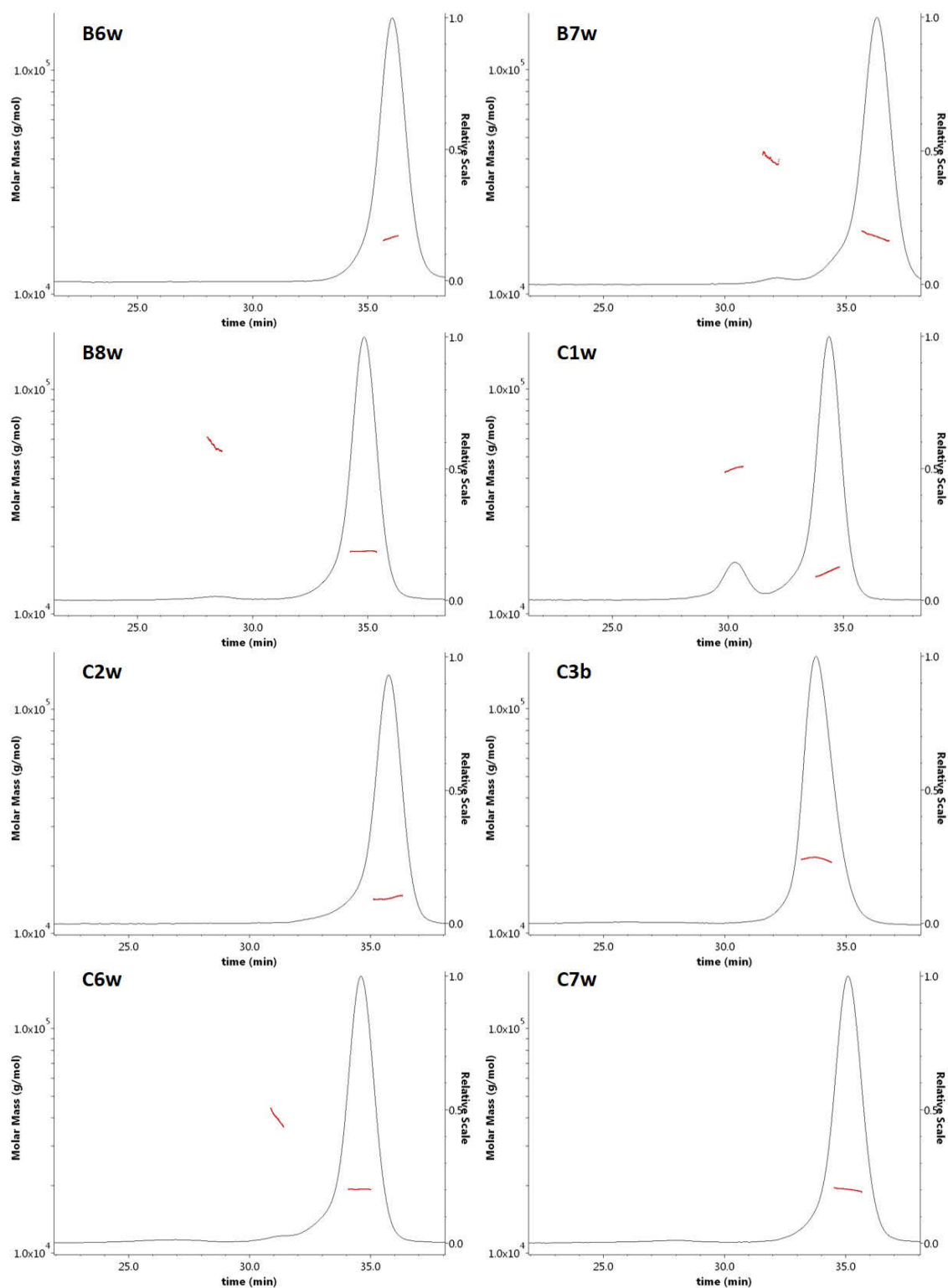


Figure B.2: SEC-MALS elution profiles of B6w, B7w, B8w, C1w, C2w, C3b, C6w and C7w. Left vertical axis: molar mass [g/mol] (indicated in red). Right vertical axis: UV absorbance at 280 nm (indicated in black). Bottom axis: Elution time [min].

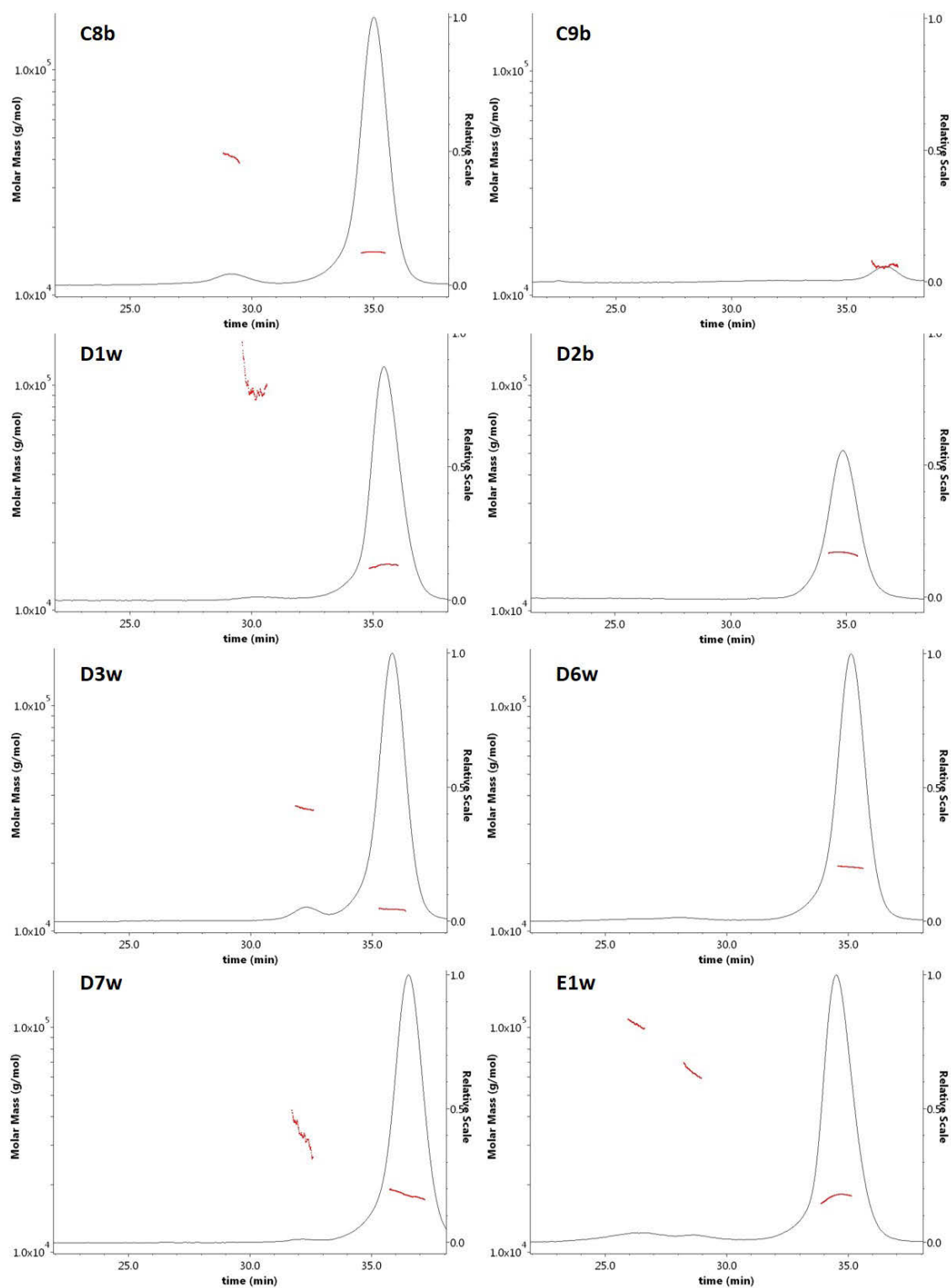


Figure B.3: SEC-MALS elution profiles of C8b, C9b, D1w, D2b, D3w, D6w, D7w and E1w. Left vertical axis: molar mass [g/mol] (indicated in red). Right vertical axis: UV absorbance at 280 nm (indicated in black). Bottom axis: Elution time [min].

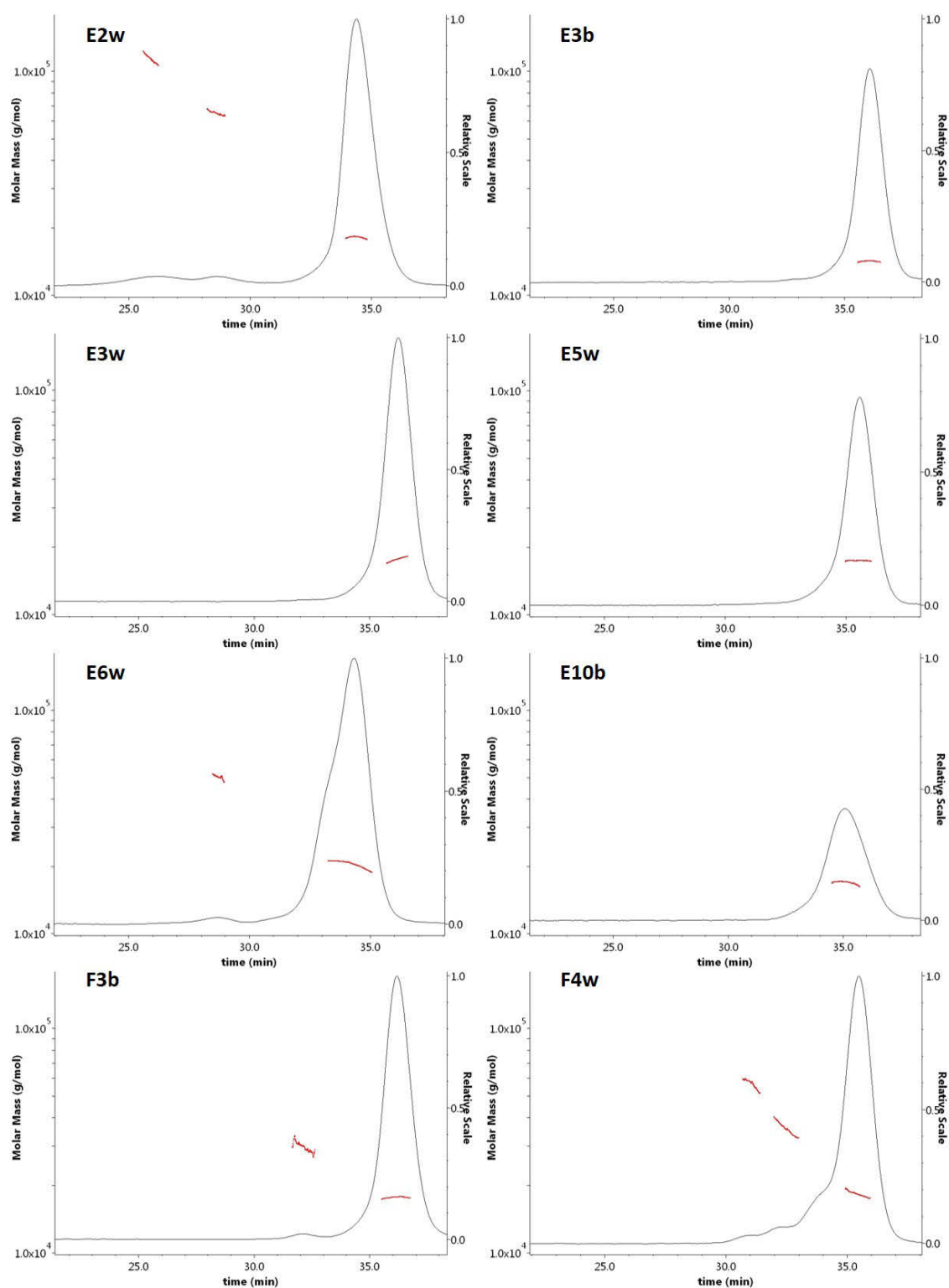


Figure B.4: SEC-MALS elution profiles of E2w, E3b, E3w, E5w, E6w, E10b, F3b and F4w. Left vertical axis: molar mass [g/mol] (indicated in red). Right vertical axis: UV absorbance at 280 nm (indicated in black). Bottom axis: Elution time [min].

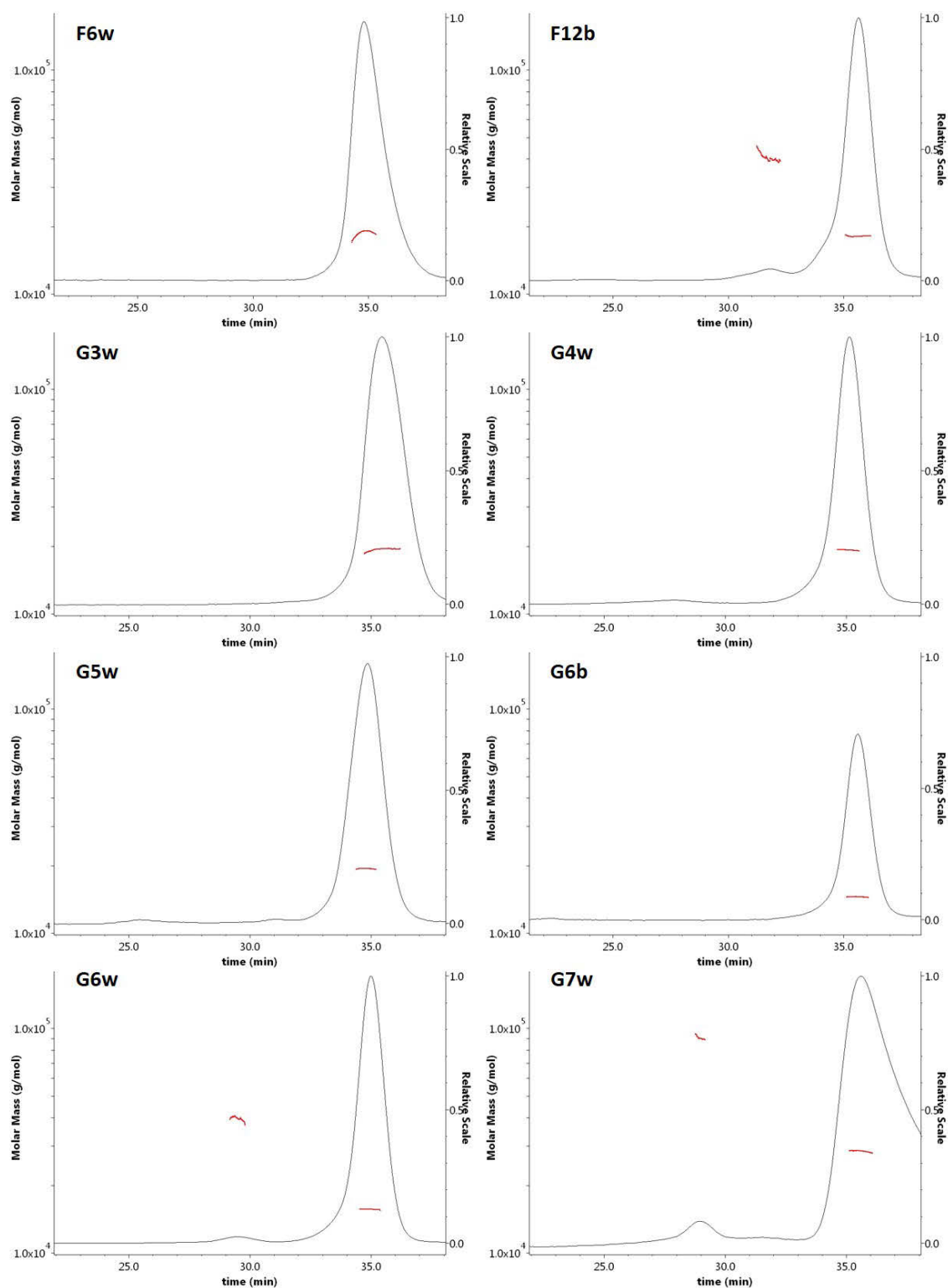


Figure B.5: SEC-MALS elution profiles of F6w, F12b, G3w, G4w, G5w, G6b, G6w and G7w. Left vertical axis: molar mass [g/mol] (indicated in red). Right vertical axis: UV absorbance at 280 nm (indicated in black). Bottom axis: Elution time [min].

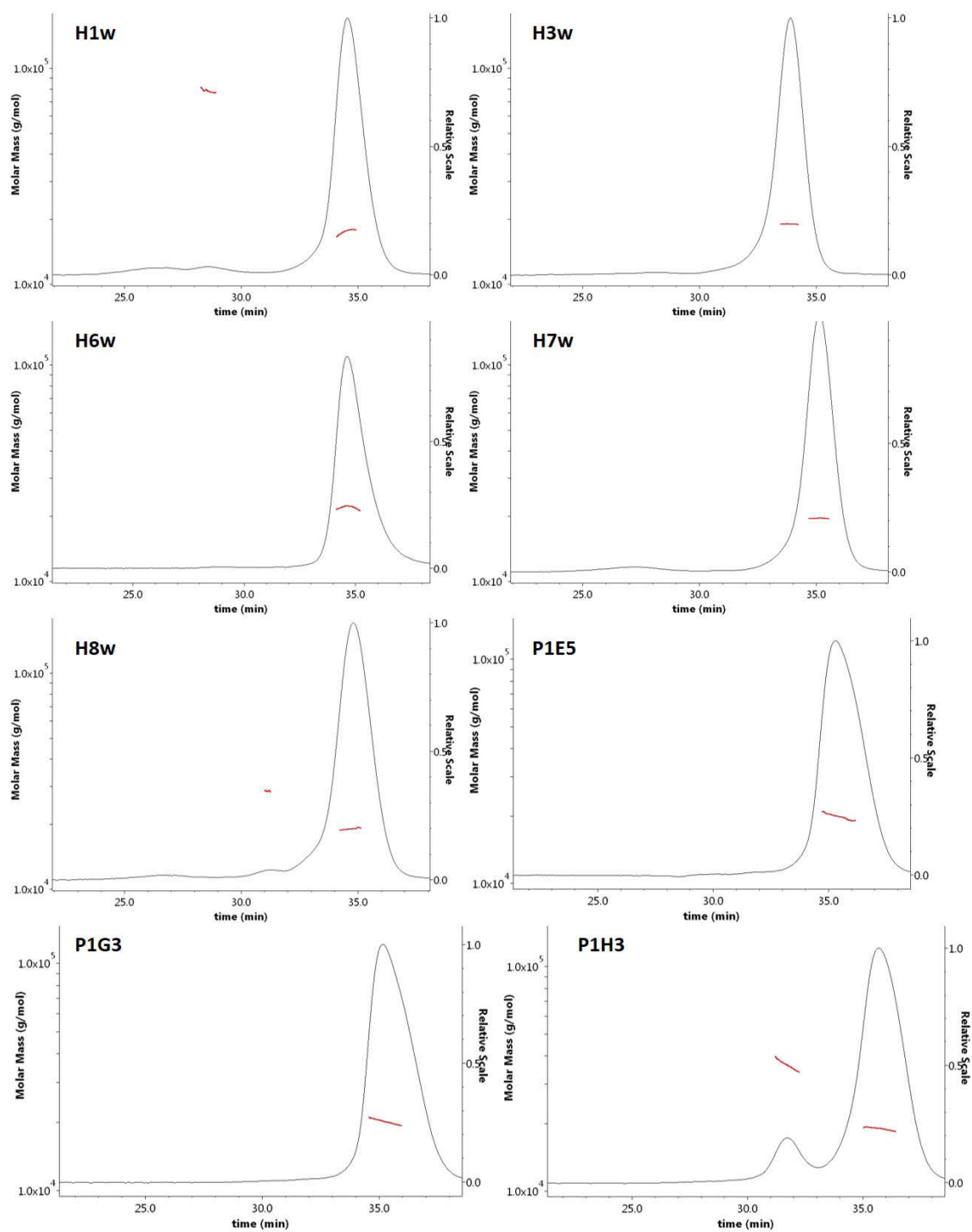


Figure B.6: SEC-MALS elution profiles of H1w, H3w, H6w, H7w, H8w, P1E5, P1G3 and P1H3. Left vertical axis: molar mass [g/mol] (indicated in red). Right vertical axis: UV absorption at 280 nm (indicated in black). Bottom axis: Elution time [min].

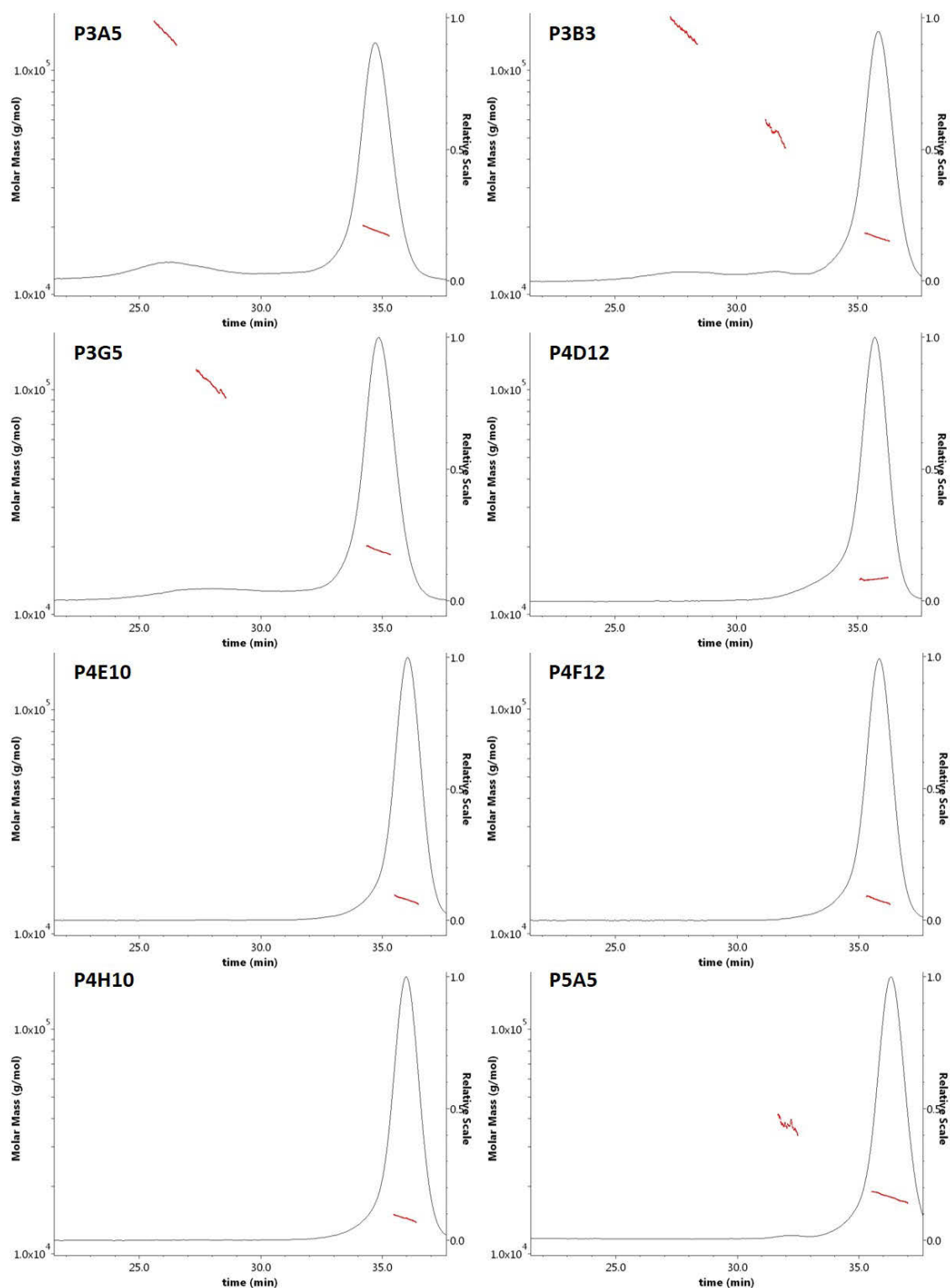


Figure B.7: SEC-MALS elution profiles of P3A5, P3B3, P3G5, P4D12, P4E10, P4F12, P4H10 and P5A5. Left vertical axis: molar mass [g/mol] (indicated in red). Right vertical axis: UV absorbance at 280 nm (indicated in black). Bottom axis: Elution time [min].

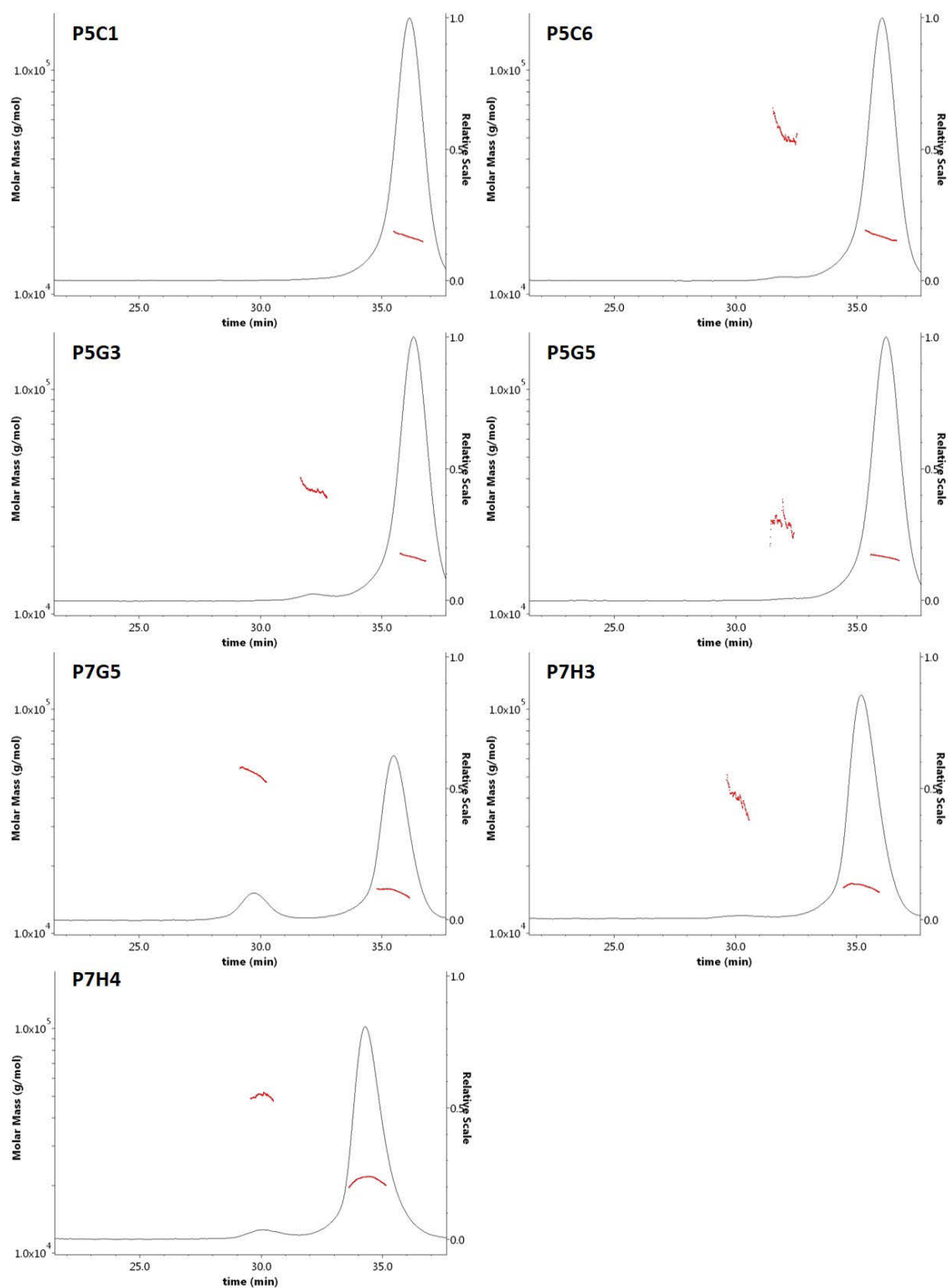


Figure B.8: SEC-MALS elution profiles of P5C1, P5C6, P5G3, P5G5, P7G5, P7H3 and P7H4. Left vertical axis: molar mass [g/mol] (indicated in red). Right vertical axis: UV absorbance at 280 nm (indicated in black). Bottom axis: Elution time [min].

# **Appendix C**

## **Surface Plasmon Resonance**

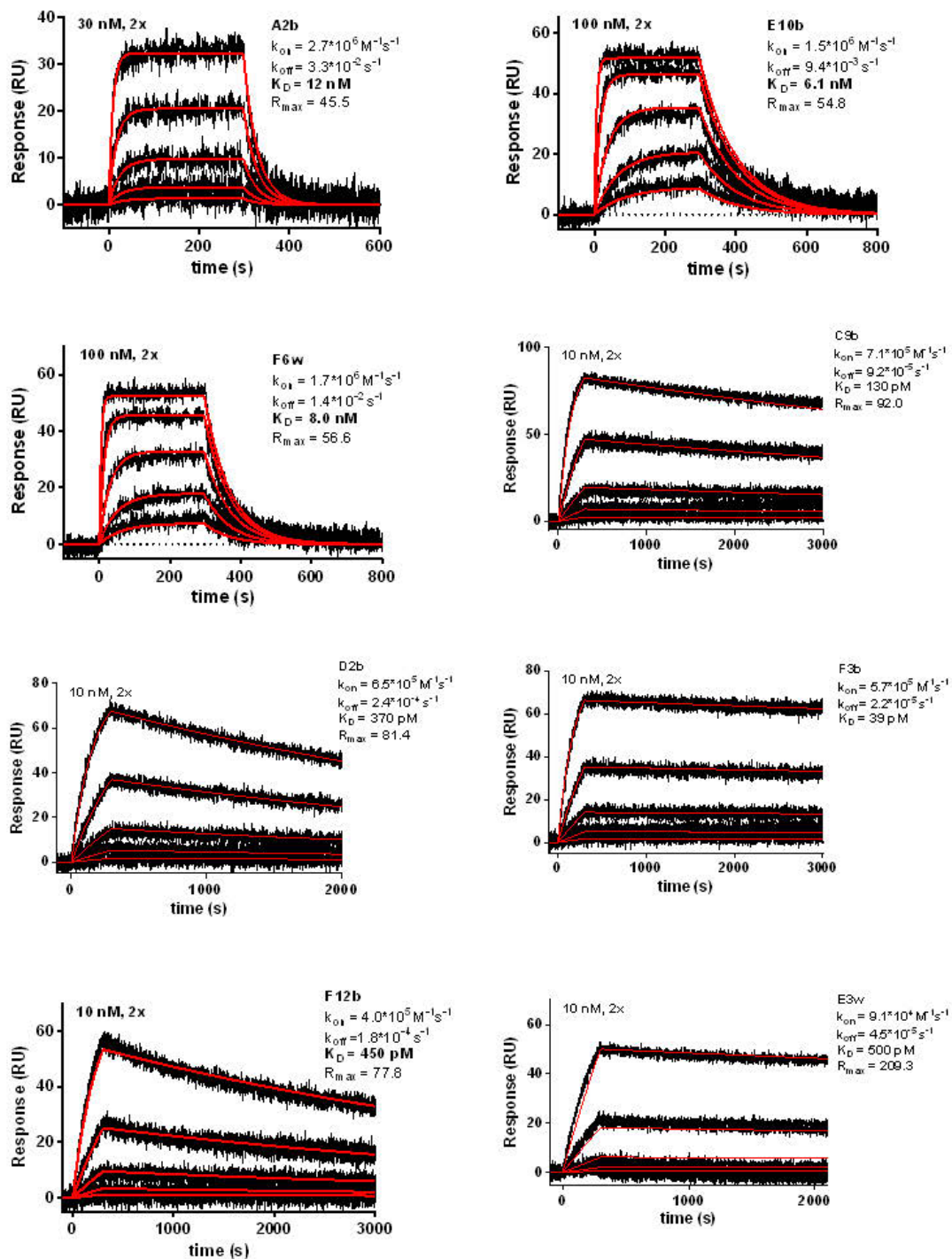


Figure C.1: Kinetic data of A2b, E10b, F6w, C9b, D2b, F3b, F12b, E3w

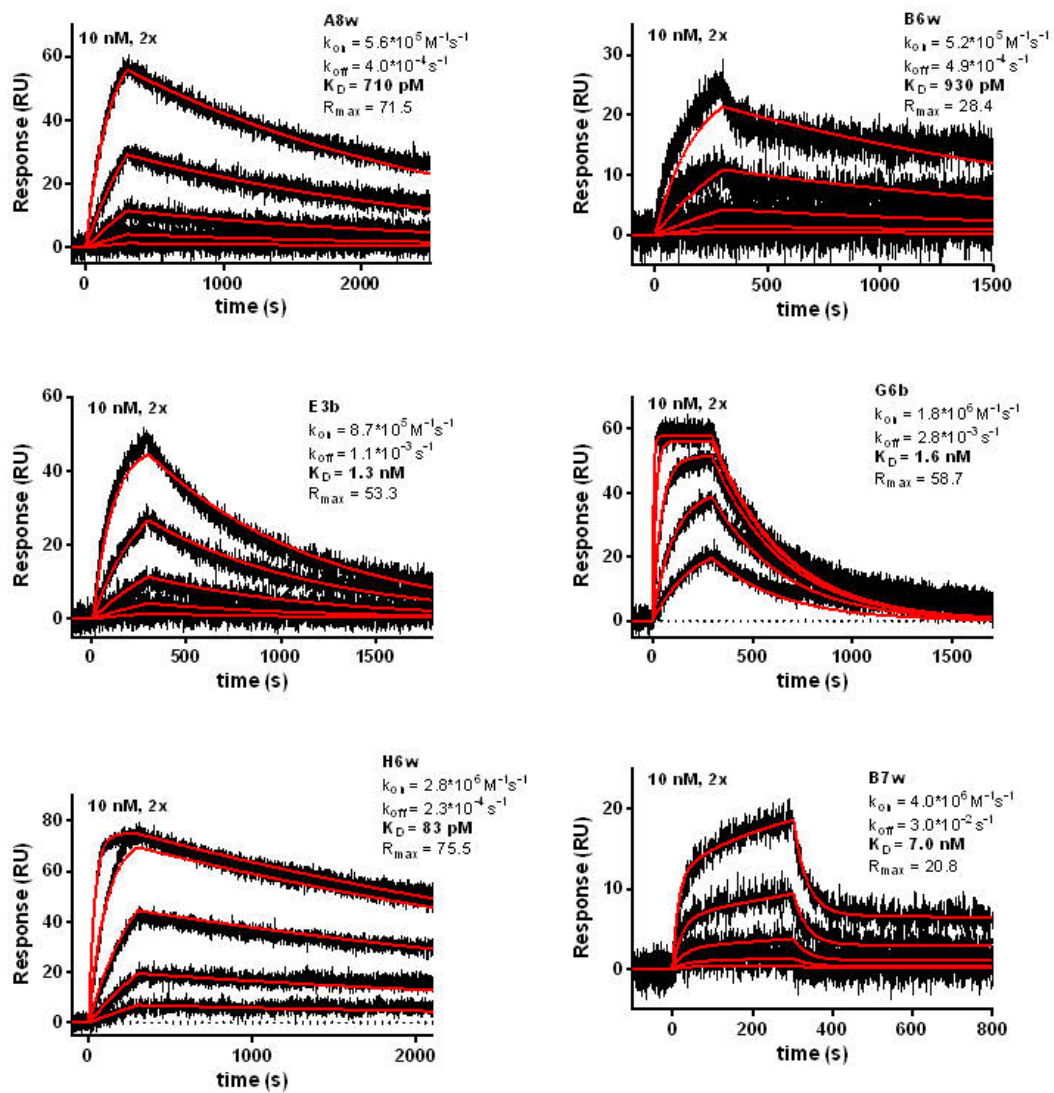


Figure C.2: Kinetic data of A8w, B6w, E3b, G6b, H6w, B7w

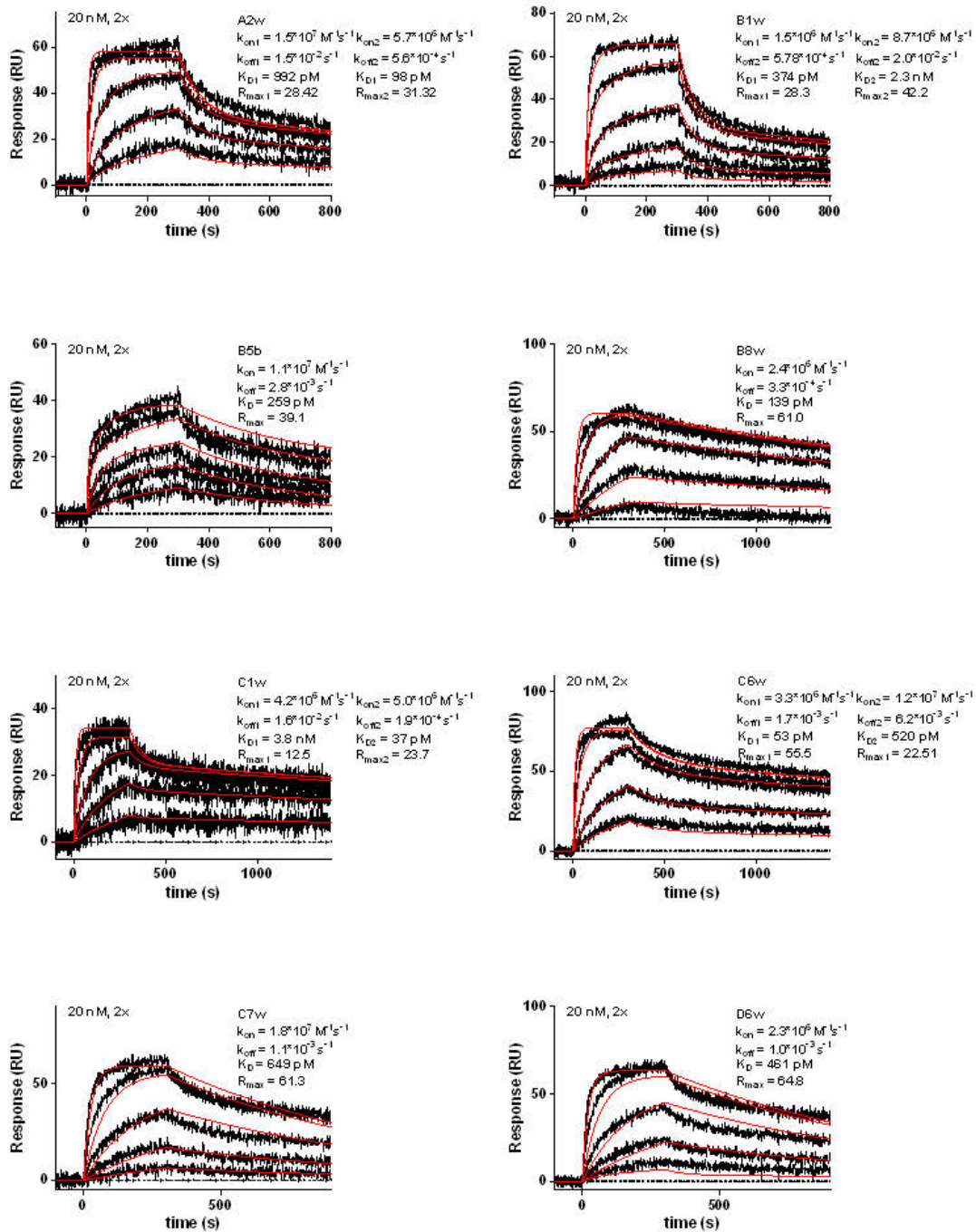


Figure C.3: Kinetic data of A2w, B1w, B5b, B8w, C1w, C6w, C7w, D6w

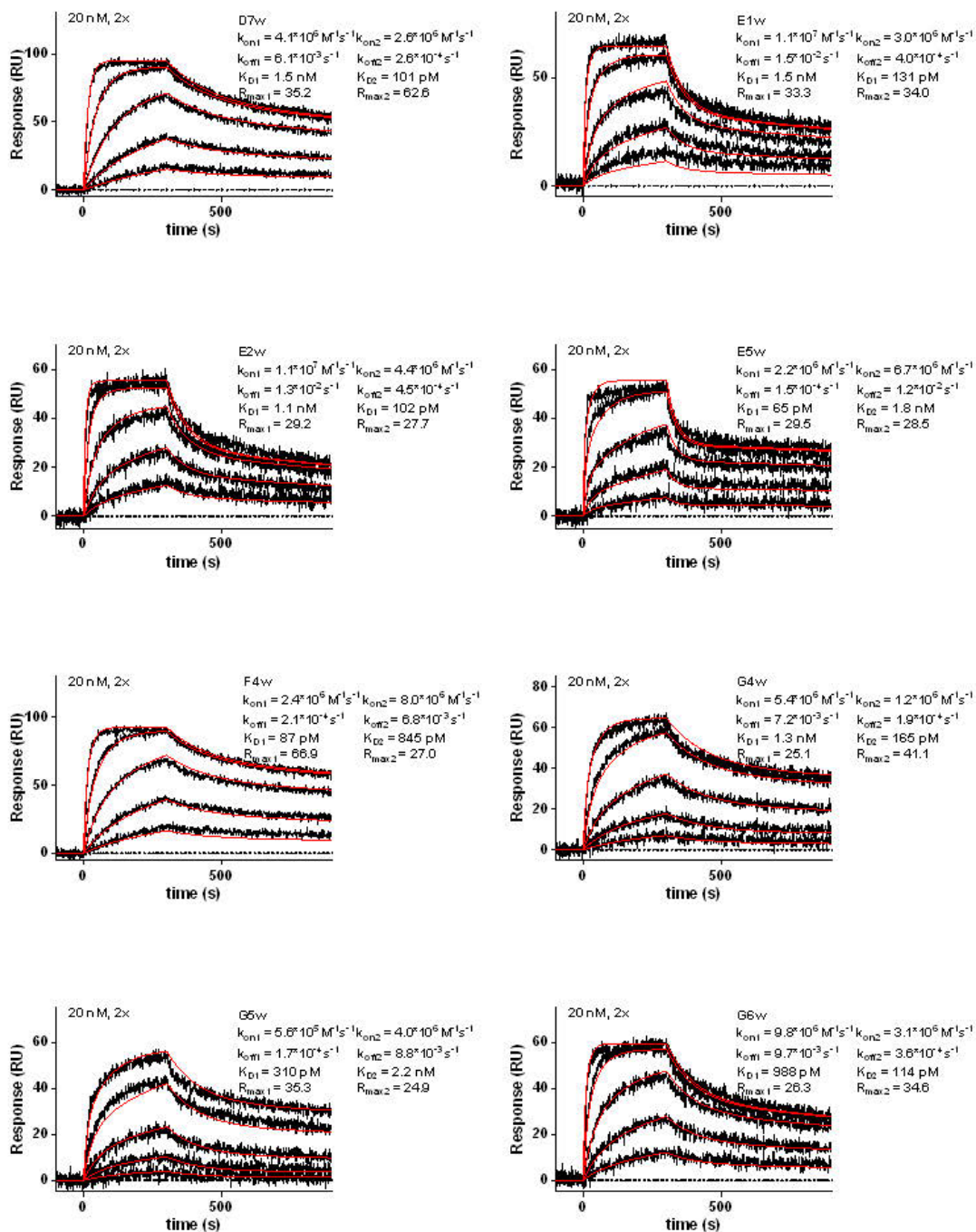


Figure C.4: Kinetic data of D7w, E1w, E2w, E6w, F4w, G4w, G5w, G6w

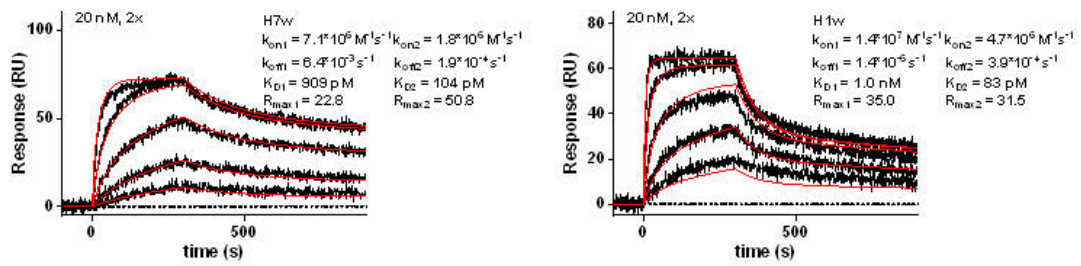


Figure C.5: Kinetic data of H1w, H7w

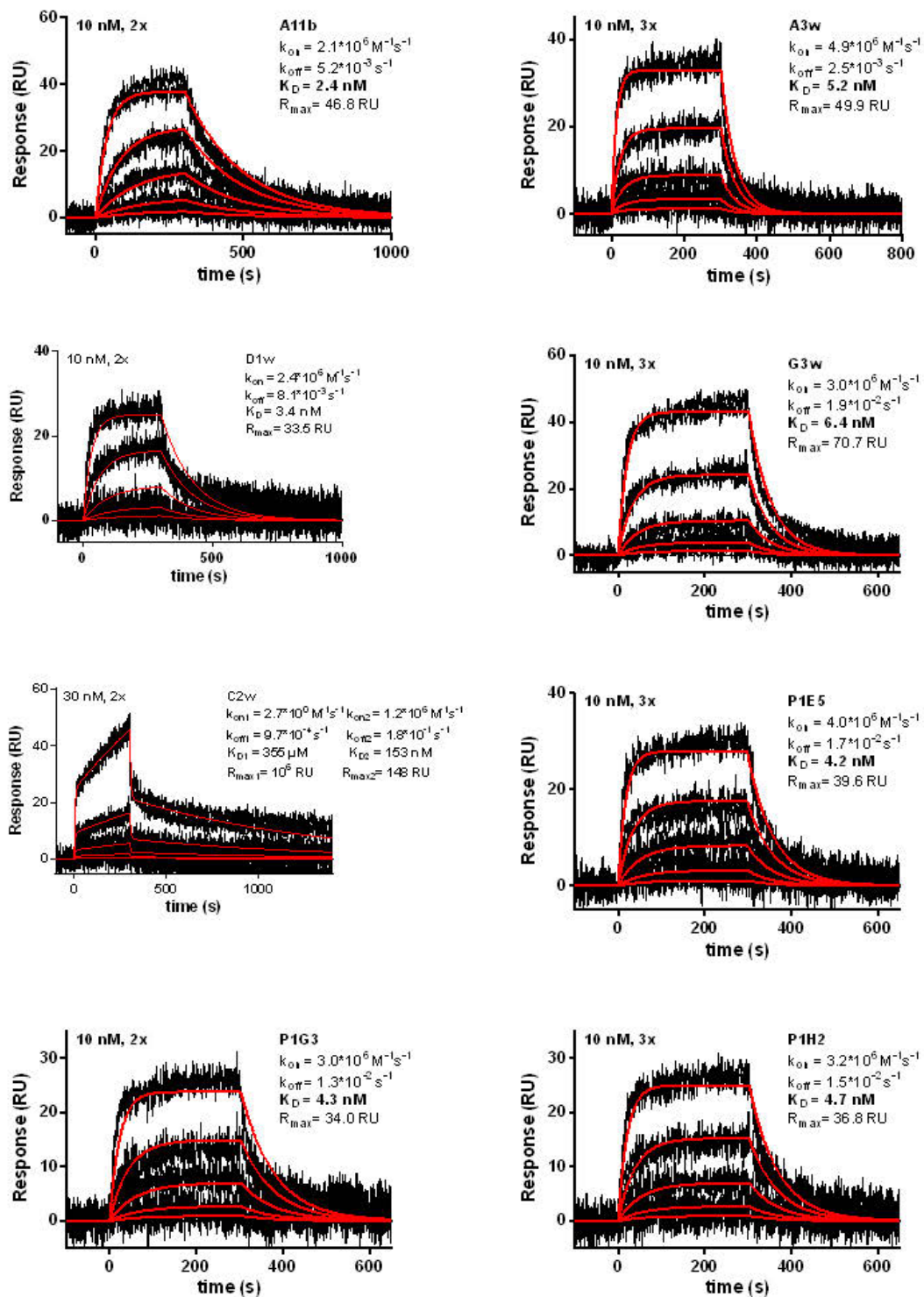


Figure C.6: Kinetic data of A11b, A3w, D1w, G3w, C2w, P1E5, P1G3, P1H2

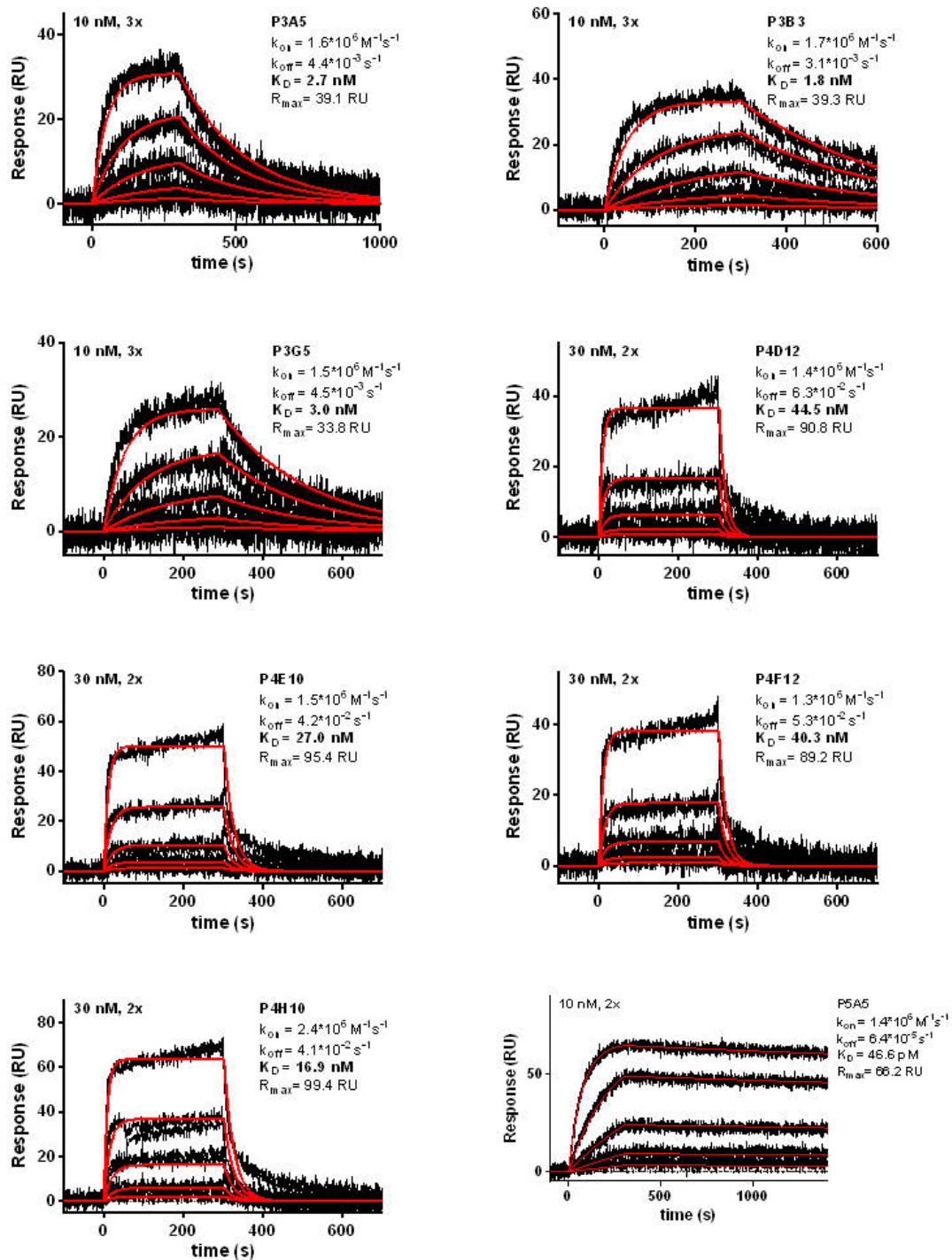


Figure C.7: Kinetic data of P3A5, P3B3, P3G5, P4D12, P4E10, P4F12, P4H10, P5A5

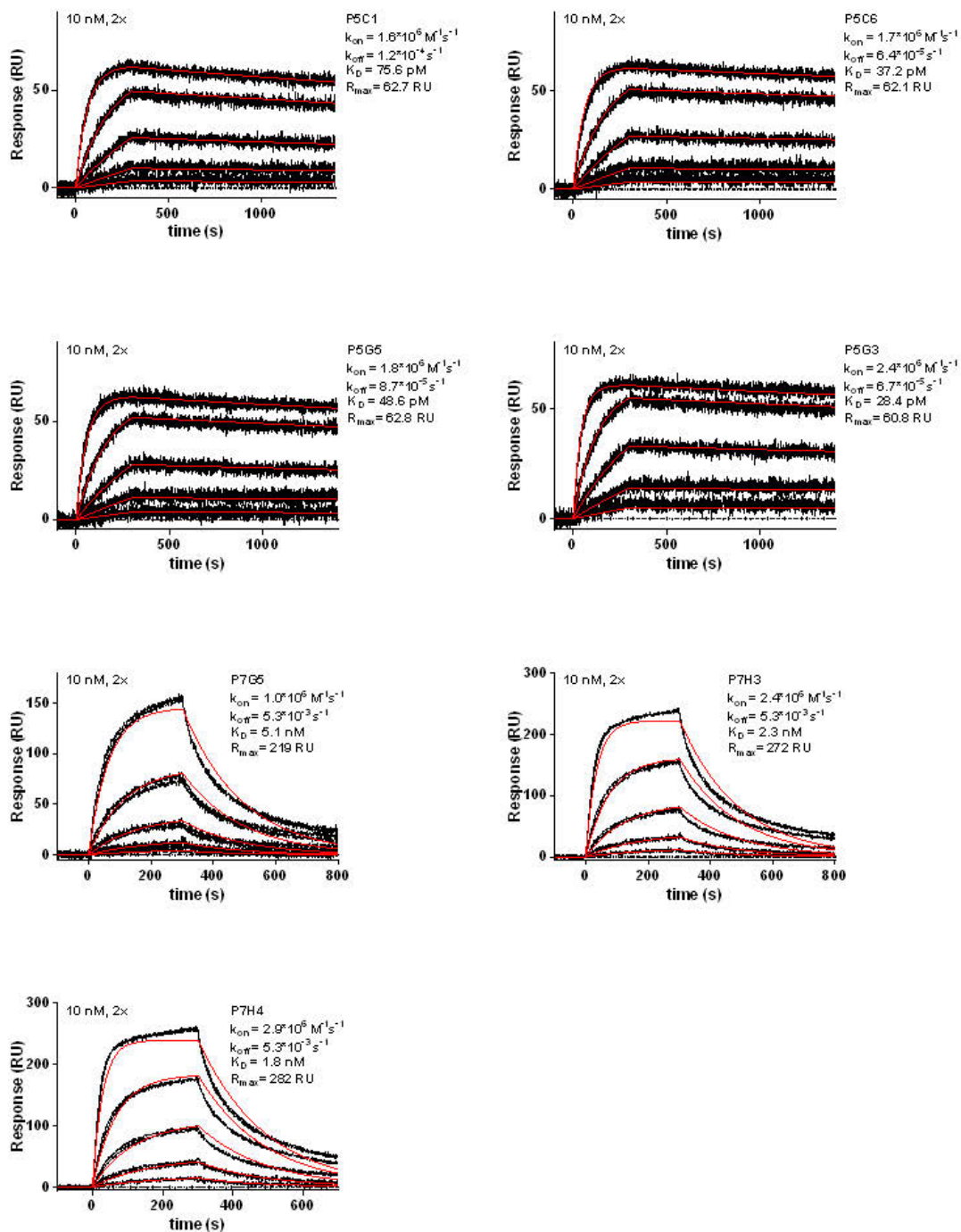


Figure C.8: Kinetic data of P5C1, P5C6, P5G5, P5G3, P7G5, P7H3, P7H4

## 1.1 Human ROR1

Human receptor tyrosine kinase-like orphan receptor 1 (hROR1) is a transmembrane protein within the receptor tyrosine kinase family that is highly conserved among species.[12] Its structure consists of an extracellular region including an immunoglobulin-like domain (Ig), followed by cysteine-rich frizzled domain (FZD) and a kringle domain (KRD), linked to the membrane via transmembrane domain. The intracellular region consists of a tyrosine kinase domain with weak to moderate kinase activity followed by two serine/threonine-rich domains and a proline rich domain, to be seen in figure 31.[13, 14, 15] In contrast to other related receptors, human ROR1 possesses multiple N-glycosylation sites. Posttranslational modification at these sites are considered as necessary for the trafficking and function of the receptor. [16] Many investigations and experiments have been performed in order to elucidate the function of human ROR1. Yet, the definite ligand and involved signalling pathways are still unknown and knowledge of the key biological function is still incomplete.[17, 18]

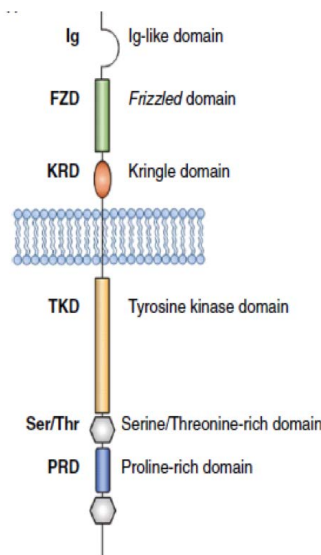


Figure 1.1: Structure of human ROR1. Receptor consisting of three extracellular domains, including Immunoglobulin domain (Ig), Frizzled domain (FZD) and Kringle domain (KRD), transmembrane domain and four intracellular domains including Tyrosine kinase domain (TKD), two Serine/Threonine rich domains (Ser/Thr) and a Proline rich domain (PRD). Adapted from N. Borchering et al. [17]

Besides the missing knowledge about key biological functions, human ROR1 is considered to play an essential role in embryonic patterning and neurogenesis, underpinned by its high degree of conservation among species and its strong expression profiles during development.[19, 20] In early stages of fetal development the receptor ROR1 is highly expressed in a great variety of tissues from all three germ lines, including neural crest cells, head mesenchyme, specialised sense organs, lung, skeletal and urogenital tissues. Knockdown of the receptor ultimately led to aberrant development of neural tissue and respiratory dysfunction within 24 hours after birth.[21, 22] Further studies revealed retarded growth, severe skeletal defects, urogenital and female infertility in ROR1-deficient mice. These findings highlight the receptor as a crucial factor for normal development.[22,

tions when it comes to stability, folding, aggregation propensity and rapid evolvability of those molecules and variants they confer. When using antibodies in more ambitious formats, such as fusions, the limitations in their biophysical properties become even more apparent.[41, 42] This increases the demand for alternative molecular scaffolds in order to enable additional innovative therapeutic approaches and investigations.

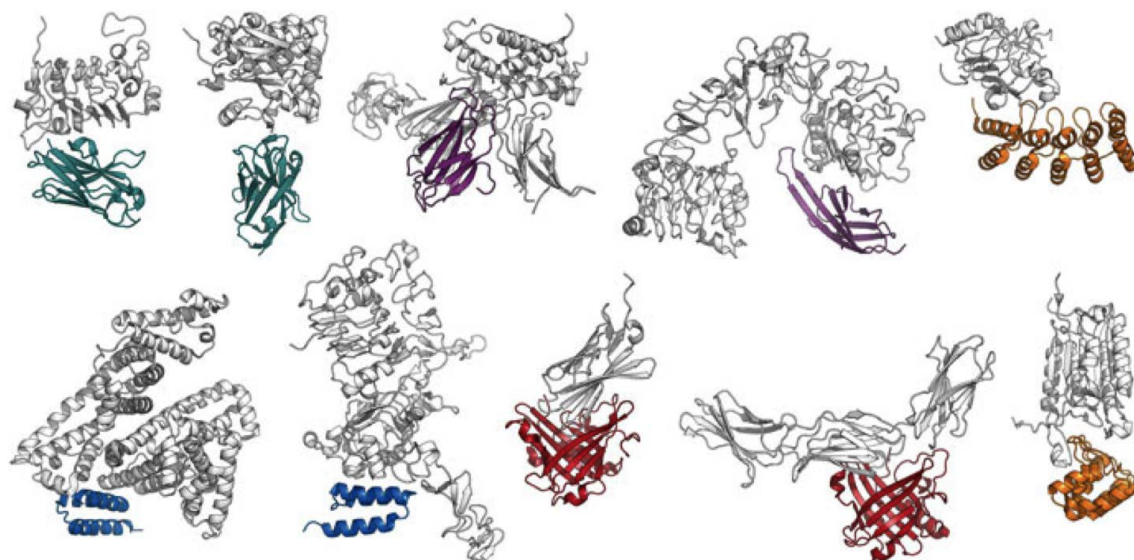


Figure 1.2: Structural comparison between alternative protein scaffolds. Each scaffold in complex with a biomedically relevant protein. Green: Nanobodies in complex with a EGFR fragment and ricin. Violet: Adnectins in complex with IL23 heterodimer and the EGFR extracellular region. Orange: DARPins in complex with a HER2 fragment and caspase 3. Blue: Affibodies in complex with albumin and the HER2 extracellular region. Red: Anticalins in complex with the CTLA-4 extracellular domain and ED-B. Adapted from A. Rosenberg et al. [44]

Enhanced by the need for novel alternative molecular scaffolds for therapeutic approaches and novel investigative strategies, a large effort was made in the past two decades to elucidate novel and potential binding scaffolds. As of today, more than 50 different protein scaffold have been proposed with emphasis on small single-chain proteins that possess high thermodynamic stability, lack of required posttranslational modifications and are missing free cysteines.[46, 64, 65] Due to the high technical demands on proteins for biopharmaceutical development and applications, only four scaffolds out of this great variety of constructs were finally able to mature beyond initial model case studies. These four protein scaffolds, Adnectins, Affibodies, Anticalins and DARPins constitute the most advanced approaches in this field and are of today the only alternative scaffold considered to yield products with a commercial value.[66, 44]

### *Adnectins*

One of the more promising classes of alternative proteins are Adnectins. Very similar designs have also been called Monobodies and Centyrins. A fibronectin type III domain (FN3), comprised of a 10 kDa autonomous domain that was first found in the abundant extracellular matrix proteins fibronectin and tenascin, as well as in a variety of multido-

round	1st	2nd	3rd	4th
target	250 nM	100 nM	20 nM	2 nM
washing	6 x 2'	2 x 2'	2 x 2'	2 x 2'
		5', 10'	6 x 10'	6 x 10'
		5', 10'		
competition	na	na	na	455 x

Figure 1.5: Conditions for ribosome display selection for DARPins binding human ROR1. Each selection round is indicated with the amount of target used for panning step, duration and number of cycles for washing steps and amount of unbiotinylated competitor used for off-rate selection. Adapted from Dreier et al. (unpublished)

that no unspecific binding by reagents used in the basic assay composition occurred. The negative control using target but no DARPins resulted in a signal ratio of about 0.148, showing a signal very similar to the negative control of reagents only and confirmed that no unspecific binding of reagents to the target occurs. The third negative control, including the DARPin off7 specifically binding Maltose Binding Protein (MBP), but in the absence of MBP as target, resulted in a signal ratio of about 0.148, therefore showing a similar signal as the first and second negative control, confirming no unspecific binding of DARPins to the extracellular domain of human ROR1.

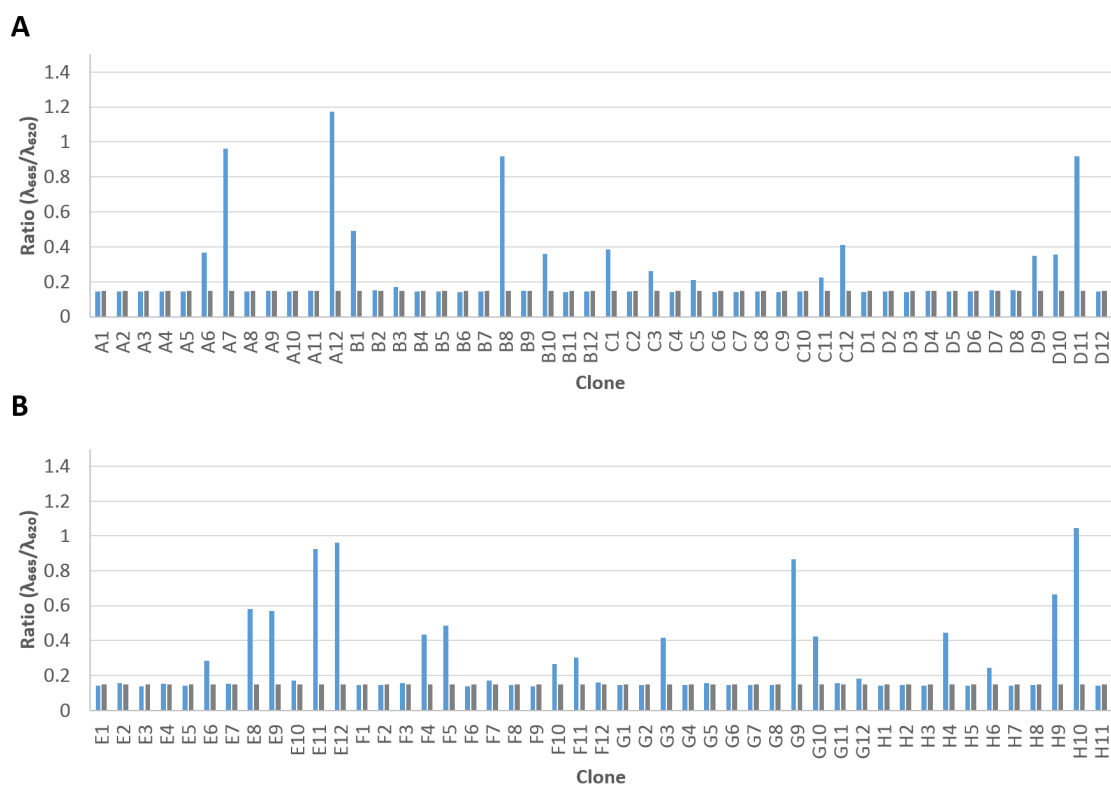


Figure 3.1: Homogenous Time Resolved Fluorescence of clones from the naive library N2C obtained after the third selection round against human ROR1 ECD using ribosome display. Signal plotted as the ratio of detected counts at 665 nm over detected counts at 620, measured in 1:10,000 dilution of crude extract. Blue: measured signal of setup including DARPin, Gray: negative control using reagents only. A: clone A1 - D12, B: clone E1 - H11. The name of each clone refers to its position on the respective expression plate

As shown in Figure 3.1, DARPins from the naive library containing N2C DARPins [106], that were obtained from the third selection round by using ribosome display, showed a clear ratio between counts at 665 nm and 620 nm, respectively, over background. A clear shift towards 665 nm and therefore binding to the extracellular domains of human ROR1 could be suspected. A significant number of clones show only a marginal increase in signal ratio compared to the signal of background at a dilution of 1:10,000 ranging from 0.14 to 0.19. About a third of the analysed clones showed a signal significantly higher than the background, ranging from a signal ratio of 0.40 to 1.2.

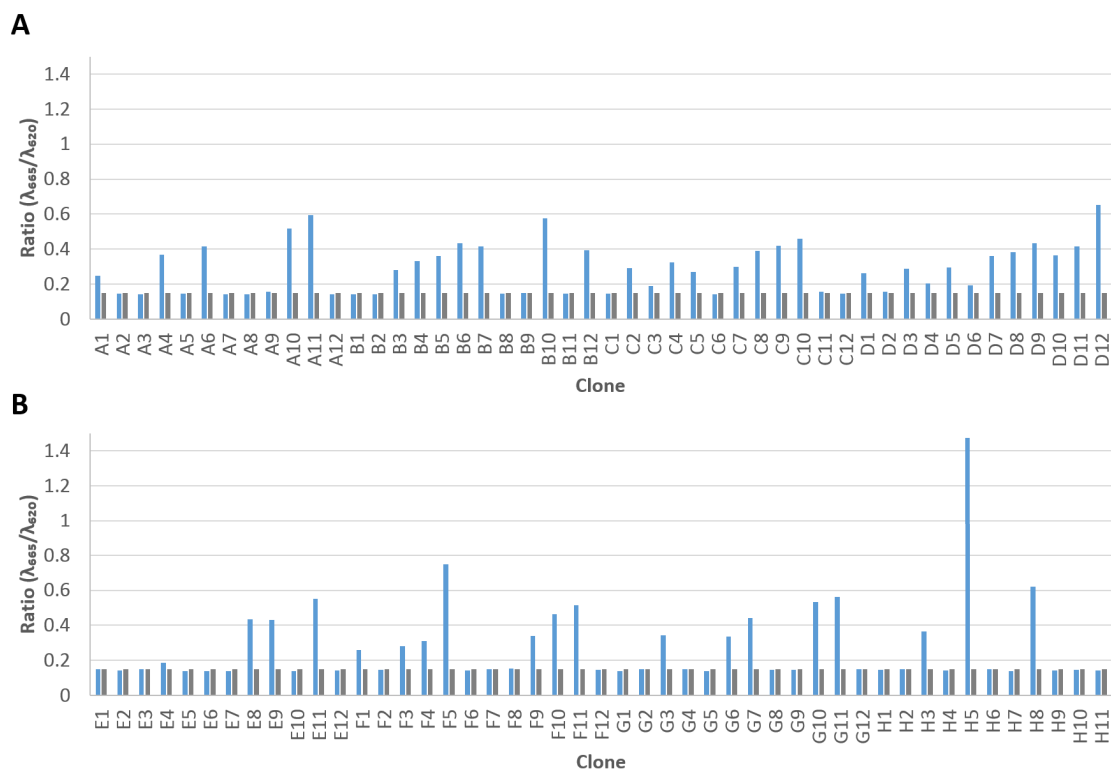


Figure 3.2: Homogenous Time Resolved Fluorescence of clones from the naive library N3C obtained after the third selection round against human ROR1 ECD using ribosome display. Signal plotted as the ratio of detected counts at 665 nm over detected counts at 620, measured in 1:10,000 dilution. Blue: measured signal of setup including DARPin, Gray: negative control using reagents only. A: clone A1 - D12, B: clone E1 - H11. The name of each clone refers to its position on the respective expression plate

Similarly, clones selected from the naive library containing N3C DARPins [106], that were obtained from the third selection round by using ribosome display, showed a clear increased ratio between counts at 665 nm and 620 nm, respectively, over background to be seen in Figure 3.2, indicating a binding of the extracellular domains of human ROR1.

Clones from the library containing N3C DARPins showed signals that were significantly over background, resulting in 48% of analysed clones that showed a significant signal of binding to human ROR1 ECD. These clones are ranging in signal ratios from 0.20 to 1.45. About 52% of the analysed clones showed only a marginal or no increased ratio of signals compared to the measured negative control.

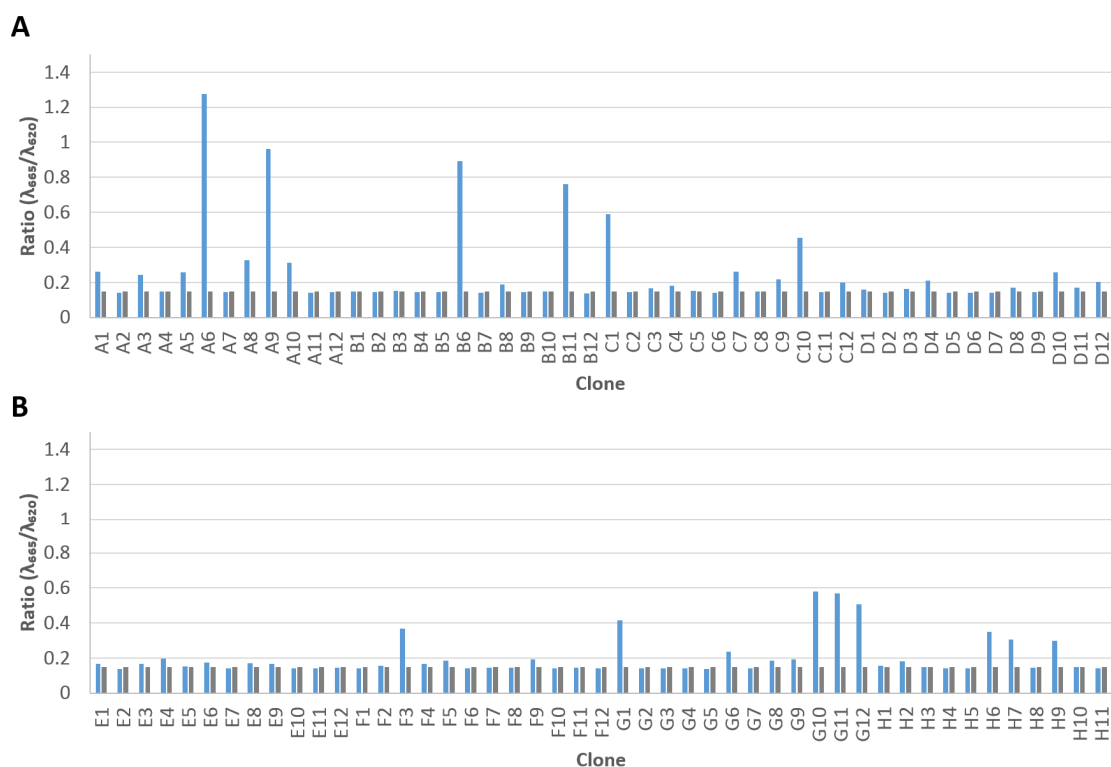


Figure 3.3: Homogenous Time Resolved Fluorescence of clones from the naive library r+nr obtained after the third selection round against human ROR1 ECD using ribosome display. Signal plotted as the ratio of detected counts at 665 nm over detected counts at 620, measured in 1:10,000 dilution. Blue: measured signal of setup including DARPin, Gray: negative control using reagents only. A: clone A1 - D12, B: clone E1 - H11. The name of each clone refers to its position on the respective expression plate

Figure 3.3 shows that DARPins derived from the library where N3C DARPins with stabilised Ccap [109] and N3C DARPins with either randomised and non-randomised capping repeats [106] were mixed in equimolar amounts (r+nr) from the third selection round showed distinct increased signals ratios above background. About 23% of clones analysed from library r+nr from selection round 3 showed a significantly higher signal than the negative controls and therefore significant binding to the extracellular domains of human ROR1. The ratio of counts at 665 nm to 620 nm, equivalent to the proximity of target and ligand, in case of the analysed positive clones of r+nr from the third round was between 0.20 and 1.30. About 77% of analysed clones showed only marginal or no signal over background.

#### Screening of DARPins from selection round 4

All negative controls, consisting of a measurement setup with reagents only, a setup with target only without DARPins and a setup with target and the MBP binding control DARPin off7, showed a similar ratio of counts at 665 nm wavelength to counts at 620 nm ranging between 0.151 and 0.143. Similar to the negative controls of the HTRF screening of DARPins from the third selection round this represents a rather low ratio and therefore a low interference of signal from the background can be expected. Still, at

very high dilutions of 1:10,000 the difference between ratios obtained from the negative controls and ratios obtained from DARPs binding the target human ROR1 ECD can be rather small. Therefore only clones that show a distinct signal over background will be followed further.

An obtained signal of 665 nm to 620 nm of around 0.143 in the measurement setup, where only reagents but no target or DARPs were added, confirmed no unspecific binding by reagents used in the basic assay composition. The negative control using target but no DARPs resulted in a signal ratio of about 0.148, showing a signal very similar to the negative control of reagents only and confirming that no unspecific binding of reagents to the target occurs. The third negative control, including the DARPin off7 specifically binding Maltose-Binding-Protein, resulted in a signal ratio of about 0.151. Therefore showing a similar signal as the first and second negative control and confirming no unspecific binding of DARPs to the extracellular domain of human ROR1.

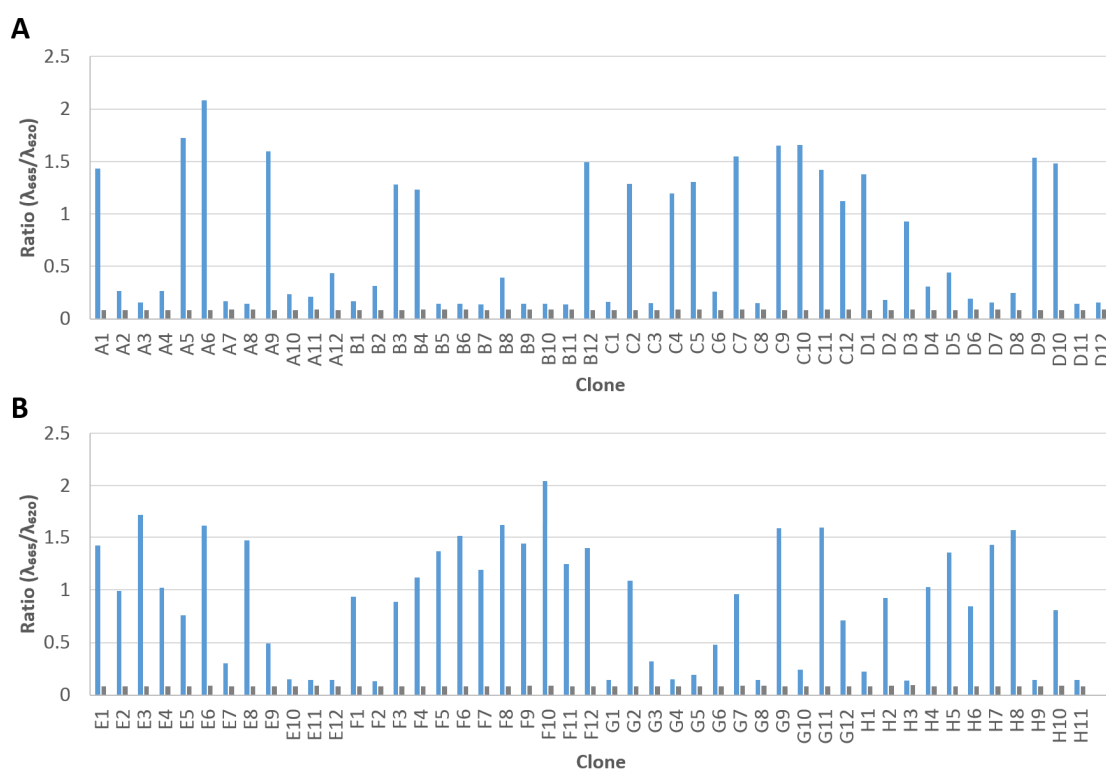


Figure 3.4: Homogenous Time Resolved Fluorescence of clones from the naive library N2C obtained after the fourth selection round against human ROR1 ECD using ribosome display. Signal plotted as the ratio of detected counts at 665 nm over detected counts at 620, measured in 1:10,000 dilution. Blue: measured signal of setup including DARPin, Gray: negative control using reagents only. A: clone A1 - D12, B: clone E1 - H11. The name of each clone refers to its position on the respective expression plate

As seen in Figure 3.4, DARPs from the naive library containing N2C DARPs [106], that were obtained from the fourth selection round by using ribosome display, showed a clear increased ratio between signals at a wavelength of 665 nm and 620 nm, respectively, over background. This indicated a shift towards 665 nm and therefore binding to the extracellular domains of human ROR1. All analysed clones that evolved from the

fourth selection round showed a clear signal over background, with more than 42% of all analysed clones showing signal ratios higher than 1.0. The highest signal was obtained at a signal ratio of 2.2. Only 32% of analysed clones showed a signal lower than 0.25. The rest of DARPin of N2C from selection round four exhibited a ratio between 0.2 and 1.0.

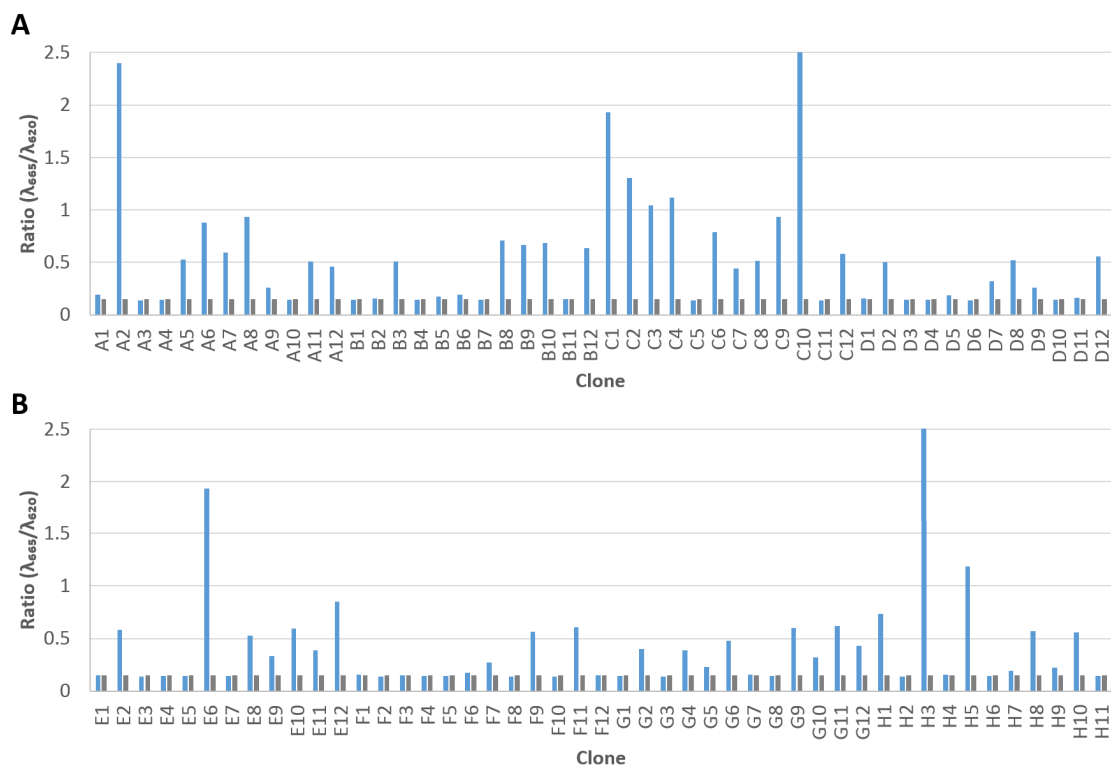


Figure 3.5: Homogenous Time Resolved Fluorescence of clones from the naive library N3C obtained after the fourth selection round against human ROR1 ECD using ribosome display. Signal plotted as the ratio of detected counts at 665 nm over detected counts at 620, measured in 1:10,000 dilution. Blue: measured signal of setup including DARPin, Gray: negative control using reagents only. A: clone A1 - D12, B: clone E1 - H11. The name of each clone refers to its position on the respective expression plate

Clones from the naive library containing N3C DARPins [106] that were obtained from the fourth selection round by using ribosome display, showed a clear ratio between counts at 665 nm and 620 nm, respectively, over background to be seen in Figure 3.5, indicating a binding of the extracellular domains of human ROR1, with 67% of analysed DARPins showing a signal that is significantly higher than background. Only 9% of clones showed a signal ratio than was higher than 1.0, with a maximum in ratio at about 3.1. All other positive clones are ranging in signal ratios of 0.25 to 0.95.

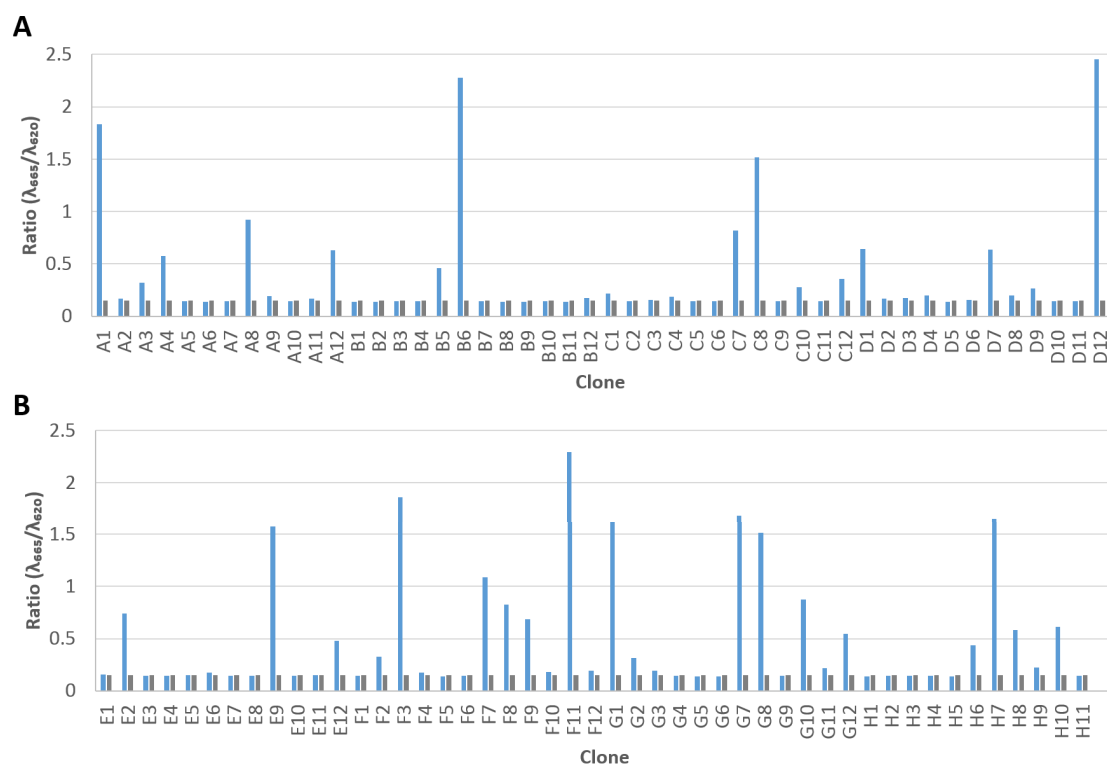


Figure 3.6: Homogenous Time Resolved Fluorescence of clones from the naive library r+nr obtained after the fourth selection round against human ROR1 ECD using ribosome display. Signal plotted as the ratio of detected counts at 665 nm over detected counts at 620, measured in 1:10,000 dilution. Blue: measured signal of setup including DARPin, Gray: negative control using reagents only. A: clone A1 - D12, B: clone E1 - H11. The name of each clone refers to its position on the respective expression plate

Figure 3.3 shows that DARPins derived from the library where N3C DARPins with stabilised Ccap [109] and N3C DARPins with either randomised and non-randomised capping repeats [106] were mixed in equimolar amount (r+nr) from the third selection round showed distinct signals ratios above background. Ratios of counts towards a signal at 665 nm could be observed that were significantly higher than the background, indicating a binding of the target human ROR1 ECD. About 50% of the analysed clones showed a distinct signal ratio over background. About 13% of the analysed clones showed signal ratios that were higher than 1.0, including a highest measured ratio of signals at 2.45.

Within analysed clones from both selection rounds (round 3 and 4) a significant number of clones that showed a signal over background could be identified. Notably, DARPins that evolved from the fourth round showed on average 5- to 10-fold higher signals than DARPins that evolved from the third round. Sixty clones that showed the highest signal ratios and were considered to putatively bind human ROR1 were further analysed by Sanger sequencing, in order to identify the sequence of the putative binder as well as to evaluate its similarities and putative conclusions towards distinct families and properties. Further clones that represented cys-containing DARPins and identical sequences were eliminated from further characterisation.

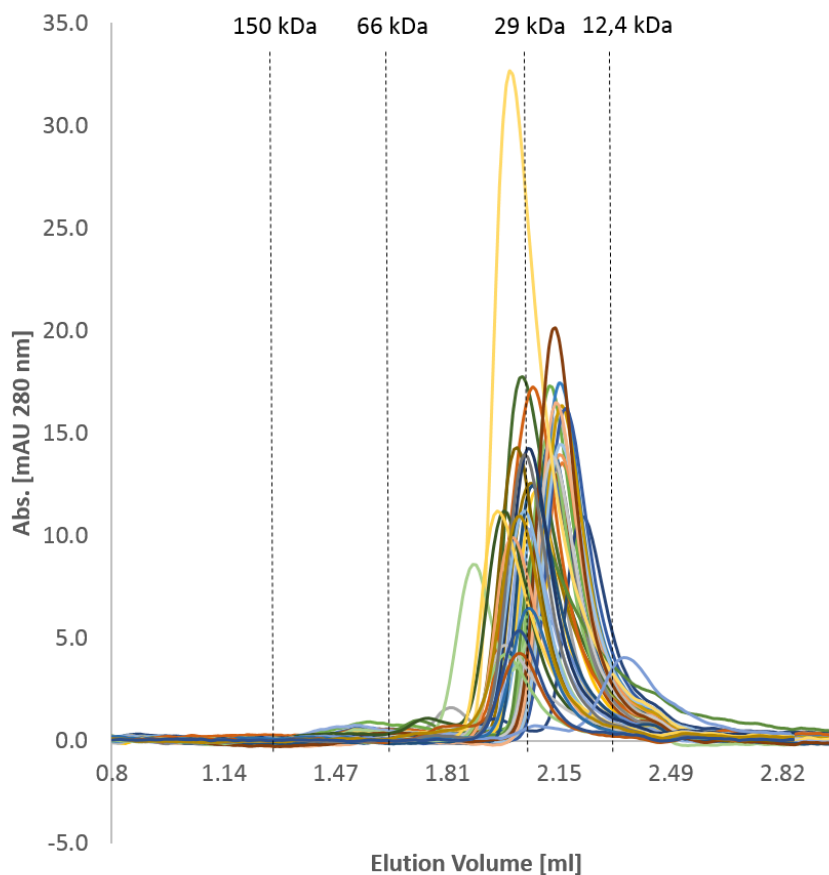


Figure 3.9: Analytical SEC of DARPins evolved from round three and four of ribosome display selection. Curves represent the elution profile of each single clone as detected using absorbance at 280 nm, after purification and removal of Imidazole by buffer exchange. For each run 50  $\mu$ l of a 10  $\mu$ M protein-solution was loaded onto a Superdex 200 increase column with 1  $\times$  PBS pH 7.4 at a flow rate of 0.4 ml/min using an ÄKTAmicro chromatography system. All curves plotted as Abs. [mAU 280 nm] vs. elution volume [ml]. The elution profile of the MW standard (150 kDa, 66 kDa, 29 kDa and 12.4 kDa) is represented by dashed black vertical lines.

Figure 3.9 shows the summary of analytical size exclusion chromatography of selected DARPins, evolved from the third and fourth round of ribosome display selection after removal of imidazole by buffer exchange to 1  $\times$  PBS, pH 7.4. All 45 clones analysed in Figure 3.9 represent the most promising candidates, regarding a monomeric elution profile.

It can be seen that the vast majority of the analysed DARPins from ribosome display selection round 3 and 4 showed an elution profile at  $OD_{280}$  that was characteristic for monomers. Only 6 out of 46 analysed clones (C1w, D3w, G7w, B7w, E10b and C9b) showed a slight tendency for a second peak at the approximate size of 30 to 40 kDa, which would represent the potential size of DARPin dimers. A single clone (B5b) eluted in a profile that was characteristic for dimers, to be seen as a second peak at the approximate size of a dimeric N3C DARPin. The signal intensity of this first eluting peak seemed to be larger than the second peak, which was considered to represent monomeric DARPins, suggesting a strong tendency for dimerisation.

### 3.1.6 Qualitative ELISA

In order to test the specific binding of the purified DARPins to the target human ROR1 ECD a qualitative ELISA of 45 of the initially 570 clones was performed.

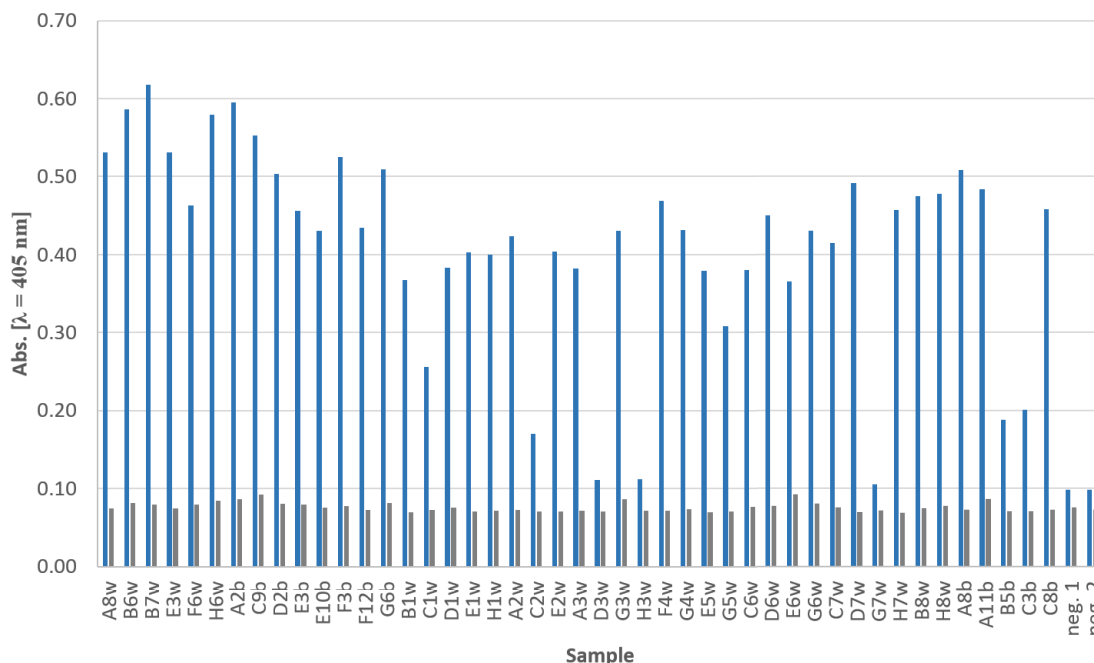


Figure 3.10: ELISA to test binding of purified DARPins to the human ROR1 ECD. A qualitative ELISA was used to analyse the binding of DARPins to the protein human ROR1 ECD. Hundred  $\mu\text{l}$  of 100 nM target was immobilised via Streptavidin after 1.0 h in each well. Hundred  $\mu\text{l}$  of 100 nM DARPIn was incubated for 1.5 h. Bound DARPins were detected using anti MRGS-His<sub>4</sub> antibody + secondary antibody coupled to AP. After addition of pNPP as substrate OD<sub>405</sub> was determined. The absorption at 405 nm was plotted on y-axis. Blue: Absorption of the respective DARPins. Gray: Negative control without target. Neg.1 refers to the negative control where no primary antibody was used. Neg. 2 refers to the negative control where no DARPIn was used.

As can be seen in Figure 3.10, the results of the qualitative ELISA for binding of human ROR1 were plotted as signal obtained after one hour of incubation with substrate, as represented by absorbance at  $\lambda = 405$  nm on the y-axis.

The majority DARPins were able to bind to the immobilised protein human ROR1 ECD. On average an absorption of 0.43 after 1.5 h of incubation was measured. Almost all clones reached an absorption that was significantly higher than the background signal, suggesting a promising specific binding of the target by the selected clones, with B7w, a putative dimer, showing the strongest measured signal of 0.62. Only three DARPins, D3w, H3w and G7w, exhibited a signal that was only marginally higher than the background, suggesting a very weak or even an absence of binding to the target human ROR1.

The negative control with missing primary antibody, shown as 'neg.1' on the right panel of the x-axis, showed an absorption that is equivalent to the background signal. With increased incubation time, the signal remained constantly low, confirming the specific binding of the secondary antibody, to the primary antibody (Table 2.22). The negative control where no DARPins were applied, shown as 'neg.2' on the right panel of the

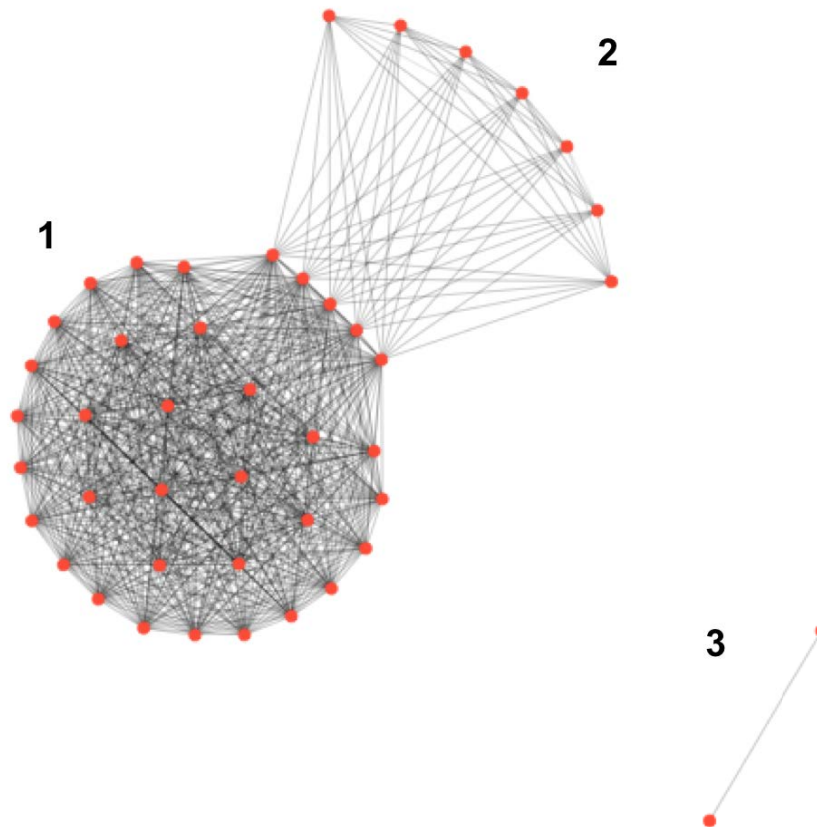


Figure 3.13: Summary of results of epitope binning on extracellular domain of human ROR1. The node plot shows different epitope regions bound by selected and characterised DARPins. Each red dot represents the respective DARPin binned. Grey connecting lines represent missing binding when binned against respective DARPin, representing binding of the same epitope region. Missing grey line between dots indicate binding on different epitope region. Number 1, 2 and 3 indicate the three regions targeted.

As of Figure 3.13 a third very rare epitope region, bound by only 5% of the selected DARPins, can be seen, representing a rather unfavoured unique binding area during directed evolution. Other than region one and two, this identified epitope showed no binder with overlapping binding of other regions, revealing a distinct binding region that is targeted by the two clones. Again as well as for the other two unique regions both clones binding this area are connected with each other, suggesting again binding of well defined small epitope regions that lie in overlapping proximity to each other. Notably, both clones binding this area evolved from the N2C library, while for epitope 1 and 2 binders from the libraries N2C, N3C and r+nr were found. A summary of the epitope regions for the tested DARPins is depicted in Table 3.8.

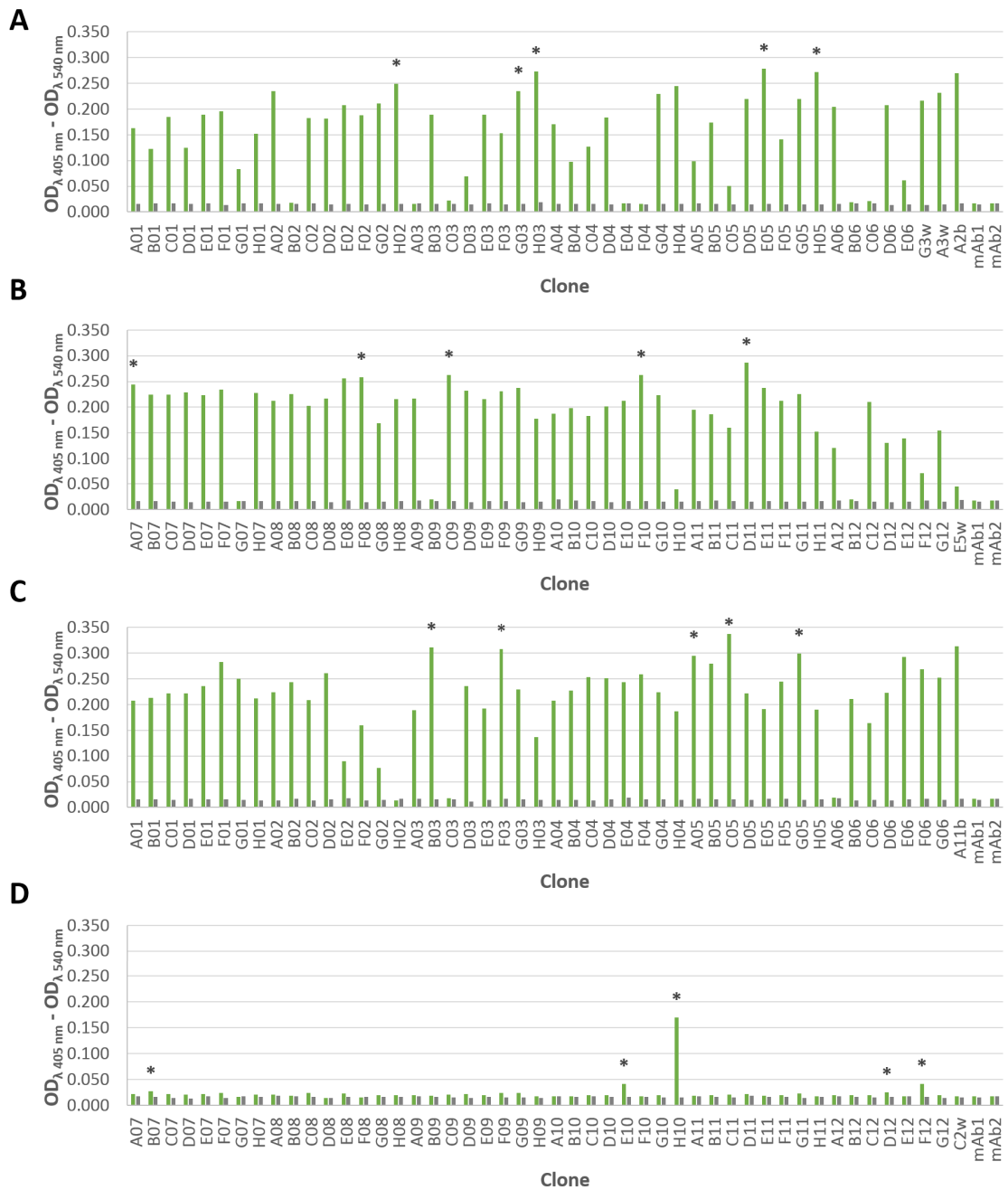


Figure 3.17: Crude extract ELISA of clones evolved from off-rate selection. Signal plotted as the difference in absorption at 405 nm and 540 nm wavelength. All samples were measured and plotted in a 1:5,000 dilution. Green: measured absorption of samples including target human ROR1 ECD and respective DARPin. Gray: negative control using reagents and DARPins only. (A) Clones evolved from P1 (44 clones). (B) Clones evolved from P2 (45 clones). (C) Clones evolved from P3 (45 clones). (D) Clones evolved from P4 (45 clones). mAb1: negative control using target and first antibody only. mAb2: negative control using target and second antibody only. The name of each clone refers to its position on the respective expression plate. Clones that were selected for further sequence analysis are highlighted with \*.

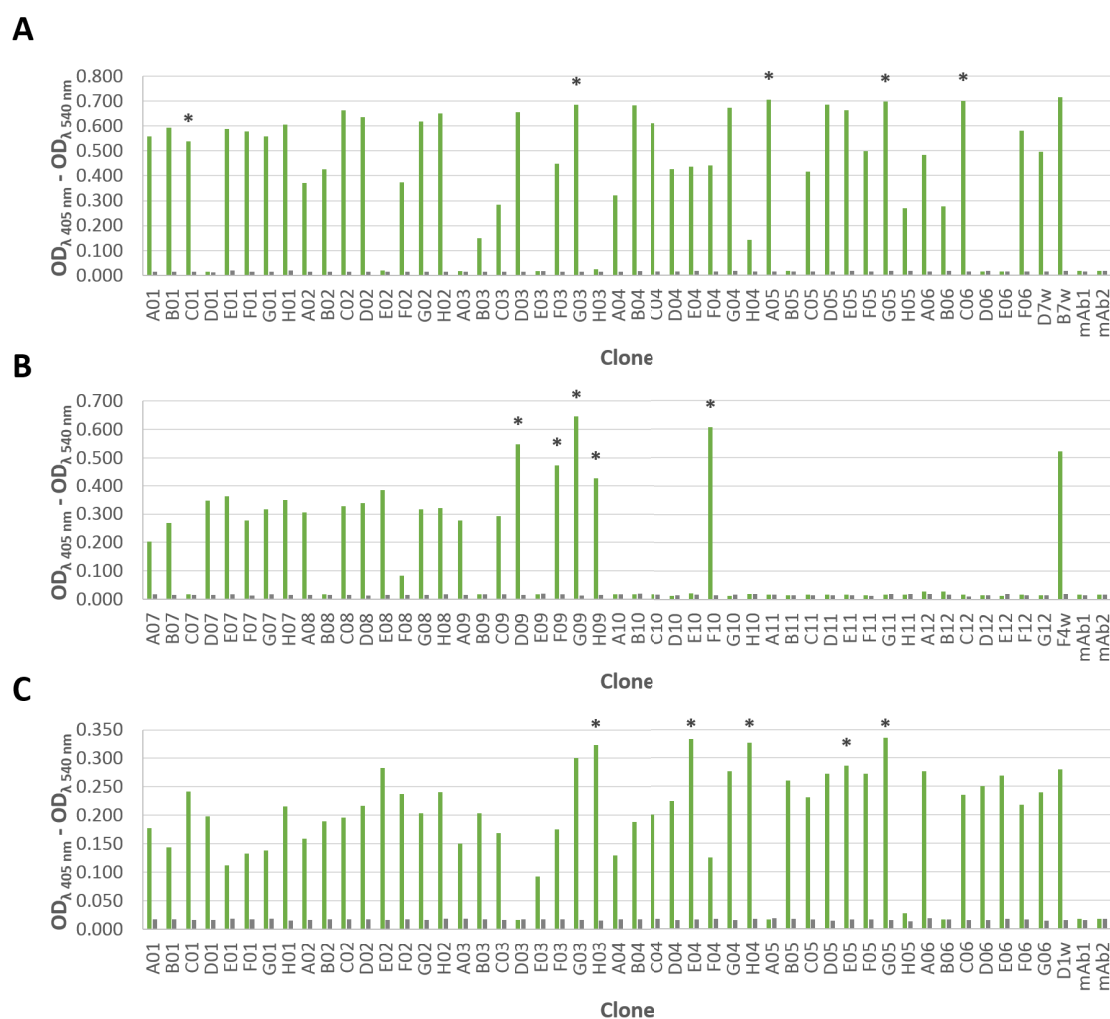


Figure 3.18: Crude extract ELISA of clones evolved from off-rate selection. Signal plotted as the difference in absorption at 405 nm and 540 nm wavelength. All samples were measured and plotted in a 1:5,000 dilution. Green: measured absorption of samples including target human ROR1 ECD and respective DARPin. Gray: negative control using reagents and DARPins only. (A) Clones evolved from P5 (44 clones). (B) Clones evolved from P6 (45 clones). (C) Clones evolved from P7 (45 clones). mAb1: negative control using target and first antibody only. mAb2: negative control using target and second antibody only. The name of each clone refers to its position on the respective expression plate. Clones that were selected for further sequence analysis are highlighted with \*.

Figure 3.17 shows the results of the crude extract ELISA for the screening for putative binder of human ROR1 ECD, that evolved from the sixth round of ribosome display selection. (A) Shows the results of the screening of clones evolved from the first pool (P1) derived from the sixth round of ribosome display selection. The parental clones derived from the first pool, indicated as G3w, A3w and A2b on the right panel of Figure 3.17, showed a distinct increase in signal compared to the respective negative controls where target was omitted. The signal intensities ranged between 0.220 and 0.270. The parental clone A2b, that showed the lowest affinity of parental DARPins as determined by SPR (Section 3.1.8) showed the highest signal with 0.270. Almost all selected clones

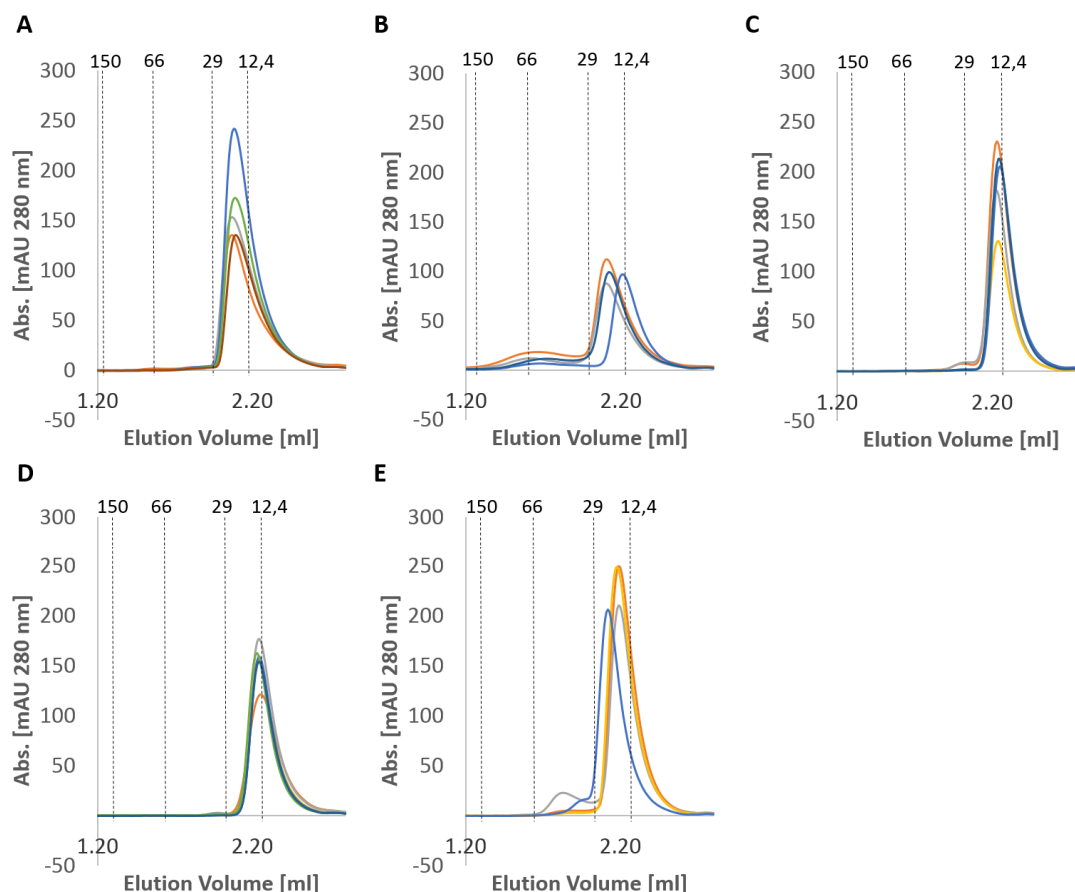


Figure 3.27: Analytical SEC of DARPins from the first pool evolved from round six of ribosome display selection. [A] DARPins evolved from pool P1. The parental clones are indicated as orange (G3w), light gray (A3w) and yellow (A2b) line. [B] DARPins evolved from pool P3. The parental clone is indicated as orange line (A11b). [C] DARPins evolved from pool P4. The parental clone is indicated in orange (C2w). [D] DARPins evolved from pool P5. The parental clones are indicated as orange (D7w) and gray (B7w). [E] DARPins evolved from pool P7. The parental clone is indicated in orange (D1w). Curves represent the elution profile of each single clone at  $OD_{280}$ , after purification and removal of imidazole by buffer exchange. For each run 50  $\mu$ l of a 10  $\mu$ M protein-solution was loaded onto a Superdex 200 column with  $1 \times$  PBS pH 7.4 at a flow rate of 0.4 ml/min. All curves plotted as Abs. [mAU 280 nm] vs. elution volume [ml]. The elution profile of MW standard (150 kDa, 66 kDa, 29 kDa and 12.4 kDa) is represented by dashed black vertical lines.

### 3.3.5 Multi Angle Light Scattering (MALS)

To confirm the results obtained by SEC alone, SEC coupled to MALS was performed. With multi angle light scattering one can determine the actual molecular mass of the protein in their eluting peak independent of their elution profile. For this purpose all DARPins as analysed in Section 3.3.4 were analysed using SEC-MALS. For each run 50  $\mu$ l of a 50  $\mu$ M protein-solution was loaded onto a Superdex 200 column with  $1 \times$  PBS pH 7.4 at a flow rate of 0.5 ml/min and the eluting protein detected by UV detection at  $OD_{280}$ ,